UNIVERSITY OF TRENTO - Italy
Department of Civil, Environmental and Mechanical Engineering

Doctoral School in Civil, Environmental and Mechanical Engineering

Topic 1. Civil and Environmental Engineering – 33rd cycle 2017/2020

Doctoral Thesis – January 2021

Daniele Riccadonna

Acoustic methods for timber structural health assessment

Supervisors

Prof. Maurizio Piazza, DICAM – University of Trento

Dr. Ivan Giongo, DICAM – University of Trento

University of Trento
Doctoral School in Civil, Environmental and Mechanical Engineering
http://web.unitn.it/en/dricam
Via Mesiano 77, I-38123 Trento
Tel. +39 0461 282670 / 2611 - *dicamphd@unitn.it*

University of Trento
Ph.D. program in Civil, Environmental and Mechanical Engineering
XXXIII Cycle

Ph.D. Program Coordinator: Prof. Luca Deseri

Final examination. May 3rd 2021

Board of examiners:
Dr. Mayank Mishra, Indian Institute of Technology, Bhubaneswar, India
Prof. Mariapaola Riggio, Oregon State University, USA
Dr. Nicola Tondini, University of Trento, Italy

This page intentionally left blank.

INDEX

ABSTRACT

The aim of the thesis is the evaluation of the feasibility of a new Non-Destructive Testing (NDT) technique for structural timber assessment based on the sound recordings analysis of impact hammer tests. The research workflow can be summarised as follows. First, an extensive bibliographic study was carried out both on the current state-of-the-art of timber assessment methods and on the physical aspects specific to the examined technique (i.e. wave propagation, structural vibration, sound radiation, etc.). Second, a series of experimental tests were performed to examine the potentiality of the proposed diagnostic technique to identify decay and/or damage inside solid wood beam elements. The recorded audio data were then analysed using a specifically developed MATLAB® code, extracting several parameters to be used as reference to deduce information about the timber element condition.

In the bibliographic survey, carried out at the beginning of the PhD work, a series of European and International documentation and guidelines about structural timber assessment were reviewed and analysed. A summary of the most common Non-Destructive Testing (NDT) and Semi-Destructive Testing (SDT) techniques was compiled, with a more detailed inquiry into the so-called stress-wave based techniques since they are closely related to the topic of the thesis. A general overview of the theory of wave propagation, both in solid media and fluid media, was then reported setting the stage for a clearer understanding of the sound radiation phenomenon involved in the proposed assessment method. The principles of audio analysis and digital audio recording were studied, and different types of data post-processing procedure were considered but a particular emphasis was reserved to frequency domain analysis and spectral audio features extraction.

For the experimental part of the thesis a first step was taken by testing 10 salvaged timber beam specimens (i.e. timber elements recovered from a structure being dismantled), 5 of them in sound conditions and 5 of them in decayed conditions as confirmed by visual examination, moisture content measurement and static testing (i.e. evaluation of the element modulus of elasticity). After these preliminary investigation,

additional testing was performed on 20 new-sawn timber beam specimens (spruce solid wood grade C24) evaluating the influence of different variables, such as type of boundary conditions, point of impact or type of microphone used for the recording (i.e. smartphone built-in microphone and calibrated electret microphone). Six of the total 20 specimens were chosen for further testing after two alternative damage scenarios were applied to the timber beams. A horizontal crack, one eighth of the total beam span long and located at the mid-height of the cross section, was applied either at the beam ends (simulating shear failure) or at the midspan section (simulating failure perpendicular to the grain for hanging loads). Results appear promising, however further testing is required to extend the method validity and statistical relevance.

This page intentionally left blank.

1 INTRODUCTION

It is well known that timber played a major role in the history of civilization, being second probably only to masonry in terms of use in the field of building and construction since humans passed from nomadism to sedentism. The success of timber can be found in its numerous qualities. It is a natural resource widely available across the world and economically feasible to harvest. It has remarkably high mechanical properties per unit weight and it can be easily machined and fabricated into elements having different shapes and sizes covering a wide range of structural needs [1]. After a slow decline of wood-based constructions that began at the dawn of the Industrial Revolution in favour of "modern" materials such as steel and concrete, in the last two decades timber has experienced a renewed interest in both the research and the practice of buildings and structures thanks to an increased awareness toward environmentally sustainable materials and thanks to the development of new engineered wood products and connections (e.g. Cross Laminated Timber CLT, Laminated Veneer Lumber LVL and self-tapping screws just to cite a few).

The quality of environmental sustainability that has revived the appeal of timber as structural material could reveal a double-edged sword. In fact, this property relies on the fact that wood is a natural, biodegradable, and renewable resource, with the lowest carbon footprint among the main building materials. However, this makes timber structural elements more sensitive to the interaction with the surrounding environment if compared to other materials, and more vulnerable to modification of the original mechanical properties due to biotic and/or abiotic attacks. For this reason, to ensure a consistent level of structural safety over the entire life-span of the timber construction, adequate design strategies and proper maintenance plans aimed at a common "durability" goal should be adopted. As part of this plan, the development of specific assessment procedures and methods plays an important role for the on-site periodical evaluation of the mechanical properties of the material and the related structural capacity of the elements. These procedures and methods can be applied also for the

appraisal of the conservation status of both historic and heritage timber structures, with different grades of invasiveness and detail based on the cultural value and historical significance of the considered construction. It is not surprising then that during the last years a vast number of research works and considerable academic effort have been dedicated to the topic of timber assessment methods and procedures.

1.1 THESIS OUTLINE

Within this research framework, the presented thesis is aimed at developing a specific assessment method for timber structures based on the recording of the radiated sound from impact tests (using smartphone built-in microphones) and on the subsequent analysis of the registered acoustic signal. The thesis is organized as follows in six main chapters, including both the Introduction and Conclusions sections.

Chapter 2 – State-of-the-art on timber structure assessment methods

In order to provide context for the proposed acoustic assessment method, Chapter 2 reports an up to date and extensive state-of-the-art on structural timber diagnostic techniques and assessment procedures to the best of the author's knowledge. The chapter begins by describing the guidelines developed in the last decade by the European Cooperation in Science and Technology (COST) association are reported for both historic and heritage structures ([2] and [3]) and more "modern" timber constructions [4]. A list of the most common diagnostic techniques for structural timber is then presented distinguishing Non-Destructive Testing (NDT) techniques [5] from Semi-Destructive Testing (SDT) techniques [6]. A more detailed literature research was carried out regarding the so-called stress-wave methods [7] since they are closely related to the method proposed in this work. These techniques rely on the common operating principle of using the propagation of a stress wave inside the inspected element as a diagnostic tool to infer information about the mechanical properties of the material and/or the geometry of the structure. Additional sub-grouping of the stress-wave methods can be obtained based on which aspect of the wave propagation is measured (structural acceleration or sound radiation), based on the frequency content of the stress wave source (sonic or ultrasonic methods) and based on the type of analysis and post-processing performed on the recorded data (time domain or frequency domain methods).

Chapter 3 – Theoretical basis of wave propagation and structural vibration

In Chapter 3 a brief overview on the theory of wave propagation inside solid media and fluid media is presented to lay the foundation for the understanding of the physical

phenomenon of sound radiation from acoustic impact tests. The book "Sound and structural vibration – Radiation, transmission and response" from Fahy and Gardonio [8] is used as main reference for the mathematical concepts. Emphasis is given to the relation between bending waves in solid medium and longitudinal waves in fluid medium because bending waves are commonly recognised to be the main contributors to sound radiation from vibrating structures (also known as structure-borne sound). In the second part of the Chapter the principles of structural dynamic testing are reported and, in particular, the main notions of Experimental Modal Analysis (EMA) using an impact hammer as input source ([9] and [10]). Even if not directly employed in this work, the concepts of EMA can be transposed to the proposed acoustic impact testing method.

Chapter 4 – Proposed acoustic timber assessment method

Chapter 4 starts by describing the so-called tapping (sounding) method [4], known to literature as a qualitative approach to obtain a rough evaluation of a timber element condition in the first stages of an on-site survey. The operator carrying out the assessment hits the element with a blunt object and based on the radiated sound can make an expert estimate of the health condition of the structure. Based on this starting point, the chapter reports on a proposal for improving the method by replacing the subjective sound perception of the inspector with the recording of the sound with a smartphone built-in microphone and the following analysis of the registered signal. The main concepts of acoustics are covered within the chapter, with notes also on the fundamentals of microphone technology and digital audio recording. For the registered signal analysis and data post-processing part, a thorough review of frequency analysis procedures is included, ranging from the basis of Fourier Transform methods to octave analysis, combined time-frequency analyses (Short Time Fourier Transform STFT and Wavelet Transform) and cepstrum analysis. The last section of the chapter treats of the specific procedure used to analyse the data gathered during the experimental part of the presented research work. It is reported the mathematical definition of four time-domain based and fourteen frequency-domain based signal descriptors used to represent the acoustic recordings and to perform the assessment of the timber element conditions. Finally, are stated the main working hypotheses relative to the capability of the method to identify decay and/or damage in timber beam elements, which will then put to test in Chapter 5. Based on a literature overview of analogous diagnostic methods and on theoretical considerations it is assumed that:

- Wood decay, and specifically the biodegradation caused by wood-decaying fungi, induces a decrease of the strength and stiffness properties of timber (e.g. modulus of elasticity, modulus of rupture, surface hardness, etc.).

- This change of the mechanical properties of the wood material influences the dynamic (both vibrational and acoustical) response of the timber element. Compared to sound material, decayed timber may exhibit lower frequency content in the radiated sound, lower amplitudes value of the acoustic signal with similar input forces, and more damped vibrational and acoustical response.
- Mechanical damage, particularly the most common type consisting in cracks perpendicular to the grain, may affect primarily the geometrical properties of a timber beam element (i.e. cross section features like area and geometric moment of inertia).
- This modification of the geometrical features of the element may lead to change in the propagation pattern of stress-wave inside the element also affecting the excitation of flexural bending modes which in turn correlate to the overall frequency content of the radiated sound.

Chapter 5 – Experimental campaign, outcomes and analyses

Chapter 5 is dedicated at reporting the results of two separated experimental campaigns carried out with the intention of testing the proposed acoustic method and evaluating its ability to detect timber element decay and damage. The first campaign [11] was aimed at assessing the ability of the technique to detect differences in sound radiation between timber elements in relatively sound conditions and timber elements with an advanced state of decay. A total of ten salvaged timber beam specimens (i.e. timber elements recovered from a structure being dismantled, five in good conditions and five in bad conditions) were utilised for the test, measuring firstly mechanical parameters such as the modulus of elasticity, the average global density, and the average moisture content. For the acoustic tests two mid-market smartphones were used for the recording and two alternative configurations were assumed: impact in the beam longitudinal direction and impact in the beam transverse direction at the midspan section. Other parameters that may affect the test outcomes, such as microphone-to-sound-source distance and impact tool type, were considered and investigated. The second experimental campaign was aimed at addressing aspects of the proposed acoustic method not examined in the previous investigation. A selection of twenty new timber beam specimens with two different geometries (ten with a 2 m span length and a cross-section of 100×100 mm^2 and ten with a 4 m span length and a cross-section of 140×180 mm^2) was adopted for the tests. All the specimens were made of spruce solid wood (grade C24) and the relevant mechanical properties (modulus of elasticity, global density, and moisture content) were assessed for each of them prior to the acoustic impact testing. As regards the test configuration, only the option with the impacts in the transverse direction was selected for this campaign. The impact sound was recorded using two mid-market smartphones and a calibrated microphone to be used as benchmark for evaluating the

reliability of the smartphones recording outcomes. The influence of parameters on sound radiation such as the location of the impacts and the element boundary conditions was studied thanks to a specific setup capable of hindering the rotations of the specimen extremities. Finally, after testing the beams in intact conditions, horizontal cuts were created on six of the specimens by using a chainsaw to simulate the typical cracks perpendicular to the grain direction, often found in timber elements. The acoustic impact tests were then repeated on the damaged specimens to evaluate the potential of the method to identify also the presence of longitudinal cracks inside timber beam elements.

Chapter 6 – Conclusions

In the final section a summary of the main findings of the research is reported together with a proposal for future studies in this field and opportunities for further investigation.

1.2 REFERENCES

[1] I. Smith and M. A. Snow, "Timber: An ancient construction material with a bright future" *The Forestry Chronicle*, vol.84, no. 4, 2008.

[2] H. Cruz, D. Yeomans, E. Tsakanika, N. Macchioni, A. Jorissen, M. Touza, M. Mannucci and P. B. Lourenço "Guidelines for on-site assessment of historic timber structures" *International Journal of Architectural Heritage*, vol. 9, no. 3, pp. 277-289, 2015.

[3] M. Riggio, D. D'Ayala, M. A. Parisi and C. Tardini "Assessment of heritage timber structures: Review of standards, guidelines and procedures" *Journal of Cultural Heritage*, vol. 31, pp. 220-235, 2018.

[4] P. Dietsch and H. Kreuzinger "Guideline on the assessment of timber structures: Summary" *Engineering Structures*, vol. 33, pp. 2983-2986, 2011.

[5] M. Riggio, R. W. Anthony, F. Augelli, B. Kasal, T. Lechner, W. Muller and T. Tannert "In situ assessment of structural timber using non-destructive techniques" *Materials and Structures*, vol. 47, pp. 749-766, 2014.

[6] T. Tannert, R. W. Anthony, B. Kasal, M. Kloiber, M. Piazza, M. Riggio, F. Rinn, R. Widmann and N. Yamaguchi "In situ assessment of structural timber using semi-destructive techniques" *Materials and Structures*, vol. 47, pp. 767-785, 2014.

[7] U. Dackermann, K. Crews, B. Kasal, J. Li, M. Riggio, F. Rinn and T. Tannert "In situ assessment of structural timber using stress-wave measurements" *Materials and Structures*, vol. 47, pp. 787-803, 2014.

[8] F. Fahy and P. Gardonio, "Sound and structural vibration – Radiation, transmission and response" 2nd ed., Oxford: Academic Press, 2007.

[9] O. Døssing "Structural testing. Part 1. Mechanical mobility measurements" Bruel & Kjaer, Naerum, Denmark, 1988.

[10] O. Døssing “Structural testing. Part 2. Modal analysis and simulation” Bruel & Kjaer, Naerum, Denmark, 1988.
[11] D. Riccadonna, G. Schiro, D. Casagrande, M. Piazza and I. Giongo, “On the use of sound spectral analysis for the in situ assessment of structural timber” *Proceedings of the 11th International Conference on Structural Analysis of Historical Constructions SAHC*, Cusco, Perú, 2018.
[12] D. Riccadonna, I. Giongo, D. Casagrande and M. Piazza, “Acoustic testing for the preliminary assessment of timber beams – A pilot study” *International Journal of Architectural Heritage*, vol. 13, no. 7, 2019.

2 STATE-OF-THE-ART ON TIMBER STRUCTURE ASSESSMENT METHODS

2.1 WHY IS TIMBER STRUCTURES ASSESSMENT NEEDED?

Even if it may seem superfluous or common knowledge one should start to answer this question by defining what timber is and how it was, and it is used in the building and construction field. Timber is a natural, hygroscopic and anisotropic building material and it is used in a variety of ways in the civil construction industry either as part of a structure (e.g. a wide majority of floors and roofs of both historical and new buildings) or as main building element ranging from light-frame wall structures to heavy frame, Cross-Laminated-Timber (CLT) wall and large span structures.

The fact that timber is a natural material implies that it is not a homogeneous material such as steel or concrete, despite of also concrete may be argued to be not homogeneous. Nonetheless, timber presents features coming from the natural growing process of the plant which radically change the mechanical properties of the material composing full-scale building element to that of the "pure" material (i.e. clear wood) [1]. These features may be various (e.g. knots, slope of grain, juvenile wood, shrinkage cracks, pole defect, etc.) and generally are considered as defects when calculating the capacity of the full-scale timber element, lowering its resistance to external action. This is usually not a concern when assessing modern buildings since the effects of these defects are already taken into account in the strength grading of the timber structural material [2]. However, when evaluating historical constructions, or in absence of information about the design of a modern structure, the presence, location and dimension of timber natural defects should be reported because they can greatly impact the response of the structure to new or modified load levels.

Linked to the natural growing process of the plant there is also the fact that timber is an anisotropic material: it has a primary direction of resistance (longitudinal), coincident

to the axis of the tree (i.e. parallel to the grain), and two secondary directions (radial and tangential) orthogonal to the tree axis (i.e. perpendicular to the grain), lying on the plane where the growth rings of the plant can be discerned. This modelling of the material can be further simplified recognising that, for timber elements sawn sufficiently far away from the tree pith, the two secondary directions have very similar mechanical properties and can be considered as a unique transversal direction. Therefore, the timber material can be deemed to be orthotropic having a principal direction, parallel to the grain, and a secondary direction, perpendicular to the grain. Due to the particular loading conditions for which the material was "designed" by nature [1], the strength and stiffness properties in the direction parallel to the grain are much higher than that perpendicular to the grain. In particular, the tensile strength perpendicular to the grain represents the lowest resistance for any type of timber product and wood species ([3] and [4]), making the timber structural element particularly prone to damage for actions operating in that direction (e.g. suspended loads, excessive shrinkage deformations, etc.). Indeed, as reported in literature ([5] and [6]), the most common type of mechanical damage to timber beam elements and timber large-span structure is cracking along the grain direction. This type of damage needs to be assessed because it can modify the timber element geometric properties (i.e. cross-section properties) influencing both the load bearing capacity and serviceability of the structure. To give a simple example let us imagine a 4-meter long solid wood beam (grade C24 [3]) with a 100x140 mm^2 cross-section, the characteristic bending capacity of the element can be evaluated as the product of the material bending strength and the elastic section modulus:

$$M_{R,k} = f_{m,k} \cdot W_{el} = 24\ MPa\ \cdot \frac{100 \cdot 140^2 mm^3}{6} = 7.84\ kNm \qquad \text{(Eq. 2-1)}$$

Assuming that the perpendicular crack runs along all the beam width and length halfway up the cross section, the beam can be viewed as a composite system where two distinct beams act in parallel and the bending capacity can be calculated as:

$$M_{R,k} = 2 \cdot \left(24\ MPa\ \cdot \frac{100 \cdot 70^2 mm^3}{6}\right) = 3.92\ kNm \qquad \text{(Eq. 2-2)}$$

Obviously, this is the worst-case scenario where the capacity of the element is halved, however it is useful to evidence how a modification of the geometric properties of a timber element (e.g. elastic section modulus) can significantly influence the capacity and stiffness of the structure.

Finally, the timber material is hygroscopic meaning that it reacts with the surrounding environment exchanging moisture with air. Water in wood can be contained either as "free" water in the natural porosities of the material or as "bounded" water in the

material micro-structure [1]. Since the chemically bounded water can considerably affect the mechanical properties of timber, the measurement of the element moisture content (i.e. percentage of water mass contained with respect to dry wood mass) should always be part of every timber structure assessment. In particular, it should be assessed if the measured moisture content of the element is compatible with the limit values to which the structure is supposed to operate (e.g. for a recently designed structure the values set by the European Code for the three service classes [7]). Additionally, the moisture content of timber is related to the probability of biotic attacks (i.e. destruction of wood material by living organisms). It exists a threshold value of the moisture content, generally set at 18÷20% [1], above which the timber material can become colonised by wood-decaying fungi and start to rot, especially when the high humidity values are kept constant for long period of time. In an engineering perspective this can impact both the load-carrying capacity and serviceability of the structure since the degradation of the material micro-structure lead to significant reduction of the material resistance and stiffness properties [8]. Referring to the former example of a solid wood beam (Eq. 2-1), the wood decay caused by fungi reduces the load bearing capacity of the element lowering the mechanical properties of the material while the geometric properties of the section remain unchanged. Another common cause of wood decay is constituted by wood-boring insects, which are generally less limited by the environmental condition compared to wood-decaying fungi and can infest also dry timber material. Signs of infestation are the presence of small tunnels plus related exit holes and dust on the surface of the affected timber element. By a structural point of view, the effect of insect attack can be seen as a mix of mechanical damage and decay; the material micro-structure is not affected by the presence of wood-boring insects, but in a macroscopic view the sum of the caused mechanical damage (i.e. missing material) can be regarded as an overall reduction of the material strength and stiffness properties correlated to the decrease in material density [9].

To sum up, the assessment of existing timber structures is an important area of research due to the intrinsic nature of wood material and its interaction with the surrounding environment which make timber prone to modification of the pre-existing structural capacity. This is particularly true in the light of the growth in usage of timber as structural material for large-span structures and high-rise buildings over the past two decades. Because these constructions are classified into high consequence classes in terms of structural robustness, appropriate maintenance plans should be prepared which cannot be exempted from the adoption of procedures and methods to assess the material integrity.

As regards the main aspects to be aware of when assessing existing timber structures, we can summarise them into four main categories:

1) *Natural defects*: related to the natural growing process of the plant, they can reduce the capacity of full-scale timber element. Particularly important to assess when operating on historical timber structures made of solid wood material.
2) *Mechanical damage*: often linked to the orthotropic nature of the timber material, in particular to the limited resistance to tension operating perpendicular to the grain direction (e.g. cracks along the grain). It can affect the serviceability and capacity of the structure by modifying the geometric properties of the composing timber elements.
3) *Moisture Content*: related to the hygroscopic nature of wood material. Important to assess either because the increase in moisture content by its own can reduce the mechanical properties of the material and because it is strictly related to the probability of biotic attacks.
4) *Biotic attacks and decay*: generally subdivided in two macro groups: wood-decaying fungi attack and wood-boring insects attack. Both of them, with different degrees, are related to the moisture content of the timber element and in general to the surrounding environmental conditions. In terms of structural capacity decay reduces the mechanical properties of the material due to degradation of the material micro-structure (wood-decaying fungi) and reduction of global density of the material (wood-boring insects).

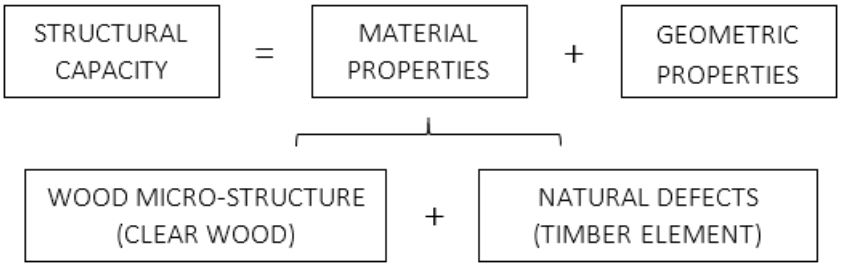

Figure 2-1 Simple schematic representation of the factors influencing the structural capacity of timber elements

The next part of this chapter is organised as follows: first is reported a literature review of the guidelines and procedures proposed for the assessment of existing timber structures. Then, a brief description of the most common Non-Destructive Testing (NDT) and Semi-Destructive Testing (SDT) techniques for the inspection and diagnosis of timber elements. Finally, a thorough bibliographic survey of NDT techniques based on stress-wave measurements is presented and discussed.

2.2 GUIDELINES FOR THE ASSESSMENT OF TIMBER STRUCTURES

Highlighting the importance of the assessment of existing timber structures, the past decade has seen increasing attention by the researching community with several task groups in the European Cooperation in Science and Technology (COST) association working on guidelines to present the currently available assessment methods and to define procedure for their application ([10], [11] and [12]). In a certain way we can say that these guidelines provide a list of the assessment methods (diagnostic techniques for the timber material) together with a method for the assessment, meaning a list of steps needed to carry out the assessment. The approach is very similar considering either historic and heritage timber structures ([10] and [11]) or more modern timber structures such as large-span structures or high-rise buildings [12].

The reasons for planning the assessment of an existing timber structure may be various:

- Identified inadequacies or errors in the design or construction process of the structure (including possible modifications from the original design).
- Change of use of the building and consequent change of load levels.
- Detection of material decay due to biotic attacks suffered by part of the structure.
- Detection of mechanical damage due to exceptional loading conditions or other factors.
- Apparently inadequate serviceability of the building or suspected impairment of the construction structural safety.
- End of the expected lifetime of the structure.

Aim of the assessment and some fundamental principles to keep in mind are:

- The inspection and the measurements performed during the building survey should provide sufficient data for the analysis of the building history, the evaluation of structural safety and for helping in the decision-making process about the eventual intervention.
- In doing so, the assessment methods used should have a minimal impact on the original material, structural systems and other parts composing the existing building.

As reported in the guidelines for the assessment of historic timber structures developed within the COST Action IE0601 [10], the procedure to carry out the assessment can be subdivided in two distinct phases each of one composed by different steps. A preliminary survey which is composed by:

1) *Desk survey*: it involves collecting all the information and documentation available on the building (e.g. technical drawings for modern buildings or information about the construction technologies for historic structures). It should also require a confrontation with the building owner for clarifying accepted alterations and intentions about the final intervention.
2) *Visual survey*: primary examination of the building to plan the following steps and to identify the proper ways to execute the work and gather the required measurements in safety.
3) *Measured survey*: collection of the geometrical disposition of the timber structures and of the timber elements size. It should also report obvious signs of damage or decay and evidence of alterations from the original design (when possible).
4) *Structural analysis*: to determine the expected force levels on the timber structure and identify the zones with the higher amount of stress due to the operating load or the eventual increase of load for change of use of the building.
5) *Preliminary report*: it should resume the results of the four previous steps providing a highlight of the most critical parts of the timber structures (i.e. high stress levels, evidence of damage and/or decay, etc.). It should serve as a basis for planning the (eventual) second stage of the assessment, also supplying an estimation of the costs of the additional work.

If the data provided by the preliminary survey are not enough to arrive at a final decision a second stage of the assessment can be prepared:

6) *Detailed survey*: based on the outcomes and observations of the preliminary surveys, the most critical zones of the timber structures should be assessed with Non-Destructive Testing (NDT) techniques or Semi-Destructive Testing (SDT) techniques. A visual strength grading of the timber elements can also be performed together with the evaluation of the wood species (especially when dealing with historic structures with unknown material). Moreover, the adequacy of the timber joints should also be evaluated.
7) *Diagnostic report*: once the conditions of the timber structures are determined with an acceptable degree of accuracy, hypotheses about the causes of damage, decay or impairment of function can be formulated with suggestions on how to address the repairment and structural rehabilitation phase. Additional structural analyses should also be carried out to evaluate the force and stress levels on the structure with the updated mechanical properties after the detailed survey and with the proposed reinforcement intervention.
8) *Detailed design of intervention*: the last step of the assessment should be the programming and preparation of the intervention on the existing structure if this

is the decision taken after the detailed survey. An appropriate maintenance plan should also be outlined to guarantee the effectiveness of the intervention over time.

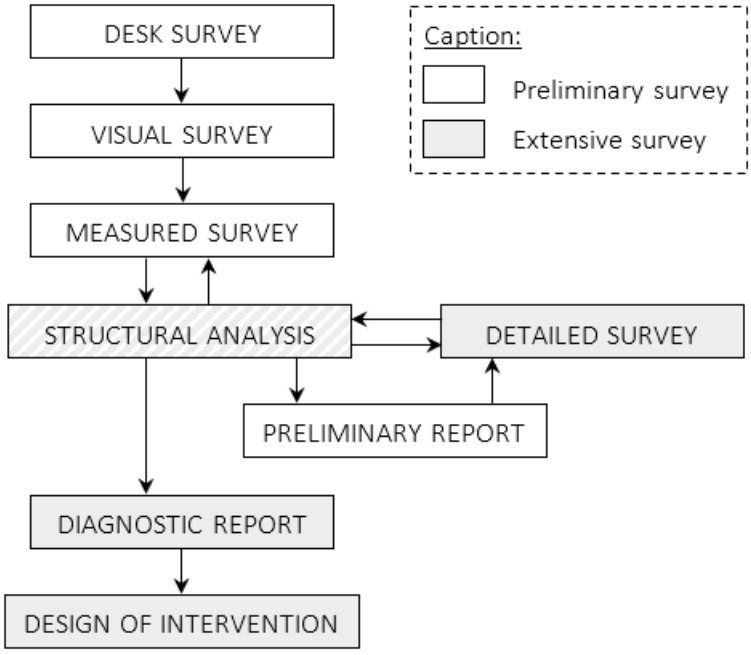

Figure 2-2 Steps required for the assessment of an existing timber structures (adapted from [10])

The layout, developed for historical and heritage timber structures, can be adopted also for modern existing structures, as it was similarly described in the guideline for the assessment of large-span timber structures [12]. All the authors agree that the most critical part of the assessment is the actual evaluation of the mechanical parameters of the wood material and the identification of the damaged and/or decayed zones via NDT or SDT methods because is generally the part containing the highest degree of uncertainty. In fact, up to date does not exist a unique method capable of define completely the capacity of a timber element; on the contrary, a combination of different techniques have to be adopted, each of which grants different information about material properties, presence of damage or decay, etc. When several methods provide similar results one can be adequately confident that the outcomes do not represent a false positive, for example for the identification of damaged or decayed area.

However, most of the assessment methods currently available give qualitative information (e.g. presence or not of decay, extension of decayed area), while only few

are able to deliver quantitative data that can be used in the structural analysis stage (i.e. updating of analytical or numerical model). Moreover, the methods that give quantitative measurements generally evaluate stiffness parameter or other mechanical properties of the material (e.g. Modulus of Elasticity MOE or global density ρ) that are then correlated to strength parameters such as the Modulus of Rupture MOR for bending actions. This correlation is too low to ensure an adequate level of confidence for brittle failure of timber member such as bending or shear failure [12].

This means that there is still room of improvement and that research in this field should focus on the optimization of the currently available methods and in parallel on the development of new methods to provide the highest amount of information to the engineer that have to perform the assessment in practice.

2.3 NON-DESTRUCTIVE TESTING (NDT) TECHNIQUES

In literature already exist a wide number of works ([13], [14], [15], [16] and [17]) aimed at summarising the most common NDT and SDT methods used for the on-site assessment of timber structures. In this section it will be reported a short review of the Non-destructive Testing methods based on the work of the RILEM Technical Committee AST 215 "In situ assessment of structural timber" reported in [13]. The term Non-Destructive Testing means that the inspected element, in its form and properties, is not altered by the diagnostic technique in no way.

2.3.1 VISUAL INSPECTION AND VISUAL GRADING

Type	NDT	
Measured parameter	Geometry and locations of natural defects	
Estimated parameter	Strength class of the element	
Information	Qualitative	
	Global	
Detection of	Natural defects	Yes
	Moisture	Limited
	Decay	Limited
	Damage	Limited
	Hidden internal details	-

Visual inspection is the first and most obvious type of NDT technique and it is the base for every other following assessment method. It includes a basic geometric survey of the timber elements, timber joints and the identification of the operating load on the structure. It can help to identify evident signs of moisture accumulation, biotic attacks, and mechanical damage and to detect critical areas where further thorough inspections are needed. Together with the usual visual inspection a visual strength grading of the various timber elements can be performed, particularly useful in the case of historic structures or in absence of documentation of the resistance properties of the timber material. The visual strength grading, coupled with the identification of the wood species, allows to sort the timber elements in specific strength classes (range of mechanical properties) on the basis of the observed natural features [2]. However, one should keep in mind that there are different limitations for the application of visual grading in the assessment of existing timber structure. First, the procedures and standards usually adopted were developed for new sawn solid timber and there are limited indications for the use on-site or for glued laminated timber. Secondly, not always the whole surface of the timber element is visible due to impediments from other part of the structure or due to coating of the material (e.g. decorated or painted elements in heritage structure). Lastly, there is an inevitable degree of subjectivity of the measurement because the collection and interpretation of the outcomes depend on the training and experience of the person who carries out the measurement.

2.3.2 MOISTURE CONTENT MEASUREMENT

Type		Measured property	Range of validity
Oven-dry method	SDT	Mass	Entire MC range
Hygrometric method	SDT	Air relative humidity (RH)	Entire MC range
Resistance method	SDT	Wood electrical resistance*	Below FSP
Capacitance method	NDT	Wood dielectric properties*	Below FSP

* Calibration required for temperature and wood species

Since the moisture content (MC) greatly affects the mechanical properties of the timber material and is also associated to the risk of bio-deterioration, its measurement is of crucial importance and should be always performed when assessing an existing timber structure. There are different ways for determining the MC of a timber element, spacing from direct measurement of the water mass to indirect measurement via evaluation of the electrical properties of the material. Here will be shortly described:

- The oven-dry method [18].

- The hygrometric method.
- The resistance method [19].
- The capacitance method [20].

It should be noted that all these methods provide local measurement of the MC; since the MC in a timber element can vary across the section and the longitudinal axis, an appropriate grid of measurements should be prepared to provide an estimation of the MC distribution across the whole element.

Type	Oven-Dry method (SDT)	
Measured parameter	Mass	
Estimated parameter	Moisture Content	
Information	Quantitative	
	Local	
Detection of	Natural defects	-
	Moisture	Yes
	Decay	-
	Damage	-
	Hidden internal details	-

The oven-dry method allows the direct measurement of the timber moisture content by removing small samples from the inspected element; hence it can be classified as a Semi-Destructive Testing (SDT) method. In addition, it cannot provide immediate on-site measurement since it requires two subsequent measurement of the mass of the extracted samples as is and after oven dried.

$$MC_{\%} = \frac{m_{sample} - m_{oven-dry}}{m_{oven-dry}} \cdot 100 \qquad \text{(Eq. 2-3)}$$

Type	Hygrometric method (SDT)	
Measured parameter	Air Relative Humidity (RH)	
Estimated parameter	Moisture Content	
Information	Quantitative	
	Local	
Detection of	Natural defects	-
	Moisture	Yes
	Decay	-

	Damage	-
	Hidden internal details	-

The hygrometric method is based on the observation that the moisture content (MC) of timber is influenced by the surrounding air volume relative humidity (RH) and vice-versa. For the measurement there are two different procedure: measurement on extracted samples or measurement directly on the element. Both of them are Semi-Destructive in nature since the direct measurement requires to bore a hole to place the instrumentation (hygrometer and thermometer) inside the element. Additionally, the measuring instrumentation and the samples should be placed inside air-tight container to avoid influence from the surrounding environment. Frequent readings of the air relative humidity are taken until the hygroscopic equilibrium between wood and air is reached (threshold value after due consecutive readings); from that RH value and the measured temperature value, an estimation of the timber MC is drawn.

Type	Resistance method (SDT)	
Measured parameter	Wood electrical resistance*	
Estimated parameter	Moisture Content**	
Information	Quantitative	
	Local	
Detection of	Natural defects	-
	Moisture	Yes
	Decay	-
	Damage	-
	Hidden internal details	-

* Influenced by local density values (e.g., wood species, growth rate, etc.). Calibration required.

** Below Fibre Saturation Point (FSP, MC≈25÷30%)

The measurement is performed with a hand-held moisture meter composed by an ohmmeter connected to two pin-type electrodes; these electrodes must be fixed to the timber element, so the testing method should be considered as moderately destructive. Generally insulated electrodes are used (i.e. only the tip not covered by insulation material) since they are less influenced by surface moisture that might not represent the correct MC value for the whole element. Specific procedure for the estimation of the global MC of the element are reported in the standard [19]; it is generally advisable to avoid the ends of the elements (minimum distance of 50 mm) to avoid the influence of

unbound water absorbed for capillarity. The measurements must be taken on sound wood, free of defects or material discontinuity. A minimum of three readings for each measurement location should be taken and the effects of glue lines (for glued laminated timber), wood extractives and other eventual chemical treatment should be taken into account because they can influence the electrical properties of the material.

Type	Capacitance method (NDT)	
Measured parameter	Wood dielectric properties*	
Estimated parameter	Moisture Content**	
Information	Quantitative	
	Local	
Detection of	Natural defects	-
	Moisture	Yes
	Decay	-
	Damage	-
	Hidden internal details	-

* Influenced by local density values (e.g., wood species, growth rate, etc.). Calibration required.

** Below Fibre Saturation Point (FSP, MC≈25÷30%)

The capacitance method exploits the relation between the timber MC and the wood dielectric properties linked to the transit of electric alternate current (AC). This is the only completely Non-Destructive method for estimating the timber MC because surface electrodes are used for the measurement. This advantage comes at the cost of increased limitations on the assessment procedure. Indeed, in addition to similar limitations as already expressed for the resistance method, the capacitance method is more sensitive to parameters such as temperature, grain direction, AC frequency and wood density. In particular, the high dependence on wood density requires proper calibration either for wood species and for the ratio of sapwood and heartwood material in the measurement location.

2.3.3 DIGITAL RADIOSCOPY

Type	NDT
Measured parameter	Absorption of electromagnetic (EM) radiation (x-rays)*
Estimated parameter	-
Information	Qualitative

	Local	
Detection of	Natural defects	Limited
	Moisture	Limited
	Decay	Limited
	Damage	Limited
	Hidden internal details	Yes

* Influenced by local density values (e.g., wood species, growth rate, etc.) and local moisture content values. Calibration required.

The principle underlying timber assessment using digital radioscopy is the same principle for the diagnosis of human body. High energy electromagnetic (EM) radiation with determined frequency (i.e. x-rays) can easily penetrate timber material but are preferentially absorbed by metal connectors or other dense material. Hence, digital radioscopy is one of the best assessment methods to identify hidden details inside the timber cross-section or evaluate the capacity of metallic timber joints, but it can also give rough estimate of the extent of decayed or damaged zone inside the element. Among the limitations of this method there are the necessity to access at least two opposite sides of the element under consideration and the need of qualified technician to perform the measurement together with precise and rigorous safety measures due to the hazard of working with high-energy radiation.

2.3.4 GROUND PENETRATING RADAR (GPR)

Type	NDT	
Measured parameter	Reflection of electromagnetic (EM) radiation*	
Estimated parameter	-	
Information	Qualitative	
	Local	
Detection of	Natural defects	Limited
	Moisture	Limited
	Decay	Limited
	Damage	Limited
	Hidden internal details	Limited

* Influenced by local density values (e.g., wood species, growth rate, etc.) and local moisture content values. Calibration required.

The GPR assessment method utilizes electromagnetic radiation to investigate the timber material: an antenna emits an EM signal and estimate about the material condition are drawn by analysing the reflected signal captured by a receiver. The advantage over digital radioscopy is that the access at only one face of the element is required; the disadvantages are that the interpretation of the results is less straightforward and depending on the frequency of the EM radiation adopted there is a limitation on the depth of penetration of the radiation or the resolution of the results. Higher frequencies imply lower wavelengths and can provide more detailed results but are also more subjected to attenuation therefore travelling shorter distances.

2.4 SEMI-DESTRUCTIVE TESTING (SDT) TECHNIQUES

Proceeding on the review of the assessment methods for structural timber here will be reported a lists of Semi-Destructive Testing methods based on the work of the RILEM Technical Committee AST 215 "In situ assessment of structural timber" reported in [14]. The term Semi-Destructive Testing is used because the application of these techniques requires a minimal but not negligible alteration of the original element (e.g. extraction of small samples or residual hole/surface alteration due to testing).

2.4.1 RESISTANCE DRILLING

Type	SDT	
Measured parameter	Drilling resistance (Torque)	
Estimated parameter	Wood density	
Information	Quantitative	
	Local	
Detection of	Natural defects	Limited
	Moisture	-
	Decay	Yes
	Damage	Yes
	Hidden internal details	Limited

Resistance drilling is based on the measurement of the torque required to bore a hole in an existing timber element registered with an instrumented drill; these recordings are linked to relative density profiles since the drilling resistance of timber is strictly related to the density of the material. This enables to infer information from change in the

density profile (e.g. pocket of decay, cracks or voids, etc.); a "normal" density profile recorded across the grain will exhibit an alternate behaviour due to the natural growth rings of the tree with peaks in correspondence of the heartwood and relative drops on the sapwood. Among the different assessment method resistance drilling is one of the most reliable for detecting and quantifying the amount of decay or damage of the timber element. However, it gives a very local measure, not only in the longitudinal direction but also in the cross section of the element, and it is moderately destructive (diameter of the drill-bit generally between 1.5÷3 mm). Hence, it should be coupled with other preliminary NDT or SDT techniques and used to confirm or disprove doubt about the material condition in certain critical zones.

2.4.2 COMPRESSION TEST OF RADIAL CORE

Type	SDT	
Measured parameter	Compression strength, Modulus of Elasticity (MOE)	
Estimated parameter	Strength properties of the element	
Information	Quantitative	
	Local	
Detection of	Natural defects	-
	Moisture	-
	Decay	-
	Damage	-
	Hidden internal details	-

This assessment method provides estimate of the strength properties of the timber element under examination but does not give information about the eventual presence of decay or damage. It is more destructive compared to other SDT methods since it requires the extraction of cylindrical samples in the radial direction (perpendicular to the growth rings) with a diameter of 5 mm and height of 50 mm; the holes that remain after sampling can be plugged with other material, however this drawback should be kept in mind especially when working with historic and heritage structures. The cylindrical samples then can be tested in a laboratory facility to determine their compression strength and MOE and deduce information about the global strength of the timber element.

2.4.3 TENSILE TEST OF MICRO-SPECIMEN

Type	SDT	
Measured parameter	Tensile strength, Modulus of Elasticity (MOE)	
Estimated parameter	Strength properties of the element	
Information	Quantitative	
	Local	
Detection of	Natural defects	-
	Moisture	-
	Decay	-
	Damage	-
	Hidden internal details	-

The tensile test of micro-specimen is used to give estimate values for the strength properties of the timber element under examination. Small specimens of triangular cross-section (side dimension of almost 10 mm) are cut out the surface of the timber element along the fibre direction. These samples are then tested in laboratory to evaluate the tensile strength and stiffness (MOE) properties. Due to the high variability of the ratio of heartwood and sapwood inside these small samples several tests must be performed to ensure results with proper statistical validity.

2.4.4 GLUE LINES TEST (RADIAL CORE SAMPLES)

Type	SDT	
Measured parameter	Shear strength	
Estimated parameter	Quality of the glue lines	
Information	Quantitative	
	Local	
Detection of	Natural defects	-
	Moisture	-
	Decay	-
	Damage	-
	Hidden internal details	-

This method is similar to the compression test on radial core, but it is performed on existing glued laminated timber when doubt exist about the load-carrying capacity of the glue lines. The extracted samples have cylindrical shape and must obviously contain a glue line; they are then testes in laboratory and the maximum shear strength recorded. After the failure of the sample, the two exposed side can be chemically treated to determine if the failure happened in the wood material or at the interface, giving therefore an indication of the quality of the bond.

2.4.5 SCREW WITHDRAWAL

Type	SDT	
Measured parameter	Screw withdrawal strength	
Estimated parameter	Wood density, MOE, and Modulus of Rupture (MOR)	
Information	Quantitative	
	Local	
Detection of	Natural defects	-
	Moisture	-
	Decay	Limited
	Damage	-
	Hidden internal details	-

The screw withdrawal test allows to make assumption about the strength of an existing timber element correlating the value of measured extraction resistance of a customised screw with values of density, modulus of elasticity and modulus of rupture of the element. These regression relationships are provided by existing database of tests performed both on hardwood and softwood species. In general, to provide a mean value of withdrawal resistance as a function of the drilling depth, at least three different coaxial measurements of the maximum withdrawal force should be taken for each location.

2.4.6 NEEDLE PENETRATION

Type	SDT
Measured parameter	Indentation depth
Estimated parameter	Wood density
Information	Quantitative

	Local	
Detection of	Natural defects	-
	Moisture	-
	Decay	Limited
	Damage	-
	Hidden internal details	-

The needle penetration test requires the use of a handheld device (known with the commercial name of *Pilodyn*) constituted by a spring-loaded striker, available with three different impact energy levels (i.e. 6 J, 12 J and 18 J) and with different striker (needle) geometry. The indentation depth, using the same impact energy and striker geometry, depends primarily on the material density and therefore is also related to the relative direction of impact perpendicular to the grain (radial or tangential), to the wood species and to the presence of natural defects such as knots or reaction wood. Hence, to derive consistent results is important to properly calibrate the measurement depending on the species of the examined element and to impact the element with consistent direction during the various measurement.

2.4.7 PIN PUSHING

Type	SDT	
Measured parameter	Pin pushing resistance (Force)	
Estimated parameter	Wood density	
Information	Quantitative	
	Local	
Detection of	Natural defects	Limited
	Moisture	-
	Decay	Yes
	Damage	Yes
	Hidden internal details	Limited

In a certain way one can say that the pin pushing test is a mix between the needle penetration test and the resistance drilling method. The device used is formed by a toothed rack that drives a pin indentor (diameter equal to 25 mm) through the timber element by means of a couple of manually driven cranks. The resistance to penetration

as a function of the indentation depth is measured by a load cell with a 100 Hz sampling rate allowing to plot resistance profile analogous to the resistance drilling method. Differently to the resistance drilling method the direction of measurement should always be radial because when performing tangential readings, the pin tends to deviate toward the softer sapwood material.

2.4.8 HARDNESS TEST

Type	SDT	
Measured parameter	Surface hardness	
Estimated parameter	Modulus of elasticity (MOE)	
Information	Quantitative	
	Local	
Detection of	Natural defects	-
	Moisture	-
	Decay	Limited
	Damage	-
	Hidden internal details	-

The hardness test used for the assessment of existing timber structures is known with the name of Piazza-Turrini hardness test. It is a modified version of the Janka-hardness test which in turn consists in the application of a standard Brinell hardness test to a piece of clear wood. It is measured the force needed to impress a steel hemisphere (10 mm diameter) inside the timber element external surface (perpendicular to the grain) to a depth of 5 mm. Several measurements for each location are taken and the mean represents the hardness of the wood material in that location. An estimation of the modulus of elasticity of the timber element is then derived using an empirical relationship with the hardness value, accounting for parameters like the moisture content and the wood species.

2.5 STRESS-WAVE BASED TECHNIQUES

Among the Non-Destructive Testing (NDT) techniques a wide subgroup of methods can be identified based on the common principle of using the propagation of stress-wave inside the inspected element to deduce information about its conservation status and/or mechanical properties. In this section it will be reported an extensive overview about

the stress-wave methods for the assessment of timber structures found in literature. As a basis it will be used the work of the RILEM Technical Committee AST 215 "In situ assessment of structural timber" reported in [15] integrated with other bibliography sources when necessary.

A definition of stress wave can be propagation of energy inside a carrying medium in the form of particle displacement (i.e. pressure variations for fluid media, deformations in solid media), generally due to an external input source. Based on this definition further classifications can be derived inside the stress wave methods group:

- *Sonic or ultrasonic methods*: this subdivision depends on the frequency content of the input signal used for the assessment: if the maximum frequency is below the human hearing threshold (i.e. 20 kHz) the method is said to be sonic or acoustic, if the maximum frequency is superior to 20 kHz the method is called ultrasonic. However, this is not only a question of nomenclature: higher frequency means smaller wavelengths and therefore ultrasonic methods can detect smaller defects or imperfections inside the material. This advantage of ultrasonic method is counterbalanced by the fact that higher frequency means also higher attenuation; therefore, ultrasonic waves can travel shorter distance with respect to sonic waves.
- *Sound-based or vibration-based methods*: this classification depends on how the effects of the stress wave propagation inside the timber element are observed and measured. A wide majority of the stress wave methods measure the stress wave directly on the timber element by means of accelerometer sensor evaluating the vibration of the structure (vibration-based methods). Depending on the attachment procedure of the sensor to the structure these methods could be considered NDT or moderately destructive (SDT, e.g. screw fastening). Other methods instead exploit the relation between vibration of the element and radiated sound using microphone sensor to record the signal (sound-based methods).
- *Time domain or frequency domain methods*: finally, depending on how the recorded signal is post-processed to obtain information and data, one can distinguish between time domain or frequency domain methods. Time domain methods usually infer data about the condition of a timber element calculating the speed of the propagating wave in the material. Frequency domain methods on the other hand evaluate the spectrum of the recorded signal by means of a Fourier Transform and based on the spectral characteristics derive information on the conservation status of the material or on its mechanical properties.

2.5.1 TIME-OF-FLIGHT METHOD

Type	NDT, sonic, vibration-based, time domain	
Measured parameter	Time	
Estimated parameter	Speed of sound*	
Information	Qualitative	
	Global/Local	
Detection of	Natural defects	Limited
	Moisture	-
	Decay	Limited
	Damage	Limited
	Hidden internal details	-

* Influenced by local density values (e.g., wood species, growth rate, etc.) and local moisture content values. Calibration required.

The time-of-flight methods is one of the most used technique to assess the condition of timber structural elements ([15] and [21]) and also of timber logs and standing trees ([22] and [23]). For the measurement procedure are used an instrumented hammer, with a sensor triggering the start of recording when impacting the element surface, and a receiving sensor (e.g. an accelerometer) that stops the recording when detecting the incoming stress wave.

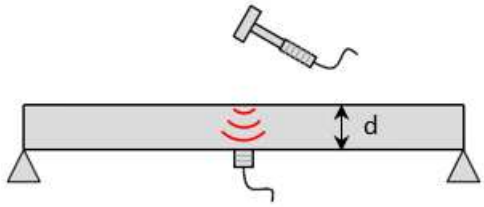

Figure 2-3 Representation of the time-of-flight method applied in the transverse direction

$$c = \frac{d}{t_{flight}} \quad \text{(Eq. 2-4)}$$

Knowing the distance between the input source and the output measurement the speed of sound inside the material can be derived (Eq. 2-4). Since sound propagates faster inside dense and rigid material the measured stress wave velocity can be used as an

indicator of the condition of the timber material (e.g. presence of decay or damage). Decay caused by fungi generally reduces the mechanical properties of timber by degrading the wood microstructure whereas decay caused by insects reduces the global density of the material; both are linked to decreased sound velocity. Mechanically damaged timber (e.g. cracks) on the other hand may exhibit lower speed of sound due to the longer distance that the wave has to travel to reach the receiving sensor.

The measurements can be performed either in the transverse and in the longitudinal direction. The first provide data about a limited section of the element (local information) and performing several recordings over the whole element length can be a viable method to obtain a mapping of its internal condition. The latter tend to mediate the effect of (possible) presence of decay or damage in different location giving an indication about the global condition of the timber element (see also paragraph 2.5.2 Resonance method).

Besides the internal condition of the material the speed of stress wave propagating inside a timber element can depend on different parameters which have to be checked to obtain reliable information during the assessment:

- *Wood species* ([15], [21] and [22]): not surprisingly because wood density and other mechanical properties vary largely between different species.
- *Indirect or direct longitudinal measurement* ([22] and [23]): some authors observed that the sound speed measured in the longitudinal direction in standing trees were significantly higher than that measured in logs cut from the same trees. They supposed and proved that this deviation stems from the different wave propagation mechanism in the two measurement setups: for standing trees the longitudinal velocity can be measured only in an indirect way (see Figure 2-4), placing the input and receiving sensors on the side of the tree. For logs on the other hand a direct measurement can be performed placing the sensors on the two extremes in the longitudinal direction. This difference influences the type of wave transmitted through the wood medium: for direct measurement are transmitted quasi-longitudinal waves whereas for indirect measurement are transmitted pure longitudinal wave. As will be exposed in Chapter 3 Theoretical basis of wave propagation and structural vibration, for a material with equal mechanical properties the travelling speed (also known as phase speed) of these two types of wave is different and pure longitudinal waves are faster than quasi-longitudinal waves.

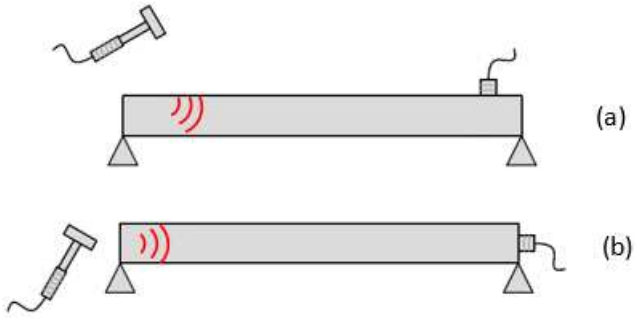

Figure 2-4 Time-of-flight method in the longitudinal direction: indirect (a) and direct (b) measurement

- *Grain angle* ([15], [21] and [24]): stress wave travel faster in the direction parallel to the grain with respect to the perpendicular direction with a ratio ranging between one fifth and one third (e.g. for douglas fir $v_{\parallel} = 5000\ m/s$, $v_{\perp} = 1200\ m/s$ [21]). A quadratic relationship using the Hankinson formula can be assumed for all the other direction ranging from parallel to perpendicular to the grain [24].
- *Annual ring orientation* ([15] and [21]): for measurement in the transverse direction (i.e. perpendicular to the grain) there is also a dependence of the stress wave velocity with the orientation of the annual growth rings (tangential and radial directions). The lowest speed is for impact in an intermediate direction (angle of 45° with respect to the annual rings) between tangential (0°) and radial direction (90°). From this minimum the speed grows either for increasing and decreasing angle with a maximum value in the radial direction (e.g. $v_{radial\ 90°} = 1500\ m/s$, $v_{tangential\ 0°} = 1200\ m/s$ and $v_{45°} = 1000\ m/s$ [21]).
- *Moisture content* ([15], [21], [25] and [26]): the effect of moisture content on the stress wave velocity is partially different in the case of transverse measurement with respect to longitudinal measurement. In both cases below the fibre saturation point FSP ($MC \cong 28 \div 30\%$) the sound speed increases for decreasing value of moisture content. Above the FSP the influence of MC variation is negligible for measurement in the transverse direction [21] whereas for measurement in the longitudinal direction there is still a slightly dependence with increasing speed for decreasing MC values ([25] and [26]).

- *Preservative treatment* ([15] and [21]): wood treated with oil-borne preservatives shows lower stress wave velocities (reduction of almost 40%) with respect to untreated wood [21].
- *Presence of wood knots* ([21], [27] and [28]): the presence of wood knots clearly influence the stress wave propagation speed since they can be considered as 90° deviation in grain direction: when performing transverse measurement they act as parallel to the grain timber, when performing longitudinal measurement as perpendicular to the grain timber [21]. Several authors agree on the influence of wood knots on stress wave measurement ([27] and [28]), however from the collected data is generally difficult to infer the number, location and size of such defects.

2.5.2 RESONANCE METHOD

Type	NDT, sonic, vibration-based/sound-based, frequency domain	
Measured parameter	Fundamental frequency	
Estimated parameter	Modulus of Elasticity (dynamic)*	
Information	Quantitative	
	Global	
Detection of	Natural defects	Limited
	Moisture	-
	Decay	Limited
	Damage	Limited
	Hidden internal details	-

* Influenced by local density values (e.g., wood species, growth rate, etc.) and local moisture content values. Calibration required.

Even if based on similar principle, the resonance method ([24] and [29]) is rarely used for the assessment of existing timber structures. Usually it is adopted for the quality assessment (i.e. presence of decay, [30] and [31]) or the strength grading of harvested timber logs ([32] and [33]). This is most likely due to the calculation of the stress wave velocity from frequency domain measurement instead of time domain; indeed, the fundamental frequency of the element used to estimate the velocity in the resonance method is highly dependant on the element boundary conditions, a parameter difficult to evaluate in the case of on-site assessment. Most of the measurements carried out on timber logs are taken simulating free-free boundary conditions by using rubber bands supports or other compliant devices.

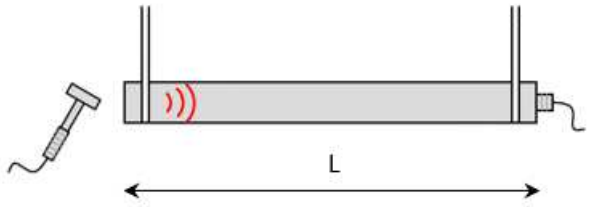

Figure 2-5 Representation of resonance method (direct longitudinal measurement)

$$c_L = 2f_0L \quad \text{(Eq. 2-5)}$$

$$MOE_{dyn} = \rho \cdot c_L^2 \quad \text{(Eq. 2-6)}$$

If it weren't for the limitation about the boundary condition, the resonant method constitutes a flexible technique since the measurement can be performed either in the longitudinal direction or in the transverse direction and the recording can be done either using vibration sensors (accelerometers, [30] and [31]) or acoustic sensors (microphones, [34] and [35]).

2.5.3 ACOUSTIC TOMOGRAPHY

Type	NDT, sonic/ultrasonic, vibration-based, time domain	
Measured parameter	Time	
Estimated parameter	Map of velocity*	
Information	Qualitative	
	Local	
Detection of	Natural defects	-
	Moisture	-
	Decay	Yes
	Damage	Yes
	Hidden internal details	Limited

* Influenced by local density values (e.g., wood species, growth rate, etc.) and local moisture content values. Calibration required.

Based on multiple time-of-flight measurements (Figure 2-6) the acoustic tomography technique ([15], [16], [36] and [37]) allows for the mapping of the stress wave velocity inside a timber element cross section thanks to post-processing of the collected data with specific algorithms. Either sonic or ultrasonic wave can be used for the assessment based on the type of input source used while for the receiving sensors vibration-based

devices are used (i.e. accelerometers). This method can be used to evaluate either structural timber element or standing trees and logs; a possible limitation for its application on timber structures may be that best results are obtained when access from all sides of the inspected element is guaranteed, which is not always the case for on-site assessment (e.g. timber joists of a composite floor, etc.).

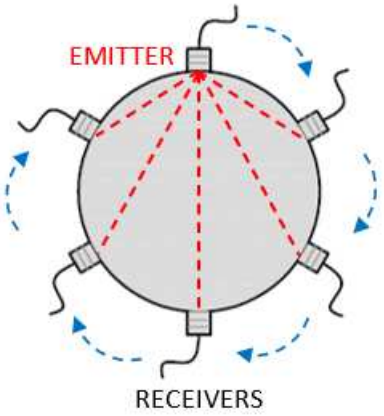

Figure 2-6 Scheme of an acoustic tomography measurement on a round cross section (e.g. tree trunk)

However, the method has been proven to be effective on detecting and sizing internal decay zones of standing trees during on-field assessment as confirmed by the resistance drilling SDT method [36]. The clarity of the tomography results can then be improved by considering the anisotropic properties of timber material in the post-processing algorithm facilitating the interpretation of the results by the assessment operator [37].

2.5.4 ULTRASONIC ECHO

Type	NDT, ultrasonic, vibration-based, time domain	
Measured parameter	Time*	
Estimated parameter	Geometric property (depth)	
Information	Qualitative	
	Local	
Detection of	Natural defects	-
	Moisture	-
	Decay	Limited
	Damage	Limited

	Hidden internal details	Limited

* Influenced by local density values (e.g., wood species, growth rate, etc.) and local moisture content values. Calibration required.

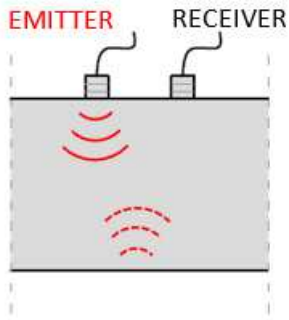

Figure 2-7 Representation of an ultrasonic echo measurement

The ultrasonic echo method ([15], [16], [38] and [39]), as the name suggest, is based on the reflection of an emitted stress wave on the opposite side of the examined element (back wall echo). Usually, frequency in the range of 50 kHz (i.e. ultrasonic) are used as compromise between sufficient resolution of the results and minimal attenuation over distance of the signal. Knowing the stress wave velocity (from previous time of flight measurement or assuming a mean value from data found in literature) one can estimate the depth where the acoustic signal rebounded from the returning stress wave time. If this calculated depth is close to the real dimension of the element and the signal is clear, the timber material can be considered as sound and undamaged. Any area where the signal is weak/vanishing or where the stress wave is reflected from shorter distance (with respect to the whole depth) should be investigated in detail as possible location of damage or decay.

2.5.5 MODAL ANALYSIS

Type	NDT, sonic, vibration-based, frequency domain	
Measured parameter	Frequency Response Function (FRF)	
Estimated parameter	Modal features	
Information	Qualitative	
	Global	
Detection of	Natural defects	Limited
	Moisture	-

	Decay	Limited
	Damage	Limited
	Hidden internal details	-

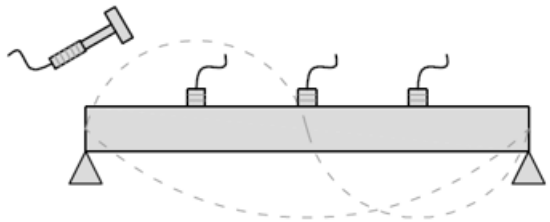

Figure 2-8 Representation of a single-input-multi-output experimental modal analysis measurement

In the group of the stress-wave based assessment methods a certainly attractive technique is the Experimental Modal Analysis (EMA) technique which allows to kill two birds with one stone. Besides of providing data usable to assess the timber element condition, the acceleration measurements can be used to investigate the dynamic properties and the vibration performance of the inspected element to check the satisfaction of the target serviceability requirements as defined in the standards (e.g. vibrations limitation of timber floors). The EMA is a powerful tool to measure and comprehend the dynamic behaviour of every type of structure, it is used in several engineering fields ranging from the automotive and electronic industry to the analysis of large civil structures such as bridges or multi-stories buildings. A thorough description of the principles of the EMA and its application is reported in Chapter 3 Theoretical basis of wave propagation and structural vibration.

Based on the original work of Kim and Stubbs [40], a modal-based damage-detection method for timber beam elements was developed in the early 2000s [41]. This method is known in literature as the Damage Index (DI) method and is based on measuring experimentally the modal strain energy of the inspected element and evaluating its variation from a baseline undamaged model (numerical or analytical). The modal strain energy of a rectangular cross-section timber beam for the i-th mode is defined as:

$$U_i = \frac{1}{2}\int_0^L E(x)I[\Phi_i''(x)]^2 dx \qquad \text{(Eq. 2-7)}$$

Where $E(x)$ represents the distribution of the modulus of elasticity along the beam axis, I is the second moment of area of the cross section and $\Phi_i''(x)$ is the second derivative (i.e. curvature) of the i-th mode shape measured at the x coordinate (for the

experimentally derived data Shannon's sampling theory [41] is used to derive new mode shape vectors by interpolation increasing the spatial resolution of the results, physically limited to the number of sensors used for the measurement). Discretizing the beam into *j* elements, the modal strain energy for the i-th mode of the single j-th element can be written as:

$$U_{ij} = \frac{(EI)_j}{2} \int_j [\Phi_i''(x)]^2 dx \qquad \text{(Eq. 2-8)}$$

With the integral applied only to the j-th element and the modulus of elasticity assumed constant over its length. The fraction of modal strain energy contained in the j-th element is expressed as:

$$F_{ij} = \frac{U_{ij}}{U_i} \qquad \text{(Eq. 2-9)}$$

This fraction is clearly comprised between 0 and 1 for every j-th element. Now, defining the damaged state of the beam with the apex * and the undamaged state without the apex, a damage indicator for the j-th element and the i-th mode can be defined as:

$$\beta_{ij} = \frac{1 + F_{ij}^*}{1 + F_{ij}} \qquad \text{(Eq. 2-10)}$$

Deriving the expression as a function of the mode shape curvatures:

$$\beta_{ij} = \frac{\left\{\int_j \left[\Phi_i''^*(x)\right]^2 dx + \int_0^L \left[\Phi_i''^*(x)\right]^2 dx\right\} \cdot \int_0^L [\Phi_i''(x)]^2 dx}{\left\{\int_j \left[\Phi_i''(x)\right]^2 dx + \int_0^L \left[\Phi_i''(x)\right]^2 dx\right\} \cdot \int_0^L \left[\Phi_i''^*(x)\right]^2 dx} \qquad \text{(Eq. 2-11)}$$

To account for all the available modes a summation is applied on both the numerator and denominator obtaining the damage indicator β_j for a single j-th element. To improve the "readability" of the results, the damage indicator values β_j are assumed to be random variables and are transformed in a standard normal space:

$$Z_j = \frac{\beta_j - \mu_{\beta j}}{\sigma_{\beta j}} \qquad \text{(Eq. 2-12)}$$

Where $\mu_{\beta j}$ represents the mean of the β_j values and $\sigma_{\beta j}$ the standard deviation of the β_j values. A threshold value for the Z_j variable is then selected judgementally to establish if damage is present in correspondence of the j-th element. The method has been proven to be effective in detect damage applied to timber beams in the form of reduction of cross-section [42]; some limitations of the method are that it is prone to false-positive locations of damage and that because is based on the evaluation of mode

shape curvatures it gives reliable results only when significant flexural vibration can be excited and measured. The first limitation is not a big deal since few false-positive damage locations can be considered acceptable for a global assessment method which is then coupled with more localized techniques (e.g. resistance drilling) to check the actual presence of damage. The second limitation instead is more bounding since it means that the method is not appliable to elements with low slenderness value or in the proximity of the element supports.

Other similar methods are present in literature based on the comparison of a sound/undamaged model of the tested element and its experimental measures. Hu and Afzal [43] used a damage indicator based on the discrete Laplacian transform of a parameter representing the difference of the mode shape coordinates (assumed as the amplitude peak of the FRF) for the damaged and undamaged element. Choi et al [44] proposed a new version of the damage index method, called Modified Damage Index (MDI) method, with a slightly different definition of the damage indicator (Eq. 2-13) and with the mode shape curvature normalised to the maximum value of the corresponding mode for each considered mode.

$$\beta_{ij} = \frac{\int_j \left[\Phi_i''^*(x)\right]^2 dx \cdot \int_0^L [\Phi_i''(x)]^2 dx}{\int_j \left[\Phi_i''(x)\right]^2 dx \cdot \int_0^L \left[\Phi_i''^*(x)\right]^2 dx} \qquad \text{(Eq. 2-13)}$$

The MDI method improves the ability of the DI method to detect damage especially in the case of multiple damage locations. Samali et al [45] applied the DI method extended to plate like structures (DI-P method) successfully detecting the presence of damage inflicted to the beam elements of a multi-joist timber-to-timber composite floor.

Kouroussis et al [46] proposed a method to assess the mechanical properties of a timber element based on a modal updating procedure of a numerical model using the data acquired during the EMA of the examined element in free-free boundary conditions. Santos et al [47] used the results of an EMA performed on multi-joist timber-to-timber composite floor to evaluate the presence of damage at the floor supports. The support damage was simulated in laboratory by completely removing the support at different joist ends location; an effective method to detect and locate the support damage was found to be the qualitative assessment of the floor mode shapes, particularly using higher mode shapes.

2.5.6 IMPACT TEST AND WAVEFORM ANALYSIS

Type	NDT, sonic, vibration-based, time domain/frequency domain
Measured parameter	Signal spectrum*

Estimated parameter	Spectral features	
Information	Qualitative	
	Local	
Detection of	Natural defects	Limited
	Moisture	-
	Decay	Limited
	Damage	Limited
	Hidden internal details	-

* Influenced by local density values (e.g., wood species, growth rate, etc.) and local moisture content values. Calibration required.

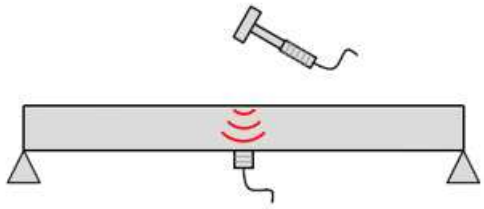

Figure 2-9 Representation of an acoustic impact test in the transverse direction

Similar to the time-of-flight method for the measurement setup, it was recently proposed a damage detection method based on transverse stress wave recordings and analysis of the registered signal waveform either in the time domain and in the frequency domain. The method was used to inspect either glued laminated timber elements [48] and harvested timber logs ([49] and [50]). The method is based on the study of the entire registered signal waveform either in the time domain or in the transformed frequency domain; to simplify the comparison of different measurements moment analysis (intended as statistical moment, ed.) is used to derive single parameters used as signal descriptors. For the signal time history, the time centroid T_C and the time energy centroid T_{EC} are used as signal descriptors:

$$T_C = \frac{\sum_{i=1}^{n} A_i t_i}{\sum_{i=1}^{n} A_i} \quad \text{(Eq. 2-14)}$$

$$T_{EC} = \frac{\sum_{i=1}^{n} A_i^2 t_i}{\sum_{i=1}^{n} A_i^2} \quad \text{(Eq. 2-15)}$$

Where n is the number of time samples, A_i is the amplitude of the signal at the time step t_i. For the signal spectrum, the spectral centroid S_C and the frequency energy centroid F_{EC} are used as signal descriptors:

$$S_C = \frac{\sum_{i=1}^{N} S_i f_i}{\sum_{i=1}^{N} S_i} \quad \text{(Eq. 2-16)}$$

$$F_{EC} = \frac{\sum_{i=1}^{N} S_i^2 f_i}{\sum_{i=1}^{N} S_i^2} \quad \text{(Eq. 2-17)}$$

Where N is the total number of frequencies in the spectrum, S_i is the amplitude of the spectrum in correspondence of the frequency f_i. In addition, the authors proposed the analysis of the frequency content of the signal over time (i.e. spectrogram analysis) by applying a Continuous Wavelet Transform (CWT). For a more detailed description of the analysis refers to [49] and [50], in synthesis CWT allows to obtain the main frequency components of the signal and the associated damping ratio. By experimental testing, the authors found a positive relationship between the presence of damage/decay and the time centroid/time energy centroid and the estimated signal damping ratios, namely for damaged/decayed element stress wave amplitude and energy is more delayed over time and the signal results also more attenuated with respect to sound material. As regards the frequency content instead it was found a negative relationship, with decayed material showing most of the energy content concentrated in the low frequency zone whereas signals recorded on sound material presented also high frequency components.

2.5.7 ACOUSTIC EMISSION TECHNIQUE

Type	NDT, sonic/ultrasonic, vibration-based/sound-based, time domain/frequency domain	
Measured parameter	Sound radiation	
Estimated parameter	Crack propagation/wood-boring insect activity	
Information	Qualitative	
	Local	
Detection of	Natural defects	-
	Moisture	-
	Decay	Limited
	Damage	Limited
	Hidden internal details	-

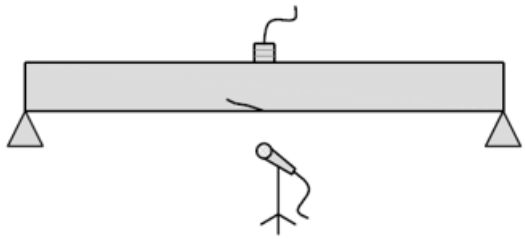

Figure 2-10 Representation of a crack propagation monitoring via acoustic emission technique

The acoustic emission technique ([17] and [51]) cannot be fully considered as an assessment method since the measured parameter (acoustic emission) is not intentionally generated by an operator but it is "naturally" produced by the timber element. Acoustic emission is defined as a phenomenon whereby transient elastic waves are generated by rapid release of energy from localised sources within a material [51]. These elastic waves can have a wide range of frequencies varying from sonic to ultrasonic values (indicatively 10 ÷200 kHz) and for this reason piezoelectric sensors are normally used for the measurement. Due to the nature of acoustic emission, this technique has the potential to be integrated in passive monitoring systems [17] for the structural health assessment of timber elements. Research in literature has shown that the cumulated number of AE events (i.e. number of recordings above a certain amplitude threshold value) is linked to the reaching of the timber elements elastic limit due to the propagation of cracks inside the material ([51], [52] and [53]).

Moreover, the setup used to measure the acoustic emission generated from crack propagation can be adapted to identify also the activity of wood-boring insects inside existing timber elements ([54] and [55]).

2.6 REFERENCES

[1] M. Piazza, R. Tomasi and R. Modena "Strutture in legno: Materiale, calcolo e progetto secondo le nuove normative europee" Milano: Hoepli Editore, 2005. (In italian)

[2] International Organization for Standardization (2018). ISO 9709:2018 (EN): Structural timber - Visual strength grading - Basic principles. ISO, Geneva, Switzerland.

[3] European Committee for Standardisation (2016). EN 338:2016: Structural timber -Strength classes. CEN, Brussels, Belgium.

[4] European Committee for Standardisation (2013). EN 14080:2013: Timber structures – Glued laminated timber and glued solid timber – Requirements. CEN, Brussels, Belgium.

[5] S. Franke, B. Franke and A. M. Harte "Failure modes and reinforcement techniques for timber beams - State of the art" *Construction and Building Materials*, vol. 97, pp. 2-13, 2015.
[6] P. Dietsch and S. Winter "Structural failure in large-span timber structures: A comprehensive analysis of 230 cases" *Structural Safety*, vol. 71, pp. 41-46, 2018.
[7] European Committee for Standardisation (2014). EN 1995-1-:2004+A2:2014: Eurocode 5 – Design of timber structures, Part 1-1, General - Common rules and rules for buildings. CEN, Brussels, Belgium.
[8] G. Cartwright, W. G. Campbell and F.H. Armstrong "The influence of fungal decay on the properties of timber I – The effect of progressive decay by Polyporus hispidus, Fr., on the strength of English ash (Fraxinus excelsior, L.)" *Proceeding of the Royal Society B - Biological Sciences*, vol. 120, no. 816, pp. 76-95, 1936.
[9] L. Nunes, J. L. Parracha, P. Faria, P. Palma, A. Mauricio and M. F. C. Pereira "Towards an assessment tool of anobiid damage of pine timer structures" *Proceedings of the International Association of Bridge and Structural Engineering (IABSE) Symposium*, Guimarães, Portugal, 2019.
[10] H. Cruz, D. Yeomans, E. Tsakanika, N. Macchioni, A. Jorissen, M. Touza, M. Mannucci and P. B. Lourenço "Guidelines for on-site assessment of historic timber structures" *International Journal of Architectural Heritage*, vol. 9, no. 3, pp. 277-289, 2015.
[11] M. Riggio, D. D'Ayala, M. A. Parisi and C. Tardini "Assessment of heritage timber structures: Review of standards, guidelines and procedures" *Journal of Cultural Heritage*, vol. 31, pp. 220-235, 2018.
[12] P. Dietsch and H. Kreuzinger "Guideline on the assessment of timber structures: Summary" *Engineering Structures*, vol. 33, pp. 2983-2986, 2011.
[13] M. Riggio, R. W. Anthony, F. Augelli, B. Kasal, T. Lechner, W. Muller and T. Tannert "In situ assessment of structural timber using non-destructive techniques" *Materials and Structures*, vol. 47, pp. 749-766, 2014.
[14] T. Tannert, R. W. Anthony, B. Kasal, M. Kloiber, M. Piazza, M. Riggio, F. Rinn, R. Widmann and N. Yamaguchi "In situ assessment of structural timber using semi-destructive techniques" *Materials and Structures*, vol. 47, pp. 767-785, 2014.
[15] U. Dackermann, K. Crews, B. Kasal, J. Li, M. Riggio, F. Rinn and T. Tannert "In situ assessment of structural timber using stress-wave measurements" *Materials and Structures*, vol. 47, pp. 787-803, 2014.
[16] K. J. Vössing and E. Niederleithinger "Nondestructive assessment and imaging methods for internal inspection of timber" *Holzforschung*, vol. 72, no. 6, pp. 467-476, 2018.
[17] P. Palma and R. Steiger "Structural health monitoring of timber structures – Review of available methods and case studies" *Construction and Building Materials*, vol. 248, 2020.

[18] European Committee for Standardisation (2002). EN 13813-1: Moisture content of a piece of sawn timber. Determination by oven dry method. CEN, Brussels, Belgium.
[19] European Committee for Standardisation (2002). EN 13813-2: Moisture content of a piece of sawn timber - Part 2: Estimation by electrical resistance method. CEN, Brussels, Belgium.
[20] European Committee for Standardisation (2005). EN 13183-3: Moisture content of a piece of sawn timber – Part 3: Estimation by capacitance method. CEN, Brussels, Belgium.
[21] R. J. Ross, R. F. Pellerin, N. Volny, W. W. Salsig and R. H. Falk "Inspection of timber bridges using stress wave timing non-destructive evaluation tools – A guide for use and interpretation" Department of Agriculture, Forest Service, Forest Products Laboratory, Madison (WI), US, Tech. Rep. FPL-GTR-114, 1999.
[22] X. Wang, R. J. Ross and P. Carter "Acoustic evaluation of wood quality in standing trees. Part 1. Acoustic wave behaviour" *Wood and Fiber Science*, vol. 39, no. 1, pp. 28-38, 2007.
[23] X. Wang "Acoustic measurements on trees and logs: a review and analysis" *Wood Science and Technology*, vol. 47, pp. 965-975, 2013.
[24] H. Xu, G. Xu, L. Wang and L. Yu "Propagation behaviour of acoustic wave in wood" *Journal of Forestry Research*, vol. 25, no. 3, pp. 671-676, 2014.
[25] M. Yamasaki, C. Tsuzuki, Y. Sasaki and Y. Onishi "Influence of moisture content on estimating Young's modulus of full-scale timber using stress wave velocity" *Journal of Wood Sciences*, vol. 63, pp. 225-235, 2017.
[26] D. F. Llana, G. Íñiguez-González, R. D. Martínez and F. Arriaga "Influence of timber moisture content on wave time-of-flight and longitudinal natural frequency in coniferous species for different instruments" *Holzforschung*, vol. 72, no. 5, pp. 405-411, 2018.
[27] C. C. Gerhards "Effect of knots on stress waves in lumber" Department of Agriculture, Forest Service, Forest Products Laboratory, Madison (WI), US, Res. Pap. FPL-384, 1982.
[28] J. Qin, X. Liu, K. Van Den Abeele and G. Cui "The study of wood knots using acoustic non-destructive testing methods" *Ultrasonics*, vol. 88, pp. 43-50, 2018.
[29] M. J. Frampton "Acoustic studies for the non-destructive testing of wood" Ph.D. Thesis, University of Canterbury, Christchurch, New Zealand, 2019.
[30] J. B. Barré, F. Bourrier, L. Brancheriau, D. Bertrand and F. Rey "Effects of fungal decay on elasticity and damping of small-diameter silver fir logs assessed by the transverse vibration resonant method" *Wood Science Technology*, vol. 52, pp. 403-420, 2018.
[31] F. Xu, X. Wang, E. Thomas, Y. Liu, B. K. Brashaw and R. J. Ross "Defect detection and quality assessment of hardwood logs: Part 1 – Acoustic impact test and wavelet analysis" *Wood and Fiber Science*, vol. 50, no. 3, pp. 291-309, 2018.

[32] L. Brancheriau and H. Baillères "Use of the partial least squares method with acoustic vibration spectra as a new grading technique for structural timber" *Holzforschung*, vol. 57, pp. 644-652, 2003.
[33] F. Arriaga, J. Monton, E. Segues and G. Íñiguez-Gonzalez "Determination of the mechanical properties of radiata pine timber by means of longitudinal and transverse vibration methods" *Holzforschung*, vol. 68, no. 3, pp. 299-305.
[34] N. Sobue "Instantaneous measurements of elastic constants by analysis of the tap tone of wood" *Journal of the Japan Wood Research Society*, vol. 32, no. 4, pp. 274-279, 1986.
[35] D. Ouis "Vibrational and acoustical experiments on logs of spruce" *Wood Science and Technology*, vol. 33, pp. 151-184, 1999.
[36] X. Wu, G. Li, Z. Jiao and X. Wang "Reliability of acoustic tomography and ground-penetrating radar for tree decay detection" *Applications in Plant Sciences*, vol. 6, no. 10, 2018.
[37] L. Panosso Perlin, R. Caldas de Andrade Pinto and A. do Valle "Ultrasonic tomography in wood with anisotropy consideration" *Construction and Building Materials*, vol. 229, 2019.
[38] M. Krause, K. Mayer and U. Effner "Ultrasonic echo methods for structural timber" *Proceedings of the COST Workshop – Highly performing timber structures: Reliability, assessment, monitoring and strengthening*, pp. 77-82, Biel, Switzerland, 2014.
[39] M. Krause, U. Dackermann and J. Li "Elastic wave modes for the assessment of structural timber: ultrasonic echo for building elements and guided waves for pole and pile structures" *Journal of Civil Structural Health Monitoring*, vol. 5, pp. 221-249, 2014.
[40] J. T. Kim and N. Stubbs "Model-uncertainty impact and damage-detection accuracy in plate girder" *Journal of Structural Engineering,* vol. 121, no. 10, pp. 1409-1417, 1995.
[41] S. T. Peterson, D. I. McLean, M. D. Symans, D. G. Pollock, W.F. Cofer, R.N. Emerson and K. J. Fridley "Application of dynamic system identification to timber beams. I" *Journal of Structural Engineering*, vol. 127, no. 4, pp. 418-425, 2001.
[42] S. T. Peterson, D. I. McLean, M. D. Symans, D. G. Pollock, W.F. Cofer, R. N. Emerson and K. J. Fridley "Application of dynamic system identification to timber beams. II" Journal of Structural Engineering, vol. 127, no. 4, pp. 426-432, 2001.
[43] C. Hu and M. T. Afzal "A statistical algorithm for comparing mode shapes of vibration testing before and after damage in timbers" *Journal of Wood Science*, vol. 52, pp. 348-352, 2006.
[44] F. C. Choi, J. Li, B. Samali and K. Crews "Application of modal-based damage-detection method to locate and evaluate damage in timber beams" *Journal of Wood Science*, vol. 53, pp. 394-400, 2007.

[45] B. Samali, J. Li, F. C. Choi and K. Crews "Application of the damage index method for plate-like structures to timber bridges" *Structural Control and Health Monitoring*, vol. 17, pp. 849-871, 2010.
[46] G. Kouroussis, L. Ben Fekih and T. Descamps "Assessment of timber element mechanical properties using experimental modal analysis" *Construction and Building Materials*, vol. 134, pp. 254-261, 2017.
[47] P. G. Santos, L. Bernardo, A. Dias, L. Godinho and A. C. Pereira "Damage detection on timber floors' supports through dynamic analysis" *International Journal of Architectural Heritage*, vol. 11, no. 8, pp. 1133-1142, 2017.
[48] F. Xu, X. Wang, M. Teder and Y. Liu "Acoustic impact testing and waveform analysis for damage detection in glued laminated timber" *Holzforschung*, vol. 71, no. 10, pp. 197-208, 2017.
[49] F. Xu, X. Wang, E. Thomas, Y. Liu, B. K. Brashaw and R. J. Ross "Defect detection and quality assessment of hardwood logs: Part 1 – Acoustic impact test and wavelet analysis" *Wood and Fiber Science*, vol. 50, no. 3, pp. 291-309, 2018.
[50] F. Xu, Y. Liu, X. Wang, B. K. Brashaw, L. A. Yeary and R. J. Ross "Assessing internal soundness of hardwood logs through acoustic impact test and waveform analysis" *Wood Science and Technology*, vol. 53, pp. 1111-1134, 2019.
[51] S. Kawamoto and R. S. Williams "Acoustic emission and Acousto-Ultrasonic techniques for wood and wood-based composites" Department of Agriculture, Forest Service, Forest Products Laboratory, Madison (WI), US, Tech. Rep. FPL-GTR-134, 2002.
[52] M. Diakhate, E. Bastidas-Arteaga, R. Moutou Pitti and F. Schoefs "Cluster analysis of acoustic emission activity within wood material: Towards a real-time monitoring of crack tip propagation" *Engineering Fracture Mechanics*, vol. 180, pp. 254-267, 2017.
[53] H. S. Sousa, J. S. Machado, J. M. Branco and P. B. Lourenço "Detection of shear crack propagation on timber elements using acoustic emission tests" *Proceedings of the International Symposium on Structural Health Monitoring and Nondestructive Testing*, Saarbruecken, Germany, 2018.
[54] R. L. Lemaster, F. C. Beall and V. R. Lewis "Detection of termites with acoustic emission" *Forest Product Journal*, vol. 47, no. 2, pp. 75-79, 1997.
[55] J. G. M. Creemers "Use of Acoustic Emission (AE) to detect the activity of common European dry-woodboring insects: Practical considerations" *Proceedings of the International Symposium of Non-Destructive Testing in Civil Engineering*, Berlin, Germany, 2015.

This page intentionally left blank.

3 THEORETICAL BASIS OF WAVE PROPAGATION AND STRUCTURAL VIBRATION

3.1 BASICS OF WAVE PROPAGATION ANALYSIS

A thorough study on wave propagation in the field of vibro-acoustic is reported in the book "Sound and structural vibration – Radiation, transmission and response" [1]. The following section refers mainly to this work, reporting a summary of the information needed for the rest of the thesis.

The general definition for wave is transport of a disturbance (i.e. perturbation from a stable equilibrium position) or energy through space with not associated (absolute) motion of the medium occupying the space. Basic physical phenomena to which waves are subjected are:

- *Reflection*: change of wave direction from hitting a reflective surface.
- *Refraction*: change of wave direction from entering a new medium.
- *Diffraction*: wave circular spreading from entering small openings or wave bending around small obstacles (dimension comparable to the wavelength of the wave).
- *Interference*: superposition of two distinct waves encountering with each other.
- *Dispersion*: dependence of wave phase velocity from wave frequency (as will be illustrated in more detail later).

Waves can be categorised in two main groups:

- *Stationary waves* (or standing waves): are waves that remains in a constant position in space. This may be due to two reasons: the medium is moving in the opposite direction to the wave or two waves are moving in opposite directions forming a stationary interference pattern.

- *Travelling waves* (or propagating waves): are waves that vary both in time and space.

Regarding the wave motion another classification can be defined:

- *Longitudinal waves*: are waves whose disturbance moves parallel to the wave direction (e.g. sound waves in fluids or compression waves in solids).
- *Transverse waves*: are waves whose disturbance moves perpendicular to the direction of propagation (e.g. shear waves in solids).

To describe the nature of wave motion and the mathematical relationship between variations in time and space is convenient to adopt the complex exponential representation because it eases the operations of derivation and integration found in the governing (differential) equations of wave motion and it allows a simpler and more neat definition of the Fourier Transform to analyse the frequency content of a certain wave.

Let us assume now a simple harmonic variation in time, this can be represented in a trigonometric form as:

$$g(t) = A\cos(\omega t + \Phi) \qquad \text{(Eq. 3-1)}$$

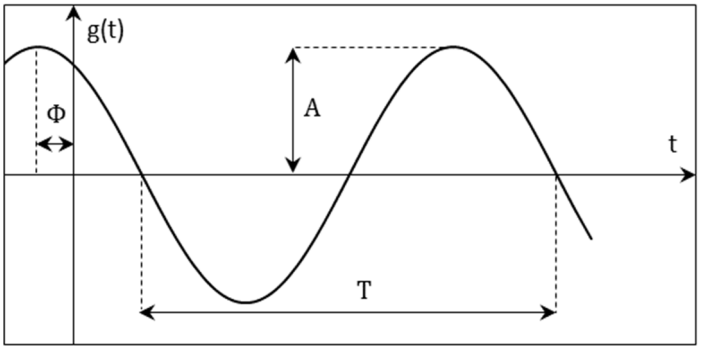

Figure 3-1 Simple harmonic variation in time

Where:

- A is the amplitude.
- Φ is the initial phase.
- T is the period.
- $f = 1/T$ is the frequency.
- $\omega = 2\pi/T$ is the angular frequency.

Exploiting the Euler's formula this can be represented also in a complex exponential form:

$$g(t) = Re\{Be^{i\omega t}\} \quad \text{(Eq. 3-2)}$$

Where:

- B is the complex amplitude.
- i is the imaginary unit ($i^2 = -1$).
- $Re\{...\}$ stands for the real part of the complex number in parentheses (often in wave analysis this is omitted and taking only the real component is implied).

The complex amplitude by its own can be represented in the three different complex number forms: cartesian or algebraic (Eq. 3-3), polar trigonometric (Eq. 3-4) and polar exponential (Eq. 3-5):

$$B = a + ib \quad \text{(Eq. 3-3)}$$

$$B = A(\cos\Phi + i\sin\Phi) \quad \text{(Eq. 3-4)}$$

$$B = Ae^{i\Phi} \quad \text{(Eq. 3-5)}$$

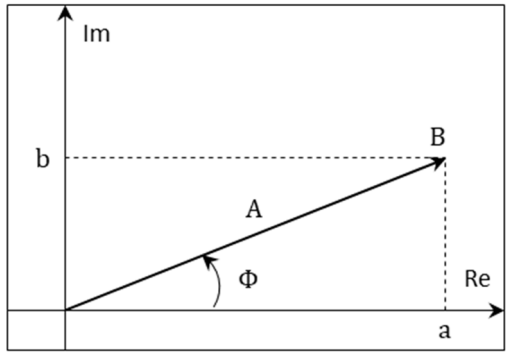

Figure 3-2 Representation of the complex amplitude in the Argand-Gauss plane

The real amplitude A represents the module of the complex amplitude vector, whereas the initial phase Φ represents the orientation of the complex amplitude vector in the complex plane (Argand-Gauss plane) at time equal to zero. Conversion between forms can be performed by using the following relations:

$$A = \sqrt{a^2 + b^2} \qquad \Phi = arctan\left(\frac{b}{a}\right) \quad \text{(Eq. 3-6)}$$

$$a = A\cos\Phi \qquad b = A\sin\Phi \quad \text{(Eq. 3-7)}$$

A simple harmonic variation in time can be defined in the complex plane as the projection on the real axis of a complex rotating vector $Be^{i\omega t}$ (also termed as *phasor*) rotating with angular speed ω.

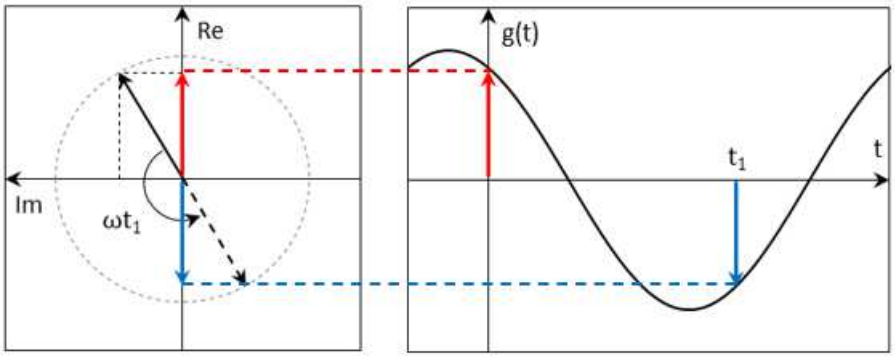

Figure 3-3 Phasor representation of a simple harmonic variation in time

Thus far it was considered only a simple harmonic variation in time (i.e. stationary wave). If now we consider also the possibility of the wave to propagate in one space dimension x, we will see that the harmonicity of the wave variation in time reflects also in space with the wave propagating away from the origin with a definite speed c following a sinusoidal spatial disturbance pattern.

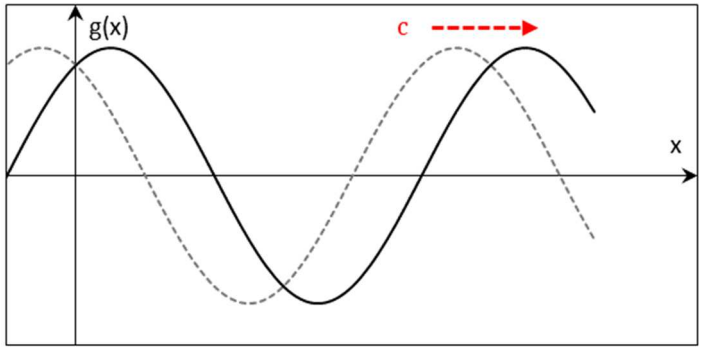

Figure 3-4 One dimensional travelling wave with propagation speed equal to c

Assuming a linear response for the medium carrying the wave, the frequency of the propagating wave will be the same at any point in space to that of the generator. The disturbance at the point of generation can be written as:

$$g(x = 0, t) = Re\{Be^{i\omega t}\} \qquad \text{(Eq. 3-8)}$$

Let consider now the disturbance at a distance x_1 from the point of generation, its phase will lag the phase of the generator by an angle equal to the product of the angular frequency ω and the time taken for the wave to travel the corresponding distance ($t_1 = x_1/c$):

$$g(x_1, t) = Re\left\{Be^{i\left(\omega t - \frac{\omega x_1}{c}\right)}\right\} \quad \text{(Eq. 3-9)}$$

The propagation speed c is also called the *phase speed* c_{ph}. The reason for that definition can be clarified using a phasor representation (Figure 3-5) to plot the combined effect of space and time variations:

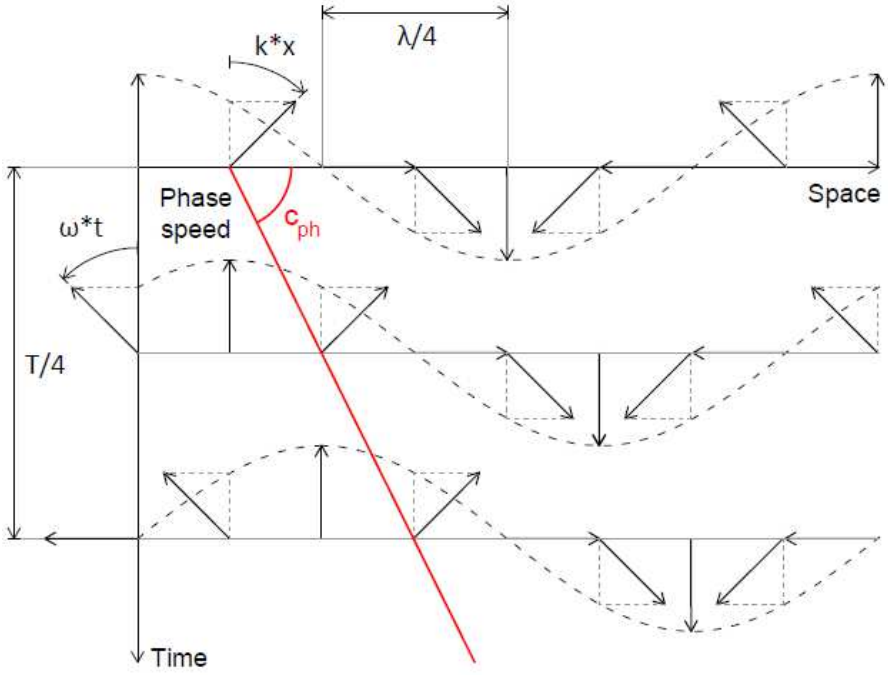

Figure 3-5 Phasor representation of sinusoidal variations in time and space (reworked from [1])

The angle c_{ph} in the space-time graph, for which the phasor orientation remains the same, is called *phase speed* of the wave because an observer travelling at this speed in the direction of wave propagation sees no change in phase.

The quantity ω/c_{ph} in (Eq. 3-9) is termed *angular wavenumber* (also known as angular spatial frequency) k and represents the phase change per unit distance such as the angular time frequency represents the phase change per unit time:

$$\omega = \frac{2\pi}{T} = [Hz] \quad \text{(Eq. 3-10)}$$

$$k = \frac{\omega}{c_{ph}} = \frac{2\pi}{\lambda} = \left[\frac{1}{m}\right] \quad \text{(Eq. 3-11)}$$

The analogy for wave in space and time is reported in Table 3-1 and Figure 3-6:

Table 3-1 Analogy for wave properties in space and time

Domain	Period	Frequency	Fourier Transform
Space	Temporal period T	Angular frequency ω	Time Fourier Transform
Time	Wavelength λ	Angular wavenumber k	Wavenumber Transform

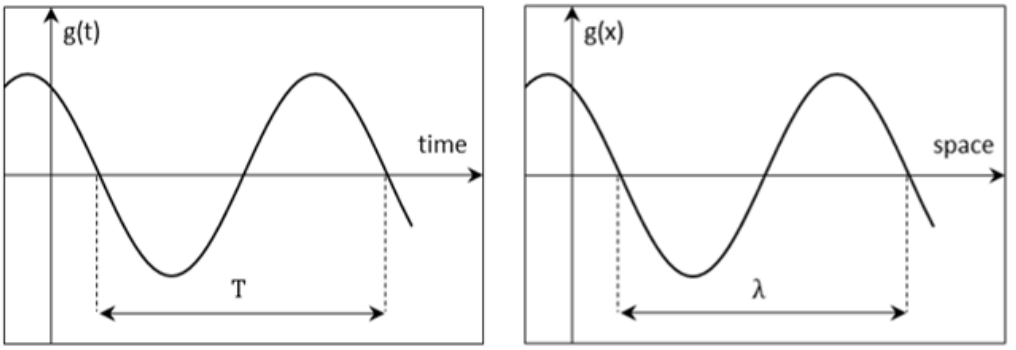

Figure 3-6 Graphical representation of the analogy for wave properties in space and time

Differently from the angular frequency ω, the angular wavenumber k can assume either positive and negative values indicating waves propagating in the negative and positive x direction respectively (Figure 3-7).

$$g^{+}(x,t) = Re\{Be^{i(\omega t - kx)}\} \quad \text{(Eq. 3-12)}$$

$$g^{-}(x,t) = Re\{Be^{i(\omega t + kx)}\} \quad \text{(Eq. 3-13)}$$

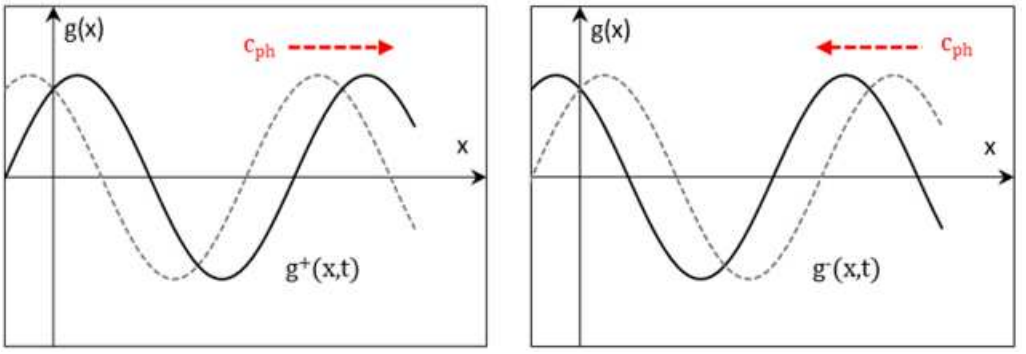

Figure 3-7 Graphical representation of travelling waves with positive and negative wavenumbers

The form of the relation which links the angular wavenumber k and the angular frequency ω is termed the *dispersion relation*:

$$k = f(\omega) = \frac{\omega}{c_{ph}(\omega)} \qquad \text{(Eq. 3-14)}$$

This relation indicates whether a wave will propagate through a medium unaltered in its basic spatial pattern: if this is true the wave is said to be non-dispersive. That happens only if the relation between k and ω is linear (i.e. constant phase speed c_{ph}, independent from ω). The dispersion relation can be a property of the wave itself (e.g. sound waves are non-dispersive, bending waves in solids are dispersive) as well as of the type of wave-bearing medium. It should be noted that the non-dispersive nature of a wave is related only to the spatial form properties of the wave, whereas the amplitude of the wave may decrease as the distance from the generation increases when the wave propagates through space.

The dispersion curves are of great importance for studying the wave interaction in coupled media, such as in *vibro-acoustic* problems, because the interaction is much stronger at the frequency where the dispersion curves of the two media intersect with each other. In addition, the dispersion curves also indicate the speed at which energy is transported. This speed is called *group speed* c_g and is defined by (Eq. 3-15).

$$c_g = \frac{\partial \omega}{\partial k} \qquad \text{(Eq. 3-15)}$$

$$c_{ph} = \frac{\omega}{k} \qquad \text{(Eq. 3-16)}$$

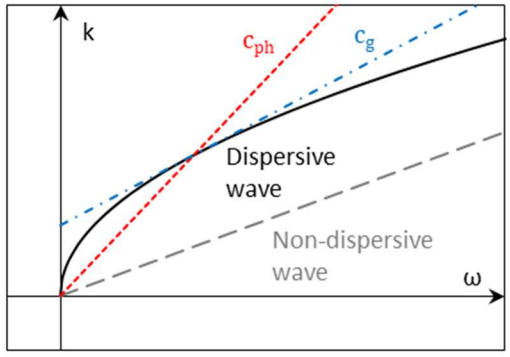

Figure 3-8 Graphical representation of phase speed and group speed for a dispersive wave

As can be noted by the example graph of Figure 3-8 for non-dispersive wave (linear relation between k and ω) phase speed c_{ph} (secant value) and group speed c_g (derivative

value) are equals. In a more didascalic way, group speed can be seen as the propagation speed of the spatial form of a wave packet (i.e. envelope shape) and phase speed as the propagation speed of the carrier wave within the envelope (Figure 3-9).

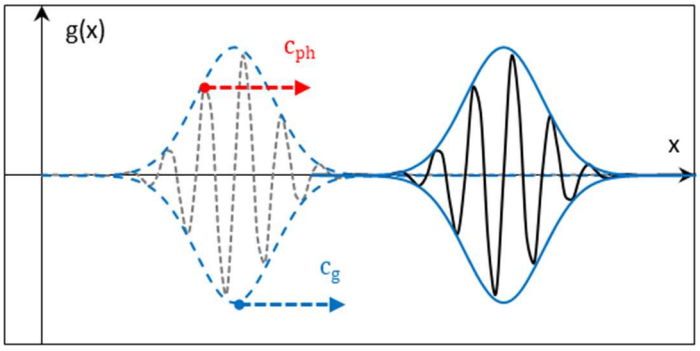

Figure 3-9 Graphical representation of phase and group speed of a sinusoidal pulse

3.1.1 SOUND WAVES IN FLUIDS

From the linearised forms of continuity equation (conservation of mass):

$$\frac{\partial \rho}{\partial t} + \rho_0 \left(\frac{\partial v_x}{\partial x} + \frac{\partial v_y}{\partial x} + \frac{\partial v_z}{\partial z} \right) = 0 \qquad \text{(Eq. 3-17)}$$

And momentum equations (Euler's force equation):

$$\frac{\partial \rho}{\partial x} + \rho_0 \frac{\partial v_x}{\partial t} = 0 \qquad \text{(Eq. 3-18)}$$

$$\frac{\partial \rho}{\partial y} + \rho_0 \frac{\partial v_y}{\partial t} = 0 \qquad \text{(Eq. 3-19)}$$

$$\frac{\partial \rho}{\partial z} + \rho_0 \frac{\partial v_z}{\partial t} = 0 \qquad \text{(Eq. 3-20)}$$

It can be derived the *wave equation*, governing the propagation of sound waves through a homogeneous, inviscid, isotropic, compressible fluid in three dimensions:

$$\nabla^2 p = \frac{1}{c^2} \frac{\partial^2 p}{\partial t^2} \qquad \text{(Eq. 3-21)}$$

Where ρ_0 is the mean fluid density, v_x, v_y and v_z are the particle velocities and ∇^2 is the Laplace operator ($\nabla^2 f = \sum_{i=1}^{3} \partial^2 f / \partial x_i^2$). The quantity p is the *acoustic pressure*, intended as variation of pressure Δp about the fluid equilibrium pressure p_0 and c

represents the frequency independent speed of sound in the fluid (sound waves in fluid are non-dispersive):

$$c = \sqrt{\frac{Bp_0}{\rho_0}} \qquad \text{(Eq. 3-22)}$$

Where B is the adiabatic bulk modulus and p_0 is the fluid mean pressure. Considering the planar version of the wave equation where the only variations in space can happen in two orthogonal directions (Eq. 3-21) becomes:

$$\frac{\partial^2 p}{\partial x^2} + \frac{\partial^2 p}{\partial y^2} = \frac{1}{c^2}\frac{\partial^2 p}{\partial t^2} \qquad \text{(Eq. 3-23)}$$

Assuming a simple harmonic time dependence this may be rewritten as:

$$p(x, y, t) = p(x, y)e^{i\omega t} \qquad \text{(Eq. 3-24)}$$

$$\frac{\partial^2 p}{\partial x^2} + \frac{\partial^2 p}{\partial y^2} = -k^2 p \qquad \text{(Eq. 3-25)}$$

(Eq. 3-25) is known as two-dimensional *Helmholtz equation*. Assuming also a harmonic variation for the propagation in space the solution to the equation becomes:

$$p(x, y, t) = \tilde{p}e^{-ik_x x - ik_y y}e^{i\omega t} \qquad \text{(Eq. 3-26)}$$

$$k_x^2 + k_y^2 = k^2 \qquad \text{(Eq. 3-27)}$$

Therefore, "*only a certain combination of* k_x *and* k_y *will satisfy the wave equation at any specific frequency ω and the direction of wave propagation is indicated by the wavenumber vector k*" [1].

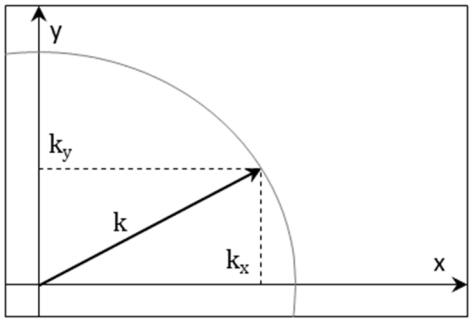

Figure 3-10 Two dimensional wavenumber vector and components [1]

In terms of sound radiation by vibrating structure is useful to refer to the linearised momentum equations because they can be seen as *fluid boundary conditions* relating

the orthogonal movement of fluid particles (acceleration) near the interface to variations in the global fluid pressure gradient. Assuming again a simple harmonic variation in time for the particle velocities, the relation between pressure gradient and orthogonal acceleration reduces to a relation between pressure gradient and particle velocity:

$$v_y = \widetilde{v_y} e^{i\omega t} \quad \text{(Eq. 3-28)}$$

$$\left.\frac{\partial \rho}{\partial y}\right|_{y=0} = -i\omega\rho_0 v_y\big|_{y=0} \quad \text{(Eq. 3-29)}$$

In vibro-acoustic sound radiation is commonly measured in terms of radiated sound power. This is defined as the integral over the entire structure surface of the product of local surface pressure and normal surface velocity:

$$W = \int_S p_{surface} \cdot v_\perp dS \quad \text{(Eq. 3-30)}$$

Given that acoustic disturbances radiated by all parts of the structure propagates to all the other parts, the local fluid boundary conditions are not sufficient to determine uniquely the relation between surface pressure and normal velocity. In theory, to obtain accurate results, one should know the normal velocity distribution over the whole surface in terms of phase and amplitude for all the interested frequencies.

3.1.2 LONGITUDINAL WAVES IN SOLIDS

For pure longitudinal waves the direction of propagation of the wave matches completely the direction of solid particles displacement. In theory this can happen only in an unbounded solid medium where the phenomenon known as *Poisson effect* (i.e. lateral strain due to longitudinal stress) is inhibited. In this case also the well-known Hooke's law ($\sigma_{xx} = E\varepsilon_{xx}$ where the elasticity constant E is defined as *Young modulus*) is no more valid and the relation between longitudinal stress σ_{xx} and longitudinal strain ε_{xx} becomes:

$$\sigma_{xx} = B\varepsilon_{xx} \quad \text{(Eq. 3-31)}$$

The solid *bulk modulus* B and the longitudinal strain ε_{xx} are defined as:

$$B = \frac{E(1-\nu)}{(1+\nu)(1-2\nu)} \quad \text{(Eq. 3-32)}$$

$$\varepsilon_{xx} = \frac{\partial \xi}{\partial x} \qquad \text{(Eq. 3-33)}$$

Where ν is the material Poisson's ratio and ξ is the solid particles displacement in the direction of the applied stress.

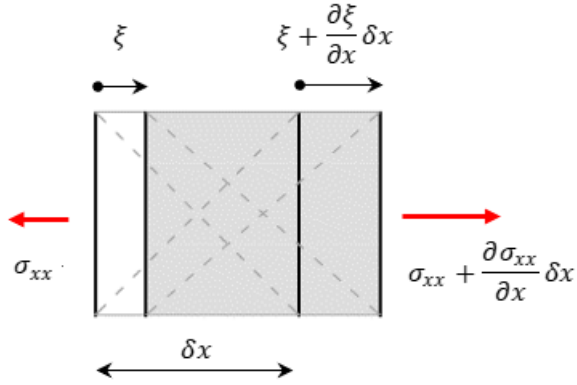

Figure 3-11 Displacements and stresses in longitudinal waves for an infinitesimal solid element [1]

$$\rho \delta x \frac{\partial^2 \xi}{\partial t^2} = \frac{\partial \sigma_{xx}}{\partial x} \delta x \qquad \text{(Eq. 3-34)}$$

Substituting the constitutive relation in the equation of motion (Eq. 3-34) the governing wave equation (Eq. 3-35) may be obtained:

$$\frac{\partial^2 \xi}{\partial x^2} = \left(\frac{\rho}{B}\right) \frac{\partial^2 \xi}{\partial t^2} \qquad \text{(Eq. 3-35)}$$

Where ρ is the solid mean density. This equation has the same form for the one-dimensional equation for sound wave in fluids. Hence, longitudinal waves in solids are non-dispersive and have phase speed equal to:

$$c_L = \sqrt{\frac{B}{\rho}} \qquad \text{(Eq. 3-36)}$$

3.1.3 QUASI-LONGITUDINAL WAVES IN SOLIDS

For finite solid elements, such as plates and beams, the presence of longitudinal stress will produce also associated lateral strains. For this reason, the wave motion is not purely longitudinal and the term "quasi-longitudinal" is used. The change of the

constitutive equation yields to different formulation for the wave phase speed. For thin plates:

$$\sigma_{xx} = \frac{E}{1-\nu^2}\varepsilon_{xx} \quad \text{(Eq. 3-37)}$$

$$\frac{\partial^2 \xi}{\partial x^2} = \frac{1}{c_L'}\frac{\partial^2 \xi}{\partial t^2} \quad \text{(Eq. 3-38)}$$

$$c_L' = \sqrt{\frac{E}{\rho(1-\nu^2)}} \quad \text{(Eq. 3-39)}$$

For beams:

$$\sigma_{xx} = E\varepsilon_{xx} \quad \text{(Eq. 3-40)}$$

$$\frac{\partial^2 \xi}{\partial x^2} = \frac{1}{c_L''}\frac{\partial^2 \xi}{\partial t^2} \quad \text{(Eq. 3-41)}$$

$$c_L'' = \sqrt{\frac{E}{\rho}} \quad \text{(Eq. 3-42)}$$

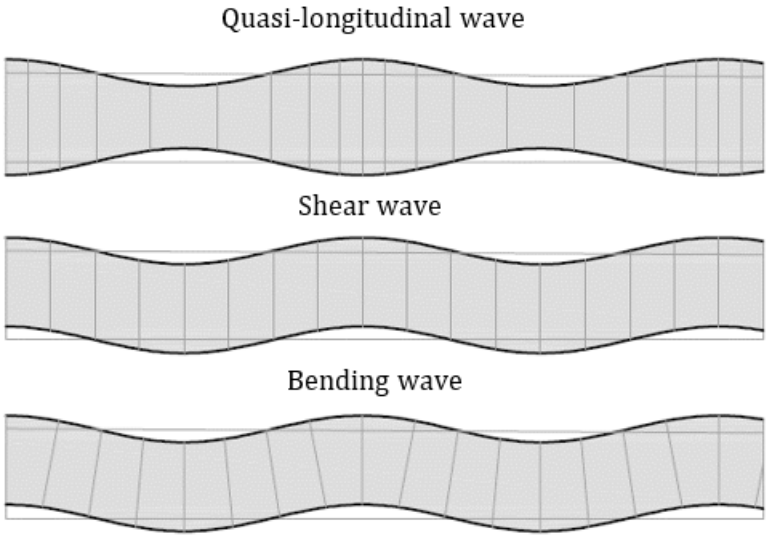

Figure 3-12 Transverse deformation pattern of wave in bounded solid media (i.e. beams or plates); for quasi-longitudinal wave transverse deformation exaggerated for clarity [1]

3.1.4 SHEAR WAVES AND TORSIONAL WAVES IN BEAMS

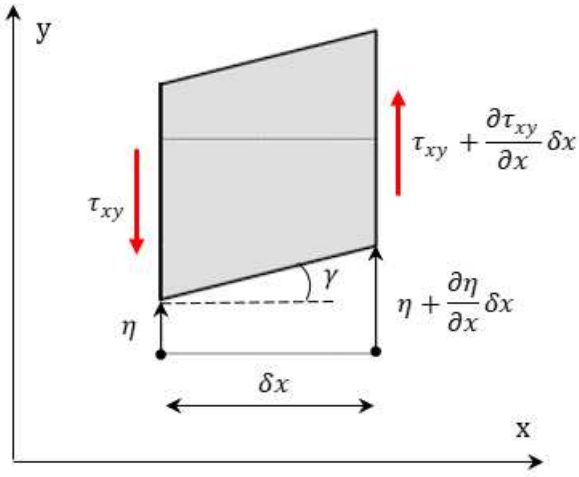

Figure 3-13 Vertical displacements, shear strain and stresses for an infinitesimal beam element [1]

Considering the case of shear deformation in the plane xy with associated differential transverse displacement $\partial\eta/\partial x$, the differential vertical shear stress $\partial\tau_{xy}/\partial x$ induces a vertical acceleration $\partial^2\eta/\partial t^2$ of the infinitesimal element $\rho\delta x\delta y$. The equation of motion yields:

$$(\rho\delta x\delta y)\frac{\partial^2\eta}{\partial t^2} = \frac{\partial\tau_{xy}}{\partial x}\delta x\delta y \qquad \text{(Eq. 3-43)}$$

The constitutive equation for shear stress is:

$$\tau_{xy} = G\gamma \qquad \text{(Eq. 3-44)}$$

$$G = \frac{E}{2(1+\nu)} \qquad \text{(Eq. 3-45)}$$

Where G is the shear modulus of elasticity and γ is the shear strain or shear deformation angle. Substituting (Eq. 3-44) in (Eq. 3-43) the shear wave equation for solid media can be obtained, which has similar form to the longitudinal and quasi-longitudinal wave equations indicating that also shear waves are non-dispersive.

$$\frac{\partial^2\eta}{\partial x^2} = \frac{1}{c_S^2}\frac{\partial^2\eta}{\partial t^2} \qquad \text{(Eq. 3-46)}$$

$$c_S = \sqrt{\frac{G}{\rho}} = \sqrt{\frac{E}{2\rho(1+\nu)}} \quad \text{(Eq. 3-47)}$$

Comparing the phase speed one may notice that shear waves are slower than quasi-longitudinal waves in beams, generally with a ratio of 0.6 for many structural material [1]. In vibro-acoustic shear waves are less important with respect to bending waves, especially for analysis at low frequencies, but can play a major role in the process of vibration transmission in complex structures or composite plates and beams.

For torsional waves the procedure to obtain the wave equation is similar to that of the shear wave and yields to:

$$\frac{\partial^2\theta}{\partial x^2} = \frac{1}{c_T^2}\frac{\partial^2\theta}{\partial t^2} \quad \text{(Eq. 3-48)}$$

$$c_T = \sqrt{\frac{GJ}{I_p}} \quad \text{(Eq. 3-49)}$$

Where GJ represents the torsional stiffness of the beam and I_p is the polar moment of inertia per unit length.

3.1.5 BENDING WAVES IN BEAMS

Among all the types of wave, bending waves are the most important in the field of vibroacoustic for two reasons:

1) Bending waves induce substantial orthogonal displacement of the surface separating structure and fluid, which is directly related to the ability of generating pressure gradient in the adjacent fluid and radiate sound.
2) Structure where bending waves propagate can have similar transverse impedance (see section 3.2.3) in terms of magnitude to that of sound waves in adjacent fluid, thus facilitating energy exchange between the two media.

Bending waves cannot be classified neither as longitudinal nor as transverse waves because they cause mainly transverse displacements, but the associated stresses are directed in the longitudinal direction. Let us assume an infinitesimal element of a beam in bending deformation under the assumption of small displacements and pure bending theory (*Euler-Bernoulli* assumption: plane cross-sections remain plane):

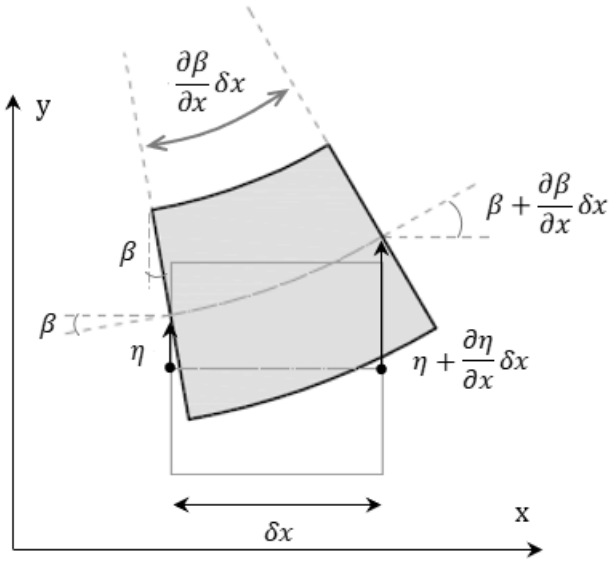

Figure 3-14 Vertical displacements and section rotations for a beam in bending [1]

$$\beta = \frac{\partial \eta}{\partial x} \qquad \text{(Eq. 3-50)}$$

Because there is no external applied force in the longitudinal direction of the beam, the equilibrium equation requires that:

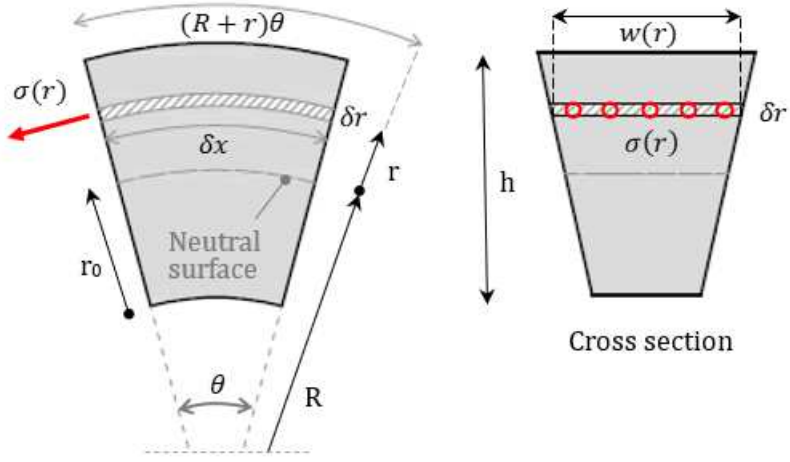

Figure 3-15 Pure bending deformation of a beam with a generic cross-section [1]

$$\int_{-r_0}^{h-r_0} \sigma(r)w(r)dr = 0 \qquad \text{(Eq. 3-51)}$$

$$\varepsilon(r) = \frac{|(R+r)\theta - \delta x|}{\delta x} \qquad \text{(Eq. 3-52)}$$

Because we have assumed a simple beam in bending (zero lateral constraint) the constitutive relation for the longitudinal stresses is the Hooke's law $\sigma(r) = E\varepsilon(r)$. Consideration about the curvature (Figure 14 and Figure 15) gives:

$$\frac{1}{R} = \frac{\theta}{\delta x} = -\frac{\partial \beta}{\partial x} = -\frac{\partial^2 \eta}{\partial x^2} \qquad \text{(Eq. 3-53)}$$

Hence, strains and stresses as a function of r can be rewritten as:

$$\varepsilon(r) = (R+r)\cdot\frac{\theta}{\delta x} - 1 = -r\frac{\partial^2 \eta}{\partial x^2} \qquad \text{(Eq. 3-54)}$$

$$\sigma(r) = -Er\frac{\partial^2 \eta}{\partial x^2} \qquad \text{(Eq. 3-55)}$$

In general, if the external bending moment is not constant along the longitudinal axis x, also the beam curvature should vary with x. Therefore, the corresponding variation of $\sigma(r)$ should be balanced in the longitudinal direction by horizontal shear stresses.

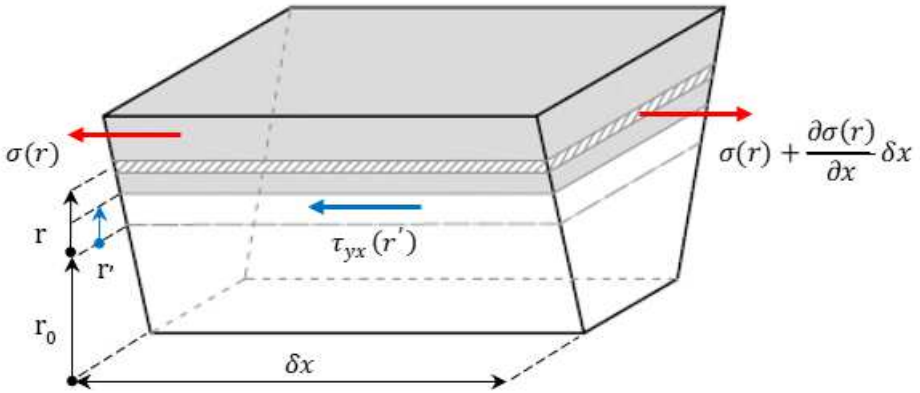

Figure 3-16 Longitudinal equilibrium between axial stresses and horizontal shear stresses [1]

$$\tau_{yx}(r')w(r') = \int_{r'}^{h-r_0} \frac{\partial \sigma(r)}{\partial x} w(r)dr \qquad \text{(Eq. 3-56)}$$

Substituting (Eq. 3-55) in (Eq. 3-56) yields to the following equation for a general cross-section:

$$\tau_{yx}(r') = -\frac{E}{w(r')}\frac{\partial^3\eta}{\partial x^3}\int_{r'}^{h-r_0} rw(r)dr \qquad \text{(Eq. 3-57)}$$

Assuming a simple rectangular cross-section of uniform width w and $r_0 = h/2$:

$$\tau_{yx}(r') = -\frac{E}{2}\frac{\partial^3\eta}{\partial x^3}\left[\left(\frac{h}{2}\right)^2 - (r')^2\right] \qquad \text{(Eq. 3-58)}$$

Which is the well-known parabolic relationship for shear stresses with a maximum that occurs at the neutral surface ($r' = 0$). The horizontal shear stresses τ_{yx} are then complemented by the vertical component τ_{xy} of equal magnitude and distribution.

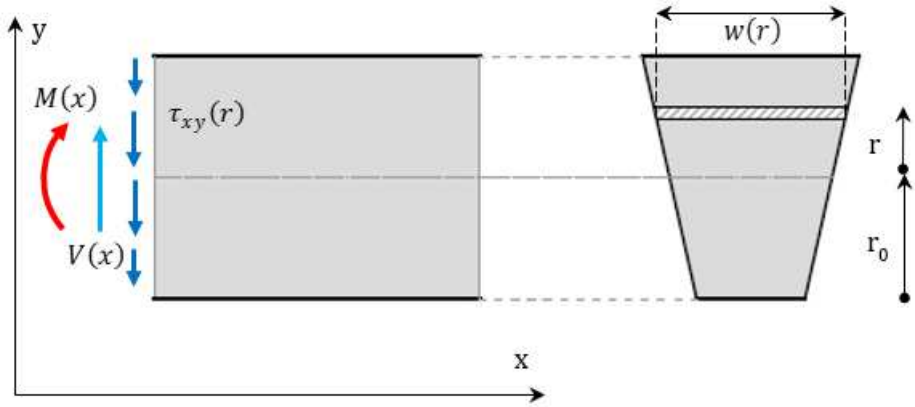

Figure 3-17 Distribution of shear stresses in a beam in bending [1]

The total shear force is given by the integration of the vertical shear stresses over the cross-section area:

$$V(x) = -\int_{-r_0}^{h-r_0} \tau_{xy}(r)w(r)dr \qquad \text{(Eq. 3-59)}$$

For the general cross-section:

$$V(x) = E\frac{\partial^3\eta}{\partial x^3}\int_{-r_0}^{h-r_0}\frac{1}{w(r')}\left[\int_{r'}^{h-r_0} rw(r)dr\right]w(r')dr' \qquad \text{(Eq. 3-60)}$$

Integration by parts yields to:

$$V(x) = EI\frac{\partial^3 \eta}{\partial x^3} \quad \text{(Eq. 3-61)}$$

Where I stands for the second moment of area of the cross section, calculated as:

$$I = \int_{-r_0}^{h-r_0} w(r) r^2 dr \quad \text{(Eq. 3-62)}$$

The bending moment acting on the cross section instead is related to the longitudinal axial stresses:

$$M(x) = \int_{-r_0}^{h-r_0} \sigma(r) w(r) r dr = -EI\frac{\partial^2 \eta}{\partial x^2} \quad \text{(Eq. 3-63)}$$

Thus far it was assumed that plane sections remain plane; however, the presence of shear stresses cause distortion of the cross-section and this assumption is no more strictly correct. Nevertheless, these deformations are rather small compared to the bending effects and can be neglected in the case of slender beams (high ratio l/h, with l the distance between two opposing transverse forces and h the height of the beam cross section).

Considering an infinitesimal element of the beam of linear distributed mass m, the equation of motion in the transverse direction gives:

$$\frac{\partial V}{\partial x} = -m\frac{\partial^2 \eta}{\partial t^2} \quad \text{(Eq. 3-64)}$$

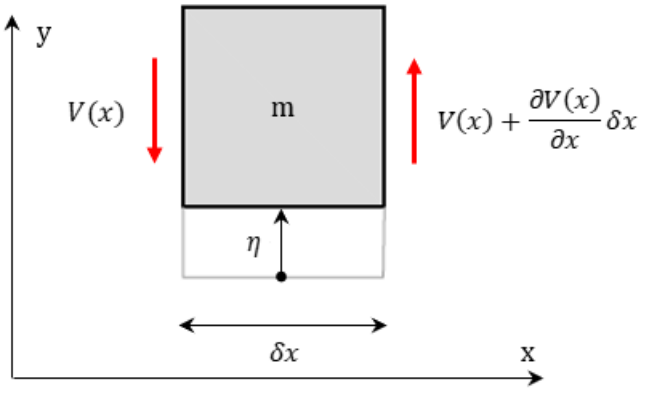

Figure 3-18 Transverse forces on an infinitesimal beam element [1]

Substituting the shear force relation (Eq. 3-61) in the equation of motion yields to the governing equation for bending wave in slender beams:

$$EI\frac{\partial^4\eta}{\partial x^4} = -m\frac{\partial^2\eta}{\partial t^2} \quad \text{(Eq. 3-65)}$$

Bending waves are a hybrid between longitudinal and transverse waves and for this reason the spatial derivative is of the fourth and not the second order. Considering a simple harmonic propagating wave, the equation reduces to:

$$\eta(x,t) = \tilde{\eta}e^{i(\omega t - kx)} \quad \text{(Eq. 3-66)}$$

$$EIk^4 = m\omega^2 \quad \text{(Eq. 3-67)}$$

Which gives four roots for the wavenumber k, two imaginary and two real:

$$k = \pm i\sqrt[4]{\frac{m\omega^2}{EI}} \qquad k = \pm\sqrt[4]{\frac{m\omega^2}{EI}} \quad \text{(Eq. 3-68)}$$

The complete solution can thus be written as:

$$\eta(x,t) = \left[\tilde{A}e^{-ik_Bx} + \tilde{B}e^{ik_Bx} + \tilde{C}e^{-k_Bx} + \tilde{D}e^{k_Bx}\right]e^{i\omega t} \quad \text{(Eq. 3-69)}$$

The first two terms in parentheses are real and are called *propagating waves*, indicating respectively waves propagating in the positive and negative direction. The last two terms are imaginary and are called *near-field terms* (sometimes termed also as evanescent waves), relating to effects that rapidly decay over distance from the point of generation. The bending wave wavenumber k_B and phase speed c_B are:

$$k_B = \sqrt[4]{\frac{m\omega^2}{EI}} \quad \text{(Eq. 3-70)}$$

$$c_{ph\,B} = \frac{\omega}{k_B} = \sqrt{\omega}\sqrt[4]{\frac{EI}{m}} \quad \text{(Eq. 3-71)}$$

It can be noticed that the phase speed $c_{ph\,B}$ is dependent from the square root of frequency ω, hence bending waves are dispersive. The group speed for definition is:

$$c_{g\,B} = \frac{\partial\omega}{\partial k} = \frac{\partial}{\partial k}\left(k_B^2\sqrt{\frac{EI}{m}}\right) = 2c_{ph\,B} \quad \text{(Eq. 3-72)}$$

The range of validity of the defined wave equation is limited to the point where shear contribution can be considered as negligible. To evaluate a definite value for this limit let us assume a cantilever beam subjected to a concentrated load on the tip:

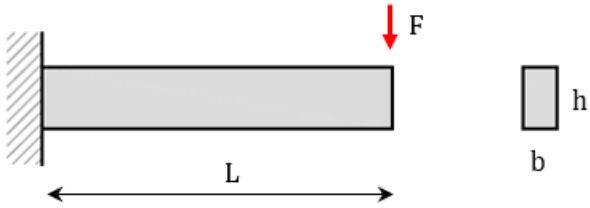

Figure 3-19 Cantilever beam with concentrated load on the tip

The shear and bending contribution to the vertical displacement can be calculated as:

$$w_S = \frac{Fl}{GA} \qquad w_B = \frac{Fl^3}{3EI} \qquad \text{(Eq. 3-73)}$$

The ratio of shear to bending deflection considering a rectangular cross-section is:

$$\frac{w_S}{w_B} = \frac{1}{2(1+\nu)}\left(\frac{h}{l}\right)^2 \qquad \text{(Eq. 3-74)}$$

For free bending waves the wavelength λ_B is defined as $2\pi/k_B$ and the distance between points of maximum and of zero displacement (or acceleration) is $\lambda_B/4$.

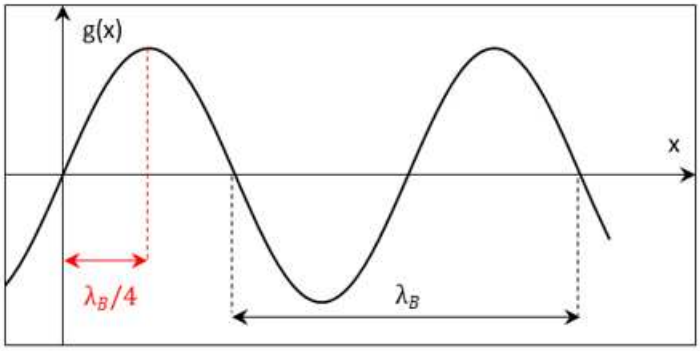

Figure 3-20 Relation between wavelength and points of zero and maximum displacement

"*In the d'Alambert view of dynamic equilibrium of bending waves, 'inertia forces' may be considered to act in opposition to elastic shear forces. Maximum inertia forces act at points of maximum acceleration, and maximum shear forces act at points of zero*

displacement" [1]. Therefore, in the ration between shear and bending deflection the length l can be substituted by the quarter of wavelength $\lambda_B/4 = \pi/2k_B$:

$$\frac{w_s}{w_B} \cong \frac{1}{2}\left(\frac{2k_B h}{\pi}\right)^2 \quad \text{(Eq. 3-75)}$$

To consider the shear contribution as negligible the ratio should be small:

$$k_B h < 1 \quad or \quad \lambda_B > 6h \quad \text{(Eq. 3-76)}$$

$$+\omega < \sqrt{\frac{EI}{m}} \cdot \frac{1}{h^2} \quad \text{(Eq. 3-77)}$$

Moving towards high frequencies the shear contribution becomes increasingly important until bending waves become very like to pure shear waves.

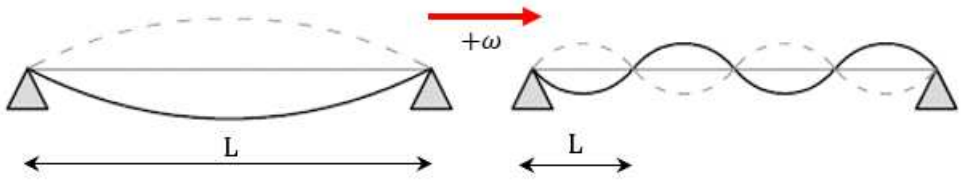

Figure 3-21 Graphical representation of decreasing beam slenderness increasing the vibration frequency (mode number)

3.1.6 BENDING WAVES IN THIN PLATES

The wave equation for a thin plate lying in the xz plane is:

$$D\left(\frac{\partial^4 \eta}{\partial x^4} + 2\frac{\partial^4 \eta}{\partial x^2 \partial z^2} + \frac{\partial^4 \eta}{\partial z^4}\right) = -m\frac{\partial^2 \eta}{\partial t^2} \quad \text{(Eq. 3-78)}$$

Where m stands for mass per unit area and D the bending stiffness of the plate per unit width (with h the plate thickness):

$$D = \frac{Eh^3}{12(1-\nu^2)} \quad \text{(Eq. 3-79)}$$

Considering a simple harmonic plane wave, substitution in the wave equation gives:

$$\eta(x,z,t) = \tilde{\eta} e^{i(\omega t - k_x x - k_z z)} \quad \text{(Eq. 3-80)}$$

$$D(k_x^2 + k_z^2)^2 = m\omega^2 \quad \text{(Eq. 3-81)}$$

Writing $k_B^2 = k_x^2 + k_z^2$ yields to a similar formulation for bending waves in thin plates to that bending waves in beams. The corresponding wavenumber k_B and phase speed c_B are:

$$k_B = \sqrt[4]{\frac{m\omega^2}{D}} \qquad \text{(Eq. 3-82)}$$

$$c_{ph\,B} = \sqrt{\omega}\sqrt[4]{\frac{D}{m}} \qquad \text{(Eq. 3-83)}$$

3.1.7 DISPERSION CURVES AND VIBRO-ACOUSTIC COUPLING

When studying the coupling between vibration in structures and acoustic wave propagation in fluid it is useful to plot the dispersion curves (wavenumber k versus frequency ω) for the two media on a common graph:

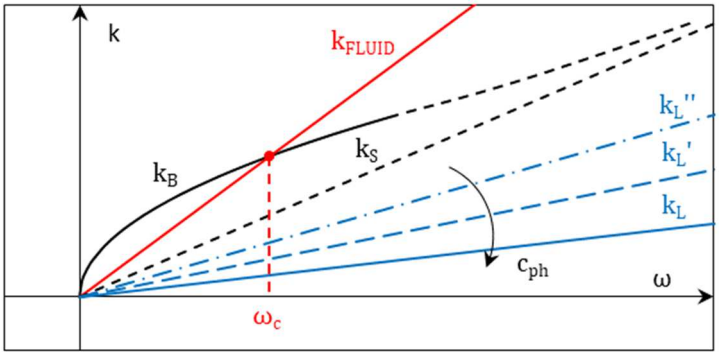

Figure 3-22 Dispersion curves for solid medium and fluid medium and highlighting of acoustic critical frequency

The phase speed c_{ph} is defined as the ratio of frequency ω and wavenumber k, so the curves with lower slopes have higher phase and group speed. The frequency at which the bending wave dispersion curve in the structure and the acoustic wave dispersion curve in the fluid meet is called the *acoustic critical frequency*. At this frequency the wavenumber (and consequently also the wavelength) of the solid medium matches that of the fluid medium and sound radiation is highly efficient, below this frequency sound radiation in the far field can be considered as negligible [2].

$$c_{ph\,B\,solid}(\omega_c) = c_{ph\,fluid}(\omega_c) \qquad \text{(Eq. 3-84)}$$

$$c_{g\ B\ solid}(\omega_c) = 2c_{g\ fluid}(\omega_c) \quad \text{(Eq. 3-85)}$$

For sufficiently high frequencies, as discussed in section 3.1.5, bending waves tend to propagate as pure shear waves and the bending wave dispersion curve has an asymptote that tends to the shear wave dispersion curve.

The representation of Figure 3-22 is valid for an infinitely extending solid medium; when the medium instead is limited by parallel boundaries in one or two dimensions the system is termed as *waveguide*. "*The presence of boundaries constrains the form of the wave pattern that can propagate in the medium and hence modifies the dispersion characteristics of the system*" [1].

Let us imagine a plate waveguide limited in one dimension (x) by simple supports to a uniform width l and unbounded in the other direction (z); the bending wave equation plus the boundary conditions in x give the dispersion relation:

$$k_{zn}^2 = k_B^2 - k_x^2 = \omega\sqrt{\frac{\overline{m}}{D}} - \left(\frac{n\pi}{l}\right)^2 \quad \text{(Eq. 3-86)}$$

$$\eta(x,z,t) = \tilde{\eta}\sin\left(n\pi\frac{x}{l}\right)e^{i(\omega t - k_{zn}z)} \quad \text{(Eq. 3-87)}$$

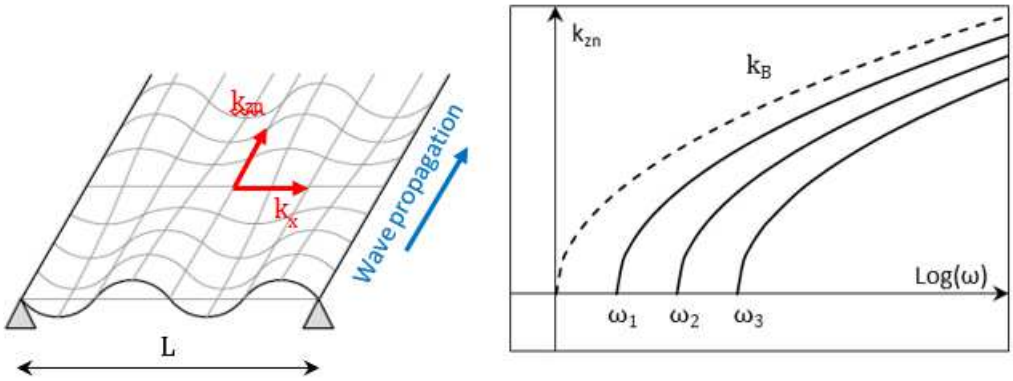

Figure 3-23 Waveguide behaviour of a simple supported plate unbounded in the z direction [1]

Where the wavenumber k_{zn} is related to the propagation in the z direction of the *waveguide modes*, which are sinusoidal standing wave pattern in the x direction. These modes are formed by interference of waves propagating in the negative and positive x direction and reflected multiple times at the boundaries. The equation shows that the only real solution, for each mode n, exist for frequency ω where k_{zn} is positive. The

frequencies at which $k_{zn} = 0$ are called *modal cut-off frequencies*, below these the associated mode cannot effectively propagate wave energy.

3.2 EXPERIMENTAL MODAL ANALYSIS (EMA)

Aim of the following section is to introduce the principles and the main features of structural dynamic testing and in particular of Experimental Modal Analysis (EMA) performed using a modal hammer. Main reference will be the guide written by Ole Døssing ([3] and [4]) for the *Bruel & Kjaer* company; this will be integrated when needed from other sources found in literature.

Many engineering fields must face with dynamic problems where the presence of time variant forces or excitations give rise to the propagation of stress waves in the structure which in turn may cause vibration and noise problems. As seen in section *3.1* the finite nature of a structure and the presence of boundary conditions yield to a dynamic response governed by specific spatial deformation patterns (*mode shapes*), formed by the interference of multiple reflected waves, for specific frequency values (*modal frequencies*). Modes can be divided into two classes:

- *Normal modes*: these modes take the form of *standing waves* with fixed node lines. The modal displacements are real and can be positive (in phase) or negative (180° out of phase).
- *Complex modes*: these modes take the form of *propagating waves* with no fixed lines. The modal displacements are complex and can have any phase value.

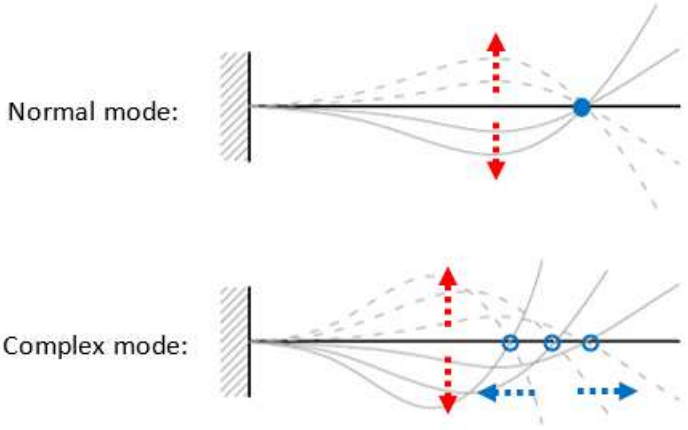

Figure 3-24 Normal mode and complex mode representation for a cantilever beam [4]

Most structures encountered in the practice of civil engineering have very light damping and exhibit normal modes; complex modes instead are generally related to high and/or localised damping (e.g. car body).

3.2.1 SIGNAL VS SYSTEM ANALYSIS

When treating with noise or vibration problem there are always three factors which should be investigated to check if they are the cause of the problem:

1) *Source*: where dynamic forces or excitation are generated (e.g. operating forces too high).
2) *Path*: how the exciting energy is transmitted and how the structure responds to the excitation (e.g. the structure is too compliant).
3) *Receiver*: how the user reacts to vibration and/or noise (e.g. user too sensitive).

Generally, engineers and designers do not consider the third factor since it is subjective; to overcome this limitation, tolerance levels are fixed by standards from statistical analyses on representative samples of the population.

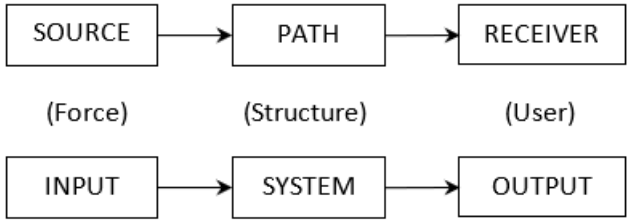

Figure 3-25 Schematic representation of typical structural dynamic problems

There are two distinct approaches to study the dynamic behaviour of a structure:

1) *Signal analysis*: it is measured only the response (output) of a structure due to some unknown excitation (in general the forces acting on the structure under service). Usually, the results are presented in the frequency domain in terms of *output spectrum*.
2) *System analysis*: both the exciting forces (input) and the response of the structure (output) are measured. The results are presented in the frequency domain as output-to-input ratio with a quantity termed as *Frequency Response Function* (FRF). Under the assumption of linear system this quantity is independent on the input magnitude and constitutes an inherent, intrinsic property of the system.

It is clear that the system analysis is a much more powerful instrument since it allows to predict the response of a structure to any type of excitation, provided that the FRF is

evaluated with sufficient accuracy and precision. However, it is not always be possible to measure the excitation forces (e.g. for a full-scale building the force levels required to obtain adequate signal-to-noise ratio in the response may cause local damage to the structure). Nevertheless, there are also specific mathematical techniques to extract system dynamic properties from output only measurement under assumption on registered signal length and excitation type (e.g. Operational Modal Analysis OMA and Enhanced Frequency Domain Decomposition EFDD technique [5]).

3.2.2 SINGLE-DEGREE-OF-FREEDOM (SDOF) MODELS

"*Models are to be used not believed*" Henri Thiel [3].

ANALYTICAL AND MATHEMATICAL MODEL

The simplest way to interpret the dynamic behaviour of a structure is to consider only a single degree of freedom (i.e. a single time variable spatial parameter). This is done by modelling the structure with the well-known system composed by a point mass m connected to a fixed basis by a linear spring k and a linear viscous damper c (Figure 3-26).

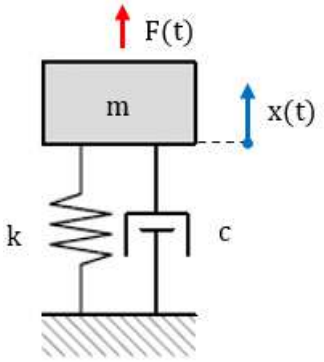

Figure 3-26 Typical representation of a SDOF dynamic system in the physical domain

$$m\ddot{x}(t) + c\dot{x}(t) + kx(t) = F(t) \qquad \text{(Eq. 3-88)}$$

The mathematical model in the time domain is obtained by writing down the dynamic equilibrium equation (Eq. 3-88) (Newton's second law) equating the internal forces (inertia, damping and elasticity) to the exciting external forces for every time step t.

SPATIAL PARAMETER MODEL

The quantity that describes the dynamic behaviour of a structure in the frequency domain is called the *Frequency Response Function* (FRF). This is a complex quantity generally represented in terms of magnitude and phase value. To define it in terms of

the analytical single-degree-of-freedom (SDOF) model parameters let us assume a simple harmonic variation for the displacement $x(t)$ and force excitation $F(t)$:

$$x(t) = \tilde{x}e^{i\omega t} = 1 \cdot e^{i\omega t} \quad \text{(Eq. 3-89)}$$

$$F(t) = \tilde{F}e^{i\omega t} = 1 \cdot e^{i\omega t} \quad \text{(Eq. 3-90)}$$

The dynamic equilibrium differential equation yields:

$$(-\omega^2 m + i\omega c + k)x(t) = F(t) \quad \text{(Eq. 3-91)}$$

The FRF in terms of displacement over force value is termed *Compliance FRF* and gives:

$$H(\omega) = \frac{x(\omega)}{F(\omega)} = \frac{1}{-\omega^2 m + i\omega c + k} \quad \text{(Eq. 3-92)}$$

Where $x(\omega)$ and $F(\omega)$ are calculated through the *Fourier Transform* as follows:

$$x(\omega) = \int_{-\infty}^{\infty} x(t)e^{-i\omega t}dt = \int_{-\infty}^{\infty} e^{i\omega t}e^{-i\omega t}dt = 1 \quad \text{(Eq. 3-93)}$$

$$F(\omega) = \int_{-\infty}^{\infty} (-\omega^2 m + i\omega c + k)e^{i\omega t}e^{-i\omega t}dt = -\omega^2 m + i\omega c + k \quad \text{(Eq. 3-94)}$$

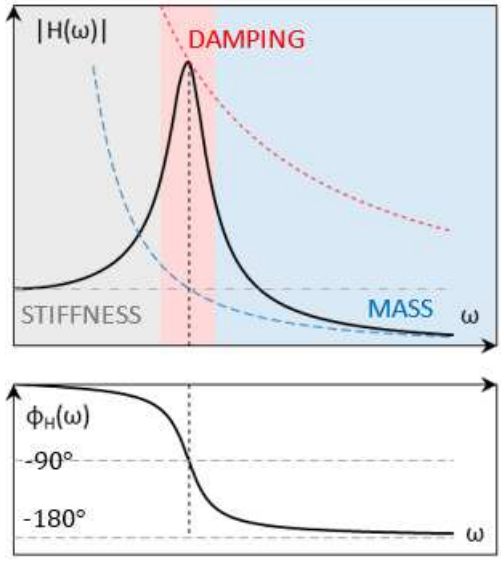

Figure 3-27 Bode plot (magnitude + phase) of a SDOF Compliance FRF

For very low frequencies ($\omega \to 0$) the dynamic equilibrium is almost equal to the static equilibrium and the response of the structure in terms of displacement is governed by the stiffness alone and is in phase with the excitation. The *Compliance FRF* (displacement over force) yields:

$$H(\omega)|_{\omega\to 0} = \frac{x(\omega)}{F(\omega)} = \frac{1}{-\omega^2 m + i\omega c + k} = \frac{1}{k} \qquad \text{(Eq. 3-95)}$$

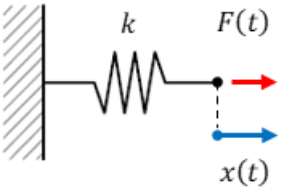

Figure 3-28 For low frequencies ($\omega \to 0$) dynamic response governed by stiffness

At increasing frequencies, the inertial forces become more important until the mass and stiffness terms cancel each other out at the so-called natural frequency ($\omega_N = \sqrt{k/m}$) and the response is controlled only by the damping term (for undamped system the displacement goes to infinity). The *Mobility FRF* (velocity over force) yields:

$$M(\omega)|_{\omega=\omega_N} = \frac{\dot{x}(\omega)}{F(\omega)} = \frac{1}{i\omega m + c - \frac{ik}{\omega}} = \frac{1}{c} \qquad \text{(Eq. 3-96)}$$

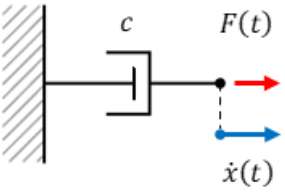

Figure 3-29 At the resonance frequency ($\omega = \omega_N$) dynamic response governed by damping

At very high frequencies, the mass term takes control and the structure becomes more and more compliant behaving as a simple mass. The *Accelerance FRF* (acceleration over force) yields:

$$A(\omega)|_{\omega\to\infty} = \frac{\ddot{x}(\omega)}{F(\omega)} = \frac{1}{m + \frac{c}{i\omega} - \frac{k}{\omega^2}} = \frac{1}{m} \qquad \text{(Eq. 3-97)}$$

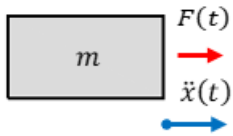

Figure 3-30 At very high frequencies ($\omega \rightarrow \infty$) dynamic response governed by mass

FRF "BLACK-BOX" MODEL

It is a non-parametric model which links the practical experimental measurements to the analytical model used to describe the dynamic behaviour of the structure. It is based in the definition of the FRF as ratio of output and input frequency spectra. It can be defined either in the frequency domain, *Frequency Response Function* $H(\omega)$, or the time domain, *Impulse Response* $h(t)$, by using the Forward and Inverse Fourier Transform to pass from one domain to the other.

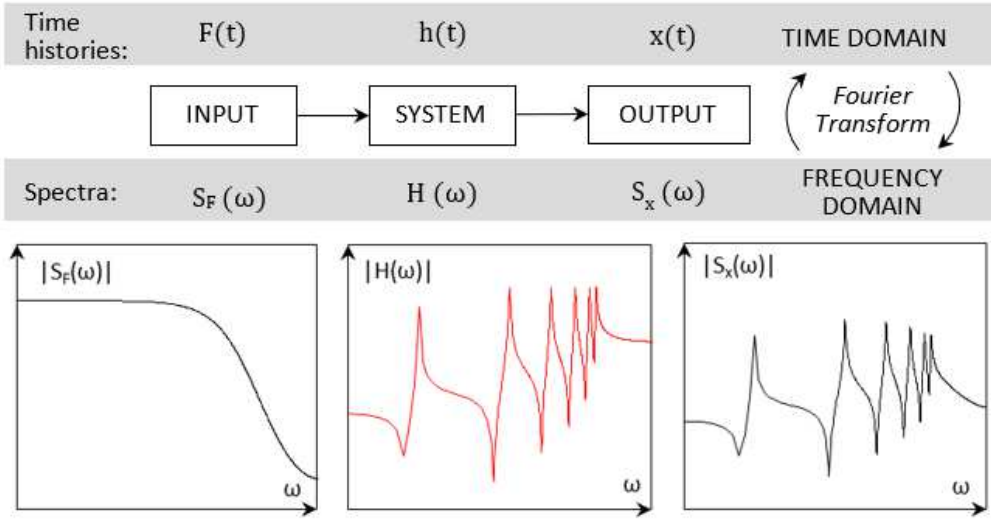

Figure 3-31 Black-box model schematic representation in the time domain and in the frequency domain

MODAL PARAMETER MODEL

The spatial parameter model described before is useful to study the behaviour of system where the mass, damping and stiffness parameters are well defined. When working with real structures this is not always the case and it can be helpful to redefine the FRF in terms of two new parameters termed as *pole location* p and *residue* R (also known as zero):

$$H(\omega) = \frac{R}{i\omega - p} + \frac{R^*}{i\omega - p^*} \quad \text{(Eq. 3-98)}$$

Where both pole location and residue are complex numbers and the apex * stands for the complex conjugate of that number. Pole location and residue can be defined in terms of the spatial parameters m, k and c:

$$R = -i\frac{1}{2m\omega_D} \qquad R^* = i\frac{1}{2m\omega_D} \quad \text{(Eq. 3-99)}$$

$$p = -\sigma + i\omega_D \qquad p^* = -\sigma - i\omega_D \quad \text{(Eq. 3-100)}$$

Where:

- $\sigma = c/2m$ is the modal damping coefficient (also known as decay rate).
- $\omega_0 = \sqrt{k/m}$ is the undamped natural frequency.
- $\omega_D^2 = \omega_0^2 - \sigma^2 = \omega_0\sqrt{1-\zeta^2}$ is the damped natural frequency.
- $\zeta = \sigma/\omega_0 = c/c_{cr} = c/2\sqrt{mk}$ is the percent of critical damping (also known as damping ratio).

The FRF again can be transformed in the time domain by using and Inverse Fourier Transform (IFT) obtaining the impulse response of the system:

$$h(t) = 2|R|e^{-\sigma t}\sin(\omega_D t) \quad \text{(Eq. 3-101)}$$

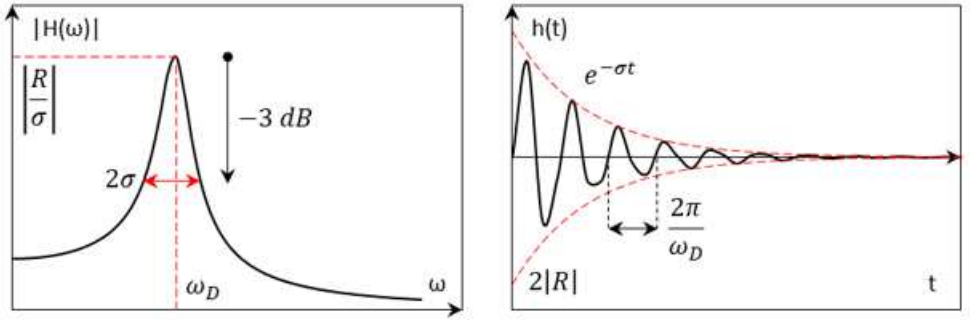

Figure 3-32 Graphical representation of FRF and impulse response of a SDOF system [4]

The pole location is a complex number where the real part σ is related to the damping properties of the system (measured as half the -3 dB frequency bandwidth of the FRF peak) and the imaginary part ω_D is the damped natural frequency of a free decaying oscillation. The pole location is then related to two modal parameters: modal damping and modal frequency; in a sense, it can be said that it defines the *shape of the FRF* (both for magnitude and phase plot).

The residue is an imaginary number and, together with the modal damping coefficient σ, carries information about the *scaling of the FRF* (Eq. 3-102). Sometimes it is also termed as "pole-strength" and it is related to the third modal parameter: the mode shape.

$$H(\omega_D) \cong \frac{R}{\sigma} \qquad \text{(Eq. 3-102)}$$

3.2.3 THE FORMS OF THE FREQUENCY RESPONSE FUNCTION (FRF)

The Frequency Response Function (FRF) is the quantity that describes the dynamic behaviour of a system; in a certain sense it can be seen as a filter which modifies the time history characteristics of a certain input giving as a result a specific output. The FRF is a complex quantity and therefore it has a magnitude $|H(\omega)|$ and a phase $\varphi_{H(\omega)}$. It is generally defined as a ratio of the output spectrum $S_x(\omega)$ over the input spectrum $S_F(\omega)$:

$$H(\omega) = \frac{S_x(\omega)}{S_F(\omega)} \qquad \text{(Eq. 3-103)}$$

Assuming a simple harmonic excitation, a straightforward interpretation of the FRF can be given with Figure 3-33.

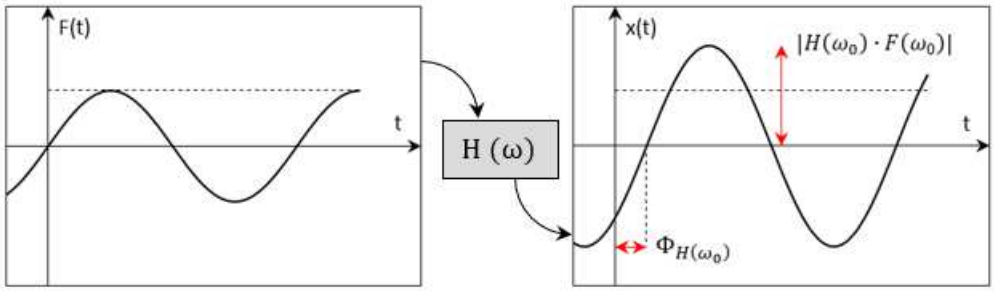

Figure 3-33 FRF black-box model considering a simple harmonic input signal [3]

The FRF describes the inherent dynamic properties of the system independently from the type of signal used for the measurements. In general, it is useful to adopt a wide frequency bandwidth for the excitation force (i.e. flat input spectrum, for example impact testing or random excitation) to reduce the measurement time during the experimental testing phase.

Typically, the FRF is defined in terms of compliance as ratio of displacement spectrum over force spectrum. However, motion can be described in terms of displacement, velocity or acceleration and the FRF can be defined as ratio of output over input or as ratio of input over output. Hence, depending on which definition is chosen, the FRF can take six different forms:

Table 3-2 The six different forms of the Frequency Response Function (FRF) [6]

	Displacement	Velocity	Acceleration
Output/Input	Compliance (Receptance)	Mobility	Accelerance (Inertance)
Input/Output	Dynamic stiffness	Impedance	Apparent mass

Where is not differently specified, the term mobility is used to describe any of the FRF forms. For measurements the FRF is evaluated in terms of accelerance whereas for modelling Compliance FRF is most used. Anyway, the transition from one form to the other is quite straightforward involving differentiation or integration in the time domain (in the frequency domain this is reduced to multiplication or division by $i\omega$ respectively) or inversion of output over input and vice versa.

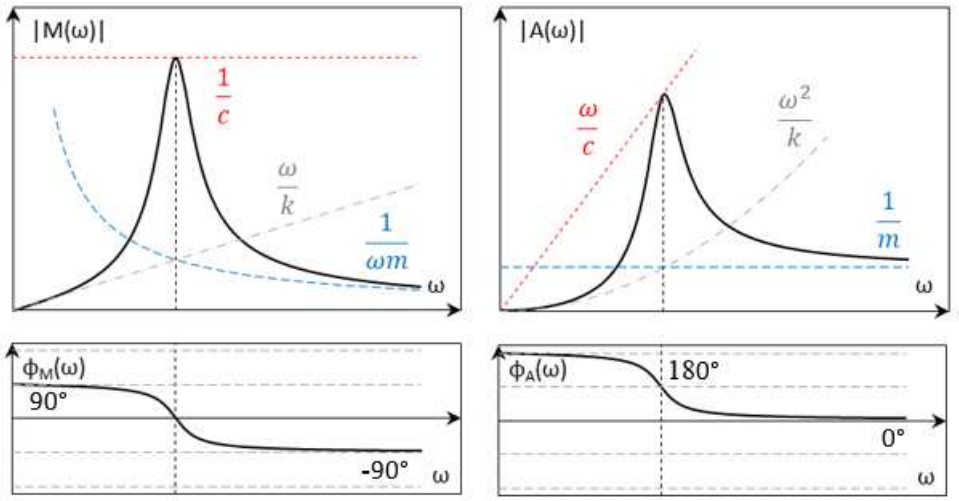

Figure 3-34 Bode plot of SDOF Mobility FRF and Accelerance FRF [3]

$$H(\omega) = \frac{S_x(\omega)}{S_F(\omega)} = \left[\frac{m}{N}\right] \qquad \text{(Eq. 3-104)}$$

$$M(\omega) = \frac{S_{\dot{x}}(\omega)}{S_F(\omega)} = i\omega \cdot H(\omega) = \left[\frac{ms^{-1}}{N}\right] \quad \text{(Eq. 3-105)}$$

$$A(\omega) = \frac{S_{\ddot{x}}(\omega)}{S_F(\omega)} = -\omega^2 \cdot H(\omega) = \left[\frac{ms^{-2}}{N}\right] \quad \text{(Eq. 3-106)}$$

3.2.4 FRF MEASUREMENT AND ESTIMATORS

In theory, the FRF is the ratio of the output spectrum over the input spectrum. In practice however, we perform several measurements to obtain the best estimate of the FRF minimizing the effect of possible errors (e.g. mechanical noise, electrical noise of instruments, etc.). Given that the FRF is a complex quantity, a simple algebraic average is not a viable method to derive a meaningful estimation of the FRF.

$$\bar{H}(\omega) \neq \frac{\sum S_x(\omega)}{\sum S_F(\omega)} \qquad \bar{H}(\omega) \neq \frac{1}{n}\sum \frac{S_x(\omega)}{S_F(\omega)} \quad \text{(Eq. 3-107)}$$

ESTIMATOR H1 (NOISE IN THE OUTPUT)

For the first estimator it is assumed that all the noise in the measurement is due to noise in the output (e.g. ambient random vibration).

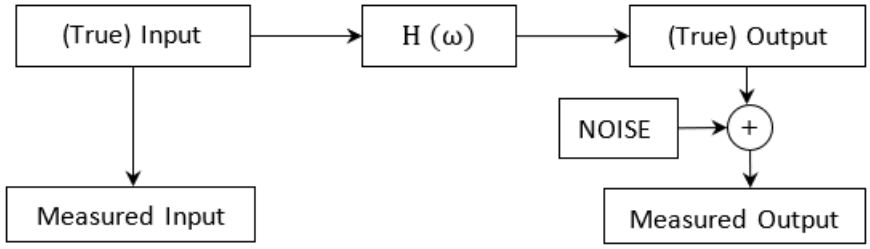

Figure 3-35 Schematic representation of FRF measurement with noise at the output [3]

The estimator H1 is defined as the ratio of the *Cross-power spectrum* $S_{Fx}(\omega)$, between response and force, and the *Auto-power spectrum* of the force $S_{FF}(\omega)$:

$$H_1(\omega) = \frac{S_{Fx}(\omega)}{S_{FF}(\omega)} \quad \text{(Eq. 3-108)}$$

These are obtained by multiplying the response and force spectrum for the complex conjugate of the force spectrum $S_F^*(\omega)$:

$$S_{Fx}(\omega) = S_F^*(\omega) \cdot S_x(\omega) \quad \text{(Eq. 3-109)}$$

$$S_{FF}(\omega) = S_F^*(\omega) \cdot S_F(\omega) \quad \text{(Eq. 3-110)}$$

Therefore, the auto-power spectrum is a real quantity while the phase information is contained in the cross-power spectrum; the FRF so defined can be averaged and for an infinite number of measurements the mean value will tend to the real FRF of the structure:

$$H(\omega) = \lim_{n\to\infty} \overline{H_1}(\omega) = \lim_{n\to\infty} \frac{\sum^n S_{Fx}(\omega)}{\sum^n S_{FF}(\omega)} \qquad \text{(Eq. 3-111)}$$

ESTIMATOR H2 (NOISE IN THE INPUT)

For the second estimator it is assumed that all the noise in the measurement is due to noise in the input (e.g. in correspondence of resonances when using shaker excitation).

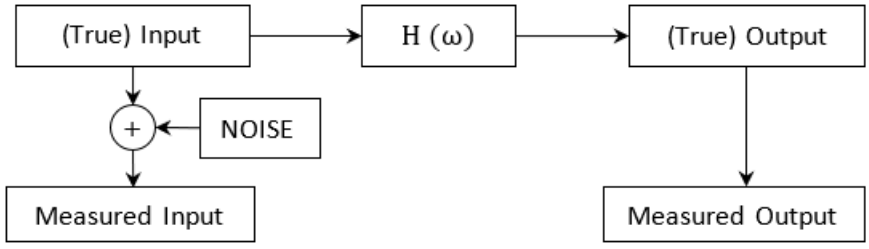

Figure 3-36 Schematic representation of FRF measurement with noise at the input [3]

The estimator H1 is defined as the ratio of the *Auto-power spectrum* of the response $S_{xx}(\omega)$ and the *Cross-power spectrum* $S_{xF}(\omega)$ between response and force:

$$H_2(\omega) = \frac{S_{xx}(\omega)}{S_{xF}(\omega)} \qquad \text{(Eq. 3-112)}$$

When noise is present both at input and output the two estimators $H_1(\omega)$ and $H_2(\omega)$ can form a confidence interval for the true FRF.

COHERENCE FUNCTION

Another important quantity can be derived by the cross-power and auto-power spectra if response and force, the so-called *Coherence Function*:

$$\gamma^2(\omega) = \frac{|S_{Fx}(\omega)|^2}{S_{xx}(\omega) \cdot S_{FF}(\omega)} \qquad 0 \le \gamma^2(\omega) \le 1 \qquad \text{(Eq. 3-113)}$$

The coherence function assesses the degree of linearity between input and output signals: a value of 1 indicates a perfect linear relationship between input and output (i.e. no noise) whereas a value of 0 indicates a random relationship between input and output (i.e. pure noise). Figure 3-37 illustrates an example of impact testing FRF measurements and how to interpret the relative coherence function.

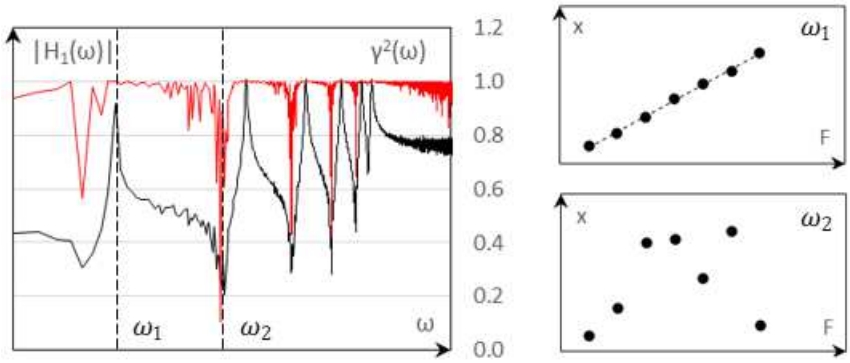

Figure 3-37 Example of H1 estimator and coherence function

In correspondence of a resonance the response of a structure is very strong, and the coherence value is generally close to 1 indicating a high repeatability of the measurement. On the other hand, in an anti-resonance the response of a structure is very weak and for this reason the signal-to-noise ratio is very low causing coherence value close to 0 (but this is somewhat expected/normal). A low value of the coherence function outside the anti-resonance zones could indicate problems/noise in the measurement (e.g. scattering of impact point location and/or impact direction).

3.2.5 FRF MEASUREMENT AND IMPACT TESTING

In this section we will see what are the steps taken to perform a *Single-Input-Single-Output* (SISO) FRF estimation, also known as dual-channel Fast Fourier Transform (FFT) analysis, through impact excitation.

To begin with, the characteristic of the instrumentation adopted to measure the excitation force and the response of the structure (i.e. modal hammer and accelerometer) must be chosen accordingly to the scope of the project:

- *Response transducer*: it is generally a piezoelectric accelerometer. The frequency range, dynamic range, sensitivity and maximum recordable signal should be selected in relation to the expected structure response. In addition, mounting condition and the mass of the transducer should be chosen suitably to not alter the local mass, stiffness and damping properties of the structure.
- *Excitation transducer*: for impact testing it is used a modal hammer, built by mounting a force transducer to a hammer. The two governing properties of the input signal are the mass of the hammer and the stiffness of the tip. The mass of the hammer should be high enough to adequately excite the mode of interest of the structure (sufficient signal-to-noise ratio of the response); a higher mass also involves narrower frequency bandwidth excitation. Another way to control

the frequency content of the input is to select different hammer tips: a hard tip (e.g. steel tip) will produce shorter impulse in the time domain and consequently excites a broader bandwidth in the frequency domain (Figure 3-38).

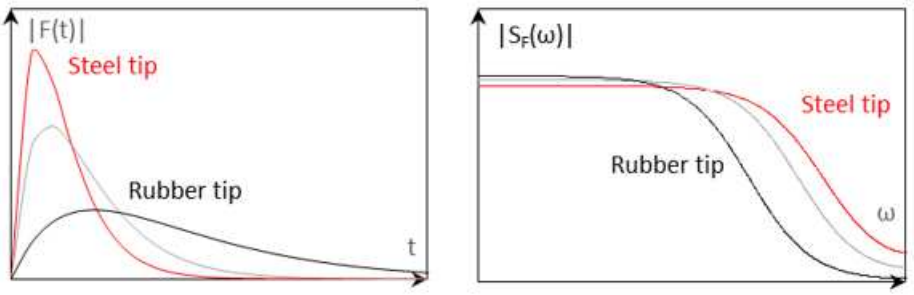

Figure 3-38 Example of input spectrum variation due to hammer tip hardness

The measurement and calculation chain for a Single-Input-Single-Output FRF estimation are schematised in Figure 3-39 (data gathering) and in Figure 3-40 (Fourier Transform and post-processing).

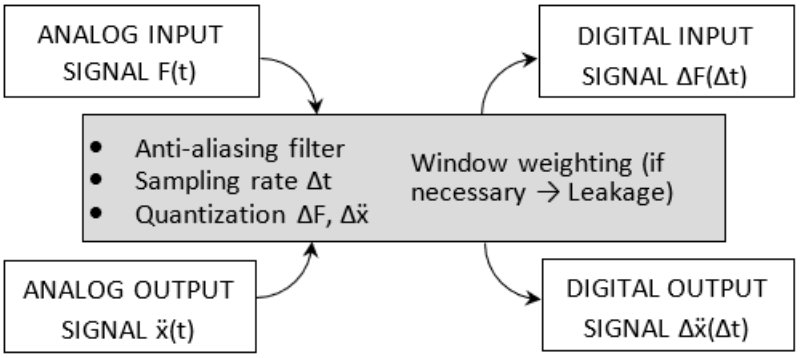

Figure 3-39 Data gathering process as first step for FRF measurement [7]

ALIASING AND LOW-PASS FILTER

Aliasing is a phenomenon which produces signal distortion when a continuous time signal is transformed into a discrete time signal with a not sufficiently high sampling rate (e.g. analog to digital conversion). The minimum sampling rate to avoid aliasing is called the *Nyquist rate* (from the Nyquist-Shannon sampling criterion) and is equal to twice the maximum frequency component of the signal to be sampled; the *Nyquist frequency* on the other hand is defined as the maximum representable frequency content of a spectrum assuming a certain sampling rate value:

$$f_{s\,Nyquist} = 2 \cdot f_{max} \qquad \text{(Eq. 3-114)}$$

$$f_{Nyquist} = \frac{f_{sampling}}{2} \quad \text{(Eq. 3-115)}$$

To ensure that the signal do not contain any frequency component higher than the chose maximum frequency a *Low-Pass filter* (also known as Anti-aliasing filter) is applied to the signal to attenuate all the frequencies above the selected limit. For example, all the audio recordings are typically sampled at 44 kHz and the corresponding Nyquist frequency is 22 kHz, almost equal to the human hearing range superior limit.

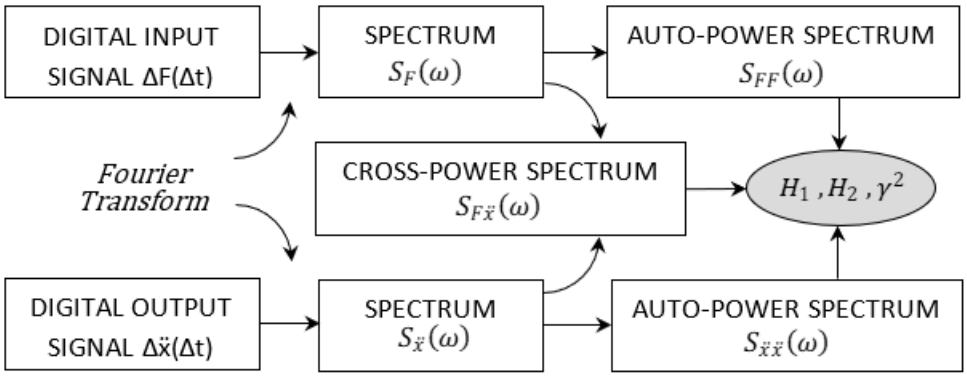

Figure 3-40 Transformation in the frequency domain and post-processing for estimating the FRF [7]

LEAKAGE AND WINDOW WEIGHTING

Leakage is a phenomenon which occurs when measuring a time signal with a measurement time shorter than the actual signal duration; the sudden truncation in the time domain induces a reduction of amplitude of the resonant frequency (assuming a simple harmonic damped signal) and a spreading (i.e. "leakage") of the spectral components over a wider frequency range.

This happens because the sudden truncation of the signal is equivalent to a short impulse, which transformed in the frequency domain has a wide flat spectrum that can be superimposed to a spectrum similar to that of the original signal.

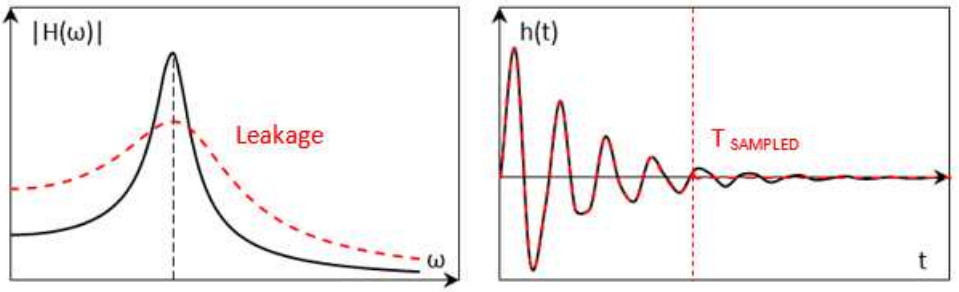

Figure 3-41 Representation of leakage due to sudden truncation of sampled time signal

There are three possible ways to reduce the influence of the leakage error on the FRF estimation:

1) *Use of the H2 estimator*: we have seen that the leakage error is related to energy spreading from otherwise sharp resonant peaks in the frequency domain. The H2 estimator is the ratio of the output auto-power spectrum to the cross-power spectrum, both characterised by sharp resonant peaks and therefore leakage error: in the ratio the errors tend to cancel each other out.
2) *Recording of the entire time signal*: when all the signal time history is captured in one sample, no truncation happens and, in theory, also no leakage because of the satisfaction of the periodicity requirement of the FFT process [7]. A rectangular window (also known as "no window") should then be used as weighting.
3) *Window weighting*: when it is not possible to record all the signal time history a window weighting function can be used transforming the time signal, before performing the Fourier Transform, by "smoothing out" the edges of the signal (time signal multiplied by the window function). Window can have different shapes and values ranging from 1 to 0 (at one or both time edges). In the case of impact testing for the input is used a transient window having a value of 1 during the period of contact and 0 elsewhere (e.g. Tukey window). For the output (free decay oscillations) is adopted an exponential window (Eq. 3-116), useful either for too short recording length (i.e. leakage error) or too long recording length (i.e. signal contaminated by noise such as instrument noise, noise-floor, or ambient noise, background noise).

$$w(t) = e^{-\frac{t}{\tau}} \qquad \text{(Eq. 3-116)}$$

DOUBLE HITS AND CLIPPING

Two other possible problems encountered when performing impact testing are double hits and signal overload (also known as clipping). Double hits may happen when the hammer is too heavy or the structure too responsive and cause distortion in the measured FRF. This error cannot be fixed in post-processing and these measurements should be excluded from the data set. One way to check for double impacts is to verify the "flatness" of the input spectrum (no drops greater than 5 ÷10 dB [8]) and the "goodness" of the coherence function.

Clipping instead is a distortion of the registered signal due to saturation (overload) of the dynamic range of the instrumentation used for recording. One way to avoid it is to reduce the impact force or to select another transducer type with a wider dynamic range and/or a higher maximum recordable signal.

SUSPENDED MASS CALIBRATION

The easiest way to calibrate the measurement chain for impact testing is to impact a freely suspended rigid mass of known weight with a mounted accelerometer on it. The measured accelerance FRF should have an amplitude equal to $1/m$ and 0° phase over the entire measurement frequency range.

$$|A(\omega)| = \frac{1}{m} \qquad \Phi_{A(\omega)} = 0° \qquad \forall\omega \qquad \text{(Eq. 3-117)}$$

3.2.6 MULTIPLE-DEGREE-OF-FREEDOM (MDOF) MODELS

Previously we have seen how to study and model the dynamic behaviour of a simple ideal structure which can move only in one direction (single degree of freedom SDOF). Real structures however are formed by many points which can move in multiple directions (multiple degree of freedom MDOF). Now we will see how this observation transfer to the models formerly defined.

ANALYTICAL MODEL (LUMPED PARAMETER MODEL)

A MDOF structure can be modelled in the physical domain as a series of masses connected by a set of springs and dampers, on which act a series of forces (Figure 3-42). Writing down the dynamic equilibrium in the time domain gives a set of coupled differential equations which can be represented using a matrix notation. The coupling indicates that the force acting on a mass may influence all the others and the analysis requires the resolution of the entire system.

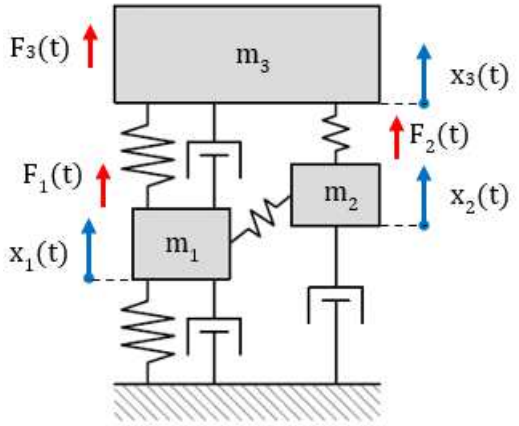

Figure 3-42 Example of a MDOF dynamic system in the physical domain [4]

$$[M]\{\ddot{x}\} + [C]\{\dot{x}\} + [K]\{x\} = \{F\} \quad \text{(Eq. 3-118)}$$

MODAL SPACE MODEL

Replacing the physical coordinates vectors $\{x\}$ in the matrix equation of motion (Eq. 3-118) with the product of the modal matrix $[\Psi]$ (columns equal to the mode shapes vectors) and the modal coordinates $\{q\}$ will give a transformation in a new domain: the modal space.

$$\{x\} = [\Psi]\{q\} \quad \text{(Eq. 3-119)}$$

The transformation into the modal space make the equation of motion to be decoupled and the solution of the entire MDOF system boils down to the solutions of a collection of SDOF models.

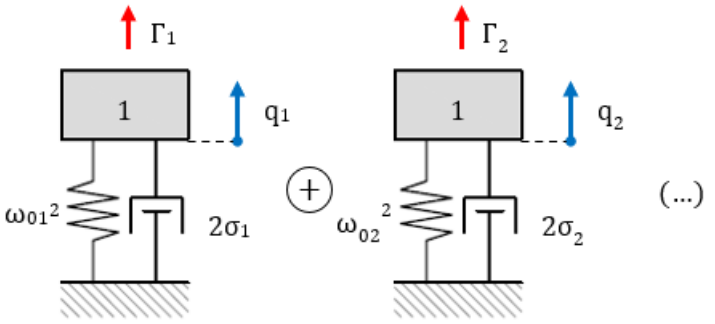

Figure 3-43 MDOF system as a collection of SDOF system in the modal space [4]

$$[I]\{\ddot{q}\} + [2\sigma]\{\dot{q}\} + [\omega_0^2]\{q\} = [\Psi]^T\{F\} = \{\Gamma\} \quad \text{(Eq. 3-120)}$$

$$\begin{cases} \ddot{q}_1 + 2\sigma_1\dot{q}_1 + \omega_{01}^2 q = \Gamma_1 \\ \dots \\ \ddot{q}_n + 2\sigma_n\dot{q}_n + \omega_{0n}^2 q = \Gamma_n \end{cases} \quad \text{(Eq. 3-121)}$$

Every single SDOF model has unit modal mass (assumption), damping equal to the modal damping (half-power bandwidth method), stiffness equal to the square of the undamped natural frequency and is excited by a modal force equal to the scalar product of the mode shape and the physical force vector.

MDOF FRF MODEL

When measuring an FRF on a real structure a degree of freedom (DOF) is defined as a set of measurement point and direction (either for excitation or response). An index i is generally used for the response DOF and an index j for the excitation DOF (x, y , z may be added to specify the measurement direction). The index r instead stands for the specific mode number of the structure.

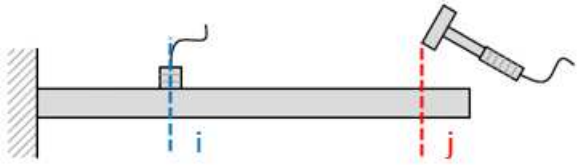

Figure 3-44 Response and excitation DOF for an impact test FRF measurement

$$H_{ij}(\omega) = \sum_{r=1}^{n} H_{ij,r}(\omega) = \sum_{r=1}^{n} \frac{S_{xi,r}(\omega)}{S_{Fj,r}(\omega)} \quad \text{(Eq. 3-122)}$$

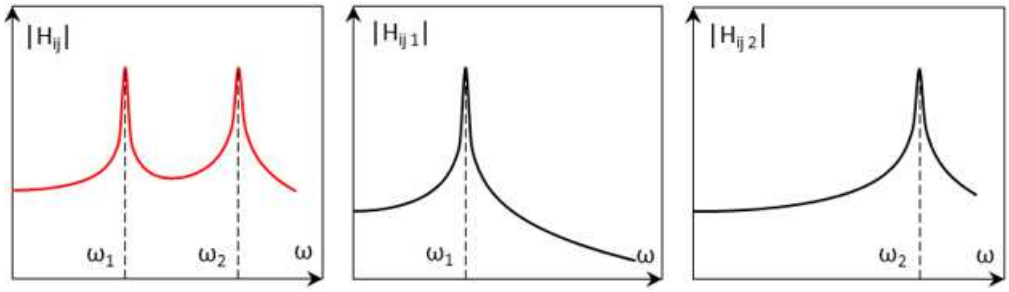

Figure 3-45 MDOF Frequency Response Function decomposed into SDOF models

MDOF MODAL PARAMETER MODEL

The FRF of a MDOF system can be described also in terms of pole locations and residues:

$$H_{ij}(\omega) = \sum_{r=1}^{n} \left(\frac{R_{ij,r}}{i\omega - p_r} + \frac{R^*_{ij,r}}{i\omega - p^*_r} \right) \quad \text{(Eq. 3-123)}$$

It is interesting to note that the pole locations depend only on the mode number r and not on the DOFs ij used for the measurement; hence, modal frequencies and modal damping are *global properties* of the system. Residues instead depends on a particular combination of DOFs and mode number and are *local properties* of the system; choosing as measurement points the nodes of a mode it will not be possible to describe the corresponding mode shapes with the FRF measurement.

In the SDOF part (section 3.2.2)we have said that the residue of the FRF is related to the third modal parameter: the mode shape. The mode shape in simple terms is a deflection pattern associate with a particular frequency (pole location). It is n inherent dynamic property of a structure in free vibration (external forces equal to zero). In theory it is a continuous function but in practice it is sampled with a defined spatial resolution (i.e. number of DOFs used for the measurement) represented in the form of a mode shape vector $\{\Psi\}_r$. The single elements of the vector Ψ_{ir} are complex number describing the magnitude and phase of relative displacements of each DOF.

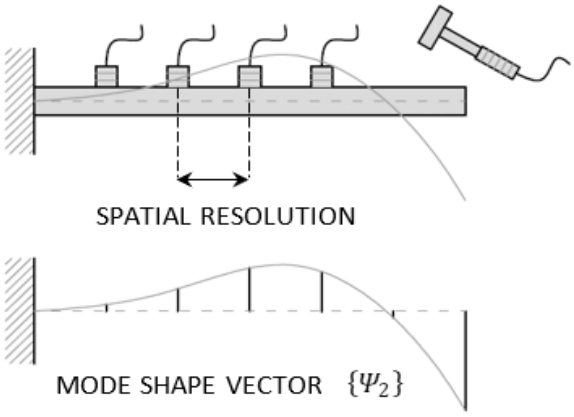

Figure 3-46 Example of Single-Input-Multi-Output impact test to identify a mode shape vector

The relation between *mode shape* and *residue* for a particular mode is a proportion between the residue value and the product of modal displacement $\Psi_{i,r}$ at the response DOF and the modal displacement $\Psi_{j,r}$ at the excitation DOF:

$$R_{ij,r} \propto \Psi_{i,r} \cdot \Psi_{j,r} \quad \text{(Eq. 3-124)}$$

The mode shape vector $\{\Psi\}_r$ describes the relative displacement of each DOF and therefore the form of the deflection but gives no information about the absolute value

of displacement (i.e. scale). The residue on the other hand has a unique value, so we can exploit the relation between residue and mode shape to obtain a definite value for the mode shape itself (i.e. scaling):

$$R_{ij,r} = a_r \Phi_{i,r} \cdot \Phi_{j,r} \quad \text{(Eq. 3-125)}$$

Where a_r is the scaling parameter and $\Phi_{i,r}$ and $\Phi_{j,r}$ the scaled modal displacements. By performing a *driving point* measurement (coincidence of response and excitation DOF) we can obtain the residue $R_{jj,r}$ for each mode:

$$R_{jj,r} = a_r \Phi_{j,r}^2 \quad \text{(Eq. 3-126)}$$

The value of the constant a_r can be calculated assuming a *unit modal mass scaling*. The modal mass for a MDOF system is a quantity defined as:

$$M_r = \{\Phi\}_r^T [M] \{\Phi\}_r \quad \text{(Eq. 3-127)}$$

For a simple SDOF system it can be written:

$$M = \Phi m \Phi \quad \text{(Eq. 3-128)}$$

$$R = \frac{1}{2i\omega_D m} = a\Phi\Phi \quad \rightarrow \quad a = \frac{1}{2i\omega_D M} \quad \text{(Eq. 3-129)}$$

And for a MDOF system assuming a unit modal mass scaling (i.e. $M_r = 1$):

$$a_r = \frac{1}{2i\omega_{D,r}} \quad \text{(Eq. 3-130)}$$

The scaled excitation modal displacements can then be evaluated and, performing transfer FRF measurements, also the scaled values of response modal displacement are obtained.

3.2.7 ASSUMPTIONS OF MODAL DESCRIPTION

The main assumption we have to make to describe the dynamic behaviour of a structure with a modal model is the *linearity* of the system. This implies:

- *Superposition*: measured FRFs are independent on the type of excitation used to measure them (e.g. random excitation, sweep sine, impact testing).
- *Homogeneity*: measured FRFs are independent on the excitation level, provided that this not exceed the instrumentation dynamic range (i.e. clipping).
- *Reciprocity*: measured FRFs between two points are independent on which of the point is used as excitation DOF or response DOF (Maxwell reciprocity theorem).

Other assumptions often overlooked are:

- *Causality*: the structure will not vibrate unless previously excited.
- *Stability*: after the excitation is removed the vibration will progressively die out.
- *Time-invariance*: the dynamic characteristic of the system (m, c and k) are constant over time.

3.2.8 MOBILITY MATRIX AND MEASUREMENT DOFS

The mobility matrix $[H]$ is the matrix that contains all the FRF measurements $H_{ij}(\omega)$ performed for the DOFs of interest. Each column of the matrix contains FRFs with common excitation DOF, each row of the matrix contains FRFs with common response DOF. The diagonal elements are called *Driving Point FRFs* whereas the off-diagonal elements are termed *Transfer FRFs*.

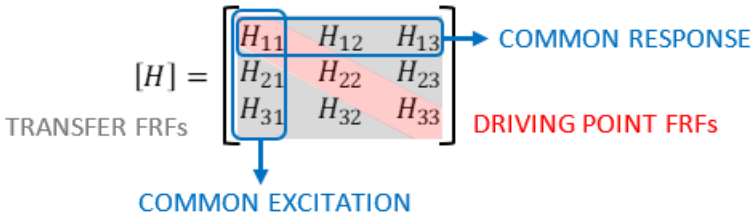

Figure 3-47 Definition of the mobility matrix and usual terminology

For n defined DOFs the number of elements of the mobility matrix (i.e. input/output combinations) are n x n. Reciprocity implies that the mobility matrix is symmetric ($H_{ij} = H_{ji}$) reducing the number of measurements needed to define it. There can be two alternative ways to determine the mobility matrix (Figure 3-48):

- *Roving excitation* (also known as roving hammer method): with a single accelerometer this allows to define a single row of the mobility matrix.
- *Roving response* (also known as roving accelerometer method): with a common excitation source (shaker or impact hammer) allows to define a column of the mobility matrix.

Performing an impact test with a single-input-multi-output (SIMO) technique and the roving hammer method enables to define the complete mobility matrix (in the direction selected for impact and accelerometers mounting). The number of DOFs required for a measurement generally depends on the purpose of the test, the geometry of the structure and the number of modes expected in the frequency range of interest.

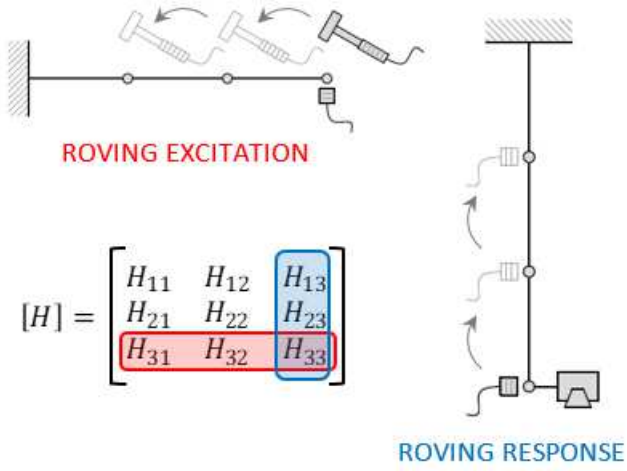

Figure 3-48 Roving excitation and roving response method to determine the mobility matrix [7]

3.2.9 PARAMETER ESTIMATION FROM FRF MEASUREMENT

Before talking of parameter extraction from experimental measurement we have to introduce the concept of *modal coupling*. Modal coupling indicates how much the response of a mode, at its specific modal frequency, is influenced by the other modes of the structure. There may be two extreme possibilities:

- *Lightly coupled modes*: simple structure with low damping will exhibit well distinct and separated modes and each of them may be treated as a SDOF system.
- *Heavily coupled modes*: complex structure with high value of damping or high modal density will not exhibit clearly distinguishable modes and the response of the structure at a particular modal frequency will be a combination of different modes.

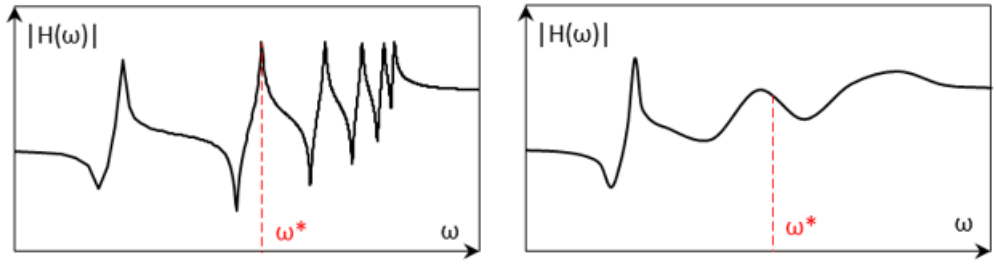

Figure 3-49 FRF examples of lightly coupled mode and heavily coupled modes

For a simple structure with lightly coupled modes the parameter estimation from FRF measurement is quite straightforward since every mode can be treated as a SDOF system:

- *Modal frequencies* can be determined with the *Peak Picking method*: every peak in the FRF corresponds to a natural frequency of the structure.
- *Modal dampings* can be determined via two alternative techniques:
    1) *Half power bandwidth method*: the modal damping is determined as half the frequency bandwidth obtained by descending of a 3 dB value (i.e. halving the power) from the FRF magnitude peak. Due to the discrete resolution in frequency and the generally narrow nature of FRF peaks, a zoom analysis (only available using shaker excitation) may be needed to obtain accurate results.
    2) *Decay rate of impulse response*: another viable solution to estimate the modal damping is to isolate a single mode in the frequency domain by using a band pass filter. The impulse response of the single mode can be determined by an Inverse Fourier Transform (IFT) and the envelope of the time signal can be determined by means of a Hilbert Transform [9]. The modal damping can be calculated as the reciprocal of the decay time ($\sigma = 1/\tau$) where the decay time τ is taken as the time for the impulse response magnitude to decay of an 8.7 dB value.

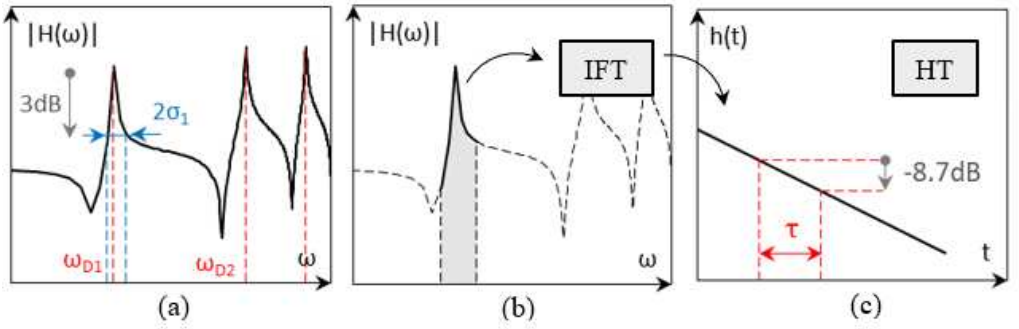

Figure 3-50 (a) Peak picking method and half-power bandwidth method for pole location extraction (b) Zoom analysis and IFT to estimate modal damping (c) Hilbert Transform of impulse response plot on a logarithmic vertical axis

- *Mode shapes* can be determined from multiple FRF measurements via the *Quadrature Picking method*. Previously (section 3.2.2), we have seen that the magnitude of the Compliance FRF at a modal frequency is almost equal to the ratio of the residue and the modal damping:

$$H(\omega_{D,r}) \cong \frac{R_{ij,r}}{\sigma_r} \quad \text{(Eq. 3-131)}$$

Since all FRF measurements are generally taken with accelerometers we have to double differentiate over time to get an Accelerance FRF (double multiplication for $i\omega_{D,r}$):

$$A(\omega_{D,r}) \cong \frac{R_{ij,r}}{\sigma_r}(-\omega_{D,r}^2) \quad \text{(Eq. 3-132)}$$

Substituting the relation of the residue with the scaled modal displacement values assuming unit modal mass it becomes:

$$R_{ij,r} = \frac{\Phi_{i,r} \cdot \Phi_{j,r}}{2i\omega_{D,r}} \quad \text{(Eq. 3-133)}$$

$$A(\omega_{D,r}) \cong \frac{\Phi_{i,r} \cdot \Phi_{j,r}}{2i\omega_{D,r}\sigma_r}(i^2\omega_{D,r}^2) = i\frac{\Phi_{i,r} \cdot \Phi_{j,r}}{2\sigma_r}\omega_{D,r} \quad \text{(Eq. 3-134)}$$

This relation says that the accelerance FRF is purely imaginary at the modal frequencies, its amplitude is proportional to the modal displacement and its sign is positive if the displacement is in phase with the excitation. So, the imaginary part of the FRF can be picked at the modal frequencies representing the modal displacement for the specified DOF. Using a *waterfall representation* (i.e. plotting imaginary parts of the FRFs in series with the measurement locations) a sampled version of the mode shape can be extracted [7].

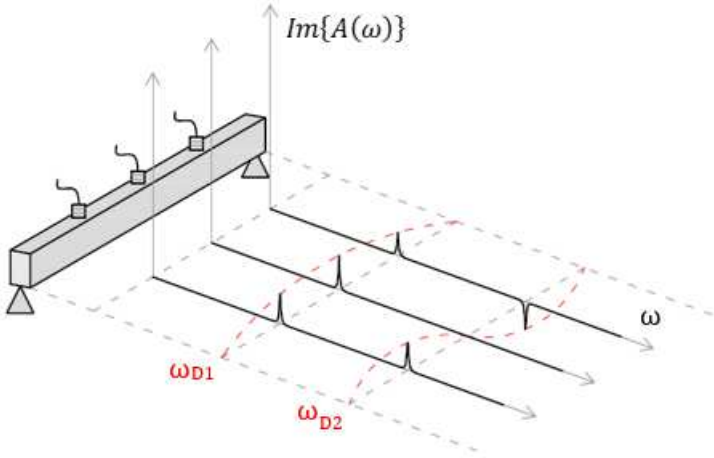

Figure 3-51 Waterfall representation of the mode shapes of a simply supported beam [7]

3.2.10 PARAMETER ESTIMATION BY CURVE-FITTING

When studying complex structures with heavily coupled modes and/or with noise contamination in the measurement the formerly described procedure is no more suitable to extract the modal parameters of the structure and *Curve-fitting techniques*, with the aid of numerical analysis, should be adopted. Curve-fitting in a general sense is the practice to determine the parameters of a certain analytical curve which have the best fit to the measured data (e.g. method of the least squares).

Before describing the Curve-fitting procedure [10] it must be said that any parameter estimation should be based on sound data and that no curve-fitter algorithm could assure a reliable parameter extraction from poor measurements (principle of "*gold-in gold-out*" [4]).

MODAL CURVE-FITTING PROCESS

1) *Selection of FRFs, frequency range and number of modes*:
   The user should choose the measurement DOFs to make the estimate, the frequency range of interest and the maximum number of modes that the algorithm will use to fit the data
2) *Selection of Curve-Fitter*:
   The user should also choose the type of algorithm to use for estimating the pole locations (modal frequencies and modal dampings) and the residues (mode shapes).
   Curve-fitters can be classified as *local* or *global* curve-fitters. The firsts fit the pole locations to one, or few, FRF measurement. The second estimate the pole locations from all the FRF measurements using a least squares method. Residues are then fitted locally to each FRF for both types.
3) *Stabilization Diagram*:
   The stabilization diagram is used to identify the real modes of the structure from the pole locations and residues estimation and edit out the computational modes. The stabilization diagram is generally displayed as an FRF magnitude plot with an additional vertical axis indicating the modal order used by the curve-fitter to extract the modal data. On the rows corresponding to the modal order number, and located in correspondence of the specific frequency, are plotted a series of symbols indicating the estimated mode and the stability of the mode compared to a previous step in the curve-fitting procedure (i.e. the previous row in the modal order axis)

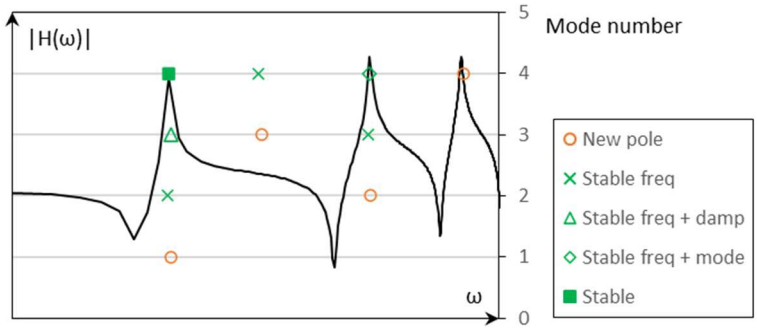

Figure 3-52 Example of a stabilization diagram used during the curve-fitting process

The tolerances for the stability criterion may be set by the operator. Typical values are: 2% for mode shape, 1% for frequency and 5% for damping.

4) *Modal Synthesis*:
When a set of stable modes is selected by the operator through the stabilization diagram, the next step is to validate the estimated modal model. Modal synthesis is used to check if there are any missing modes in the estimation process. This is done by performing an "actual curve-fitting" comparing the measured FRF with a synthetised FRF (calculated with the stable pole locations and residues values) and searching for the higher possible correlation between the two.

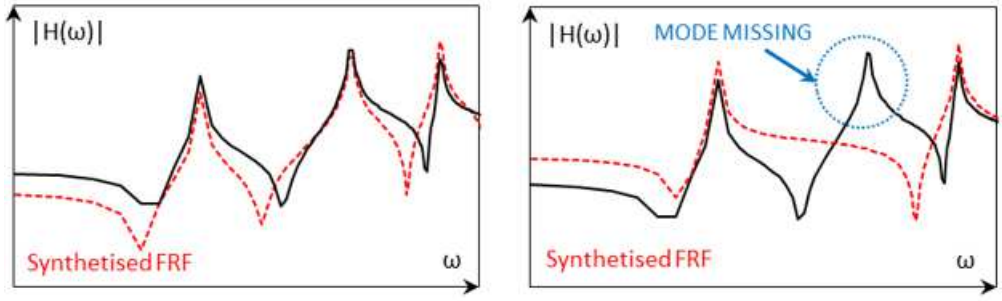

Figure 3-53 Example of modal synthesis to identify possible missing modes

5) *Modal Assurance Criterion (MAC)*:
On the other hand, to check if too many modes were selected from the stabilization diagram one can use the Modal Assurance Criterion (MAC) [11]. This implies the calculation of a MAC matrix whose values are defined as:

$$MAC(\{\Phi_r\},\{\Phi_s\}) = \frac{|\{\Phi_r\}^{*T}\{\Phi_s\}|^2}{(\{\Phi_r\}^{*T}\{\Phi_r\})(\{\Phi_s\}^{*T}\{\Phi_s\})} \quad \text{(Eq. 3-135)}$$

The MAC value is essentially the normalised scalar product of the complex modal vector (of two modes) at each common node. In simple terms it assesses the degree of similarity between two modes: if two modes are very similar the MAC value will be closer to one, if are very different it will have value closer to zero. Usually, the MAC matrix is presented adopting a "*Manhattan display*", a 3D histogram plot where the planar axes indicate the mode under comparison and the height of the columns is scale with the calculated MAC value. A "good" MAC matrix will exhibit values closer to one on the diagonal while the off-diagonal elements will be closer to zero.

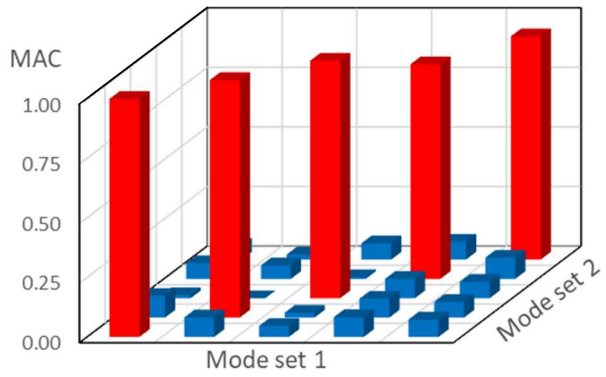

Figure 3-54 Example of MAC matrix Manhattan display for 5 mode shapes

MAC analysis can be performed in two alternatives ways: *Auto-MAC* analysis and *Cross-MAC* analysis. In the first one the mode shapes set of a certain model is compared to itself, in the latter is compared to a set of a different modal model. Examples of MAC analysis are:

- *Auto-MAC (measurement-measurement)*: performing an Auto-MAC analysis can be a viable method to detect problems in the measurement DOFs grid selection (i.e. spatial aliasing). If the response DOFs are placed on the nodes of two different mode shapes, these will have identical values equal to zero and the Auto-MAC matrix will exhibit off-diagonal elements closer to one.
- *Cross-MAC (measurement-synthetised)*: as mentioned before, comparing the mode shapes of a measured FRF and a synthetised FRF with a Cross-MAC analysis can reveal if too many modes were selected during the curve-fitting process.
- *Cross-MAC (numerical-numerical)*: the Cross-MAC analysis on a certain numerical modal model (typically using the FEM method) may be used to perform *sensitivity analysis* on the structure mode shapes

varying certain input variables (e.g. material properties, boundary conditions, etc.).

6) *Mode Indicator Function (MIF)*:
If a real structure exhibit two distinct (real) modes at the same frequency, the *Mode Indicator Function* (MIF) can be used to detect them [12]. There are different types of MIF developed through the years, here will be reported a brief description of two of them: the *Multivariate Mode Indicator Function* (MMIF) and the *Complex Mode Indicator Function* (CMIF).
The first is based on the definition of the Mode Indicator Function as the real part of the FRF divided by the magnitude of the FRF; since the FRF is purely imaginary in correspondence of a resonance frequency the MIF value will drop to zero at that frequency. The Multivariate MIF extend this analysis to multiple referenced FRF data (i.e. multiple rows or columns of the mobility matrix): each reference DOF will have a MIF and if two or more MIFs drop to zero at the same frequency this suggests the presence of two or more closely spaced modes. The Complex Mode Indicator Function (CMIF) does a similar job to the MMIF but it is more suited when there is distortion in the signal or there are complex modes (i.e. real part of the FRF different from zero at the resonant frequency). It is based on the Singular Value Decomposition (SVD) of the FRF matrix [13]; operatively, for a multiple referenced FRF measurement there are as many CMIFs as the measurement references: if these CMIFs peaks at a similar value of frequency this indicates the presence of multiple repeated modes.

3.3 REFERENCES

[1] F. Fahy and P. Gardonio, “Sound and structural vibration – Radiation, transmission and response” 2nd ed., Oxford: Academic Press, 2007.

[2] J. Torres-Romero, W. Cardenas, J. Carbajo, E. G. Segovia Eulogio and J. Ramis-Soriano, “An experimental approach to vibro-acoustic study of beam-type structures” *Archives of Acoustics*, vol. 43, no. 2, pp. 283-295, 2018.

[3] O. Døssing “Structural testing. Part 1. Mechanical mobility measurements” Bruel & Kjaer, Naerum, Denmark, 1988.

[4] O. Døssing “Structural testing. Part 2. Modal analysis and simulation” Bruel & Kjaer, Naerum, Denmark, 1988.

[5] S. Beskhyroun “Graphical interface toolbox for modal analysis” Proceedings of the 9th Pacific Conference on Earthquake Engineering, Auckland, New Zealand, 2011.

[6] Siemens Digital Industries Software, “The FRF and its many forms” [Online]. Available: https://community.sw.siemens.com/s/article/dynamic-stiffness-compliance-mobility-and-more [Accessed: 20 Apr. 2020]

[7] P. Avitable “Experimental modal analysis – A simple non-mathematical presentation” *Sound and Vibration*, vol. 35, pp. 20-31, 2001.
[8] P. Avitable “Beware of these Top-10 issues in modal testing” *Sound and Vibration*, vol. 51, no. 1, pp. 48-53, 2017.
[9] Bruel & Kjaer, Appl. Note “Practical use of the Hilbert Transform”.
[10] Siemens Digital Industries Software, “Getting started with modal curve fitting” [Online]. Available: https://community.sw.siemens.com/s/article/getting-started-with-modal-curvefitting [Accessed: 20 Apr. 2020]
[11] Siemens Digital Industries Software, “Modal Assurance Criterion (MAC)” [Online]. Available: https://community.sw.siemens.com/s/article/modal-assurance-criterion-mac [Accessed: 20 Apr. 2020]
[12] Peter Avitabile “Modal space: What is the difference between all the mode indicator function? What do they all do?” *Experimental Techniques*, vol. 31, no. 2, pp. 15-16, 2007.
[13] Peter Avitabile “Can you explain the Complex Mode Indicator Function (CMIF) again? What are these crossover frequencies?” *Experimental Techniques*, vol. 37, no. 2, pp. 3-5, 2013.

4 PROPOSED ACOUSTIC TIMBER ASSESSMENT METHOD

4.1 TAPPING (SOUNDING) METHOD IN LITERATURE

In the group of stress-wave based method for the assessment of existing timber structures can be included also the tapping (sounding) method. This was not reported in the list drafted in Chapter 2 State-of-the-art on timber structure assessment methods since it lacks the results reproducibility, objectivity, and measurable information to be fully considered as a wood diagnostic technique. Nonetheless, it is cited as a viable method for a rough evaluation of the element condition (location and sizing of decayed zone/hollow parts) especially in the early stage of the survey ([1] and [2]).

Table 4-1 Features of the tapping (sounding) method as reported in the COST action E55 guidelines "Assessment of timber structures" [1]

Method	Tapping (sounding)	*Frequency of application*	Frequent (Phase I)
Type	Acoustic; on-site; non-destructive	*Extent of assessment*	Local
Validity of results	Limited (qualitative; depending on experience)	*Expenditure of time/cost*	Low/Low
Constraints	Limited, qualitative information; not reproducible; interpretation of results depends on experience		

The method itself is quite simple: the surface of the timber element is beaten with a blunt object (e.g. hammer or small mallet) and the sound radiation, or differences in sound radiation, is used to make estimates about the element internal conditions. Tapping provides qualitative information about the extension of decay from fungi or insects and about the location and sizing of hollow parts. It allows a rapid screening of

the element but is also strongly dependant on the experience of the inspector and results may vary between different operators (not reproducible). In addition, interpretation of the results may be complicated by other factors affecting sound quality other then decay and usually only advanced stage of decay can be discerned by interpreting the impact sound radiation.

4.2 PROPOSED IMPROVEMENT FOR THE TAPPING METHOD – THEORETICAL BACKGROUND

In an attempt to improve the tapping (sounding) method, the advantages and disadvantages of the method were considered, trying to provide solutions for the main drawbacks of the technique while maintaining its strengths. The main advantages are:

- High cost-effectiveness.
- High measurement and analysis speed.
- Relatively local information, useful to detect critical area.

All these qualities make the tapping method an ideal solution for the preliminary survey of an existing timber structures. The main disadvantages instead are:

- Qualitative information, there are not any actually measured quantities.
- Subjectivity, results are not reproducible and can vary between different inspectors.
- Difficult interpretation of the results, depending on the experience of the inspector.

To solve part of the problems two main changes to the method are proposed:

1) *Objective and measurable data*: sound radiation can be recorded by using microphone sensors. To maintain the characteristics of low expenditure of time and cost of the tapping method smartphone built-in microphones are proposed to carry out the measurement.
2) *Post-processing and interpretation of the results*: as reported by Dackermann et al. [2]*"Changes in the tone of the sound resulting from the impact indicate different properties of the wood and can be discerned by individuals with a moderate level of experience."* These differences in sound tone and timbre can be theoretically discerned by analysing the spectral components of the sound recordings, namely performing a Fourier Transform (or other alternative frequency transform) to study the signal energy distribution over the frequency domain.

4.2.1 BASICS OF ACOUSTIC

PHYSICS OF SOUND WAVES IN AIR

In the field of acoustic, sound is defined as a variation from the equilibrium atmospheric pressure due to the propagation of longitudinal wave in air (for more detail see Chapter 3 Theoretical basis of wave propagation and structural vibration This variation from the mean atmospheric pressure is known as acoustic pressure:

$$p_{acoustic} = p_{tot} - \bar{p}_{atm} \quad \text{(Eq. 4-1)}$$

Due to its oscillatory nature, sound can be studied using an elementary sinusoidal waveform (pure tone):

$$p(t) = A \cdot \sin(2\pi \cdot f \cdot t) \quad \text{(Eq. 4-2)}$$

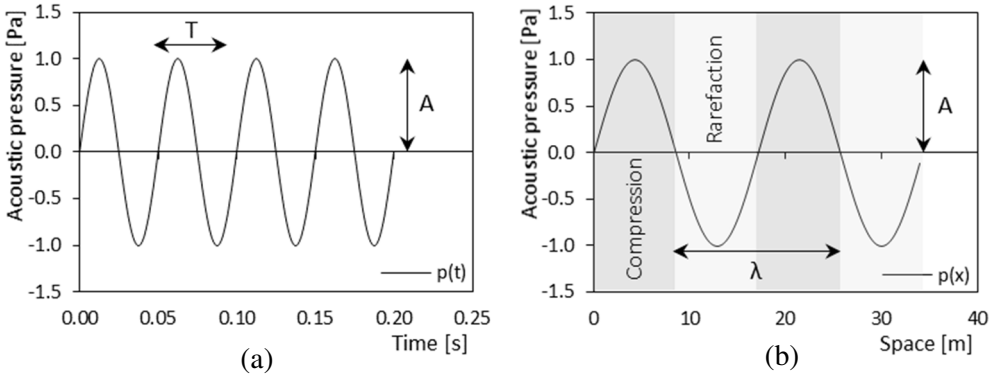

Figure 4-1 Representation of a 20 Hz pure tone acoustic wave in the time domain (a) and in the space domain (b)

Where:

- A is the amplitude of the acoustic pressure measured in Pascal [Pa] which can be described using the maximum value p_{max} or the Root Mean Square (RMS) value p_{rms} calculated as the square root of the averaged squared amplitudes of the period under consideration (for sinusoidal wave $p_{rms} \cong 0.707 \cdot p_{max}$).
- f is the frequency measured in Hertz [Hz], representing the number of pressure variations per unit time (seconds).
- $T = 1/f$ is the period, namely the time taken to complete one cycle of the acoustic wave, measured in seconds [s].

- $\lambda = c/f$ is the wavelength, namely the distance travelled by the acoustic wave during a single cycle, measured in meters [m].
- c is the speed of sound propagation in air. Since sound waves in fluids are non-dispersive this represent either the phase speed and the group speed of the propagating waves (see Chapter 3 Theoretical basis of wave propagation and structural vibration).

It is worth remembering that the speed of sound is related to the wave propagation (sequence of compression and rarefaction zones); sound waves transfer energy and not matter: the mean air particles velocity is equal to zero. The speed of sound in air depends on the ambient pressure and temperature. At 20° C and 1 atmosphere pressure the speed of sound is equal to 343 m/s. For varying temperature, the speed of sound can be calculated as [3]:

$$c = 332 + 0.6 \cdot T_{Celsius} \quad \text{(Eq. 4-3)}$$

Or alternatively using the equation of state for gases [3]:

$$c = \sqrt{\frac{\gamma R T_{Kelvin}}{M}} \quad \text{(Eq. 4-4)}$$

Where γ is the ratio of specific heats ($\gamma = 1.402$ for air), R is the universal gas constant ($R = 8.314\ J/\ (°K \cdot mole)$), T_{Kelvin} is the temperature expressed in Kelvin degrees and M is the molecular weight ($M = 0.029\ kg/mole$).

What is perceived as sound by human are acoustic pressure wave in the frequency range between 20 Hz and 20.000 Hz. Using the speed of sound for air at 20° C the relation between frequencies and wavelengths can be derived (Table 4-2).

Table 4-2 Relationship between frequencies and wavelengths in air

Frequency [Hz]	Wavelength [m]
20	17
1000	0.34
10000	0.034
20000	0.017

The description of a sound wave reported in (Eq. 4-2) and Figure 4-1 is valid for a pure tone monochromatic sound, that is a sound composed by a single frequency component and therefore a perfect sinusoidal waveform. However, sound usually can have more than a single frequency component ranging from pure tone polychromatic sound (signal

composed by a limited number of frequency components), complex sound (the frequency content is comprised inside specific frequency intervals named frequency bands) and noise (frequency content spread across a wide range of values).

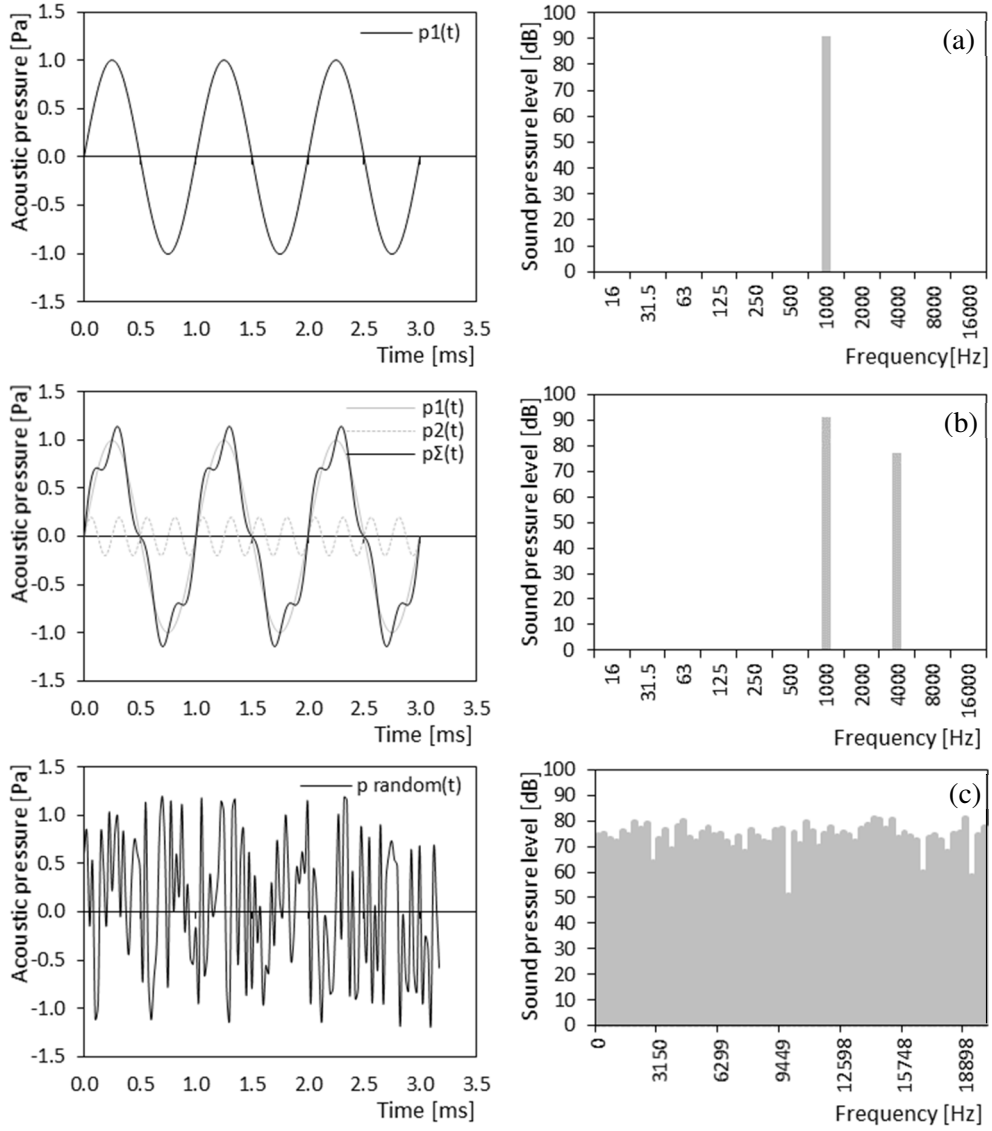

Figure 4-2 Time domain and frequency domain representations of a pure monochromatic tone (a), a pure polychromatic tone (b) and noise (c)

The frequency content analysis can be performed by using specific mathematical algorithm (e.g. Fourier Transform, more details at section 4.2.3 Data post-processing and audio features extraction) to pass from the time domain of the signal to the

frequency domain of the signal, generally called also as spectrum of the signal. An example of frequency content analysis is reported in Figure 4-2; more detail about frequency analysis will be reported in section 4.2.3 Data post-processing and audio features extraction.

QUANTIFICATION OF SOUND

Sound is a physical quantity that can be described by using three main measures ([3], [4] and [5]):

- *Sound power*: is a scalar quantity that represents the total acoustic power (rate of acoustic energy emitted for unit time) radiated by a source, measured in Watts [W].
- *Sound intensity*: is a vector quantity that represents the sound energy flowing through a specified area, measured in Watts per square meter [W/m^2].
- *Sound pressure*: is a scalar, root-power quantity (i.e. proportional to power when squared [4]) that represents the difference between the pressure caused by the sound wave propagation and the initial static equilibrium pressure of air. It is measured in Pascal [Pa].

A useful analogy for explaining sound power, sound intensity and sound pressure is the heater analogy [5], showing the similarities between heat and sound propagation as reported in Table 4-3.

Table 4-3 Heater analogy

Heater	Sound source
Heater power [W]	Sound power [W]
Heat flow [W/m^2]	Sound intensity [W/m^2]
Temperature [°C]	Sound pressure [Pa]

For definition sound intensity can be seen as:

$$I = \frac{dW}{dA} \qquad \text{(Eq. 4-5)}$$

In a free field environment (i.e. no reflected sound waves) and for plane propagating sound wave, sound intensity can be related to the root mean square sound pressure with the relation:

$$I = p_{rms} \cdot v = \frac{p_{rms}^2}{\rho \cdot c} \qquad \text{(Eq. 4-6)}$$

Where the quantity at the denominator $\rho \cdot c$ is called the specific acoustic impedance, which represents the opposition of the medium to the acoustic flow resulting from the applied acoustic pressure. The specific acoustic impedance is measured in Rayleigh [Rayl] equal to [(Pa · s)/m]; for air at 20° C and 1 atmosphere the specific acoustic impedance is equal to 414 Rayleigh. The sound power emitted by a source can be obtained by integrating the sound intensity over a surface surrounding the source:

$$W = \int_A I \cdot \hat{n}\, dA \qquad \text{(Eq. 4-7)}$$

Where the integrand is the scalar product of the sound intensity vector and the surface normal unit vector. For punctual sound source a spherical surface is usually adopted leading to:

$$W = 4\pi r^2 \cdot I \qquad \text{(Eq. 4-8)}$$

Where the magnitude of the acoustic impedance I is measured at a distance r from the sound source.

SOUND LEVELS AND DECIBEL SCALE

The range of measurable sound power, intensity and pressure can be quite large. For example, the human ear can perceive sound pressure from a minimum value of 20 μPa to a maximum value of 20 Pa. This wide range of measures (six order of magnitude) implies that a linear scale would not be the best fit to represents the acoustic quantities since the human brain is not able to distinguish all its different values. For this reason, it was introduced the Bel scale, which measures the sound level as the logarithm of the ratio of the measured quantity to a minimum reference value. To adjust the scale to the sensibility level of the human ear, a factor of ten is ante posed to the Bel value leading to the well-known definition of decibel [dB].

$$L_p = 10 \cdot \log_{10}\left(\frac{p_{rms}^2}{p_{ref}^2}\right) = 20 \cdot \log_{10}\left(\frac{p_{rms}}{p_{ref}}\right) \qquad \text{(Eq. 4-9)}$$

The quantity L_p is called Sound Pressure Level (SPL) and the reference value p_{ref} is generally fixed at 20 μPa for a pure tone at 1000 Hz, which represents the mean audibility threshold for a healthy individual. In the same way can be defined the Sound Intensity Level (SIL) L_I and the Sound Power Level (SWL) L_W:

$$L_I = 10 \cdot \log_{10}\left(\frac{I}{I_{ref}}\right) \qquad \text{(Eq. 4-10)}$$

$$L_W = 10 \cdot \log_{10}\left(\frac{W}{W_{ref}}\right) \quad \text{(Eq. 4-11)}$$

Where the reference values for sound power and sound intensity are taken equal to 1 pW (10^{-12} W) and 1 pW/m^2.

Table 4-4 Examples of sound power, sound pressure and sound decibel levels [4]

Sound source	P [W]	p [Pa]	Sound level* [dB]
Jet engine	10000	2000	160
Rifle shot	100	200	140
Pneumatic hammer (threshold of pain)	1	20	120
Outboard motor	10^{-2}	2	100
Street traffic	10^{-4}	0.2	80
Normal talk	10^{-6}	0.02	60
Library	10^{-8}	0.002	40
Whisper	10^{-10}	0.0002	20
Audibility threshold	10^{-12}	0.00002	0

* Equal for sound power, intensity, and pressure

Due to the different multiplying factor of the logarithm the relation between the decibel scale and the linear scale are different for the sound pressure with respect to sound intensity and power: doubling the sound pressure implies an increase of 6 dB ($\cong 20 \cdot \log_{10} 2$) in sound pressure level whereas doubling sound power implies an increase of 3 dB ($\cong 10 \cdot \log_{10} 2$) in sound power level. When performing mathematical operation with sound level is important to remember the logarithmic nature of the decibel scale, for example for addition and subtraction:

$$L_{p\,tot} = 10 \cdot \log_{10}\left(10^{\frac{L_{p1}}{10}} + 10^{\frac{L_{p2}}{10}} + \cdots + 10^{\frac{L_{pn}}{10}}\right) \quad \text{(Eq. 4-12)}$$

$$L_{p\,tot} = 10 \cdot \log_{10}\left(10^{\frac{L_{p1}}{10}} - 10^{\frac{L_{p2}}{10}} - \cdots - 10^{\frac{L_{pn}}{10}}\right) \quad \text{(Eq. 4-13)}$$

Inverse square law (1/r^2) [4]: assuming a point sound source positioned mid-air, its sound energy will spread over an increasing larger spherical surface. Since the sphere surface area is equal to $4\pi r^2$, the total surface will increase by a factor of 4 each time the distance r from the source is doubled. Therefore, assuming a constant sound source

power, the sound intensity will decrease by a factor of 4 each time the distance from the source is doubled. In decibel scale this is equal to a decrease of 6 dB ($\cong 10 \cdot \log_{10} 4$).

Inverse distance law (1/r) [4]: sound pressure is inversely proportional to the distance r from the sound source. Every time the distance from the sound source is doubled the sound pressure is halved. In decibel scale this is equal to a decrease of 6 dB ($\cong 20 \cdot \log_{10} 2$).

SOUND FIELDS

According to the Merriam-Webster dictionary, sound field is *"a region in a material medium in which sound waves are being propagated"*. So, sound field is used to describe the relationship between sound (energy) propagation and the geometry of the surrounding environment. There are five main sound field definitions ([3] and [6]) that are worth to be reported in this short overview: free field, near and far field, direct and diffuse (or reverberant) field.

- *Free field*: defines a region in space where sound can propagate without any impediment (e.g. outdoor, open field).
- *Near field*: is a region in space close to the sound source (usually within about two wavelengths). Sound pressure and acoustic particle velocity are not in phase. The sound field does not decrease of 6 dB each time that the distance from the sound source is doubled (Inverse distance law).
- *Far field*: begins where the near field ends (considering also a small transition zone) and goes to infinity. Sound field respond to the 6 dB rule: either sound intensity (inverse square law) and sound pressure (inverse distance law) decrease of 6 dB when the distance from the sound source is doubled.
- *Direct field*: is a region in space where the measured sound can be attributed mainly to the sound source with no or limited reflections from surrounding surfaces (e.g. indoor, close to the noise source).
- *Diffuse field*: also called reverberant field, is a region in space where reflected sound dominates. Sound pressure and particle velocity are not in phase, sound intensity is equal to zero and sound appears to have no source.

REFLECTION EFFECTS

In a free field environment, a point sound source will propagate sound energy uniformly in all directions. However typical encountered sound sources are directional, meaning that they radiate more sound energy in certain directions. To account for that a directivity factor can be defined, describing the angular dependence of sound intensity [3]. This is defined as the ratio of the sound intensity I_θ in a certain direction θ and the sound intensity I_0 of an omnidirectional sound source:

$$Q_\theta = \frac{I_\theta}{I_0} \quad \text{(Eq. 4-14)}$$

From the directivity factor can be derived the directivity index that can be summated to the specific sound power level of the sound source to obtain the total resultant sound power level:

$$DI = 10 \log_{10} Q_\theta \quad \text{(Eq. 4-15)}$$

$$L_{w\,tot} = L_w + DI \quad \text{(Eq. 4-16)}$$

Table 4-5 Directivity factors and indexes for a simple source near reflecting surfaces [3]

Situation	Q_θ	DI
Free space (omnidirectional)	1	0 dB
Centred in a large flat surface	2	3 dB
Centred at the edge of two large flat surface	4	6 dB
Centred at the corner of three large flat surface	8	9 dB

4.2.2 SOUND RECORDING USING MICROPHONE

PSYCHO-ACOUSTICS

The subjectivity of the tapping method depends not only in the different interpretation of the impact sound radiation by different inspectors but also on the different perception of sound among different person. The branch of science that studies the perception of sound and auditory physiology is known as psycho-acoustic and is based heavily on human anatomy ([3] and [7]). Some of the main concept of psycho-acoustics are reported below to understand how sound evaluation can be used for the assessment of timber elements and identify what can be the limitations of the tapping method due to human sound perception.

- *Loudness*: the human ear is able to detect sound in the frequency range of 20 Hz and 20 kHz and sound pressure level in the range of 0 dB (threshold of hearing) and 120 dB (threshold of pain). However, due to the anatomy of human ear, the perceived sound intensity is not constant across all the frequency spectrum. For this reason, it was introduced the concept of loudness (i.e. subjective perception of sound pressure) and the isophonic curve were standardised from experimental measurements on a representative sample of human population. Loudness is measured in phon, which is a decibel quantity

that matches the physical sound pressure level for a pure tone of 1 kHz (alternatively it is used the sone unit, which is a linear scale quantity linked to the phon value).

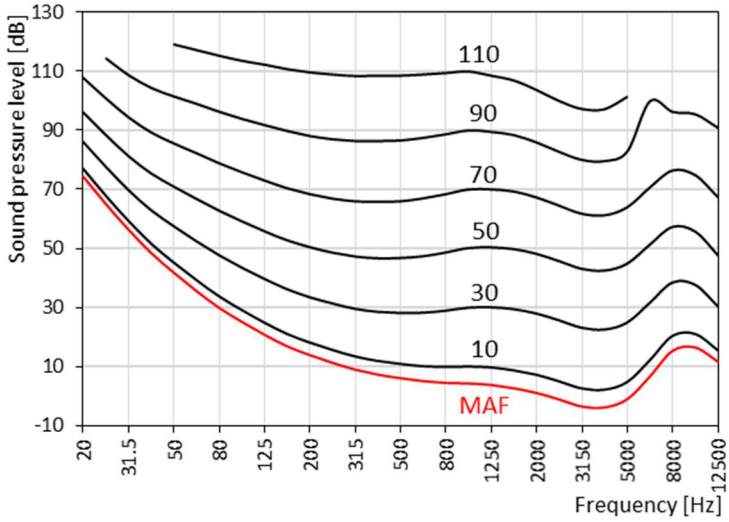

Figure 4-3 Isophonic curves according to the standard EN ISO 266 [8]. The lower curve represents the average threshold of hearing (Minimum Audible Field MAF)

- *Auditory masking*: is a concept that indicates how the perception of a sound can be affected by the presence of another sound. Two main types of making can be distinguished: temporal masking and frequency (or spectral) masking. Temporal masking is also known as non-simultaneous masking and indicates the masking effect of a sudden sound that makes inaudible other sounds preceding or following it. Spectral masking on the other hand is called also simultaneous masking and specifies how much a tone should be louder with respect to adjacent frequency components of a concurrent sound, or background noise, in order to be perceived [9]. Spectral masking is related also to the concept of auditory critical bands.
- *Critical bands*: the human ear can sense sound in the frequency range of 20 Hz and 20 kHz but, such as for the perception of sound pressure levels, the ability to distinguish different tones is not linear and varies with frequency [10]. Usually, the ear can discern more easily a small change in frequency between two tones in the low frequency domain with respect to the high frequency domain. This lead to the definition of critical bands (known also as bark scale), which roughly indicate the audio frequency ranges where a second tone can interfere with the first one via spectral masking. The scale of the critical bands,

which starts linear in the low frequencies and becomes logarithmic in the high frequencies, is related to the logarithmic spiral shape of the cochlea, the hearing organ within the inner ear.

Table 4-6 Critical bands (bark scale) of human hearing [10]

Critical band (bark)	Centre frequency [Hz]	Bandwidth [Hz]
1	60	80
2	150	100
3	250	100
4	350	100
5	450	110
6	570	120
7	700	140
8	840	150
9	1000	160
10	1170	190
11	1370	210
12	1600	240
13	1850	280
14	2150	320
15	2500	380
16	2900	450
17	3400	550
18	4000	700
19	4800	900
20	5800	1100
21	7000	1300
22	8500	1800
23	10500	2500
24	13500	3500

When two tones fall inside the same critical band, the ear perceives a modulation or beating. This is an acoustic phenomenon where two sounds of

slightly different frequencies form an interference pattern with a periodic variation in amplitude whose frequency is equal to the difference in frequencies of the two sounds.

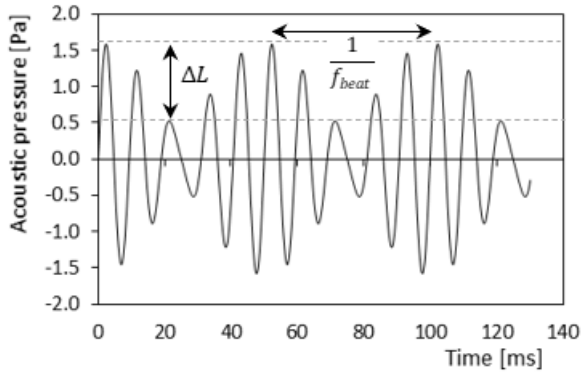

Figure 4-4 Acoustic beat resulting from the summation of two pure tones: f_1 = 100 Hz, $p_{1\,MAX}$ = 1 Pa and f_2 = 120 Hz, $p_{2\,MAX}$ = 0.6 Pa

Based on the modulation frequency f_{beat} and modulation depth ΔL two metrics are used to measure the beating phenomenon: fluctuation strength and roughness [11]. Fluctuation strength is used for frequency modulation below 20 Hz and roughness for frequency modulation above 20 Hz, with a gradual transition zone between the two. These two quantities have not yet been standardised, however indications about their calculation can be found at [12] with other usually adopted sound quality metrics.

- *Pitch and timbre*: pitch is a quality of sound that makes it possible to judge a sound as high or low based on its frequency content.

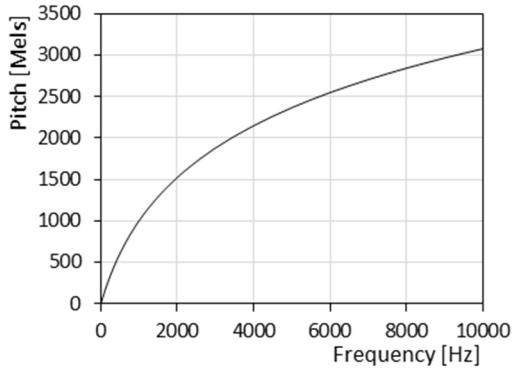

Figure 4-5 Mel scale: pitch vs frequency [7]

Based on empirical measurements it was developed a scale to indicate the relative perception of sound with different pitches with varying frequency content: the Mel scale (Figure 4-5).
Timbre on the other hand is a more complex concept that defines the quality of sound and can be used to discern between two sounds with similar pitch. Timbre is usually linked to the entire spectral composition of sound and on the evolution of sound over time.

MICROPHONE MEASUREMENT

Judging from the several characteristic features of human sound perception it is no wonder that the tapping (sounding) method for timber structures assessment gives qualitative information and difficult to replicate results, this without taking into account the skill of the inspector and the effect of aging on hearing capacity.

Therefore, to overcome this limitation while maintaining the characteristic of low cost and high measurement and analysis speed it was proposed to utilize smartphone built-in microphone for the sound recordings of impact tests, to be then post-processed and analysed to evaluate the registered sound quality and infer information about the timber element condition. This because smartphone represents a tool that it is available to most of the population, including timber structures inspectors, and it was demonstrated that can be used to perform acoustic measurement and analysis within certain limits of application ([13] and [14]).

In this section it will be reported a brief overview about smartphone built-in microphone main characteristics and digital audio recording. Smartphone manufacturer companies generally use MEMS (acronym of Micro-Electrical-Mechanical System) microphones due to their relatively good audio recording properties associated to a very small size. They have a built-in analog-to-digital converter, making them digital microphones, readily integrated with the rest of the smartphone applications. Regarding digital audio recording three topics should be discussed with more attention:

- *Sampling rate*: corresponds to the number of samples stored in one second used to discretise the continuous time signal of a sound wave. To avoid aliasing error (see also Chapter 3 Theoretical basis of wave propagation and structural vibration) the sampling rate for audio recording is usually set at 44100 Hz (i.e. Nyquist rate to measure signal with frequency content up to 22050 Hz, almost equal to the upper limit of human hearing).

$$f_{max} = \frac{f_s}{2} = \frac{44100\ Hz}{2} = 22050\ Hz \qquad \text{(Eq. 4-17)}$$

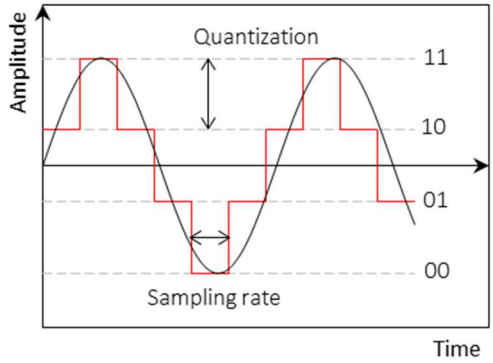

Figure 4-6 Example of digitalization of a continuous sinusoidal signal (2-bit depth resolution)

- *Quantization*: is the discretisation of the signal amplitude, needed to store a finite number of values in a digital file using binary coding. It is measured using the bit-depth metric, indicating the number of bits of information contained in each time sample. Such as for the sound levels, audio bit-depth can be defined using a logarithmic scale: decibels relative to full-scale [dBFS]. This is a negative scale because for different bit-depths it is not possible to fix a unique reference value except the maximum recordable digital level (overload).

$$dBFS = 20\log_{10}\left(\frac{Sampled\ value}{Overload}\right) \quad \text{(Eq. 4-18)}$$

For example, for a 16-bit digital audio depth:

$$A_{MAX} = 20\log_{10}\left(\frac{65536}{65536}\right) = 0\ dBFS \quad \text{(Eq. 4-19)}$$

$$A_{1/2\ MAX} = 20\log_{10}\left(\frac{32768}{65536}\right) \cong -6\ dBFS \quad \text{(Eq. 4-20)}$$

$$A_{NOISE\ FLOOR} = 20\log_{10}\left(\frac{1}{65536}\right) \cong -96\ dBFS \quad \text{(Eq. 4-21)}$$

Table 4-7 Integer and dBFS values for different bit-depth resolution

Bit-depth	Quantization steps	Signed range	dBFS
4	16	-8 to +7	24
8	256	-128 to +127	48
16	65 536	-32 768 to +32767	96

24	16 777 216	…	144
32	4 294 967 296	…	192

- *File format*: as regards the type of file format adopted to store audio track recordings there can be two alternative choices: compressed and not compressed. For audio files two typical options are the waveform audio file format for the uncompressed format and the MPEG-2 Audio Layer III for the compressed format, commonly known respectively as wave and mp3 file format. The mp3 file uses compression algorithms that work by approximating the components of sound which are assumed to be not recognisable by most of the human population based on the principle of psycho-acoustics. The difference in file size and audio quality is usually measured in bit rate, a quantity that represents the number of bits per unit time used to record the audio signal.

$$f_{bit} = f_s \cdot n_{bit} \cdot n_{channels} \quad \text{(Eq. 4-22)}$$

Where f_{bit} is the bit rate, f_s the sampling rate, n_{bit} the bit-depth and $n_{channels}$ the number of channels, which can be equal to 1 or 2 for mono or stereo recording. For example, for a wave file stereo recording using 44.1 kHz sampling rate and 16-bit depth resolution the bit rate is:

$$f_{bit} = 44.1\ kHz \cdot 16\ bit\ \cdot 2 \cong 1411 \frac{kbit}{s} \quad \text{(Eq. 4-23)}$$

The mp3 file is available with different bit rate value depending on the quality required for the recording, with the highest value set at 320 kbit/s.

Table 4-8 Example of bit rate, data storage and compression ratio of three audio file formats

	wave	mp3 (128 kbit/s)	mp3 (320 kbit/s)
Bit rate [kbit/s]	1411	128	320
1 hour recording [MB]*	635	58	144
Compression ratio	-	11:1	4:1

* 1 byte = 8 bit

Regarding the microphone specifications outline, with particular regard to MEMS microphone, main references are the application notes of the company InvenSense Inc. [15] and STMicroelectronics [16]:

- *Sensitivity*: represents the electrical signal output of the microphone for a given standard acoustic pressure input. This reference value is usually set as a 1 kHz sine wave at 94 dB Sound Pressure Level (SPL, corresponding to an acoustic pressure of 1 pascal). For analog microphone usually sensitivity is measured in mV/Pa for digital microphone in dBFS [17]. A typical value for a MEMS digital microphone is -26 dBFS [15], which means that the maximum recordable sound level (0 dBFS) is set at 120 dB SPL (ed. this is not a direct summation of dB levels but a proportion between dBFS and dB SPL).

$$Sensitivity_{dBFS} = 20\log_{10}\left(\frac{Sensitivity_{\%FS}}{Output_{REF}}\right) \quad \text{(Eq. 4-24)}$$

$$Sensitivity_{dBFS} = 20\log_{10}\left(\frac{0.05}{1}\right) = -26\ dBFS \quad \text{(Eq. 4-25)}$$

  It is worth noting that a higher sensitivity level does not necessary translate to better microphone: there is always a trade-off between sensitivity and maximum recordable signal. For near-field applications is preferable to have lower sensitivity levels to avoid the risk of signal overload and consequent distortion ([15] and [17]).
- *Signal-to-Noise Ratio (SNR)*: specifies the ratio of a reference signal (1 kHz, 94 SPL) to the noise floor level of the microphone, measured in dBFS for a digital microphone. SNR is usually presented over a 20 kHz bandwidth using an A-weighting frequency curve (i.e. correction factor based on the sensitivity of the human ear for different frequencies).

$$SNR = 20\log_{10}\left(\frac{A_{signal}}{A_{noise}}\right) \quad \text{(Eq. 4-26)}$$

  The noise floor of a microphone represents the electronic noise introduced by the instrumentation, not to be confused with the physical sound background noise. For digital audio, the noise floor level may be increased (reducing the SNR) to prevent quantization error by using additive noise techniques (e.g. dithering and noise shaping). The noise floor of a microphone is related to a specific value of SPL defined as Equivalent Input Noise (EIN):

$$EIN = 94\ dB - SNR \quad \text{(Eq. 4-27)}$$

- *Dynamic Range (DR)*: is the difference between the largest and smallest values recordable by the microphone (i.e. loudest and quietest SPLs). In terms of SPL the dynamic range can be seen as the difference between the Acoustic Overload Point (AOL, i.e. the sound signal that causes clipping in the measurement) and the Equivalent Input Noise (EIN).

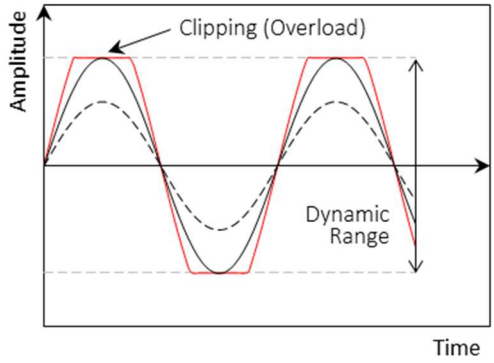

Figure 4-7 Example of signal distortion caused by clipping of a pure sinusoidal signal

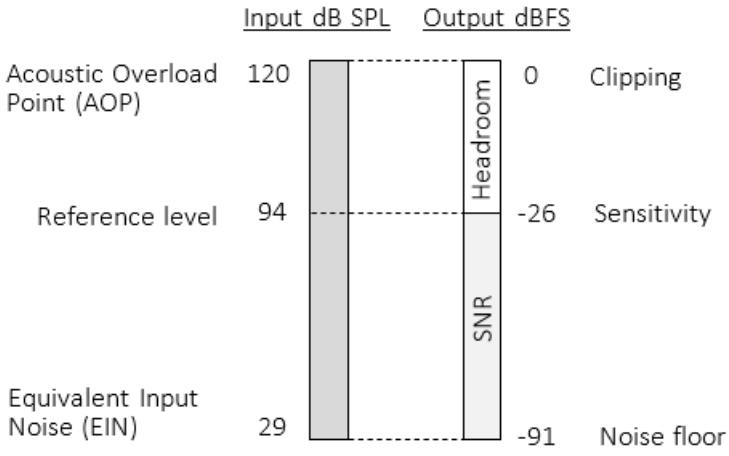

Figure 4-8 Relationship between dB SPL input and dBFS output for digital microphone [15]

- *Directionality (polar pattern)*: indicates how the microphone sensitivity changes in relation to the position of the sound source in space. It is usually described in terms of polar pattern, 2-axis polar plot showing equal sensitivity shape for different angle direction of incoming sound (Figure 4-9). Typically, microphones can be divided in two main categories: omnidirectional, meaning that they do not have a preferable orientation for sound recording (circular polar pattern), and directional, which is divided into many subgroups depending on the shape of the polar pattern. An example of an omnidirectional and directional (cardioid) polar pattern is reported in Figure 4-9. It is worth noting that polar patterns may vary with varying frequency of the recorded sound.

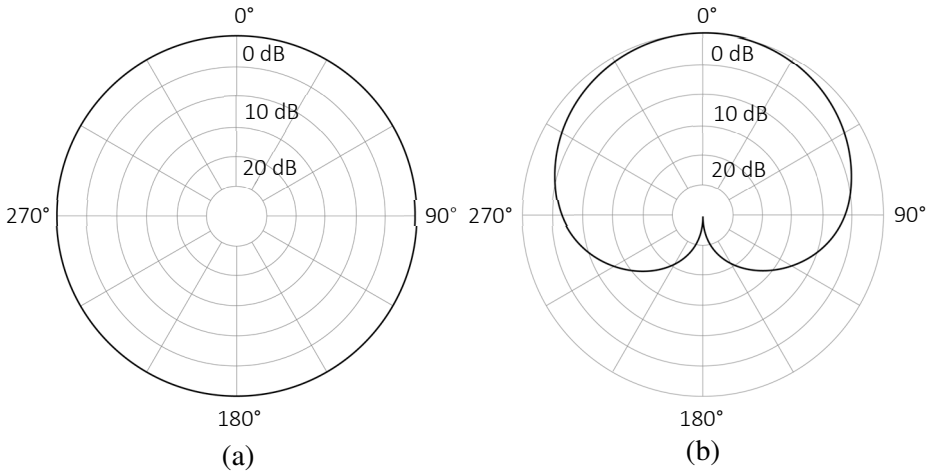

Figure 4-9 Polar patterns for an omnidirectional microphone (a) and a cardioid microphone (b)

- *Frequency response*: describes how the output level of the microphone varies across the frequency spectrum, usually reported in technical sheet as a frequency bandwidth. The high and low frequency limits are fixed as the points at which the microphone response output is 3 dB below (i.e. half power) the reference level set at 1 kHz. Another usually adopted description is a chart reporting the measured normalised output level (with respect to the amplitude value of 1 kHz signal) plot versus the sound frequency.

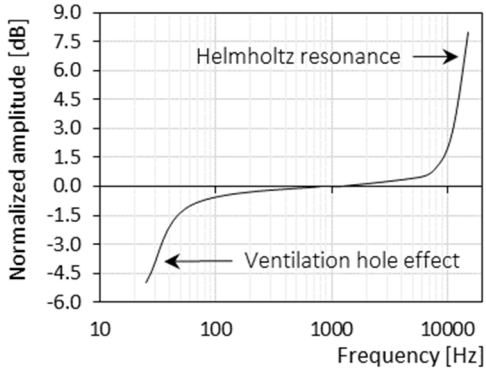

Figure 4-10 Example of frequency response for a MEMS microphone [16]

A typical frequency response for a MEMS microphone is reported in Figure 4-10. These microphones usually have a flat response, meaning a faithful

representation of the actual sound spectral components, for the mid frequencies range whereas they exhibit lower sensitivity for low frequency signal and higher sensitivity for high frequency signal. These two unwanted effects are unavoidable and are linked to the structure of the MEMS microphone body: the decrease of sensitivity is due to the geometry of the microphone back chamber and to the presence of the ventilation hole. The fictitious increase in amplitude for high frequency instead is related to the resonance of the air cavity (Helmholtz effect) in the front chamber of the microphone [16]. In the case of directional microphone (e.g. cardioid microphone of Figure 4-9) there is another aspect to consider when evaluating the frequency response: the proximity effect. This phenomenon is characterised by an increase in sensitivity of the microphone for the low frequency components of sound due to decreasing distance from the sound source [18]. An example of how it can affect the frequency response of a directional MEMS microphone is reported in Figure 4-11.

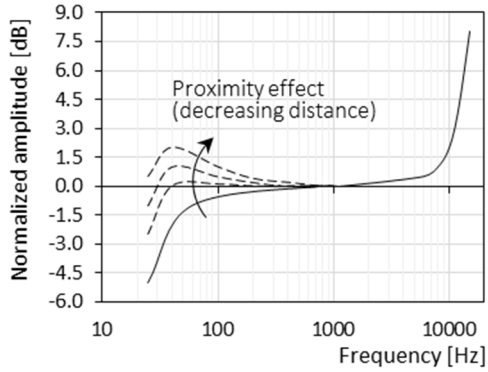

Figure 4-11 Example of proximity effect on the frequency response curve of a directional MEMS microphone

Other microphone specifications not reported in this overview are the Total Harmonic Distortion (THD) and the Power Supply Rejection Ratio (PSRR); for more details about these two quantities refers to the application notes [15] and [16].

4.2.3 DATA POST-PROCESSING AND AUDIO ANALYSIS

In the previous sections it has been established the basics of acoustics, of human perception of sound (i.e. psychoacoustics) and the main characteristics of microphone recording to be aware of. Now it remains to identify what can be the sound properties that allow the inspector to assess the integrity of a timber element and how these properties can be extracted from smartphone sound recordings.

In the field of audio analysis exist a very large number of approaches to extract significant features from an audio input to extrapolate information about speech, music and other type of sounds [19]. Broadly speaking, one can say that audio features can be extrapolated referring to two main groups: time domain (temporal features) and frequency domain (spectral features) [20]. Based on these two landmarks categories several other techniques have been developed such as the analysis of spectral content variation over time (i.e. Short-Time-Fourier-Transform STFT and wavelet transform) or cepstral analysis to determine the periodicity inside the frequency spectrum (e.g. pitch extraction from human voice recording). More details about these analyses will be reported in the following section.

Table 4-9 Main categories usually adopted for audio features extraction

Domain	Signal	Properties	Unit of measure
Time	Time history	Amplitude Time	dBFS s
Frequency	Spectrum	Amplitude Frequency (+phase)	dBFS Hz (°)
Time & Frequency	Spectrogram	Amplitude Time Frequency	dBFS s Hz
Quefrency	Cepstrum	Amplitude Quefrency	dBFS s

FOURIER SERIES, FOURIER TRANSFORM AND SPECTRAL ANALYSIS

To set the basis for audio frequency analysis (also known as spectral analysis) is important to introduce the principles of Fourier series and Fourier Transform [21], and in particular of Discrete Fourier Transform (DFT) and Fast Fourier Transform (FFT) since audio recordings are discrete signal with finite length duration.

The Fourier theorem states that a periodic function $f(t)$ of period T $(-T/2 < t \leq T/2)$ can be expressed as a summation of sinusoids functions (Fourier series):

$$f(t) = \frac{a_0}{2} + \sum_{n=1}^{\infty} a_n \cos(n\omega_0 t) + \sum_{n=1}^{\infty} b_n \sin(n\omega_0 t) \qquad \text{(Eq. 4-28)}$$

Where $\omega_0 = 2\pi/T$ is the angular frequency of the fundamental mode and the amplitude coefficients a_n and b_n are given by:

$$a_n = \frac{2}{T}\int_{-T/2}^{T/2} f(\tau)\cos(n\omega_0\tau)d\tau \quad \text{(Eq. 4-29)}$$

$$b_n = \frac{2}{T}\int_{-T/2}^{T/2} f(\tau)\sin(n\omega_0\tau)d\tau \quad \text{(Eq. 4-30)}$$

The relation reported in (Eq. 4-28) is the definition of Fourier series in sine-cosine form, but there are two other alternative representation of the Fourier series: the amplitude-phase form and the complex exponential form. The amplitude-phase form expresses the Fourier series as a summation of single sinusoids with phase shift (analog to a polar representation):

$$f(t) = \frac{A_0}{2} + \sum_{n=1}^{\infty} A_n \cos(n\omega_0 t - \phi_n) \quad \text{(Eq. 4-31)}$$

Where the amplitude A_n and phase ϕ_n are related to the Fourier coefficients of the sine-cosine form:

$$A_n = \sqrt{a_n^2 + b_n^2} \quad \text{(Eq. 4-32)}$$

$$\phi_n = arctan\left(\frac{a_n}{b_n}\right) \quad \text{(Eq. 4-33)}$$

The complex exponential form of the Fourier series is obtained by considering the Euler's formula ($e^{i\theta} = \cos\theta + i\sin\theta$):

$$f(t) = \sum_{n=-\infty}^{\infty} c_n e^{in\omega_0 t} \quad \text{(Eq. 4-34)}$$

Where the complex amplitude c_n is given by:

$$c_n = \frac{1}{T}\int_{-T/2}^{T/2} f(\tau)e^{-in\omega_0\tau}d\tau \quad \text{(Eq. 4-35)}$$

The Fourier series can be extended also to non-periodic function by making the period of the non-periodic function infinite, applying a mathematical operation called Fourier Transform [21]. The complex form of the Fourier series of a periodic function can be written as:

$$f(t) = \sum_{n=-\infty}^{\infty} \left[\frac{\omega_0}{2\pi}\int_{-T/2}^{T/2} f(\tau)e^{-in\omega_0\tau}d\tau\right] e^{in\omega_0 t} \quad \text{(Eq. 4-36)}$$

Assuming a infinite period T for a non-periodic function makes the angular frequency $\omega_0 = 2\pi/T$ become infinitesimally small. Therefore, the series of discrete value of frequency $n\omega_0$ can be now regarded as a continuous variable ω giving:

$$f(t) = \int_{-\infty}^{\infty} \frac{d\omega}{2\pi} \left[\int_{-\infty}^{\infty} f(\tau) e^{-i\omega\tau} d\tau \right] e^{i\omega t} \quad \text{(Eq. 4-37)}$$

The integrant of (Eq. 4-37) between square brackets is called the Fourier Transform (FT) of the function $f(t)$:

$$F(\omega) = \int_{-\infty}^{\infty} f(t) e^{-i\omega t} dt \quad \text{(Eq. 4-38)}$$

The Inverse Fourier Transform on the other hand is defined as:

$$f(t) = \frac{1}{2\pi} \int_{-\infty}^{\infty} F(\omega) e^{i\omega t} dt \quad \text{(Eq. 4-39)}$$

Without going too deep in the mathematical definition of the Fourier Transform and its properties, one can identify four main cases given by the combinations of two properties of the analysed time signal ([22] and [23]):

- Discrete or continuous in time.
- Finite or infinite in duration.

This is reflected also in the frequency domain, which can have discrete/continuous frequency and finite or infinite bandwidth. When time is discrete the bandwidth is finite and the frequency is discrete, and vice versa.

Table 4-10 Four Fourier Transform cases for discrete/continuous time and finite/infinite duration [23]

Signal duration		
Finite	Infinite	Time
Discrete Fourier Transform (DFT)	Discrete Time Fourier Transform (DTFT)	Discrete
Fourier series (FS)	Fourier Transform (FT)	Continuous
Discrete frequency	Continuous Frequency	

In audio signal analysis we usually have a finite time duration and a discrete time function (sampling frequency of 44.1 kHz), so we have to compute a Discrete Fourier Transform (DFT) [24]:

$$F(\omega_k) = \sum_{n=0}^{N-1} f(t_n) e^{-i\omega_k t_n} \quad k = 0,1,\dots,N-1 \qquad \text{(Eq. 4-40)}$$

Where:

- $f(t_n)$ is the input signal amplitude at time t_n (finite time history).
- $F(\omega_k)$ is the spectrum of the input signal at frequency ω_k.
- f_s is the sampling frequency measured in hertz [Hz].
- $t_n = n/f_s$ is the nth discrete time step (with n a positive integer number).
- N is the number of time/frequency samples.
- $\Delta\omega = 2\pi(f_s/N)$ is the spectrum frequency resolution.
- $\omega_k = k\Delta\omega$ is the kth discrete frequency sample (with k a positive integer number).

The Inverse Discrete Fourier Transform (IDFT) is given by:

$$f(t_n) = \sum_{k=0}^{N-1} F(\omega_k) e^{i\omega_k t_n} \quad n = 0,1,\dots,N-1 \qquad \text{(Eq. 4-41)}$$

It should be noted that the spectrum of a signal is a complex number and the Fourier Transform breaks down the signal not in a series of sinusoids but in a series of complex sinusoids (Figure 4-12).

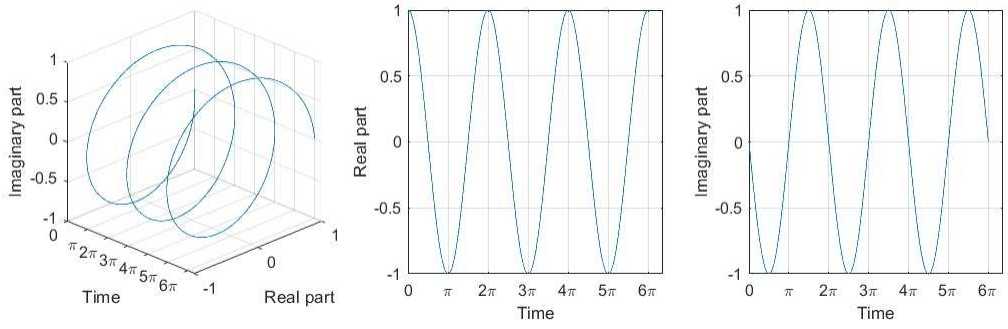

Figure 4-12 Complex sinusoid plot in the real, imaginary and time domains

Exploiting the Euler's identity, the DFT can be rewritten as:

$$F(\omega_k) = \sum_{n=0}^{N-1} f(t_n)[\cos(\omega_k t_n) - i\sin(\omega_k t_n)] \qquad \text{(Eq. 4-42)}$$

$$F(\omega_k) = F_{Real}(\omega_k) + i \cdot F_{Imaginary}(\omega_k) \qquad \text{(Eq. 4-43)}$$

These complex valued vectors are usually represented using a Bode plot, which consists in a graphical description of the spectrum magnitude $|F(\omega_k)|$ and phase $\phi_{F(\omega_k)}$ over the frequency domain.

$$|F(\omega_k)| = \sqrt{F_{Re}^2(\omega_k) + F_{Im}^2(\omega_k)} \quad \text{(Eq. 4-44)}$$

$$\phi_{F(\omega_k)} = \arctan\left(\frac{F_{Im}(\omega_k)}{F_{Re}(\omega_k)}\right) \quad \text{(Eq. 4-45)}$$

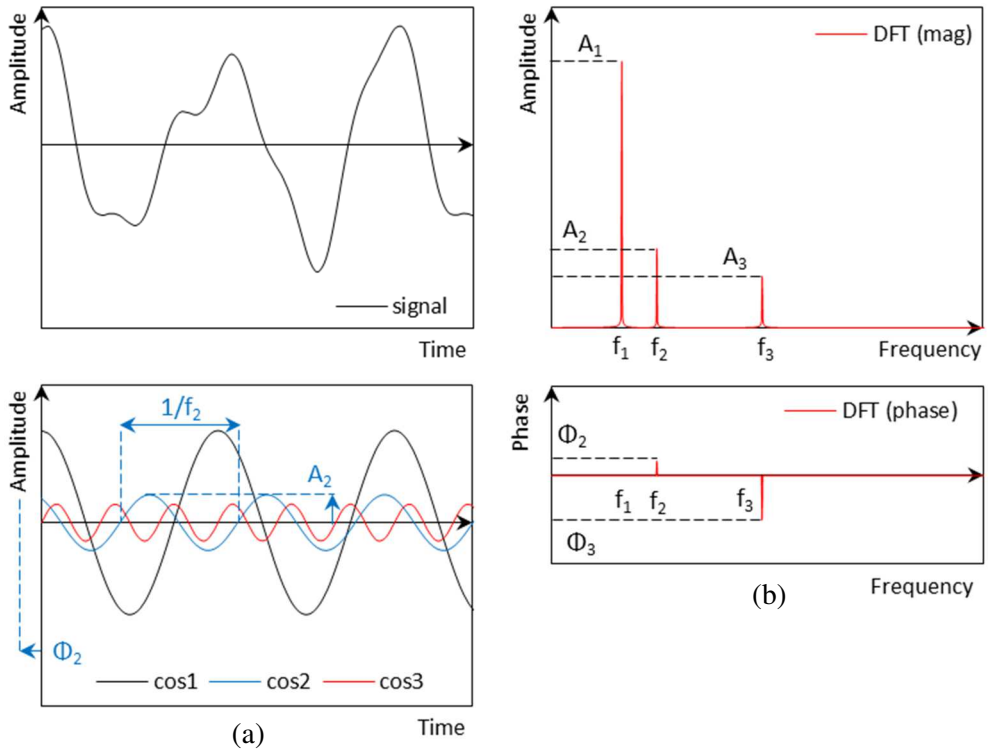

Figure 4-13 Decomposition of a time signal in a sum of cosine functions (a) and Bode plot representation of the resultant DFT signal spectrum (b)

Another important concept to point out examining the complex exponential representation of the DFT is the notion of Hermitian symmetry of the spectrum for real based signals.

$$F(\omega_k) = \sum_{n=0}^{N-1} f(t_n)[\cos(\omega_k t_n) - i\sin(\omega_k t_n)] \quad \text{(Eq. 4-46)}$$

$$\begin{aligned} F(-\omega_k) &= \sum_{n=0}^{N-1} f(t_n)[\cos(-\omega_k t_n) - i\sin(-\omega_k t_n)] \\ &= \sum_{n=0}^{N-1} f(t_n)[\cos(\omega_k t_n) + i\sin(\omega_k t_n)] \end{aligned} \quad \text{(Eq. 4-47)}$$

If the time signal $f(t_n)$ is real, then the spectrum is Hermitian (i.e. the spectrum complex conjugate is equal to the original spectrum with the frequency changed in sign):

$$F(-\omega_k) = [F(\omega_k)]^* \quad \text{(Eq. 4-48)}$$

This symmetry implies that the spectrum of a real signal is half redundant and all the negative frequency spectral samples may be disregarded, considering also that for temporal Fourier Transform negative frequencies have also little physical sense since are associated to waves travelling back in time. Therefore, spectra of sampled signals are usually plotted over a frequency range from $0\ Hz$ to $f_s/2\ Hz$ omitting the mirrored part from $f_s/2\ Hz$ to $f_s\ Hz$. Other aspects of the DFT to consider due to the finite dimension of the time signal and due to the discrete sampling frequency are:

- *Aliasing*: is a phenomenon that results in the appearance of frequency components in the spectrum different (i.e. "alias" in Latin) from the actual frequency components of the signal and is caused by the under-sampling of the signal. To avoid aliasing the Nyquist criterion must be respected, meaning that the sampling frequency should be equal to at least twice the expected maximum frequency component of the signal (i.e. Nyquist rate: $f_{s\,Nyquist} = 2 \cdot f_{max}$)

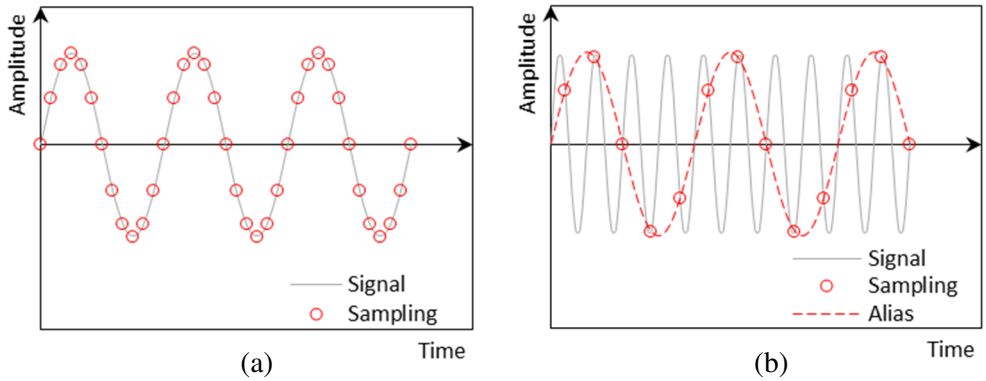

Figure 4-14 Adequately sampled signal (a) and under-sampled signal with aliasing effect (b)

When the Nyquist criterion is violated, frequency components above half the sampling frequency ($f_s/2 < f_0 \leq f_s$) appears as aliased frequency components ($f_{alias} = f_s - f_0$) due to the Hermitian symmetry of the DFT of real signals.

- *Spectral leakage*: is a type of distortion of the spectrum of a signal that may happen when we have a finite time duration of the signal. This phenomenon occurs when the sampled time duration does not respect the periodicity requirement of the Fourier Transform (i.e. when the time sample does not

contain an integer number of periods of the sinusoids used to decompose the signal). As already stated in Chapter 3 (section 3.2.5 FRF measurement and impact testing), there are two main ways to reduce the influence of leakage on the spectrum computation of the signal: include a whole integer number of periods of the signal (if the signal is transient include all the relevant temporal information, meaning using an adequately large recording duration) or if it is not possible adopt the window weighting technique (for more detail see Chapter 3).

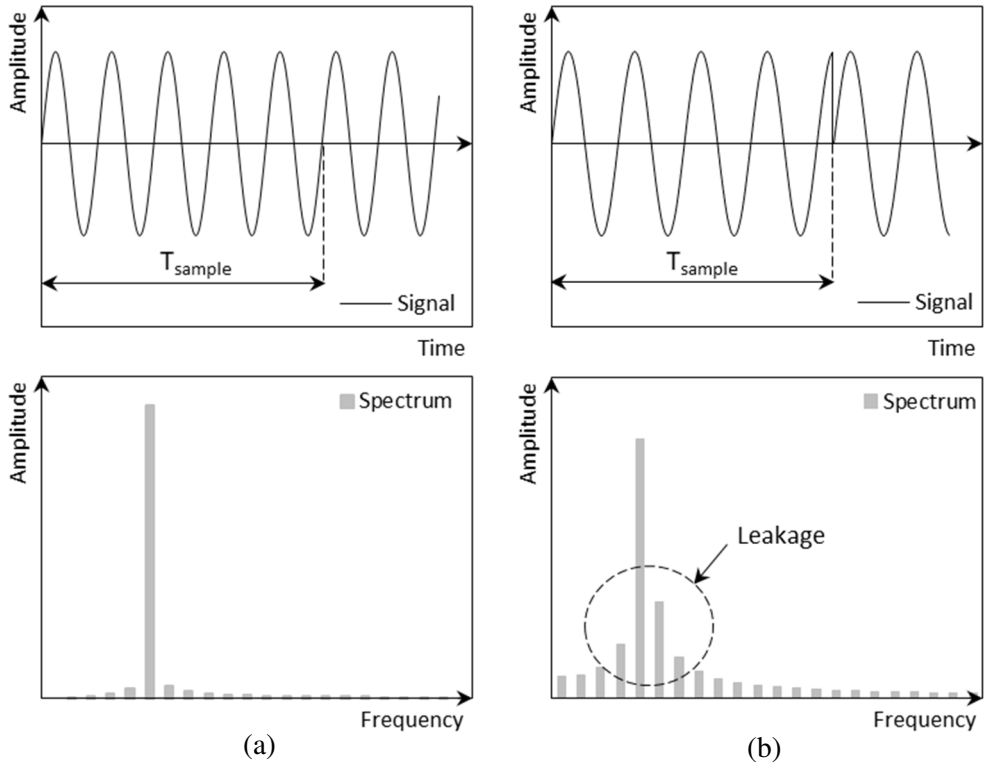

Figure 4-15 Example of spectrum with no leakage (a) and with leakage (b) due to the periodicity requirement of the DFT

- *Finite frequency resolution*: is a consequence of the finite number of samples (finite signal duration plus discrete sampling frequency) used to calculate the DFT. In particular, the frequency lines on the spectrum occur at interval equal to:

$$\Delta f = \frac{f_s}{N} \qquad \text{(Eq. 4-49)}$$

Where f_s is the sampling frequency and N is the number of points in the acquired time domain signal ($T_s = N \cdot 1/f_s$). A consequence of the finite frequency resolution is that if a signal contains two different frequencies which are separated by less than Δf, they cannot be distinguished in the DFT spectrum.

- *Computation time*: one of the major limiting factors for the application of the DFT is that it requires the resolution of N^2 complex multiplications and $N(N-1)$ complex additions; this is usually referred to by saying that the computational complexity of the DFT is equal to $O(N^2)$. To solve this problem, in 1965 it was proposed by Cooley and Tukey [25] an algorithm (named as Fast Fourier Transform FFT [26]) able to reduce the computational complexity of the DFT from an $O(N^2)$ to $O(N \log_2 N)$. The difference in computation time can be enormous, particularly for long data sets (an example is provided in Table 4-11).

Table 4-11 Difference in computation time for DFT (N^2) and FFT ($Nlog_2N$)

N	N^2	$Nlog_2N$	Saving
32	1024	160	84.4%
256	65536	2048	96.9%
1000	10^6	9966	99.0%
10^6	10^{12}	$1.99 \cdot 10^7$	≈ 100.0%
10^9	10^{18}	$2.99 \cdot 10^{10}$	≈ 100.0%

To appreciate the time saving power of the FFT algorithm let assume that a single operation takes one nanosecond to complete ($= 10^{-9}s$), for a data set of 10^9 numbers the DFT employs 10^9 seconds to complete ($\approx 31.7\ years$) whereas the FFT takes around 30 seconds. To be applied the FFT algorithm requires that the number of samples of the signal are equal to a power of two ($N = 2^n$); this is easily applied also to signal with different sample lengths by using the zero-padding technique: extending the signal length with zeros to the closest power of two.

- *Autopower and power spectral density*: the Autopower spectrum G_{XX} of a certain signal X is defined as the signal spectrum S_X multiplied by its complex conjugate S_X^* [27]:

$$G_{XX} = S_X S_X^* \qquad \text{(Eq. 4-50)}$$

$$G_{XX} = (a + ib)(a - ib) = a^2 + b^2 \quad \text{(Eq. 4-51)}$$

Due to its definition the Autopower spectrum is a real quantity equal to the squared magnitude of the signal spectrum (with no phase information). The Autopower function is usually adopted to obtain correct amplitude value when averaging multiple measurements, thanks to the removal of the phase and the squared elevation of the spectrum magnitude. Sometimes, the Autopower spectrum is reported as Autopower linear spectrum to regain the amplitude units of the original spectrum:

$$\sqrt{G_{XX}} = \sqrt{S_X S_X^*} \quad \text{(Eq. 4-52)}$$

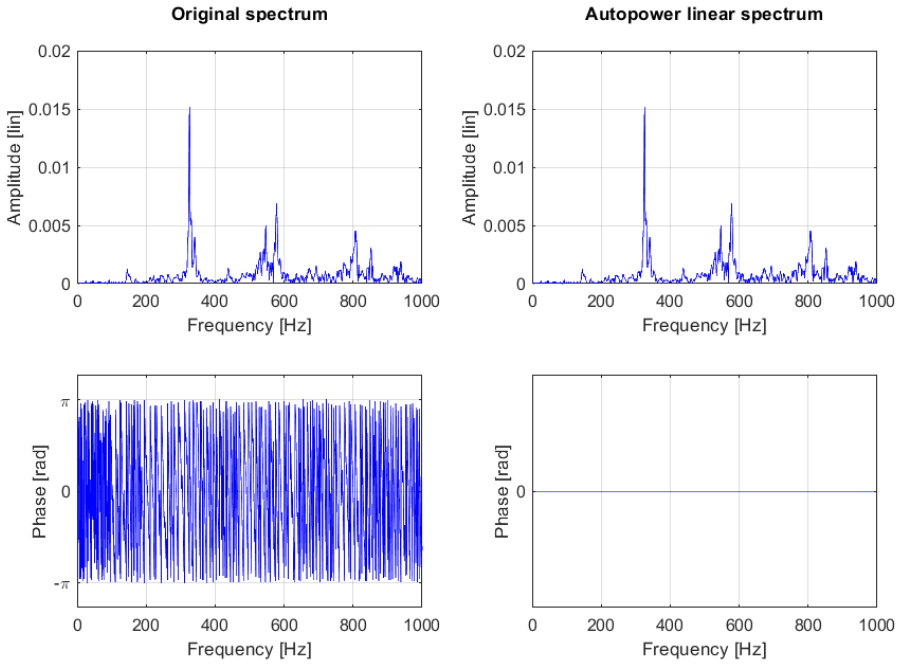

Figure 4-16 Bode plots of the original spectrum (a) and the Autopower linear spectrum (b)

The Power Spectral Density (PSD) is used to quantify the power content distribution of the signal over the entire frequency range, normalised with respect to the frequency resolution used to calculate the FFT:

$$PSD = \frac{G_{XX}}{\Delta f} \quad \text{(Eq. 4-53)}$$

This is done because when computing the FFT of the same broadband signal with different frequency resolution results in spectra having large differences

in amplitude (generally the higher the frequency resolution, small Δf, the lower the spectrum amplitudes). For transient signal also the Energy Spectral Density (ESD) is adopted, which is defined as the PSD multiplied by the acquisition time duration of the signal:

$$ESD = T\frac{G_{XX}}{\Delta f} \quad \text{(Eq. 4-54)}$$

OCTAVE ANALYSIS AND SPECTROGRAM ANALYSIS

Another effect related to the FFT analysis of an audio signal is that the finite frequency resolution Δf is constant across the entire frequency spectrum (0 Hz to 22050 HZ). This could be a problem because if a fine resolution is needed to discern the different frequency components of a signal in the low frequency domain (e.g. $\Delta f = 1\ Hz$ to distinguish frequency in the range of $20 \div 200\ Hz$), the same bandwidth is used also for the high frequency ($2000 \div 20000\ Hz$) domain where probably most of the spectral energy is related to the noise floor of the recording instrument. Moreover, as reported in section 4.2.2 Sound recording using microphone – Psycho-acoustics, the human perception of sound frequency is not linear in scale but logarithmic (i.e. existence of critical bands and Mel scale). Therefore, in acoustics is often used the Constant Percentage Bandwidth (CPB) analysis, where the spectrum resolution (i.e. bandwidth Δf) is equal to a fixed percentage of a defined centre frequency. One of the most common type of CPB analysis is the so-called Octave analysis or Octave-band analysis (which can be scaled also to fractional version: the 1/n Octave band analysis)

- FFT analysis: Constant Bandwidth (CB) analysis, the frequency resolution Δf is constant across a linear axis of frequency.
- Octave-band analysis: Constant Percentage Bandwidth (CPB) analysis, the frequency resolution Δf is constant across a logarithmic axis of frequency.

For the calculation of the Octave bands [28] two options are to determine the frequency ratio: a base-two system ($G_2 = 2$) or a base-ten system ($G_{10} = 10^{3/10} \cong 1.99$), for simplicity here is reported the base-two system. The midband frequencies are defined starting from a reference frequency of 1000 Hz; the immediate superior and inferior midband frequencies for a general 1/n Octave analysis are linked by the relation:

$$f_{m\,sup} = 2^{\frac{1}{n}} \cdot f_{m\,inf} \quad \text{(Eq. 4-55)}$$

In the same way, the bandedge frequencies (i.e. the lower and upper frequencies of a certain octave) can be calculated from the midband frequency:

$$f_{low} = 2^{-\frac{1}{2n}} \cdot f_m \quad \text{(Eq. 4-56)}$$

$$f_{up} = 2^{\frac{1}{2n}} \cdot f_m \quad \text{(Eq. 4-57)}$$

Table 4-12 Parameters of typically used fractional Octave band analyses

	Octave	1/3 Octave	1/12 Octave
f_{up}/f_{low}	2	1.260	1.059
f_{mid}/f_{low}	1.414	1.122	1.029
$\Delta f/f_{mid}$	70.7 %	23.2%	5.8%

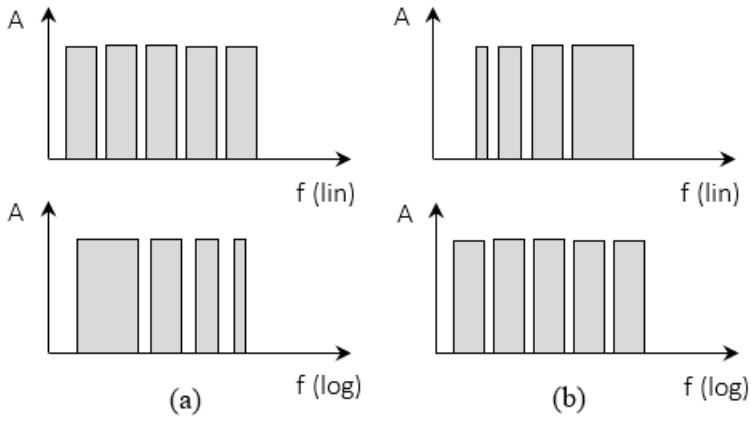

Figure 4-17 Schematic representation of frequency resolution for FFT analysis (a) and Octave-band analysis (b) [30]

For the midband frequencies of Octave band and 1/3 Octave band analysis nominal frequencies (also known as preferred frequencies [29]) are used, which can be seen as rounded values of the exact calculated midband frequencies.

Table 4-13 Calculated midband frequencies and nominal frequencies for the Octave-band analysis

$f_{mid\ calculated}$ [Hz]	$f_{mid\ nominal}$ [Hz]	$f_{low\ nominal}$ [Hz]	$f_{up\ nominal}$ [Hz]
15.625	16	11	22
31.250	31.5	22	44
62.500	63	44	88
125	125	88	177
250	250	177	355

500	500	355	710
1000	1000	710	1420
2000	2000	1420	3840
4000	4000	3840	5680
8000	8000	5680	11360
16000	16000	11360	22720

For certain type of audio analysis is also interesting to evaluate how the frequency content of the signal varies across the acquisition time duration (i.e. time-frequency analysis), however this cannot be done with a traditional Fourier Transform because the information about the temporal variation of the frequency components is "lost" during the computation of the signal spectrum. One of the most basic forms to overcome this limitation and to perform a time-frequency analysis is the calculation of a Short-Time-Fourier-Transform (STFT). In simple terms, it consists in dividing the sampled time interval into smaller time steps, each of which is transformed in the frequency domain by applying an FFT (time overlaps, and windows are applied to reduce differences between contiguous time steps).

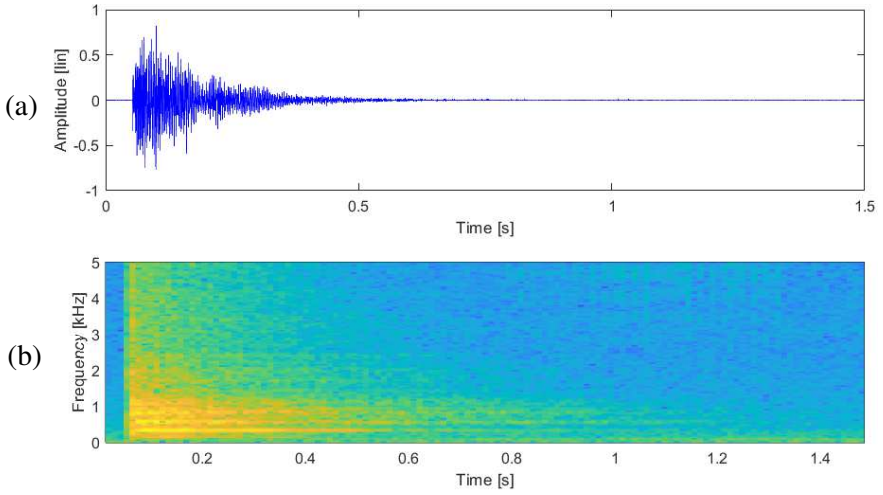

Figure 4-18 Time history (a) and STFT spectrogram (b) of an audio signal

The outcome of the STFT is then reported using a spectrogram plot: a two axes graph where the abscissa represents time, the ordinate represents frequency and the amplitude is represented by the colour intensity of the image confined in the two axes (Figure 4-18). One of the major drawback of the STFT is that it has a fixed resolution: if we

want a fine time resolution we must select a small time step but this influence also the frequency resolution of the spectrum (i.e. $\Delta f = f_s/N$) which results broader because a smaller number of samples are used to determine the spectrum, vice versa if we want a fine frequency resolution we must select larger time steps to include more samples for the calculation of the FFT. In the field of signal processing, this limitation is a manifestation of the uncertainty principle (known also as Gabor limit) which says that it is not possible to obtain simultaneous time and frequency resolution without interference.

$$\Delta t \Delta f \geq \frac{1}{4\pi} \qquad \text{(Eq. 4-58)}$$

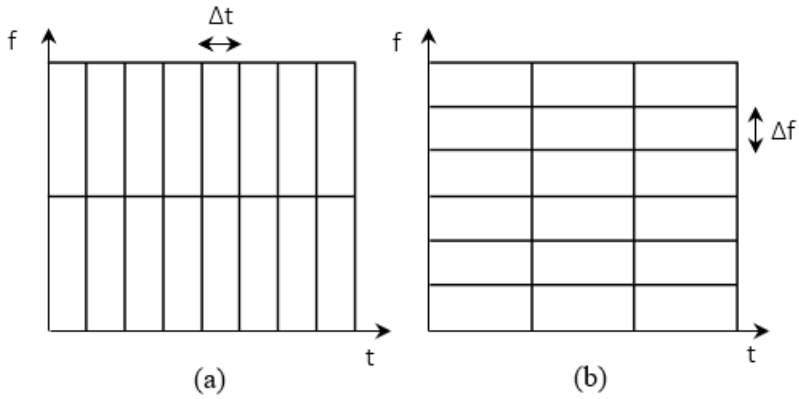

Figure 4-19 Schematic representation of the Gabor limit: STFT with fine time resolution (a) and with fine frequency resolution (b)

However, when performing time-frequency analysis of transient signal is important to have a fine frequency resolution in the low frequency domain to discern between difference frequency components, and a fine time resolution in the high frequency domain because the high frequency components tend to be damped more quickly than the low frequency components. Therefore, in place of the standard STFT analysis a Wavelet Transform is used which allows for Multi-Resolution Analysis (MRA). The Continuous Wavelet Transform (CWT) of a certain time signal $x(t)$ is defined as:

$$CWT(\tau, s) = \frac{1}{\sqrt{|s|}} \int_{-\infty}^{\infty} x(t) \psi \left(\frac{t - \tau}{s} \right) dt \qquad \text{(Eq. 4-59)}$$

Where the two variables τ and s are respectively the translation and scale parameters and the function ψ is called the mother wavelet. The term wavelet literally means small wave: an oscillatory function (wave) of finite duration (small). Mother wavelet instead implies that this function is used as prototype to reconstruct the analysed signal

(different type of mother wavelet functions can be used to perform a CWT). The translation parameter τ is used to move the mother wavelet across the signal duration, starting at time zero ($\tau = 0$) and then moving to the other time steps until the end of the signal duration ($\tau = T$); for each time step the mother wavelet is multiplied by the signal and integrated over all times. The scale parameter s indicates how much the mother wavelet is "stretched out" (or compressed) in the time domain, hence it is inversely proportional to the concept of frequency because the number of oscillations contained in the mother wavelet do not change with scale (Figure 4-20).

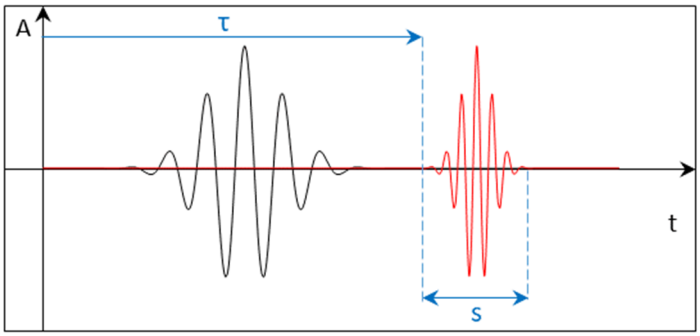

Figure 4-20 Representation of two real-valued Morlet wavelets and identification of the translation parameter τ and scale parameter s

This is the great advantage of Wavelet Transform over STFT: small scale values are related to higher frequencies and short time duration whereas large scale values are related to lower frequencies and larger time duration (Figure 4-21).

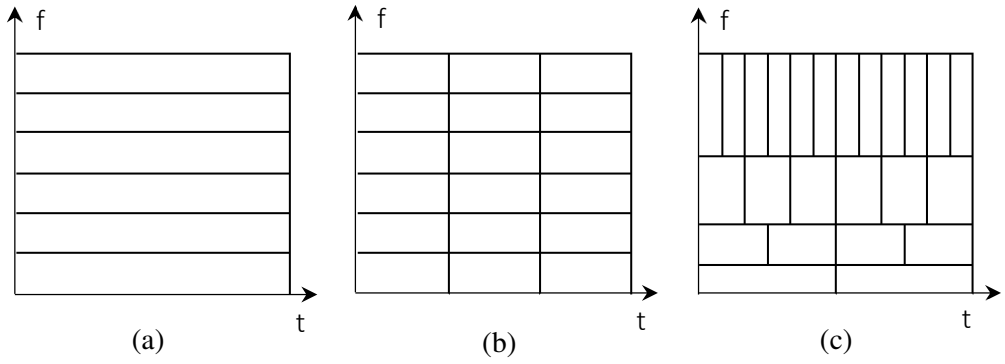

Figure 4-21 Resolution of FFT analysis (a), STFT analysis (b) and wavelet analysis (c)

The multi-resolution nature is an intrinsic property of Wavelet Transform because a transient function (i.e. wavelet) is used to analyse the time-frequency content of a signal instead of a continuous function (i.e. complex sinusoids for the STFT analysis).

CEPSTRUM ANALYSIS

The concept of cepstrum was first introduced by Bogert, Healy and Tukey in 1963 [32] with the intent of detecting echo in seismic signals. The name "cepstrum" was invented by the authors, along with a complete glossary of related terms (see Table 4-14), by paraphrasing and rearranging the consonants of spectrum because as they stated in their seminal paper: "*In general, we find ourselves operating on the frequency side in ways customary on the time side and vice versa*" ([32] and [33]).

Table 4-14 Example of cepstrum analysis terminology

Spectrum term	Cepstrum term
Frequency	Quefrency
Harmonic	Rahmonic
Filter	Lifter
Analysis	Alanysis
Phase	Saphe
Period	Repiod

The cepstrum was first defined as power cepstrum $C_p(\tau)$, calculated as the squared magnitude of the Fourier Transform (FT) of the logarithm of the autopower spectrum $G_{XX}(f)$ (for this reason it is also known as spectrum of a spectrum) [34]:

$$C_p(\tau) = \left|FT\{log(G_{XX}(f))\}\right|^2 \quad \text{(Eq. 4-60)}$$

Where the domain of the cepstrum is not the frequency domain (f), nor the time domain (t) but a new domain denominated quefrency domain (τ) and it is measured in seconds. New definition of the power cepstrum proposes the removal of the squared absolute value and the use of an Inverse Fourier Transform:

$$C_p(\tau) = IFT\{log(G_{XX}(f))\} \quad \text{(Eq. 4-61)}$$

Other definition of cepstrum are the complex cepstrum $C_c(\tau)$ and the real cepstrum $C_r(\tau)$, which are both derived from the normal spectrum of the signal S_X, one considering the phase for the calculation (complex cepstrum) and one setting the phase equal to zero (real cepstrum):

$$S_X(f) = FFT\{x(t)\} = A(f)e^{i\Phi(f)} \quad \text{(Eq. 4-62)}$$

$$C_c(\tau) = IFT\{log(S_X(f))\} = IFT\{ln(A(f)) + i\Phi(f)\} \quad \text{(Eq. 4-63)}$$

$$C_r(\tau) = IFT\{log(S_X(f))\} = IFT\{ln(A(f))\} \quad \text{(Eq. 4-64)}$$

Note that the base of the logarithm can be selected by the user and that the real cepstrum is essentially a scaled version of the power cepstrum, since also the autopower spectrum does not carry information about the signal phase.

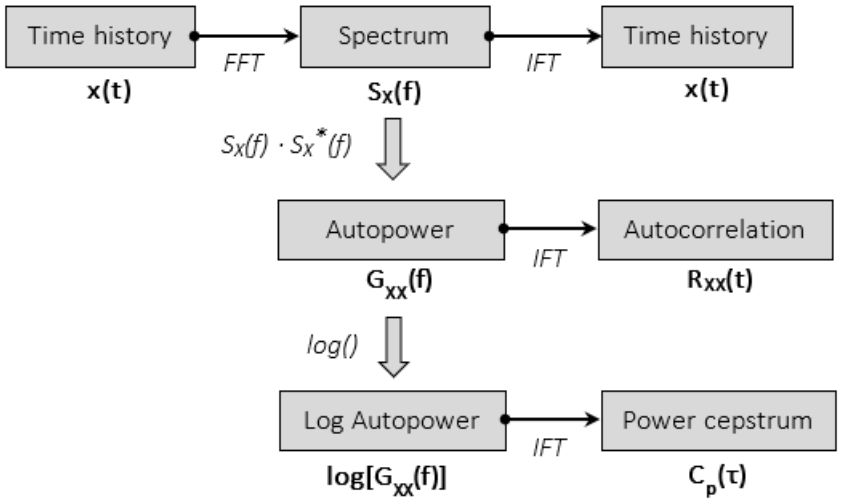

Figure 4-22 Schematic representation of the operations needed to calculate the autocorrelation function and the power cepstrum

To understand how the power cepstrum was originally developed to detect echo in seismic signals let us assume a signal with a simple echo [33]:

$$x(t) = s(t) + \alpha s(t - \tau) \quad \text{(Eq. 4-65)}$$

To report also a practical example let take the signal equal to an exponentially damped sum of three sinusoids and an echo with a time delay τ of 0.5 seconds and a reduction factor α of 0.3 (Figure 4-23).

Table 4-15 Sinusoids values for the example of echo detection via cepstrum analysis

Function	Frequency [Hz]	Phase [°]	Magnitude []
Sinusoid 1	80	0	1
Sinusoid 2	200	30	0.3
Sinusoid 3	350	-90	0.2

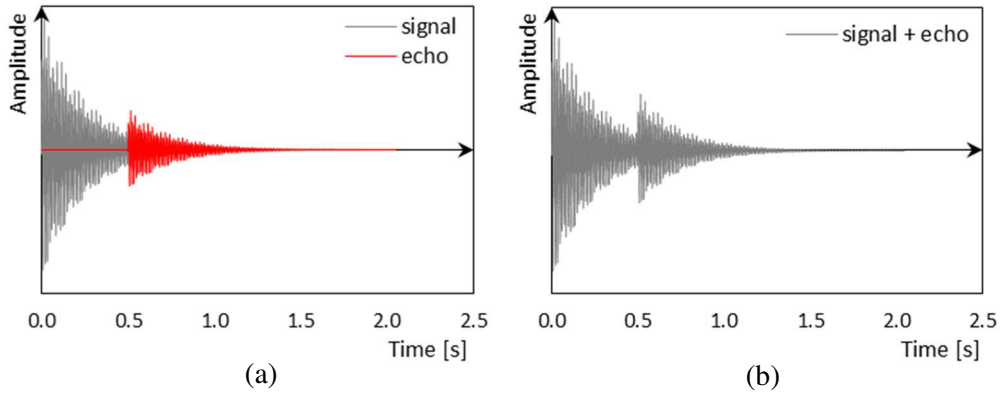

Figure 4-23 Original signal and echo separated (a) and signal with echo (b)

The autopower spectrum of the signal with echo can be proven to be equal to:

$$|S_x(f)|^2 = |S_s(f)|^2[1 + \alpha^2 + 2\alpha\cos(2\pi f\tau)] \qquad \text{(Eq. 4-66)}$$

Which can be seen to be equal to the spectrum of the original signal $|S_s(f)|^2$ with a periodic modulation function of frequency (term between squared parentheses) due to the contribution of the echo [33]. Figure 4-24 reports the spectrum magnitudes of the original signal and of the signal with echo obtained via FFT analysis (sampling frequency of 1000 Hz and rectangular time window of about 2 seconds).

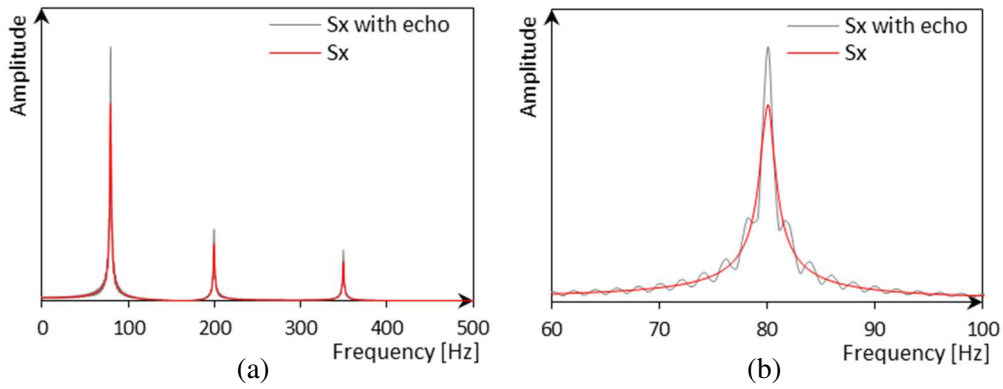

Figure 4-24 Complete spectrum of the signal with echo and without echo (a) and close-up to highlight the periodic modulation of the spectrum signal with echo

By taking the logarithm of the autopower spectrum the product of (Eq. 4-66) is turned to the sum of two components:

$$log(|S_x(f)|^2) = log(|S_s(f)|^2) + log[1 + \alpha^2 + 2\alpha\cos(2\pi f\tau)] \qquad \text{(Eq. 4-67)}$$

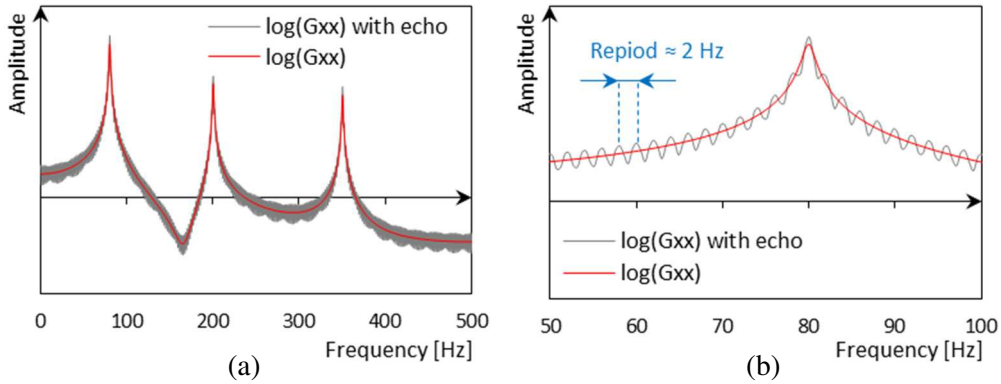

Figure 4-25 Logarithm of the autopower spectrum of a signal with echo (a) and close-up to highlight the additional periodic component due to echo (b)

The logarithm of the autopower spectrum of (Eq. 4-67) can be seen as the waveform of the complex cepstrum and it has an additional periodic component whose "frequency" is the time delay τ [33]. In traditional spectral analysis this frequency will show up in the spectrum of the waveform as a sharp peak. Therefore, if we apply the Inverse Fourier Transform (IFT) to (Eq. 4-67) a peak will appear in correspondence of the time delay τ. However, one can notice how the usual concepts of time and frequency are reversed: even if the new domain is represented in seconds it is more related to the notion of frequency. This explain why Bogert et al decided to coin a new terminology (i.e. cepstrum, quefrency domain, repiod, etc.) to avoid confusion while at the same time underlining the similarity between the new notion and the traditional type of analysis.

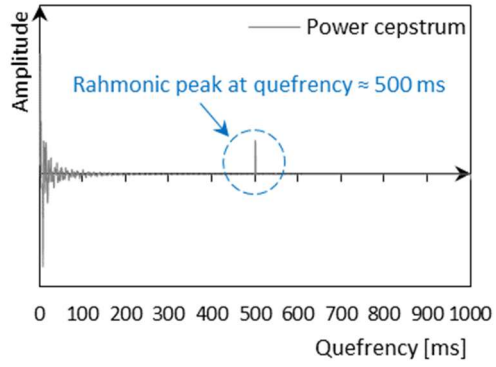

Figure 4-26 Power cepstrum of a signal with echo and rahmonic peak at quefrency equal to the echo delay τ

After the first application to detect echo in seismic signal, cepstrum analysis was used in numerous different fields ranging from speech analysis with voice pitch detection function, to medical applications such as heart rate and electroencephalogram (EEG) analysis and to machine vibration analysis with the detection of gear faults [34].

4.3 PROPOSED IMPROVEMENT FOR THE TAPPING METHOD – METHODOLOGICAL APPROACH

DATA COLLECTION CRITERIA

In this section will be presented the proposed acoustic method, outlining the main features regarding data collection criteria, signal post-processing and data analysis procedure. The method is used then to carry out the validation study based on a series of experimental tests, which will be described in detail in Chapter 5 Experimental campaign, outcomes, and analyses.

First, the sound radiation data were gathered using different microphone devices: initially, for the first experimental campaign, only smartphone built-in microphones were used. For the second campaign also a measurement calibrated microphone was employed, to be used as benchmark for the results obtained with the smartphones microphone. All the audio data were recorded digitally using the wave audio file format (audio bit-depth of 16 bit and sampling rate of 44.1 kHz).

Where not otherwise specified, the impact tests were performed using a hand wielded hammer with a hard plastic tip and the microphone-to-sound source distance (i.e. microphone distance from the impact location) was set at 1 meter. The sound signal was registered in a relatively quiet environment (an anechoic chamber was not available for the tests and it was also considered not representative of real on-site condition for the test method), starting the recording a few seconds (≈ *5 seconds*) before hitting the timber specimens and waiting a few seconds (≈ *5 seconds*) after the end of the acoustic response of the element (measured by ear) before ending the recording.

Then, using a Matlab® [35] code reported in Annex A – MATLAB Code, the audio recordings were all trimmed to the same exact time length assuming as reference the signal peak amplitude point and as lower and upper boundaries 0.1 seconds before and 1.4 seconds after the reference point. The total length of 1.5 seconds was found to be a good compromise to contain all the impact signal information without introducing too much background noise (Figure 4-27). Bearing in mind the sampling rate of 44.1 kHz, the signal duration of 1.5 seconds corresponds to a total of 66151 amplitude samples.

Because the time length of 1.5 seconds was chosen to contain all the signal information, with the signal amplitude values close to the noisefloor of the microphone sensor at the start and end of the recording, the risk of leakage while performing the spectral analysis of the signal was judged to be minimum. Therefore, a rectangular window (also known as "no-window") was applied to the signal before computing the Fast Fourier Transform (FFT). To compute the FFT the number of samples of the signal must be a power of 2; applying the technique of *zero-padding*, the signal (66151 samples) was lengthened to the next power of 2 (2^{17} = 131072) by adding a series of zeros. The spectral resolution of the FFT analysis can then be calculated as the ratio of the sampling rate over the total number of samples of the recorded signal (Δf = 44100 Hz/131072 ≈ 0.68 Hz).

SIGNAL POST-PROCESSING AND AUDIO FEAUTURES EXTRACTION

For the evaluation of the audio signals recorded during the experimental part of the thesis the two main domains of acoustic analysis were selected to compute a series of signal descriptor parameters: the time domain and the frequency domain.

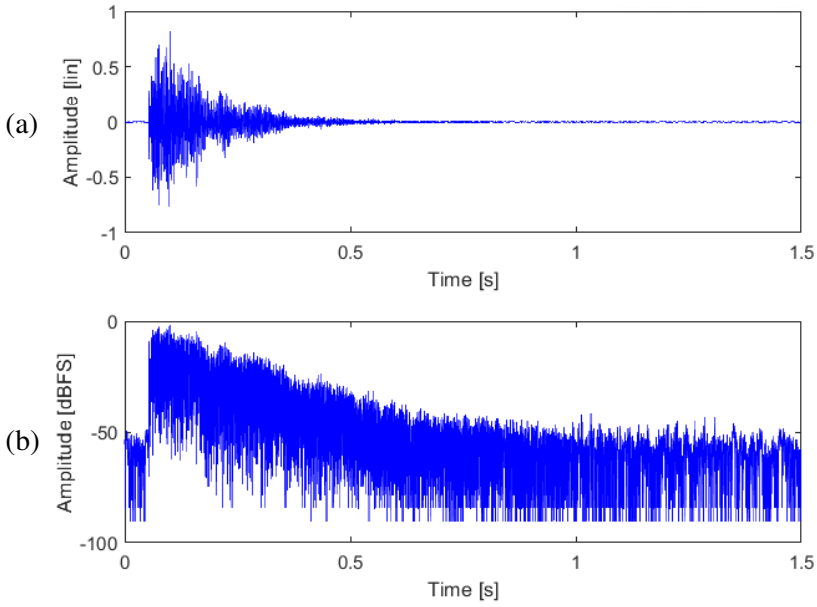

Figure 4-27 Time history of an impact test in linear scale (a) and logarithmic scale (b)

In the time domain four parameters were chosen and calculated to describe the registered transient sound signal (see also Figure 4-28):

1) **Attack Time (AT)**: measured as the time necessary for the signal amplitude to rise from an initial value equal to the 10% of the peak amplitude to a final value equal to the 90% of the peak amplitude. This parameter was already adopted in literature to categorize impact sounds recorded from objects made of different materials [36].

$$AT = t\left(A \cong 0.9 \cdot A_{peak}\right) - t\left(A \cong 0.1 \cdot A_{peak}\right) \quad \text{(Eq. 4-68)}$$

2) **Time Duration (TD)**: considered as the sum of the signal attack time AT and release rime RT, where the release time is measured as the time necessary for the signal to decrease from 90% to 10% of the signal peak value.

$$RT = t\left(A \cong 0.1 \cdot A_{peak\ fin}\right) - t\left(A \cong 0.9 \cdot A_{peak}\right) \quad \text{(Eq. 4-69)}$$

$$TD = AT + RT \quad \text{(Eq. 4-70)}$$

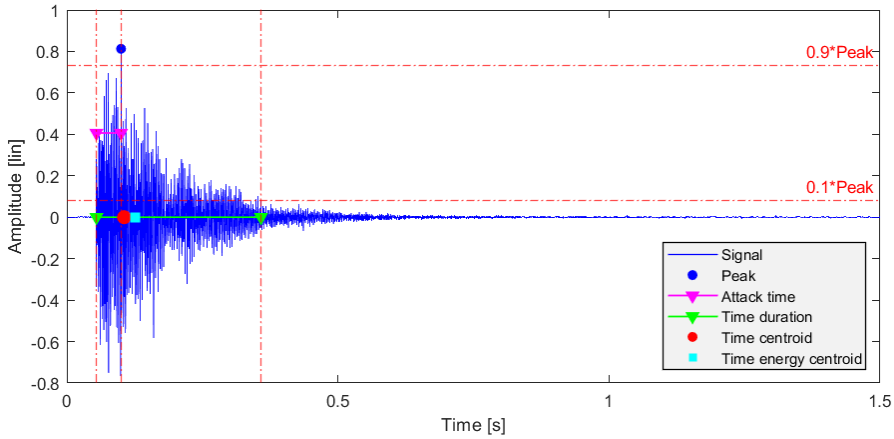

Figure 4-28 Graphical representation of the temporal descriptors for an example impact test

3) **Time centroid (TC)**: calculated by dividing the first moment of the signal time history divided by the zeroth moment of the signal time history [37]. The computation interval for the time centroid was selected equal to the time duration parameter previously determined.

$$TC = \frac{\sum_{i=1}^{n} A_i \cdot t_i}{\sum_{i=1}^{n} A_i} \quad for \quad TD_{init} \leq t \leq TD_{fin} \quad \text{(Eq. 4-71)}$$

4) **Time energy centroid (TEC)**: calculated similarly to the time centroid but assuming the square of the signal amplitude to better represent the signal energy content [38].

$$TEC = \frac{\sum_{i=1}^{n} A_i^2 \cdot t_i}{\sum_{i=1}^{n} A_i^2} \quad for \quad TD_{init} \leq t \leq TD_{fin} \qquad \text{(Eq. 4-72)}$$

In the frequency domain twelve parameters were selected to describe the shape of the signal spectrum which is related to the timbre of the sound. These spectral descriptors have been applied in a wide range of situations such as speaker identification, acoustic scene recognition and music genre classification (main references: [19] and [39]). Since the time length of the analysed sound (i.e. 1.5 seconds) was selected to contain all the valuable signal information a rectangular window (also known as "no-window") was adopted to compute the FFT of the signal.

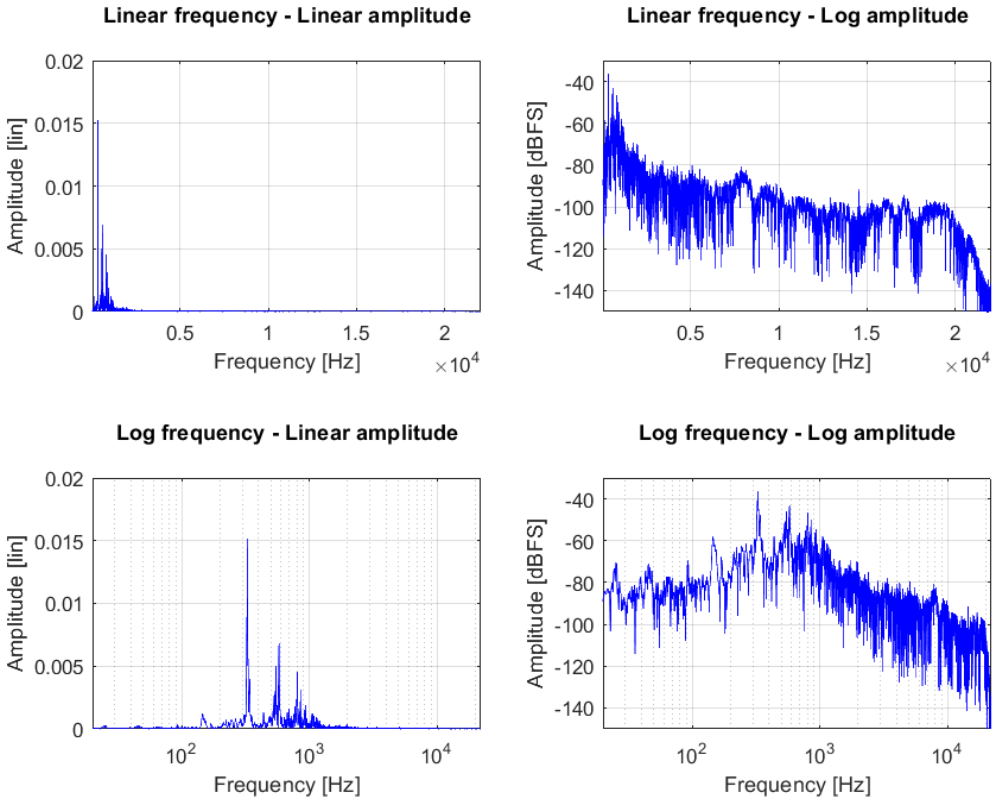

Figure 4-29 Four possible combinations of axes scale type for the spectrum representation of the considered example impact test

1) **Spectral Centroid (SC)**: calculated as the amplitude weighted mean of the frequency bins obtained through the FFT analysis of the audio signal; in other words, it represents the centre of gravity of the spectrum in term of frequency. For this reason, it is used as a measure of brightness of sounds: a sound is said

to be bright when it has more energy content in the high-frequency zone of the spectrum.

$$SC = \frac{\sum_{i=b_1}^{b_2} S_i \cdot f_i}{\sum_{i=b_1}^{b_2} S_i} \quad \text{(Eq. 4-73)}$$

Where:

- S_i is the amplitude value of the i-th bin of the discrete spectrum.
- f_i is the frequency value of the i-th bin of the discrete spectrum.
- b_1, b_2 are the bins band edges over which the spectral centroid is calculated (first and last value of the one-sided FFT spectrum).

2) **Frequency Energy Centroid (FEC):** calculated similarly to the spectral centroid but assuming the square of the spectrum amplitude to better represent the spectrum energy content [38].

$$FEC = \frac{\sum_{i=b_1}^{b_2} S_i^2 \cdot f_i}{\sum_{i=b_1}^{b_2} S_i^2} \quad \text{(Eq. 4-74)}$$

3) **Spectral Bandwidth (SB):** also known as spectral spread, it represents the standard deviation of the spectrum frequency around the reference value of the spectral centroid. It is a spectrum shape related features and it helps to discriminate between tonal sounds (having low SB values) and noise-like sounds (having high SB values).

$$SB = \sqrt{\frac{\sum_{i=b_1}^{b_2} (f_i - SC)^2 \cdot S_i}{\sum_{i=b_1}^{b_2} S_i}} \quad \text{(Eq. 4-75)}$$

4) **Spectral Crest Factor (SCF):** calculated as the ratio of the peak amplitude value in the spectrum and the arithmetic mean of the spectral amplitudes. As with the spectral bandwidth, this feature helps to distinguish between tonal sounds (higher SCF values) and noise-like sounds (lower SCF values).

$$SCF = \frac{max\{S_{i\in[b_1,b_2]}\}}{\frac{1}{b_2 - b_1}\sum_{i=b_1}^{b_2} S_i} \quad \text{(Eq. 4-76)}$$

5) **Spectral Flatness (SF):** calculated as the ratio of the geometric mean and arithmetic mean of the spectral amplitudes, it is a measure of the uniformity of the spectrum energy over the considered frequency band. Similarly to the

spectral bandwidth and the spectral crest factor, this feature allows to discriminate between tonal sounds (lower SF values) and noise-like sounds (higher SF values).

$$SF = \frac{\left(\prod_{i=b_1}^{b_2} S_i\right)^{\frac{1}{b_2-b_1}}}{\frac{1}{b_2-b_1}\sum_{i=b_1}^{b_2} S_i} \quad \text{(Eq. 4-77)}$$

6) **Spectral Entropy (SE):** calculated using the normalised Shannon entropy formula, it represents the grade of disorder of the spectrum. Therefore, it is another feature usable to separate noise (higher entropy values) from the actual signal (lower entropy values).

$$SE = \frac{-\sum_{i=b_1}^{b_2} S_i \cdot \log S_i}{\log(b_2 - b_1)} \quad \text{(Eq. 4-78)}$$

7) **Spectral Skewness (SSK):** computed as the ratio of the third moment of the spectrum and the cubic spectral bandwidth multiplied by the zeroth moment of the spectrum. It is a measure of the asymmetry of the spectrum around its mean value (i.e. spectral centroid), in other terms, it indicates when lower tones are dominant (positive skewness) or when higher tones are dominant (negative skewness).

$$SSK = \frac{\sum_{i=b_1}^{b_2}(f_i - SC)^3 \cdot S_i}{SB^3 \sum_{i=b_1}^{b_2} S_i} \quad \text{(Eq. 4-79)}$$

8) **Spectral Kurtosis (SK):** computed as the ratio of the fourth moment of the spectrum and the spectral bandwidth raised to the fourth power multiplied by the zeroth moment of the spectrum. It is a measure of the flatness of the spectrum around its mean value (i.e. spectral centroid). White noise audio signal, which have a flat spectrum, will exhibit lower kurtosis value with respect to tonal audio signal.

$$SK = \frac{\sum_{i=b_1}^{b_2}(f_i - SC)^4 \cdot S_i}{SB^4 \sum_{i=b_1}^{b_2} S_i} \quad \text{(Eq. 4-80)}$$

9) **Spectral Slope (SS):** it measures the slant of the spectrum by using a simple linear regression equation. Such as the spectral skewness it can be adopted as an indicator of the prominence of lower or higher tones in the audio signal.

$$SS = \frac{\sum_{i=b_1}^{b_2}(f_i - f_{mean}) \cdot (S_i - S_{mean})}{\sum_{i=b_1}^{b_2}(f_i - f_{mean})^2} \quad \text{(Eq. 4-81)}$$

10) **Spectral Decrease (SD):** similarly to the spectral slope it evaluates the amount of decrease of the spectral amplitudes. The formula was obtained from studies about the perception of sound by human [40] and emphasises more the contribution of the lower frequencies with respect to the higher frequencies [39].

$$SD = \frac{\sum_{i=b_1+1}^{b_2} \frac{(S_i - S_{b_1})}{i-1}}{\sum_{i=b_1+1}^{b_2} S_i} \quad \text{(Eq. 4-82)}$$

11) **Mean spectral flux (SF):** the spectral flux is used to measure the variability of the audio spectrum over time. Since it is inherently a parameter dependant on time, to obtain a single value from each test the spectral flux mean over the considered temporal frame of 1.5 seconds is adopted as signal descriptor.

$$flux(t) = \left(\sum_{i=b_1}^{b_2} |S_i(t) - S_i(t-1)|^2\right)^{\frac{1}{2}} \quad \text{(Eq. 4-83)}$$

$$flux_{mean} = \frac{1}{t_{fin}} \sum_{t=0}^{t_{fin}} flux(t) \quad \text{(Eq. 4-84)}$$

12) **Spectral Roll-Off (SRO):** is determined as the upper limit frequency bin for which the energy of the spectrum comprised in this band equal a certain percentage threshold value of the total energy of the spectrum. A typical value for the threshold in literature is set at 95% of the total energy and this will be adopted also for the presented work.

$$f_{SRO} = f_k \quad k \quad such\ that \quad \sum_{i=b_1}^{b_k} S_i = 0.95 \cdot \sum_{i=b_1}^{b_2} S_i \quad \text{(Eq. 4-85)}$$

Other two parameters that were calculated from the signal spectrum are the mean amplitude and the amplitude standard deviation of the spectrum. These two parameters were used mainly to obtain a simple graphical representation of the spectrum energy distribution along with the spectral centroid and spectral bandwidth values (see Figure 4-30).

$$A_{mean} = \frac{\sum_{i=b_1}^{b_2} S_i}{b_2} \quad \text{(Eq. 4-86)}$$

$$A_{std} = \sqrt{\frac{\sum_{i=b_1}^{b_2}(S_i - A_{mean})^2}{b_2 - b_1}} \qquad \text{(Eq. 4-87)}$$

The spectral descriptors were computed two times for every signal: firstly, on the entire frequency spectrum and then limiting the frequency band using the spectral roll-off value as upper band limit. This was done because it was found that the impact signal energy of the tested specimens was centred in the middle frequency range (≈ 100÷1000 Hz, see Figure 4-29 for an example): therefore, the evaluation of the spectral audio features on the entire frequency range could be heavily influenced by both the background noise and the noisefloor of the microphone sensor at higher frequency. In fact, all the spectral descriptors are based on weighted operation of frequency and amplitude bins; due to the FFT spectral resolution (≈ 0.68 Hz) constant on the entire frequency range the large number of noisy amplitude bins in the high frequency zone may contaminate the signal information. To support this claim in Figure 4-30 are reported the spectral centroid SC, spectral bandwidth SB and the frequency energy centroid FEC computed on the entire spectrum and on the spectrum limited to the spectral roll-off SRO value. One may notice how the spectral bandwidth greatly decrease in the latter case and also the difference between the SC and FEC values become less noticeable.

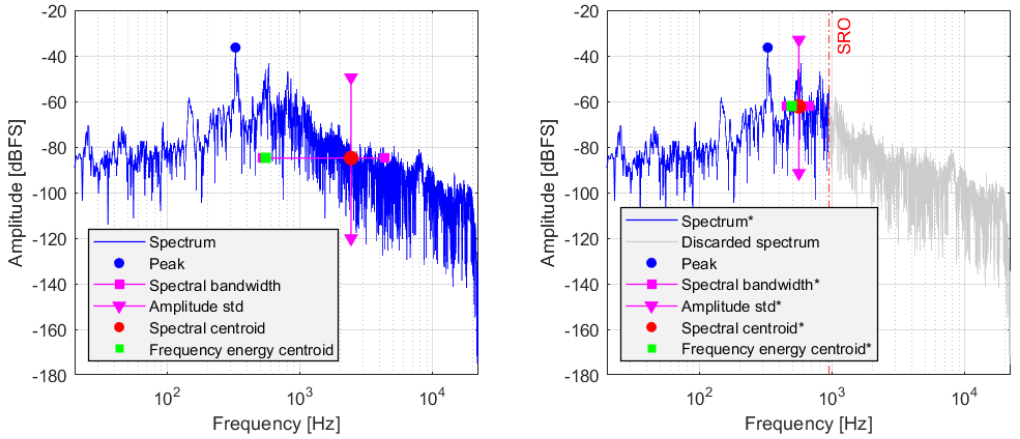

(a) (b)

Figure 4-30 Graphical representation of four spectral descriptors for the considered example impact test. Calculation on the entire spectrum (a) and on the spectrum limited to the SRO (b)

The spectral descriptors previously described were calculated applying the FFT algorithm on the entire duration of the sound recording (i.e. 1.5 seconds), to obtain a single value easier to handle for subsequent examination and statistical analyses. In

addition to that the variation of all the selected features over time was studied by performing the FFT analysis on successive windows of the signal (Hamming window type, window length of 1024 samples ≈ 0.02 s, overlap length of 512 samples) and plotting the results on the time axis (Figure 4-31). In Figure 4-31 (a) is reported also the pitch (i.e. fundamental frequency) of the sound signal obtained using the Normalised Correlation Function method [41].

(a)

(b)

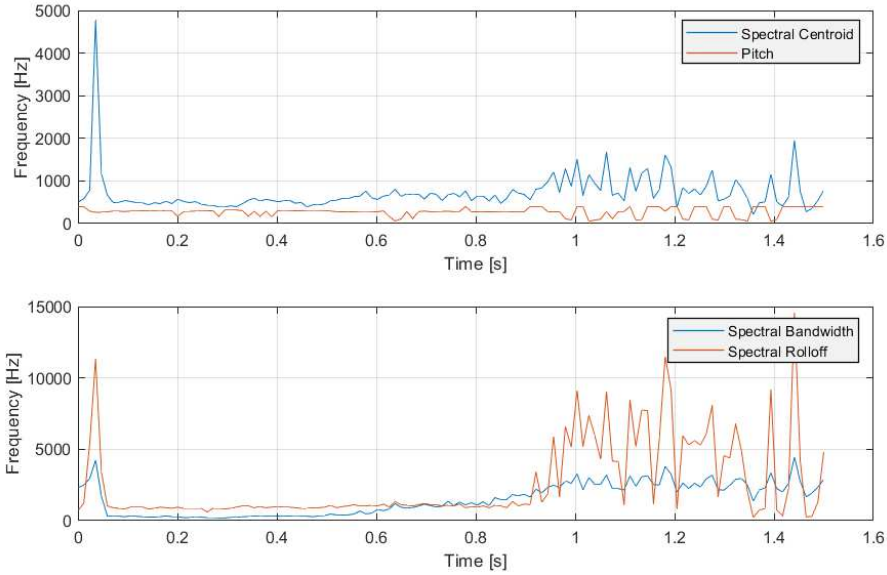

Figure 4-31 Audio features variation over time for spectral centroid and pitch (a) and spectral bandwidth and spectral roll-off (b)

Then, the Short Time Fourier Transform (STFT) and the Continuous Wavelet Transform (CWT) were computed to obtain the spectrogram and scalogram of the signal to visualize the frequency content variation over time.

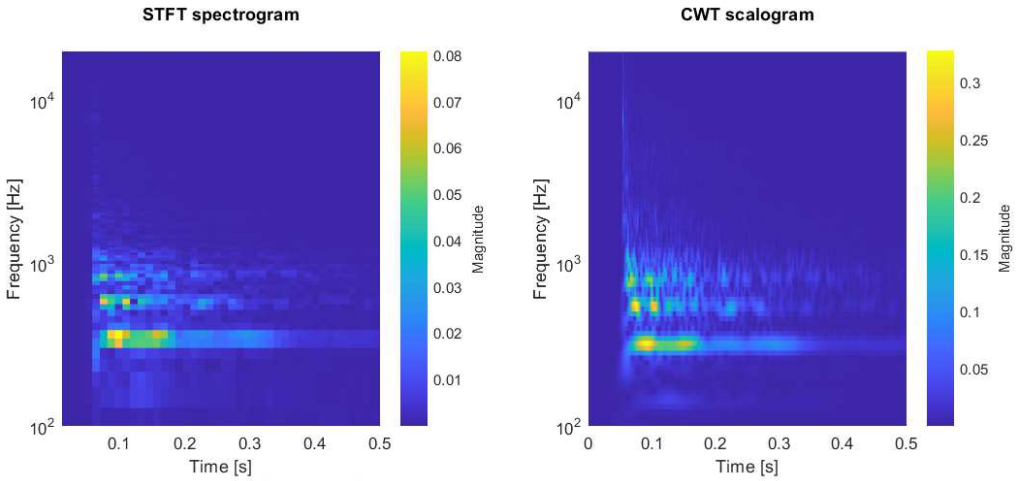

Figure 4-32 STFT spectrogram and CWT scalogram of the same considered example impact test having linear scale magnitude and limited to the first 0.5 seconds

The STFT was calculated similarly to the audio features variation over time by adopting a Hamming window with a window length of 1024 samples and an overlap length of 512 samples; the CWT on the other hand was calculated assuming a Morse type wavelet with a symmetry parameter equal to 3 and the time-bandwidth product set to 120 (resulting in larger spreads in time and narrower spreads in frequency). From the CWT analysis were also identified and extracted the ridges with the highest amount of energy content (Figure 4-33) related to the structural modes with the main contribution to sound radiation.

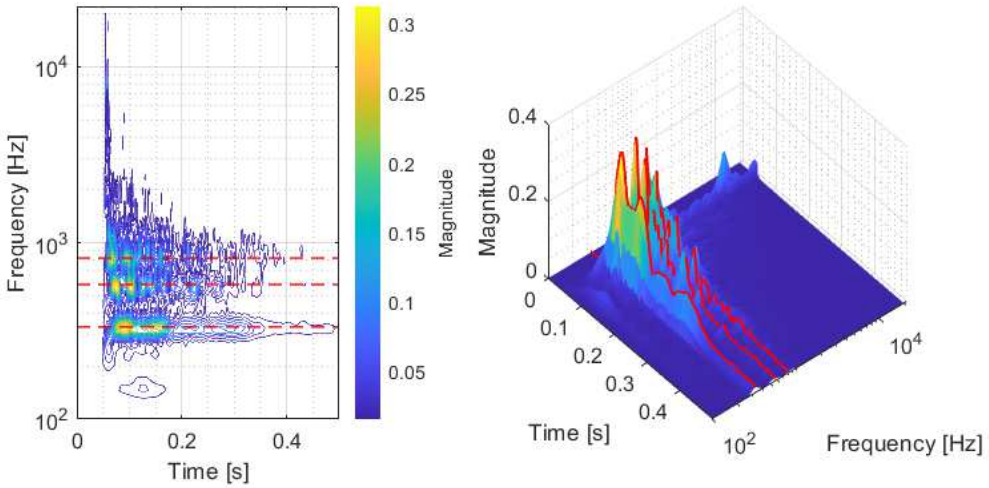

(a) (b)

Figure 4-33 Ridges of the CWT of the considered example impact test. Planar contour plot (a) and surface waterfall representation (b)

4.4 TIMBER AND SOUND

In Chapter 3 Theoretical basis of wave propagation and structural vibration it was introduced the main principles at the basis of sound radiation from vibrating structure (also known as structure-born sound). In this section it will be reported a literature overview of wood and timber material in the acoustic field with a particular emphasis on the possible influence of decay and damage on the radiated sound from timber elements.

There are four main inherent mechanical properties of wood material that play a role in sound radiation due to contact or impact loads [42]:

- The **modulus of elasticity parallel to the grain** (the modulus of elasticity perpendicular to the grain and the shear moduli may also influence the acoustic properties but typically have a linear relationship with the modulus of elasticity parallel to the grain).
- The **density** of the material.
- The **side hardness** of the material. If not directly measured may be estimated by correlation with the material density [42].
- The **loss factor** η of the material which measures the amount of vibrational energy dissipated by the material due to internal friction. (Eq. 4-88) reports the

relation between different parameter used to measure damping: the loss factor η, the quality (or amplification) factor Q, the damping ratio ζ and $\Delta\omega_{3dB}$ is the frequency bandwidth obtained by descending of a 3 dB value (i.e. halving the power) from the FRF magnitude peak at the resonance frequency ω_0.

$$\eta = \frac{1}{Q} = 2\zeta = \frac{\Delta\omega_{3dB}}{\omega_0} \quad \text{(Eq. 4-88)}$$

From the physical inherent properties of the material one can then obtain the specific acoustical properties of the same material:

- The **phase speed of quasi-longitudinal wave** inside the material (i.e. the speed at which sound travels through the material):

$$c_L'' = \sqrt{\frac{E}{\rho}} \quad \text{(Eq. 4-89)}$$

  Indicating with E the modulus of elasticity parallel to the grain and with ρ the material density.
- The **impedance** of the material defined as the product of the material sound speed and its density.

$$z = c_L'' \cdot \rho = \sqrt{E\rho} \quad \text{(Eq. 4-90)}$$

- The **sound radiation coefficient** of the material defined as the ratio of the material sound speed to its density.

$$R = \frac{c_L''}{\rho} = \sqrt{\frac{E}{\rho^3}} \quad \text{(Eq. 4-91)}$$

In particular, the ratio of sound radiation coefficient over the loss factor of the material is directly related to the intensity of the radiated sound from one-dimensional and bi-dimensional timber element [42].

In Chapter 3 Theoretical basis of wave propagation and structural vibration it was stated that bending waves are the main contributors to sound radiation from vibrating structure, especially in the case of impact transversal to the inspected element centroid axis which is probably the most typical case for the usual method of assessment. For the sake of simplicity let assume a one-dimensional beam element: the acoustic radiation frequency content is related to the bending natural frequencies of the beam. According to the Euler-Bernoulli beam theory and assuming simply supported condition these are equal to:

$$f_n = \frac{\pi}{2}\frac{n^2}{L^2}\sqrt{\frac{EJ}{\rho A}} \quad \text{(Eq. 4-92)}$$

Where n is the index of the n-th bending mode, L is the beam span length, E is the modulus of elasticity parallel to the grain, J is the moment of inertia (or more precisely the second moment of area) of the beam cross section, ρ is the mean density of the beam and A the area of the beam cross section. From Chapter 3 Theoretical basis of wave propagation and structural vibration we have to remember also that the frequency content of radiated sound due to bending vibration has also a lower bound corresponding to the acoustic critical frequency. For beams the acoustic critical frequency can be calculated by equating the wavenumber of bending wave in beams and the wavenumber of longitudinal wave in air (i.e. $k_b = k_{air}$):

$$f_c = \frac{c_{air}^2}{2\pi}\sqrt{\frac{\rho A}{EJ}} \quad \text{(Eq. 4-93)}$$

Where c_{air} is the phase speed of longitudinal waves in the air medium (i.e. sound speed in air, equal to 343 m/s at a temperature of 20°C) and the other properties are the same defined for (Eq. 4-92).

4.4.1 INFLUENCE OF DECAY

As already stated in Chapter 2 State-of-the-art on timber structure assessment methods wood decay (either caused by wood-decaying fungi or wood-boring insects) alters mainly the mechanical properties of the wood material while leaving unchanged the geometric properties of the element, at least in the early stages of biotic attack. Numerous experimental studies reported in literature ([43], [44] and [45] to cite a few) report a correlation between the biodegradation process carried out by wood-decaying fungi (measured in terms of mass loss or incubation time) and a reduction of the mechanical properties of the wood matrix (i.e. compression strength, bending strength, hardness and modulus of elasticity). The loss in stiffness (modulus of elasticity) and hardness of the material can therefore influence the vibrational and acoustical response of the material. A reduction of elastic modulus involves a reduction of the sound radiation coefficient, in turn related to less intense sound propagating from the timber element. In addition, a lower elastic modulus indicates overall lower frequency content of the radiated sound (see (Eq. 4-92) and (Eq. 4-93)). These observations are in accordance with the “conventional wisdom” which states that a hammer will produce a clear sound (i.e. relatively loud and high pitched sound) when striking sound wood, whereas the presence of decayed wood will be indicated by a dull, low-pitched sound.

During the last two decades several authors exploited this effect of biotic decay on the vibrational and acoustic properties of affected timber as a marker for the evaluation of the overall conservation status of the element ([46] and [47]) or for the detection of critical areas [48]. All the studies validate the hypothesis that the decrease of modulus of elasticity caused by wood-decaying fungi is linked to a reduction of the frequency content of both vibrations ([47] and [48]) and sound [46]. Barré et al [47] also reported a significant increase of the damping ratios of the first three bending modes for the same timber elements tested in sound and decayed conditions.

4.4.2 INFLUENCE OF DAMAGE

Differently from decay, timber damage does not alter the mechanical properties of the material but may affect substantially the geometric properties of the structural element. As seen in Chapter 2 State-of-the-art on timber structure assessment methods, the most common type of mechanical damage found in practice on real structures consists of cracks perpendicular to the grain. For this reason, most of the stress wave methods used for the detection of timber damage rely on the modification of the propagation path of sonic waves inside the material (e.g. early reflection and/or slower propagation speed). This requires the use of specific instrumentation such as an instrumented hammer and at least one accelerometer sensor.

To the best of the author knowledge, it was not found in literature any study about diagnostic techniques based on the recording of the propagated sound for the evaluation of damage in timber elements. In a pure theoretical way, it can be assumed that the modification of the geometric properties of timber element due to damage may influence mainly the frequency content of the recorded signal (Eq. 4-92). In Chapter 5 Experimental campaign, outcomes and analyses the outcomes of an experimental campaign will be reported and commented to support this claim.

4.5 REFERENCES

[1] P. Dietsch and J. Köhler “Assessment of timber structures” COST action E55 report, Aachen, Germany, Shaker Publishing Company, 2010.

[2] U. Dackermann, K. Crews, B. Kasal, J. Li, M. Riggio, F. Rinn and T. Tannert “In situ assessment of structural timber using stress-wave measurements” *Materials and Structures*, vol. 47, pp. 787-803, 2014.

[3] B. Goelzer, C. H. Hansen and G. A. Sehrndt “Occupational exposure to noise: evaluation, prevention and control” World Health Organisation (WHO), Geneva, Switzerland, 2006.

[4] Gracey & Associates “Acoustic glossary” [Online]. Available: http://www.acoustic-glossary.co.uk/ [Accessed: 25 May 2020]
[5] Siemens Digital Industries Software, “Sound Pressure, Sound Power, and Sound Intensity: What’s the difference?” [Online]. Available: https://community.sw.siemens.com/s/article/sound-pressure-sound-power-and-sound-intensity-what-s-the-difference [Accessed: 25 May 2020]
[6] Siemens Digital Industries Software, “Sound Fields: Free versus Diffuse Field, Near versus Far Field” [Online]. Available: https://community.sw.siemens.com/s/article/sound-fields-free-versus-diffuse-field-near-versus-far-field [Accessed: 25 May 2020]
[7] NeurOreille, “Psychoacoustics” [Online]. Available: http://www.cochlea.eu/en/sound/psychoacoustics [Accessed: 27 May 2020]
[8] International Organization for Standardisation (2003). ISO 226:2003 Acoustics - Normal equal-loudness-level contours. ISO, Geneva, Switzerland.
[9] Siemens Digital Industries Software, “Tone-to-Noise Ratio and Prominence Ratio” [Online]. Available: https://community.sw.siemens.com/s/article/tone-to-noise-ratio-and-prominence-ratio [Accessed: 27 May 2020]
[10] Siemens Digital Industries Software, “Critical bands in human hearing” [Online]. Available: https://community.sw.siemens.com/s/article/critical-bands-in-human-hearing [Accessed: 27 May 2020]
[11] Siemens Digital Industries Software, “Sound Modulation Metrics: Fluctuation Strength and Roughness” [Online]. Available: https://community.sw.siemens.com/s/article/sound-modulation-metrics-fluctuation-strength-and-roughness [Accessed: 27 May 2020]
[12] Salford Innovation Research Centre (SIRC) - University of Salford (Manchester), “Sound quality metrics” [Online]. Available: https://www.salford.ac.uk/research/sirc/research-groups/acoustics/psychoacoustics/sound-quality-making-products-sound-better/accordion/sound-quality-testing/sound-quality-metrics [Accessed: 28 May 2020]
[13] R. Brown and L. Evans “Acoustics and the smartphone” *Proceedings of ACOUSTICS*, Brisbane, Australia, 2011.
[14] M. Á. González and M. Á. González “Smartphone as experimental tools to measure acoustical and mechanical properties of vibrating rods” European Journal of Physics, vol. 37, no. 4, 206.
[15] InvenSense Inc., Appl. Note 1112, Microphone specifications explained, 2016.
[16] STMicroelectronics, Appl. Note 4426, Tutorial for MEMS microphones, 2017.
[17] J. Lewis “Understanding microphone sensitivity” *Analog Dialogue*, vol. 46, no. 2, 2012.
[18] A. Clifford and J. D. Reiss “Proximity effect detection for directional microphones” *Proceedings of the 131st Convention of the Audio Engineering Society*, New York, USA, 2011.

[19] F. Alías, J. C. Socoró and X. Sevillano "A review of physical and perceptual feature extraction techniques for speech, music and environmental sounds" *Applied Sciences*, vol. 6, no. 5, 143, 2016.
[20] S. Chu, S. Narayanan and C. C. Jay Kuo "Environmental sound recognition with time-frequency audio features" *IEEE Transactions on Audio, Speech, and Language Processing*, vol. 17, no. 6, pp. 1142-1158, 2009.
[21] S. Cho "Fourier Transform and its applications using Microsoft EXCEL®" Morgan & Claypool Publishers, 2018.
[22] J. O. Smith III "Spectral audio signal processing" W3K Publishing, 2011.
[23] DSPrelated.com "Fourier Transforms for continuous/discrete time/frequency" [Online]. Available: https://www.dsprelated.com/freebooks/sasp/Fourier_Transforms_Continuous_Discrete_Time_Frequency.html [Accessed: 05 Jun. 2020]
[24] DSPrelated.com "Introduction to the DFT" [Online]. Available: https://www.dsprelated.com/freebooks/mdft/Introduction_DFT.html [Accessed: 05 Jun. 2020]
[25] J. W. Cooley and J. W. Tukey "An algorithm for the machine calculation of complex Fourier series" *Mathematics of Computation*, vol. 19, no 90, pp. 297-301, 1965.
[26] National Instruments™, M. Cerna and A. F. Harvey, Appl. Note 041, The fundamentals of FFT-based signal analysis and measurement, 2000.
[27] Siemens Digital Industries Software, "The Autopower function…Demystified!" [Online]. Available: https://community.sw.siemens.com/s/article/the-autopower-function-demystified [Accessed: 10 Jun. 2020]
[28] American National Standards Institute (2004). ANSI S1.11: Specification for Octave-band and Fractional-Octave-band analog and digital filters. ANSI, Washington DC, USA.
[29] European Committee for Standardisation (1997). EN ISO 266: Acoustics – Preferred frequencies. CEN, Brussels, Belgium.
[30] Head Acoustics, Appl. Note 02/18, FFT – 1/n Octave analysis – Wavelet.
[31] R. Polikar "Wavelet tutorial – Second edition – Part 1" [Online]. Available: http://web.iitd.ac.in/~sumeet/WaveletTutorial.pdf [Accessed: 12 Jun. 2020]
[32] B.P. Bogert, M. J. R. Healy and J. W. Tukey "The quefrency alanysis of time series for echoes: Cepstrum, Pseudo-Autocovariance, Cross-Cepstrum and Saphe Cracking" *Proceedings of the Symposium on Time Series Analysis*, pp. 209-243, M. Rosenblatt Ed., Wiley, NY, 1963.
[33] A. V. Oppenheim and R. W. Schafer "From frequency to quefrency: a history of cepstrum" *IEEE Signal Processing Magazine*, vol. 21, no. 5, pp. 95-106, 2004.
[34] R. B. Randall "A history of cepstrum analysis and its application to mechanical problems" *Mechanical Systems and Signal Processing*, vol. 97, pp. 3-19, 2017.
[35] MATLAB. (2020). 9.9.0.1467703 (R2020b). Natick, Massachusetts: The MathWorks Inc.

[36] M. Aramaki, M. Besson, R. Kronland-Martinet and S. Ystad "Controlling the perceived material in an impact sound synthesizer" *IEEE Transactions on audio, speech and language processing*, vol. 19, no. 2, pp. 301-314, 2011.
[37] F. Xu, Y. Liu, X. Wang, B. K. Brashaw, L. A. Yeary and R. J. Ross "Assessing internal soundness of hardwood logs through acoustic impact test and waveform analysis" *Wood Science and Technology*, vol. 53, pp. 1111-1134, 2019.
[38] F. Xu, X. Wang, M. Teder and Y. Liu "Acoustic impact testing and waveform analysis for damage detection in glued laminated timber" *Holzforschung*, vol. 71, no. 10, pp. 197-208, 2017.
[39] The Mathworks Inc. "Spectral descriptors" [Online]. Available: https://it.mathworks.com/help/audio/ug/spectral-descriptors.html [Accessed: 12 Nov. 2020]
[40] G. Peeters "A Large Set of Audio Features for Sound Description (Similarity and Classification) in the CUIDADO Project" Technical Report; IRCAM: Paris, France, 2004.
[41] B. S. Atal "Automatic speaker recognition based on pitch contours" *The Journal of the Acoustical Society of America*, vol. 52, no. 6B, pp. 1687-1697, 1972.
[42] U. G. K. Wegst "Wood for sound" *American Journal of Botany*, vol. 93, no. 10, pp. 1439-1448, 2006.
[43] M. Venäläinen, H. Partanen and A. Harju "The strength loss of Scots pine timber in an accelerated soil contact test" *International Biodeterioration & Biodegradation*, vol. 86, pp. 150-152, 2014.
[44] M. Green, H. D. Mansfield-Williams and A. J. Pitman "Reduced hardness as an indicator of susceptibility of timbers to attack by *Euophryum confine* Broun" *International Biodeterioration & Biodegradation*, vol. 53, pp. 33-36, 2004.
[45] P. Witomski, W. Olek and J. T. Bonarski "Changes in strength of Scots pine wood (*Pinus silvestris* L.) decayed by brown rot (*Coniophora puteana*) and white rot (*Trametes versicolor*)" *Construction and Building Materials*, vol. 102, pp. 162-166, 2016.
[46] S. Yella, N. K. Gupta and M. S. Dougherty "Comparison of pattern recognition techniques for the classification of impact acoustic emissions" *Transportation Research Part C: Emerging Technologies*, vol. 15, pp. 345-360, 2007.
[47] J. B. Barré, F. Bourrier, L. Brancheriau, D. Bertrand and F. Rey "Effects of fungal decay on elasticity and damping of small-diameter silver fir logs assessed by the transverse vibration resonant method" *Wood Science Technology*, vol. 52, pp. 403-420, 2018.
[48] F. Xu, X. Wang, M. Teder and Y. Liu "Acoustic impact testing and waveform analysis for damage detection in glued laminated timber" *Holzforschung*, vol. 71, no. 10, pp. 197-208, 2017.

This page intentionally left blank.

5 EXPERIMENTAL CAMPAIGN, OUTCOMES AND ANALYSES

5.1 EXPERIMENTAL CAMPAIGN ON DECAYED SPECIMENS

OBJECTIVES	Assessment of the influence of variable parameters: ▪ Microphone-to-sound source distance ▪ Impact tool type ▪ Impact direction (longitudinal/transverse) Assessment of the influence of wood decay
TESTED MATERIAL	10 beam specimens
	Salvaged* elements (5 sound and 5 decayed)
	Softwood timber (assumed spruce species)
IMPACT TOOLS	2 hand wielded hammers (steel tip and hard plastic tip)
	Hammer weight ≈ 0.5 kg
RECORDING DEVICES	2 built-in smartphone microphones: ▪ Android™ device (Huawei™ Honor 6X) ▪ iPhone™ device (Apple iPhone™ SE 1st gen.)
ANALYSIS METHODS	Mechanical parameters: ▪ MOE (4-point bending test) ▪ Density (mass measurement) ▪ Moisture Content (resistance method)
	Acoustic analysis: ▪ Direct spectra comparison (1/12 octave) ▪ Spectral centroids dispersion graph ▪ Paired T-test on audio features ▪ Correlation with mechanical properties

* Salvaged = recovered from a building under dismantlement

To assess the effectiveness of the proposed acoustic technique for the evaluation of structural timber elements a pilot experimental investigation was carried out on a selection of 10 salvaged timber beam specimens (i.e. timber elements recovered from a structure being dismantled), with 5 specimens in a relatively good conservation status and 5 specimens in an advanced decay stage due to biotic attack. Firstly, the main mechanical parameters (static modulus of elasticity and global density) were measured for each specimen along with the individual geometric properties and moisture content of the material. Regarding the acoustic impact tests two different configurations were assumed for this campaign: one with the impact direction longitudinal, parallel to the beam axis and one with the impact direction transverse to the beam axis with the impact location coincident with the midspan section of each element. The sound recordings were made using two different mid-market smartphone devices to have a reference about the possible influence of different microphone sensors technical specifications. Furthermore, parameters that may affect the sound signal were also studied: such as the microphone distance from the sound source (to control the so-called "proximity effect", see Chapter 4 Proposed acoustic timber assessment method) and the type of impact device (to control the excited range of frequency content, see Chapter 3 Theoretical basis of wave propagation and structural vibration).

A preliminary presentation of the results of this campaign was reported in a conference paper submitted to the 11th International Conference on Structural Analysis of Historical Constructions (SAHC) held at Cusco (Perú) in the year 2018 [1]. In this section a more in-depth and updated analysis of the outcomes will be presented and discussed.

5.1.1 TIMBER SPECIMENS AND MEASURED STATIC PROPERTIES

The timber specimens adopted for the campaign were all made of spruce solid wood material salvaged from an existing structure being dismantled. All the decayed specimens exhibited visible signs of biotic attacks, indicating an advanced stage of decay, attributable to brown-rot fungi. In particular, were observed signs of brown cubical rot: crumbly wood material and cracks that form a mesh of roughly cubical pieces.

(a)

(b)

Figure 5-1 Close-up pictures of the decayed specimens: surface hyphae of the fungus (a) and internal wood damage after post-testing inspection (b)

For each specimen were measured the static modulus of elasticity (MoE_{stat}) via a four-points bending test [2], the mean value (MC_{mean}) and coefficient of variation (COV_{MC}) of the moisture content via the resistance method [3] (three measurements for each specimen: at the midspan section and at the beam ends excluding the final length of 30 cm) and the global density value (ρ) simply dividing the total mass of the element by its volume.

The results of this first evaluation of the mechanical properties of the element under examination are reported in Table 5-1 together with the geometric properties (span length and cross section dimensions). Specimens in sound conditions are labelled with a capital letter S and an identification number (e.g. S1…S5) and specimens in decayed conditions with a capital letter D and an identification number (e.g. D1…D5). The data collected about the static modulus of elasticity and the moisture content of the elements serve also as an additional validation of the distinction between sound and decayed condition based on visual assessment. In fact, comparing the mean value of modulus of elasticity for the specimens in good condition ($MoE_{S\ mean} = 5849\ MPa$) with that of the specimens in bad condition ($MoE_{D\ mean} = 3577\ MPa$) one can notice a significant decrease of stiffness properties as would be expected in the case of wood degradation by biotic attacks.

Table 5-1 Timber specimens' geometric properties, modulus of elasticity, global density, and moisture content

Specimen ID	L [m]	b [mm]	h [mm]	MoE_{stat} [MPa]	ρ [kg/m^3]	MC_{mean} [%]	CoV_{MC} [%]
S1	4.05	100	100	6587	358	8.0	10.0%
S2	3.40	90	100	6005	439	8.8	10.7%
S3	2.50	100	100	5904	438	13.3	0.9%

S4	2.50	95	100	5576	330	11.7	10.5%
S5	3.50	100	100	5175	383	7.8	5.2%
D1	1.60	100	120	2306	484	21.7	8.8%
D2	1.60	95	100	4287	494	23.8	35.1%
D3	2.10	90	90	2949	380	4.9*	10.9%
D4	2.50	70	100	4006	383	4.5*	32.7%
D5	1.65	75	100	4340	541	3.6*	4.5%

* Low MC value due to different storage conditions before testing (unintended drying Process of the specimens)

The moisture content measurements are also an indicator of the different conservation status of the two groups of specimens. The sound specimens exhibited all moisture content close to the hygroscopic equilibrium value of 12% for typical room ambient condition (temperature $T = 20°C$ and relative humidity $RH = 60\%$). Specimens D1 and D2 on the other hand shown mean moisture content values above 20%, which is typically considered as the critical MC value to set the proper conditions for the growth of wood decaying fungi. The extremely low MC value registered for specimens D3, D4 and D5 were due to the storage of these elements next in the proximity of a heat source before testing for a four-month period (the unintended drying process may have also been accelerated by the small size of the specimens). Therefore, the values reported in Table 5-1 are referred to the testing conditions, but the actual moisture content value of the elements in service was probably closer to that of specimens D1 and D2.

5.1.2 ACOUSTIC TESTS PROGRAMME

For this first campaign two mid-market smartphones were used for the audio recording: one Android™ device (*Huawei™ Honor 6X*, labelled as Smartphone A or Mic A in this work) and one iPhone™ device (*Apple iPhone™ SE 1st generation*, labelled as Smartphone B or Mic B in this work). More details about the technology and specifications of smartphone built-in microphone can be found in Chapter 4 Proposed acoustic timber assessment method. The sound was recorded adopting the Waveform Audio File Format (.wave) with an audio bit-depth of 16 bit and a sampling rate of 44.1 kHz.

The acoustic impact tests for each specimen were performed hitting the element with a hand-wield hammer in both the longitudinal and transverse direction of the beam element (Figure 5-2). In the transverse case the microphones were placed in front of the impacted edge at 1 m from the element and the beam was strike at the midspan section.

In the longitudinal case the microphones were positioned at the opposite end of the impact location at 1 m from the beam end.

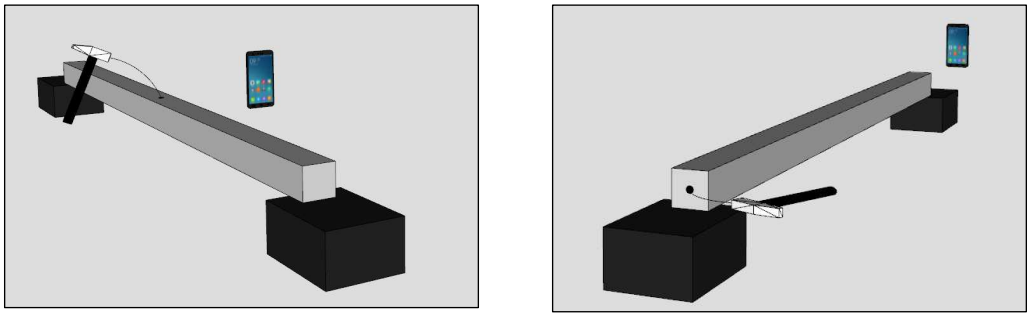

(a) (b)

Figure 5-2 Graphics for the acoustic impact tests in the transverse direction (a) and in the longitudinal direction (b). Simply supported boundary conditions for both cases

Probably the most common application method for the proposed diagnostic technique could be the impact in the transverse direction since the edges of structural elements are typically easier to reach with respect to the ends. However, in this pilot study we considered also the longitudinal case taking into account the option when the extremities of the element can be accessed (e.g. a timber structure disassembled and reused).

In addition, for all tested specimens, in both the transverse and the longitudinal direction, two different type of hammer were used to evaluate the influence of different impact devices. Both hammers were hand-wielded and had similar mass ($m_{hammer} \cong 0.5\ kg$); the main difference between the two tools was that one had a steel tip (tinners hammer) and one had a hard-plastic tip. As reported in Chapter 3 Theoretical basis of wave propagation and structural vibration the hardness of the hammer tip can influence the excited frequency content: a harder tip involves shorter impact duration and consequently excites a wider range of frequency of the structure.

Finally, for the specimen S1 also four different microphone-to-sound-source (i.e. impact location) distances (1 m, 0.5 m, 0.2 m and 0.1 m) were tested to assess the influence of the MEMS microphones proximity effect (see Chapter 4 Proposed acoustic timber assessment method) on the sound recordings. In this case the impact direction was transverse to the beam axis and the used hammer was the hard-plastic tip hammer.

In conclusion, a total of 44 different test configurations were examined (10 timber specimens considering the transverse and longitudinal cases both of which executed with a steel tip and a plastic tip hammer, plus 1 specimen tested using four different microphone-to-sound-source distances) using two smartphones for the sound recording.

Therefore, a total of 88 stored .wave files were processed using the feature extraction procedure illustrated in Chapter 4 Proposed acoustic timber assessment method and the relative outcomes will be presented in the next section.

5.1.3 OUTCOMES ANALYSIS AND DISCUSSION

The results reported in this section are presented in the form of temporal and spectral signal descriptors (Chapter 4 Proposed acoustic timber assessment method) for each impact test recording performed during the campaign. When a direct comparison between two or more sound spectra is illustrated, a 1/12 octave smoothing of the discrete spectra is adopted for the sake of clarity.

MICROPHONE-TO-SOUND-SOURCE DISTANCE

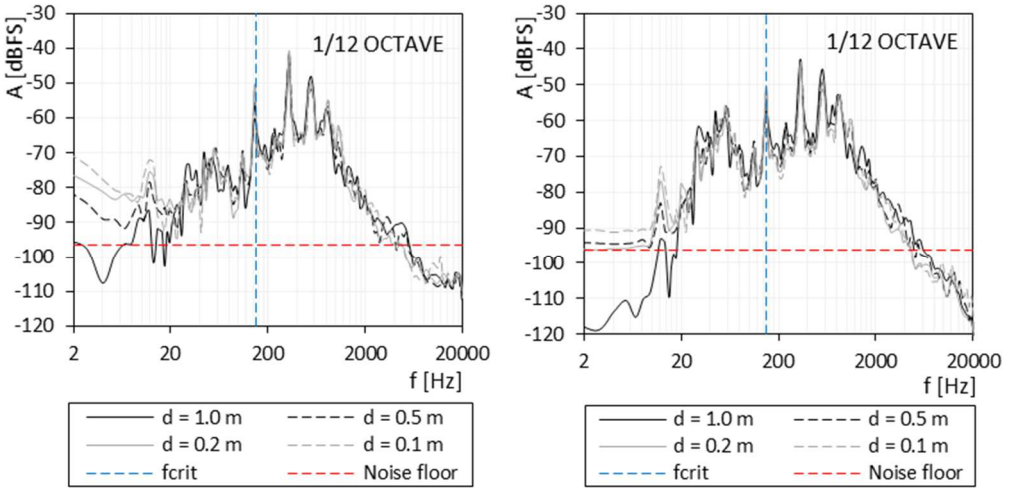

Figure 5-3 Sound spectra with 1/12 octave smoothing of transverse impact tests varying microphone-to-sound-source distance: recording by smartphone A (a) and smartphone B (b)

Specimen S1 was tested in the transverse direction using the hard-plastic tip hammer and adopting four decreasing distances from the microphone position to the impacted edge of the specimen: 1 m, 0.5 m, 0.2 m, and 0.1 m. Scope of the test was the evaluation of the influence of the smartphone MEMS microphones "proximity effect" on the recorded sound and, in particular, on the frequency content of the signal.

In Figure 5-3 is shown a comparison of the extracted sound spectra for the different recording distances with superposed the value of acoustic critical frequency for the specimen S1 and the reference value of noise-floor of the microphone using a 16-bit audio bit-depth. It can be observed that the proximity effect affects the sound recording

in a frequency range between 2 and 20 Hz. Although this may have a little influence on the final test results (since the entire affected range in most cases will fall below the threshold value of critical acoustic frequency) a microphone-to-sound-source distance of 1 meter was selected for the rest of the campaign to also reduce the risk of signal clipping due to the relatively larger sound intensity for closer distances.

IMPACT TOOL TYPE

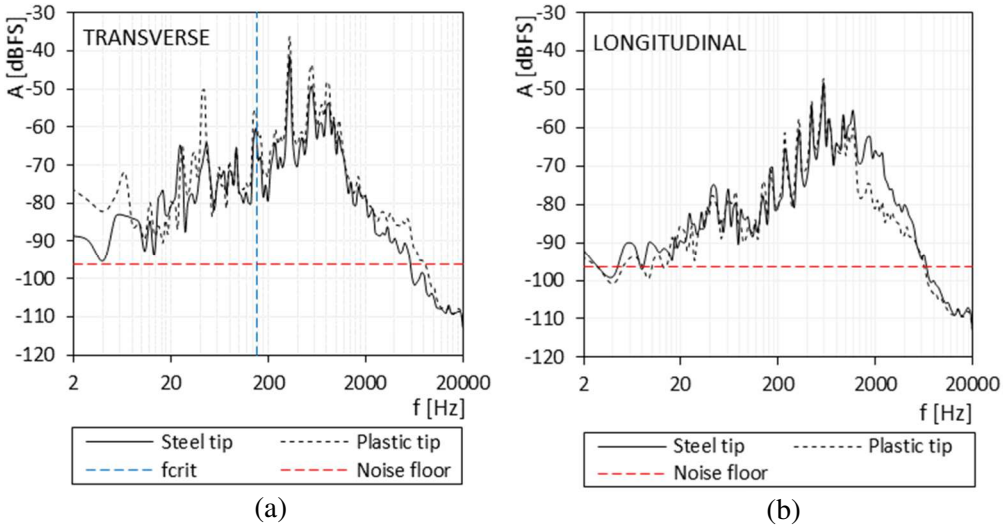

Figure 5-4 Sound spectra (1/12 octave smoothing) of specimen S1 recorded with smartphone A and impacted with different hammer tips: transverse impact (a) and longitudinal impact (b)

In Figure 5-4 is presented the comparison of sound spectra of the acoustic tests performed on specimen S1 changing the type of impact tool: a hammer with a steel tip and a hammer with a hard-plastic tip. As mentioned before, this parameter mainly influences the excited frequency range and in turn the overall frequency content of the propagated sound. As can be seen in the reported charts the type of impact tool has a slight effect when hitting the specimen in the transverse direction since both the hard (steel) and soft (plastic) tip are able to excite the bending vibrations responsible for the sound radiation. On the contrary the effect is more pronounced for the longitudinal testing configuration because only the harder tip can transfer the adequate amount of energy to activate all the longitudinal modes of the beam, which typically have much higher eigenfrequencies with respect to the bending modes.

INFLUENCE OF DECAY AND STATISTICAL ANALYSIS (T-TEST)

In Figure 5-5 are compared the sound spectra of the acoustic tests carried out on specimens S3 and D4, taken as example because of the equal span length. One can

observe that the decayed specimen exhibit lower frequency content of the acoustic signal with respect to the sound element, as would be expected due to the smaller value of modulus of elasticity and consistently with most of the literature on the subject.

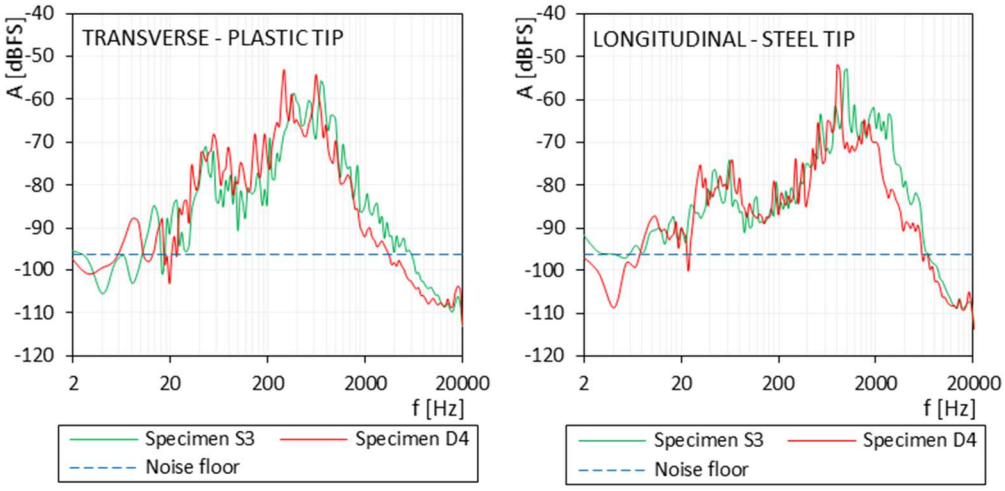

Figure 5-5 Comparison of sound spectra (1/12 octave smoothing) of tests performed on specimens S3 and D4 recorded with smartphone A: transverse (a) and longitudinal impact (b)

In order to compare all the tested specimens' frequency content on the same chart, Figure 5-6 reports the spectra boiled down to the single centroid value: on the abscissa are reported the spectral centroid value and on the ordinate the spectrum mean amplitude value. Figure 5-6 shows the results for the entire FFT frequency spectrum whereas Figure 5-7 shows the results for the spectrum limited to the upper bound set at the Spectral Roll-Off (SRO) value. From the results reported in Figure 5-6 it appears that sound specimens as a whole are characterised by higher mean amplitude values and lower spectral centroid values with respect to decayed specimens both for transverse and longitudinal impact tests. Moreover, the acoustic tests performed in the transverse direction exhibit higher spectral centroid values with respect to the tests performed in the longitudinal direction, in contradiction with what it would be expected from the theory.

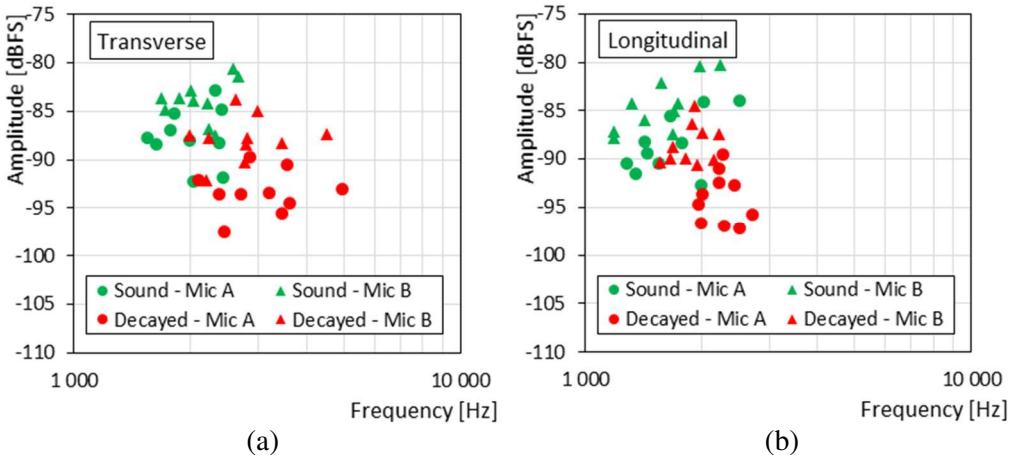

Figure 5-6 Spectral centroids and mean spectral amplitudes of all the acoustic impact test performed: transverse (a) and longitudinal impact (b)

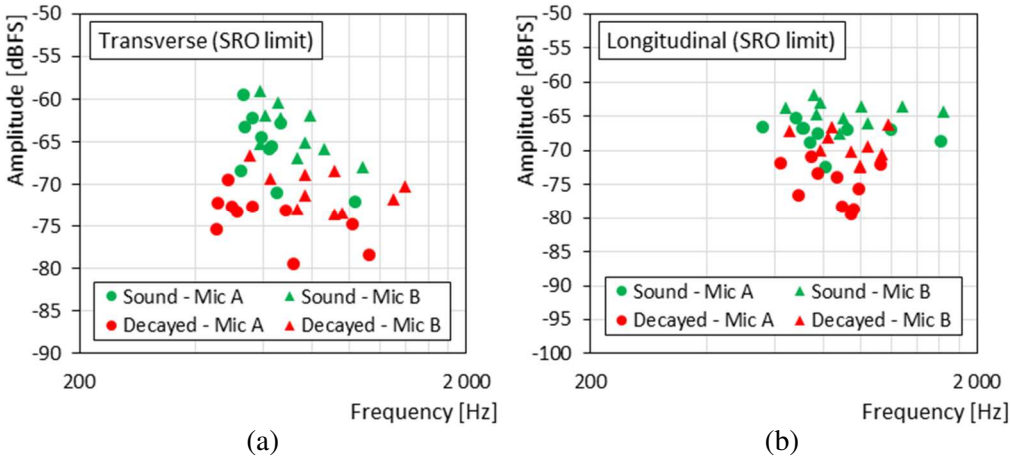

Figure 5-7 Spectral centroids and mean spectral amplitudes (limiting the spectrum to the SRO value) of all the acoustic impact test performed: transverse (a) and longitudinal impact (b)

The limit of the spectrum to the Spectral Roll-Off (SRO) value for the calculation of the relevant spectral descriptors, as proposed in Chapter 4 Proposed acoustic timber assessment method, appears to partially solve this incongruity with the theoretical predictions. In Figure 5-7 the longitudinal impact configuration shows higher frequency content with respect to the transverse impact configuration. Sound specimens also experience an increase in frequency content relative to the decayed specimens, not high enough though to what expected from theory. A more detailed discussion with a proposed explanation for this finding will be reported in the next section.

Finally, to evaluate the capability of the signal descriptors (identified in Chapter 4 Proposed acoustic timber assessment method to distinguish between sound and decayed timber elements a statistical analysis was carried out. A paired T-test was selected for the study since the predictor independent variable is categorical (sound or decayed wood material) while the outcome dependant variables are continuous (radiated sound features). It was chosen the paired T-test option and not the independent T-test because an actual independency between the samples cannot be assumed; the test is neither a "full" paired T-test since the specimens are not the same specimens examined before and after the decay attack. Nevertheless, the results can be used as an indicator of the potential of the various proposed parameters to detect differences in sound between timber in good and bad conditions. For this reason, it was opted also for the two-tailed version since it was not possible to establish a priori which of the different wood conservation stati (sound and decayed) is related to smaller or larger values of all the defined acoustic features.

The paired T-test is used to evaluate the statistical significance of the difference between the means of a reference parameter of two sample groups; in simple terms it tells if the difference of the two means is unlikely to be happened by chance. There can be two possible results of the test:

- H0 (Null hypothesis): there is not a significant difference between the means of the two groups of data.
- H1 (Alternate hypothesis): there is significant difference between the means of the two groups of data, unlikely caused by sampling error or chance.

The statistical parameter used for the test is called t-score and it is defined as:

$$t = \frac{\mu_d}{\sigma_d/\sqrt{n}} \qquad \text{(Eq. 5-1)}$$

Where μ_d is the mean value of the differences between the two sample groups A and B (having a single difference defined as $d_i = x_{i\in A} - x_{i\in B}$), σ_d is the standard deviation of the differences and n is the size of the "vector" d (equal to the size of a single sample group). Then the absolute value of the calculated t-score can be compared to the critical value of the Student's T distribution corresponding to the chosen significance value (usually set at 5%, indicated as $p = 0.05$) and to the number of degrees of freedom of the system ($df = n - 1$). If the absolute value of t-score is greater than the critical value, the null hypothesis can be rejected and the difference between the mean is said to be statistically significant (the p-value corresponding to the t-score is called the level of significance).

Considering the tests under examination, for the selection of the pair of specimens to calculate the differences was kept the order of specimens S1, …, S5 and D1, …, D5 presented in Table 5-1. To present the results for the all the tests, radar charts are adopted where on the various axes are reported the t-score value for the different acoustic features. The critical value ($p = 0.05$) is represented by a red shaded polygon, if a tested parameter falls into its area it means that the t-score value is smaller than the critical value and that the null hypothesis cannot be rejected.

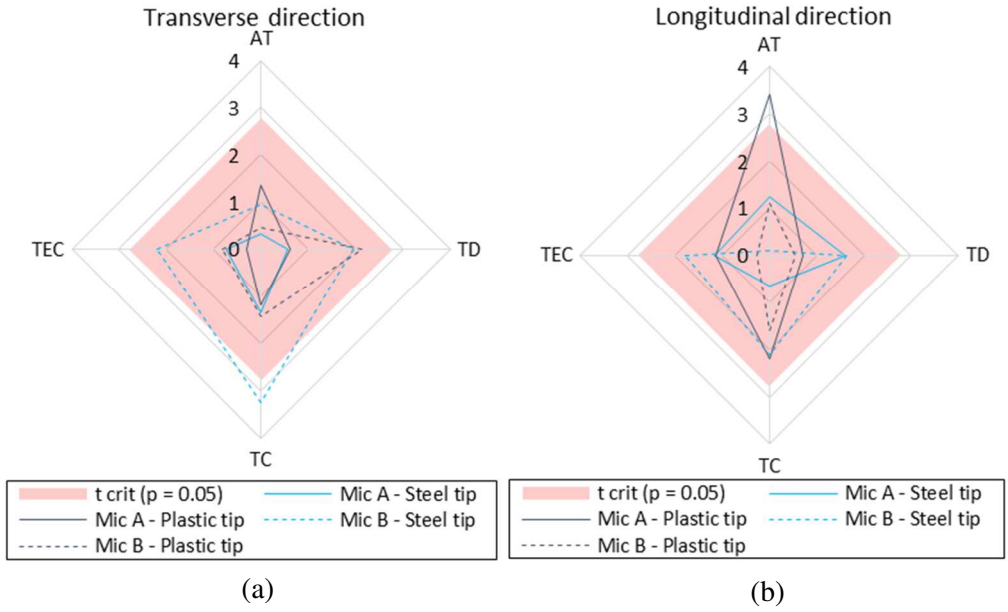

Figure 5-8 T-score values of the temporal descriptors for the transverse direction (a) and longitudinal direction (b)

Figure 5-8 shows the results for the 4 proposed temporal descriptors while Figure 5-9 and Figure 5-10 reports respectively the results for all the proposed spectral descriptors considering the entire frequency spectrum for the calculation and limiting the spectrum to the Spectral Roll-off (SRO) value. Figure 5-10 has one parameter less than Figure 5-9 because for the re-evaluation of the spectral features the SRO parameter is disregarded since it is applied as bound limit for the other parameters.

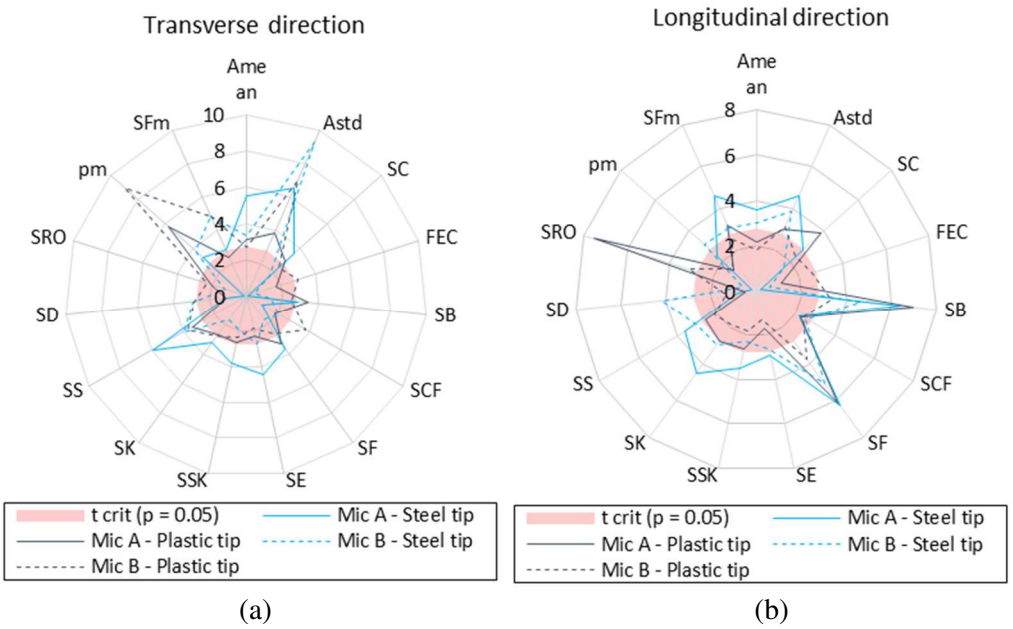

Figure 5-9 T-score values of the spectral descriptors for the transverse direction (a) and longitudinal direction (b)

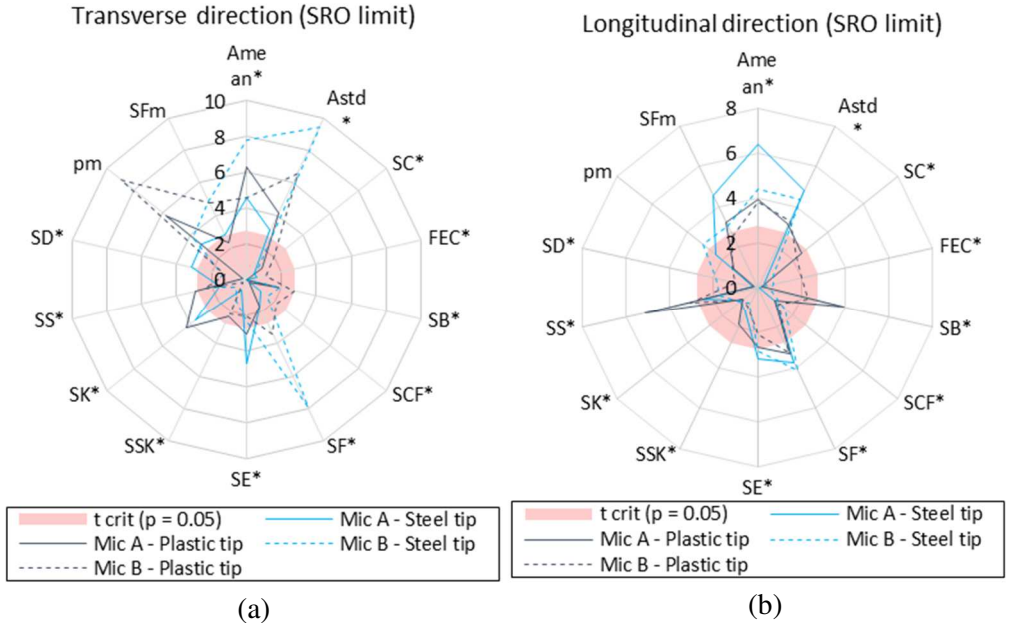

Figure 5-10 T-score values of the spectral descriptors (limiting the spectrum to the SRO value) for the transverse direction (a) and longitudinal direction (b)

From the outcomes of the t-score values for the spectral parameters it can be observed that the most reliable indicators seem to be the amplitude-based parameters (A_{mean} and A_{std}), the average values of pitch pm (especially for test in the transverse direction using a plastic tip hammer) and the average value of the spectral flux SFm (for test in the longitudinal direction using a steep tip hammer). As expected, the steel tip hammer appears to deliver better results for the longitudinal test configuration because of the higher frequency range of excitation. The parameters based on the frequency content of the signal (particularly spectral centroid SC and frequency energy centroid FEC) instead exhibited a poorer performance in identifying differences between sound and decayed material. However, a possible cause of this limitation may lie in the different geometrical dimensions of sound and decayed specimens. A more detailed discussion about this topic will be reported in the next section.

CORRELATION WITH MECHANICAL PROPERTIES

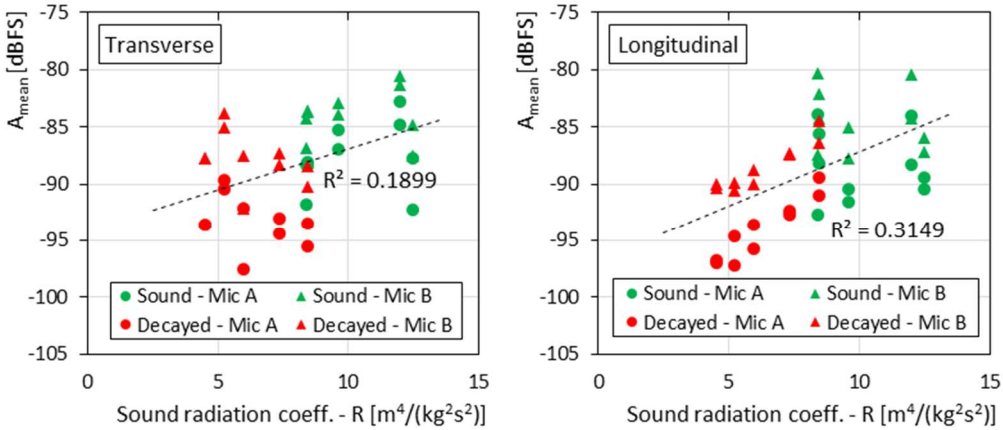

Figure 5-11 Correlation between spectrum mean amplitude and sound radiation coefficient of the various specimens: test in the transverse direction (a) and in the longitudinal direction (b)

A first interesting correlation between the static mechanical properties of the tested specimens and the related acoustic features can be obtained by linking the sound radiation coefficient to the mean amplitude value of the sound spectrum. The sound radiation coefficient discussed in Chapter 4 Proposed acoustic timber assessment method is calculated as:

$$R = \sqrt{\frac{MoE_{stat}}{\rho^3}} \qquad \text{(Eq. 5-2)}$$

It can be seen in Figure 5-11 that there is a positive correlation between the sound radiation coefficients calculated based on the static mechanical properties for each specimen and the spectrum mean amplitude value of the recorded sound. In particular, the decayed specimens exhibited lower spectral amplitude values likely due to lower sound radiation coefficient values. This phenomenon was observed both for the test in the transverse and in the longitudinal direction and for both the recording smartphones. It should be noted that the impact tool was a hand wield hammer (wielded by the same operator for each test); for this reason, the impact force, even if consistent within a certain range of values, cannot be considered constant across all the tests.

The correlation between the sound radiation coefficient and the average spectral amplitude is even more evident when limiting the spectrum to the upper frequency bound equal to the Spectral Roll-Off (SRO) as can be observed in Figure 5-12.

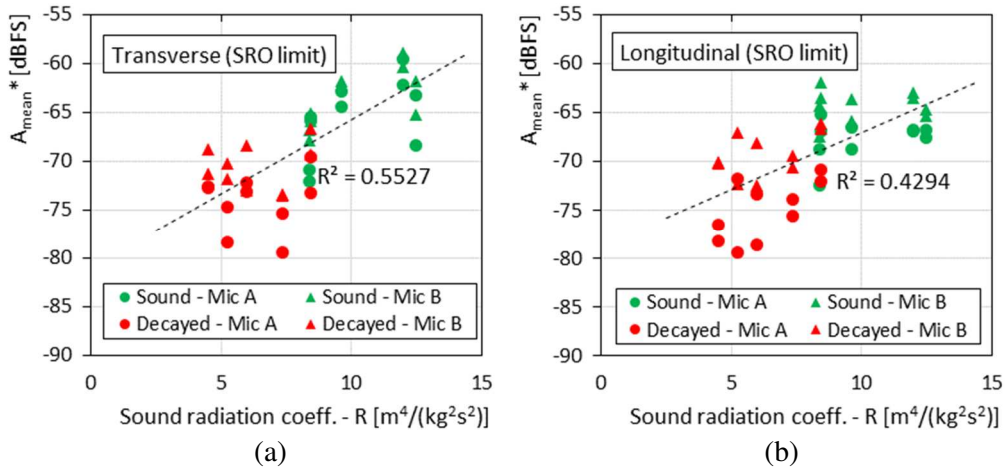

Figure 5-12 Correlation between spectrum mean amplitude (upper frequency limit at the SRO value) and sound radiation coefficient of the various specimens: test in the transverse direction (a) and in the longitudinal direction (b)

The second correlation between the geometrical and mechanical properties and the radiated sound from impact test is about the relation between the spectral centroid value and the frequency content of the structural vibrations of the beam specimens. To obtain a coefficient based on the specific geometrical and mechanical properties of each specimen let assume the Euler-Bernoulli theory for the dynamic behaviour of beam elements. The eigenfrequencies formulae for bending and longitudinal vibrations for simply supported conditions are:

$$f_{bending\,n} = \frac{\pi}{2}\frac{n^2}{L^2}\sqrt{\frac{EJ}{\rho A}} \quad \text{(Eq. 5-3)}$$

$$f_{longitudinal\,n} = \frac{n}{2L}\sqrt{\frac{E}{\rho}} \quad \text{(Eq. 5-4)}$$

From these formulations two parameters are extracted eliminating the dependence from the mode number for the sake of simplicity:

$$k_{bending} = \frac{\pi}{2L^2}\sqrt{\frac{MoE_{stat}J}{\rho A}} \quad \text{(Eq. 5-5)}$$

$$k_{longitudinal} = \frac{1}{2L}\sqrt{\frac{MoE_{stat}}{\rho}} \quad \text{(Eq. 5-6)}$$

Figure 5-13 reports the correlation between the bending and longitudinal vibration parameters and the Spectral Centroid values of each impact test. The smaller span length of the decayed specimens appears to overcome the effect of the lower modulus of elasticity caused by the decay, inducing higher frequency content for both the bending and longitudinal vibrations.

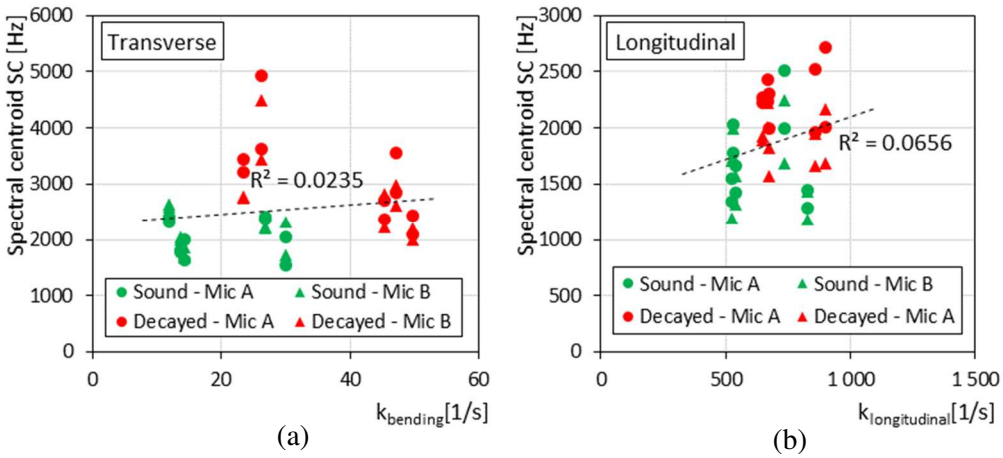

Figure 5-13 Correlation between the structural vibration parameters and the spectral centroid values for each test: impact in the transverse direction (a) and longitudinal direction (b)

This trend is also reflected in the spectral centroid values of the radiated sound and it is likely the reason because the paired T-test carried out for the frequency weighted parameters resulted in no statistically significant difference between sound and decayed

specimens. The limit of the spectrum to the Spectral Roll-Off (SRO) value for the calculation of the Spectral Centroid (SC^*) enhances the positive linear correlation between the vibrational parameter $k_{bending}$ and the SC^* value for tests in the transverse direction whereas for tests in the longitudinal direction the R^2 for the linear regression is smaller than in the case with the Spectral Centroid SC calculated with the entire spectrum (Figure 5-14).

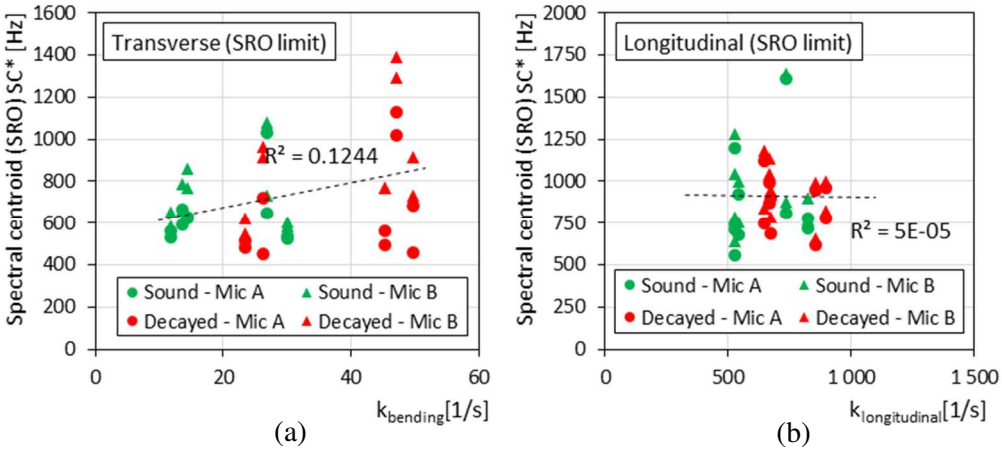

Figure 5-14 Correlation between the structural vibration parameters and the spectral centroid values (upper frequency limit at the SRO value) for each test: impact in the transverse direction (a) and longitudinal direction (b)

Finally, in Table 5-2 are reported the calculated acoustic critical frequency values f_{crit} for each tested specimen with also the sound radiation coefficients R and the defined vibrational parameters ($k_{bending}$ and $k_{longitudinal}$). The formula for calculating the acoustic critical frequency is obtained by equating the wavenumber of longitudinal wave in air with the wavenumber of bending wave in the beam specimens:

$$f_{crit} = \frac{c_{air}^2}{2\pi}\sqrt{\frac{\rho A}{MoE_{stat}J}} \qquad \text{(Eq. 5-7)}$$

It can be observed that for sound specimens the acoustic critical frequency values are lower ($f_{crit\ S\ mean} = 167\ Hz$) than that of the decayed specimens ($f_{crit\ D\ mean} = 231\ Hz$). This occurrence may also have played a role in augmenting the relative frequency content of sound radiated from decayed specimens with respect to the sound radiated from sound specimens and in turn have affected the paired T-test outcomes for frequency weighted parameters. In fact, the acoustic critical frequency is a lower bound

for the frequency content of sound, below which the intensity of sound propagation in the far field can be deemed as negligible.

Table 5-2 Sound radiation coefficient, bending and longitudinal vibration parameter and acoustic critical frequency for each timber beam specimen

Specimen ID	L [m]	MoE_{stat} [MPa]	ρ [kg/m^3]	R [m^4/(kg^{2}s^2)]	$k_{bending}$ [1/s]	$k_{longitudinal}$ [1/s]	f_{crit} [Hz]
S1	4.05	6587	358	11.98	11.9	530	151
S2	3.40	6005	439	8.44	14.3	541	175
S3	2.50	5904	438	8.39	26.9	737	177
S4	2.50	5576	330	12.47	30.1	826	158
S5	3.50	5175	383	9.60	13.6	525	176
D1	1.60	2306	484	4.52	45.3	674	248
D2	1.60	4287	494	5.96	49.7	898	220
D3	2.10	2949	380	7.33	26.3	670	259
D4	2.50	4006	383	8.45	23.5	647	201
D5	1.65	4340	541	5.23	47.2	858	229

5.2 EXPERIMENTAL CAMPAIGN ON DAMAGED SPECIMENS

OBJECTIVES	Assessment of the influence of variable parameters: ▪ Microphone device ▪ Element boundary conditions ▪ Impact location (transverse direction) Assessment of the influence of mechanical damage
TESTED MATERIAL	20 beam specimens
	New timber elements (2 alternative geometries)
	Spruce solid wood (strength grade C24)
IMPACT TOOLS	1 hand wielded hammers (hard plastic tip)
	Hammer weight ≈ 0.5 kg
RECORDING DEVICES	2 built-in smartphone microphones: ▪ Android™ device (Huawei™ Honor 6X) ▪ iPhone™ device (Apple iPhone™ 8) 1 measurement calibrated microphone: ▪ MiniDSP UMIK-1

ANALYSIS METHODS	Mechanical parameters: ▪ MOE (4-point bending test) ▪ Density (mass measurement) ▪ Moisture Content (resistance method)
	Acoustic analysis: ▪ Spectral centroids dispersion graph ▪ Paired T-test on audio features ▪ Correlation with mechanical properties

The second experimental investigation carried out was focused on the aspects not examined during the first pilot tests. In particular, the main subject of the campaign was the study of the effect of structural damage on the sound radiation from impacted timber beam specimens. The sample size of tested specimens was also increased with a selection of a first set of 10 solid-wood softwood beams with a span length of 2 m and a cross section of 100×100 mm^2 and a second set of 10 solid-wood softwood beams with a span length of 4 m and a cross section of 140×180 mm^2. As regard the acoustic testing configuration it was opted for impact in the transverse direction using a hard plastic tip hand wield hammer. The sound was recorded using two mid-market smartphones and a calibrated microphone (based on an electret sensor type) to be used as reference for assessing the reliability of the smartphones recording outcomes. The influence of the element boundary conditions was then evaluated by recording the sound of impact test performed in the midspan section for each specimen in simply supported and fixed-fixed conditions. Six specimens (three from the 2 m span length set and three from the 4 m span length set) were chosen for additional testing examining the effect of impact location different from the midspan section considering both the simply supported and fixed-fixed boundary conditions. These same specimens were then tested after the imposition of a simulated typical damage pattern for timber beam element: horizontal cuts were created at the mid-height of the cross section replicating a pass-through crack for a certain beam length. For fours specimens the cuts were applied at the beam ends (simulating shear failure cracks) and for the remaining two specimens the cuts were applied at the midspan section (simulating cracks for load perpendicular to the fibre direction).

A preliminary presentation of the results of this campaign was reported in a special issue paper of the International Journal of Architectural Heritage [5] as a follow-up article of the first SAHC conference paper. In this section a more in-depth and updated analysis of the outcomes will be presented and discussed.

5.2.1 TIMBER SPECIMENS AND MEASURED STATIC PROPERTIES

For the second experimental campaign twenty new timber specimens made of spruce solid wood (*Picea abies (L.) H. Karst*, strength grade C24 [4]) were selected for the tests. Two groups of beam geometries were considered representing standard dimensions for primary and secondary elements of typical existing wooden floors: the first group with a span length of 2 m and a cross section of 100×100 mm^2 (labelled as specimens A1, …, A10) and the second group with a span length of 4 m and a cross section of 140×180 mm^2 (labelled as specimens B1, …, B10).

As for the campaign on decayed timber elements, the mechanical properties of each specimen were experimentally determined (Table 5-3 and

Table 5-4). The static modulus of elasticity MoE_{stat} was measured with a 4-points bending test, the moisture content value via the resistance method (average value MC_{mean} and coefficient of variation CoV_{MC} assessed based on three measurement location along the beam axis) and the global density value ρ dividing the total measured mass value for the specimen volume.

Table 5-3 Measured mechanical properties for the first set of timber beam specimens: 2 m span length and cross section of 100×100 mm^2

Specimen ID	MoE_{stat} [MPa]	ρ [kg/m^3]	MC_{mean} [%]	CoV_{MC} [%]
A1	12328	451	14.4	1.2%
A2	9123	363	13.6	2.7%
A3	10089	383	15.0	1.1%
A4	11149	447	13.5	3.1%
A5	10930	444	12.1	3.4%
A6	9413	471	14.4	2.6%
A7	8370	358	14.8	6.8%
A8	8949	400	14.2	2.1%
A9	11607	405	12.8	2.0%
A10	11305	405	11.8	2.2%

Table 5-4 Measured mechanical properties for the second set of timber beam specimens: 4 m span length and cross section of 140×180 mm²

Specimen ID	MoE_{stat} [MPa]	ρ [kg/m³]	MC_{mean} [%]	CoV_{MC} [%]
B1	6013	356	13.5	4.7%
B2	9742	472	16.0	2.5%
B3	8894	446	16.4	4.2%
B4	6787	379	13.9	1.6%
B5	8475	404	12.0	3.9%
B6	6832	470	14.0	4.4%
B7	10474	447	13.9	2.1%
B8	8854	435	15.9	1.1%
B9	8486	473	15.0	12.6%
B10	8463	459	14.5	10.2%

5.2.2 ACOUSTIC TESTS PROGRAMME

As already stated at the beginning of the section for all the acoustic test it was opted for the transverse impact configuration using a hard plastic tip hand wield hammer (Figure 5-15 (a)). Three microphone devices were used for the recording: the built-in microphone of two mid-market smartphone devices and a measurement calibrated microphone. As regards the smartphones the same Android™ device of the previous campaign was used (*Huawei™ Honor 6X*, labelled as Smartphone A or Mic A in this work) while the iPhone™ device was changed (*Apple iPhone™ 8*, labelled as Smartphone C or Mic C in this work). The measurement calibrated microphone was the *MiniDSP™ UMIK-1* model (Figure 5-15 (b), labelled as Microphone D or Mic D in this work), which is an omni-directional USB measurement microphone typically used for speaker and room acoustic measurement. Here it was adopted as reference microphone to assess the goodness of the smartphones' recordings.

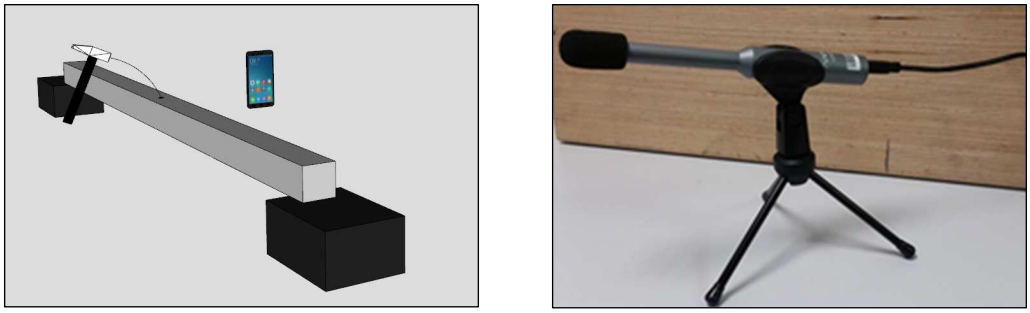

(a) (b)

Figure 5-15 (a) Test configuration for the second experimental campaign: impact in the transverse direction (b) Picture of the reference calibrated microphone: model MiniDSP™ UMIK-1

The calibration file (measured Frequency Response Function FRF of the microphone in laboratory conditions, Figure 5-16) was used to equalize the acoustic impact test recordings using a Matlab® [6] code reported in Annex A – MATLAB Code.

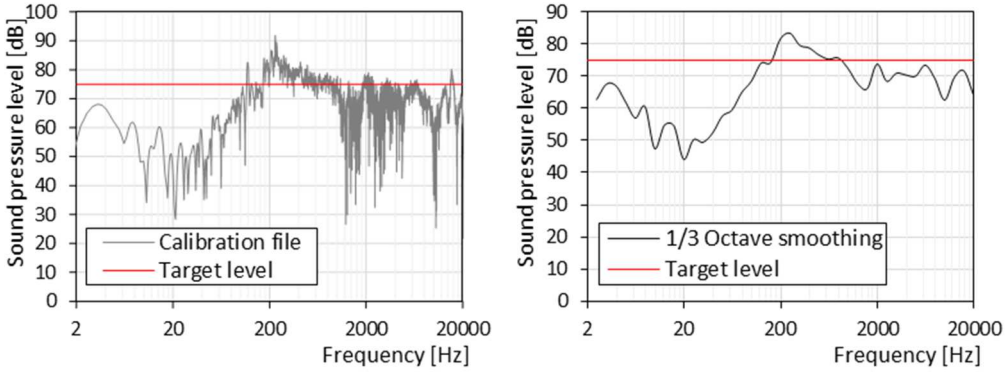

(a) (b)

Figure 5-16 MiniDSP™ UMIK-1 calibration file for a sound target level of 75 dB SPL and 1/3 octave smoothing used in the Matlab® sound equalizer

All the tested specimens were impacted in the transverse direction at the midspan section. This location corresponds to an antinode of the odd vibrational modes of the beam and a node of the even vibrational modes of the beam (Figure 5-17).

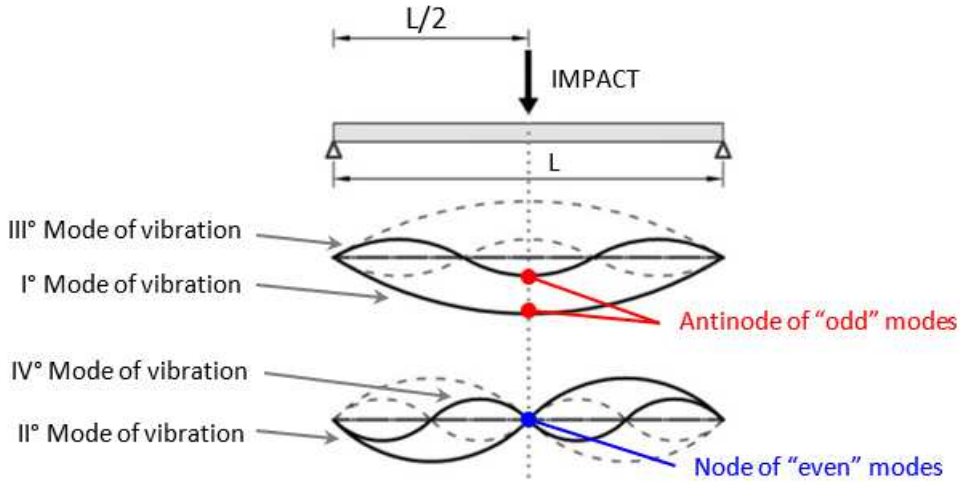

Figure 5-17 Relationship between impact location at the midspan section and vibrational modes of a simply supported beam

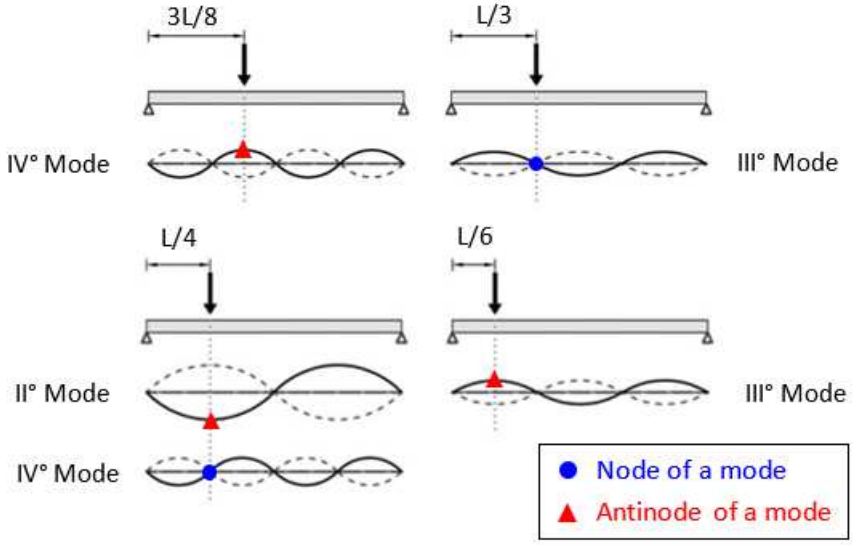

Figure 5-18 Relationship between the four selected impact locations (in addition to the midspan section) and modes excitation

As reported in Chapter 3 Theoretical basis of wave propagation and structural vibration, this implies the excitation of only the odd vibrational modes of the beam. Consequently, the sound radiation will reflect a frequency content related to these modes (considering also the lower bound imposed by the acoustic critical frequency).

To examine the influence of different impact locations on the sound radiation of acoustic impact test, six specimens (i.e. A1, A2, A3 and B1, B2, B3) were tested in four new locations, progressively closer to the beam end. Figure 5-18 shows a schematic representation of the four new test configurations and the link between the selected location and the nodes and antinodes of the first bending modes for simply supported conditions.

Figure 5-19 Setup adopted to replicate fixed-fixed boundary conditions: clamp apparatus between two wooden surfaces using two threaded rods with tightening nuts

To evaluate the influence of the boundary conditions a specific apparatus was prepared (Figure 5-19). This setup replicated the hindering of beam ends rotations of fixed-fixed conditions by clamping the extremities of the specimen between two wooden surfaces (i.e. two cross-laminated timber CLT elements) with the use of two tightened threaded steel rods.

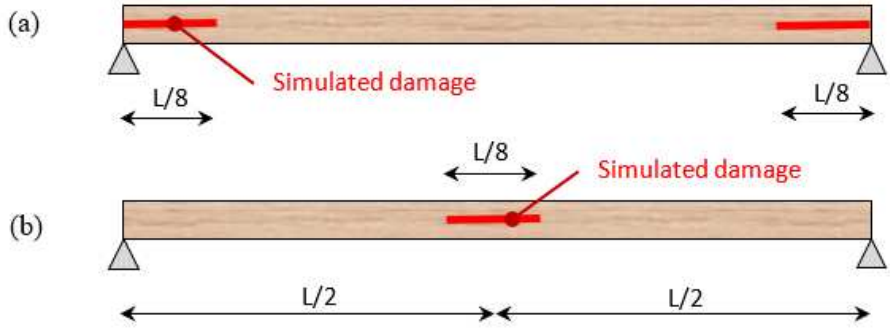

Figure 5-20 Damage scenarios: cuts at the beam ends (a) and at the midspan section (b)

All the acoustic tests performed in simply supported conditions (each specimen impacted at the midspan section and the selected six specimens impacted in the

additional four locations) were also replicated in fixed-fixed boundary conditions. Finally, the six specimens tested in the different impact locations were subjected to an imposed damage type replicating two scenarios particularly disadvantageous for the structural capacity of the timber elements (Figure 5-20). For the first case (specimens A1, A3, B1 and B3) pass-through horizontal cuts with a length equal to one eighth of the total span of the beam (i.e. 25 cm for specimens A and 50 cm for specimens B) were introduced at the two beam ends, simulating cracks due to longitudinal shear failure mode at the supports. The cuts were applied at the mid-height of the beams cross section by using a chainsaw (approximate blade thickness of 2 mm). For the second damage scenario (specimens A2 and B2) cuts of the same length were applied centred at the midspan section replicating a local tensile failure perpendicular to the grain. The acoustic impact tests were performed in all the five considered impact locations for all the six specimens with the two simulated damage scenarios.

In conclusion, a total of 128 different test configurations were examined using two smartphone and a reference calibrated microphone for the recordings:

- 20 acoustic tests for 20 specimens in simply supported conditions and with the impact location at the midspan section.
- 24 acoustic tests for 6 specimens in simply supported conditions and with four additional impact locations (3L/8, L/3, L/4, and L/6).
- 20 acoustic tests for 20 specimens in fixed-fixed boundary conditions and with the impact location at the midspan section.
- 24 acoustic tests for 6 specimens in fixed-fixed boundary conditions and with four additional impact locations (3L/8, L/3, L/4, and L/6).
- 30 acoustic tests for 6 specimens in simply supported conditions considering two simulated damage scenarios and five impact locations (L/2, 3L/8, L/3, L/4, and L/6).

Therefore, a total of 384 stored .wave files were processed using the feature extraction procedure illustrated in Chapter 4 Proposed acoustic timber assessment method and the relative outcomes will be presented in the next section.

5.2.3 OUTCOMES ANALYSIS AND DISCUSSION

CORRELATION WITH MECHANICAL PROPERTIES

Figure 5-21 shows the correlation between the sound radiation coefficient (see (Eq. 5-2) in section 5.1.3) and the average spectral amplitude for both groups of specimens (A and B), impacted at the midspan section, and reporting both the outcomes for simply supported and fixed-fixed boundary conditions.

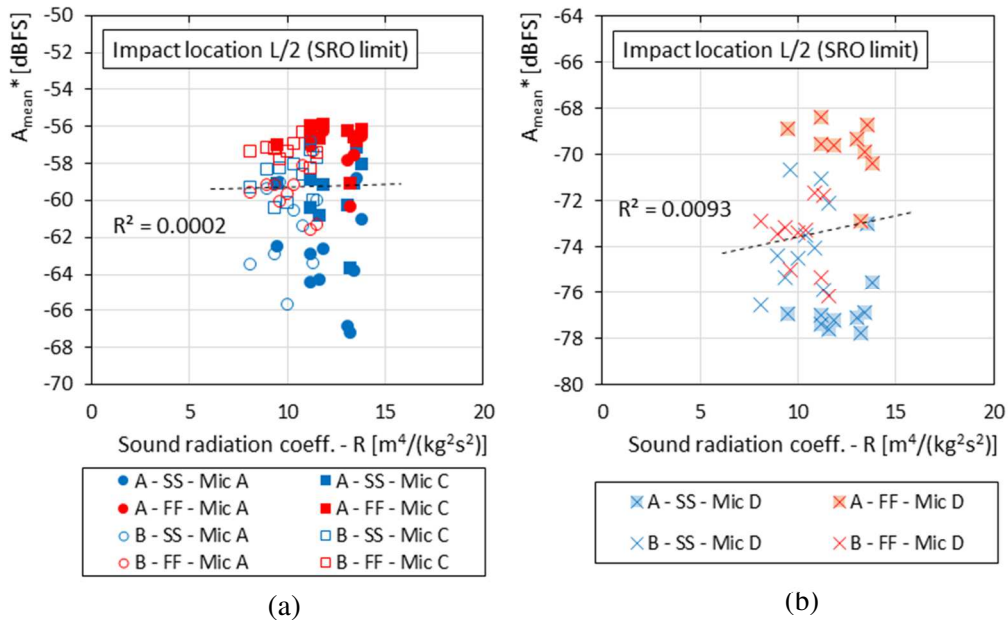

Figure 5-21 Correlation between spectrum mean amplitude (upper frequency limit at the SRO value) and sound radiation coefficient of the various specimens: smartphone microphones (a) and calibrated microphone (b). Graph legend example: Specimens A – Simply Supported – Microphone A

It was opted to maintain separate the results for the smartphone microphones (labelled as "Mic A" and "Mic C") and the calibrated microphone (labelled as "Mic D") due to different sensitivity value of the microphone sensors.

The results are not as evident as that reported for the experimental campaign on decayed specimens (section 5.1.3). The weak positive linear relation between the sound radiation coefficient and the mean spectral amplitude is likely due to the smaller range of sound radiation coefficients with respect to the former campaign on decayed specimens. A possible way to improve the clarity of the results could be the adoption of an impact device with a calibrated level of input force, however this aspect of the acoustic test was not the primary goal of the presented research work. Nevertheless, some indications from the tests performed with a hand-wield hammer can be extrapolated by the charts reported in Figure 5-21. Elements with fixed-fixed boundary conditions (represented in the charts with the colour red) exhibit higher mean spectral amplitude values compared to elements in simply supported conditions.

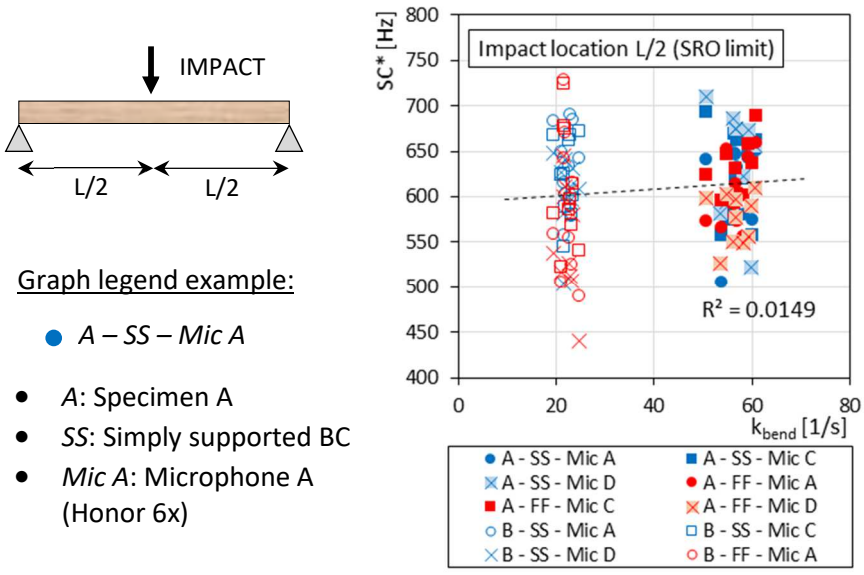

Figure 5-22 Correlation between the structural vibration parameters k_{bend} and the spectral centroid values (upper frequency limit at the SRO value) for each test: test configuration (a) and results(b)

The second correlation between acoustic and mechanical properties is reported in Figure 5-22 which presents the relation between the vibrational parameter $k_{bending}$ (see (Eq. 5-5) in section 5.1.3) and the SC^* value. The graph shows only a weak positive correlation between the two parameters as evidenced by the large scatter of SC^* values and the small R^2 number. It is interesting to note however that the different sensitivity level of the microphones used for the recording has a limited influence on the SC^* values thanks to the fact that these are obtained via a weighted operation of frequency and amplitude bins (therefore insensitive to "shifts" of amplitude constant across the frequency range).

Table 5-5 Sound radiation coefficient, bending vibration parameter and acoustic critical frequency for timber beam specimens A (span length 2 m and cross section area 100×100 mm²)

Specimen ID	L [m]	MoE_{stat} [MPa]	ρ [kg/m³]	R [m⁴/(kg²s²)]	$k_{bending}$ [1/s]	f_{crit} [Hz]
A1	2.0	12328	451	11.59	59.27	124
A2	2.0	9123	363	13.81	56.83	129

A3	2.0	10089	383	13.40	58.18	126
A4	2.0	11149	447	11.17	56.62	130
A5	2.0	10930	444	11.17	56.25	131
A6	2.0	9413	471	9.49	50.68	145
A7	2.0	8370	358	13.51	54.81	134
A8	2.0	8949	400	11.82	53.62	137
A9	2.0	11607	405	13.22	60.69	121
A10	2.0	11305	405	13.05	59.89	123

Table 5-6 Sound radiation coefficient, bending vibration parameter and acoustic critical frequency for timber beam specimens B (span length 4 m and cross section area 140×180 mm²)

Specimen ID	L [m]	MoE_{stat} [MPa]	ρ [kg/m³]	R [m⁴/(kg²s²)]	$k_{bending}$ [1/s]	f_{crit} [Hz]
B1	4.0	6013	356	20.97	11.54	88
B2	4.0	9742	472	23.18	9.63	79
B3	4.0	8894	446	22.78	10.01	81
B4	4.0	6787	379	21.59	11.17	85
B5	4.0	8475	404	23.36	11.34	79
B6	4.0	6832	470	19.45	8.11	95
B7	4.0	10474	447	24.69	10.83	74
B8	4.0	8854	435	23.01	10.37	80
B9	4.0	8486	473	21.61	8.95	85
B10	4.0	8463	459	21.90	9.35	84

INFLUENCE OF ANALYSIS PROCEDURE AND MICROPHONE

Figure 5-23 shows the comparison of the spectral centroid and mean amplitude values considering the entire spectrum for the calculation (couples SC and A_{mean}) and limiting the spectrum to the upper bound of the Spectral Roll-Off (couples SC^* and A^*_{mean}). It can be observed that the procedure of limiting the spectrum for the extraction of the frequency-based audio features helps to reduce the scattering of the outcomes (in the frequency domain) due to the adoption of different microphone devices. In fact, Figure 5-23-b exhibits a much more similar dispersion of the SC^* values comparing the

smartphone microphones (labelled as Mic A and Mic C) to the reference calibrated microphone (labelled as Mic D). The gap in amplitude values instead is most likely related to different value of microphone sensitivity, however it seems that this has not particularly affected the results of the frequency weighted parameters.

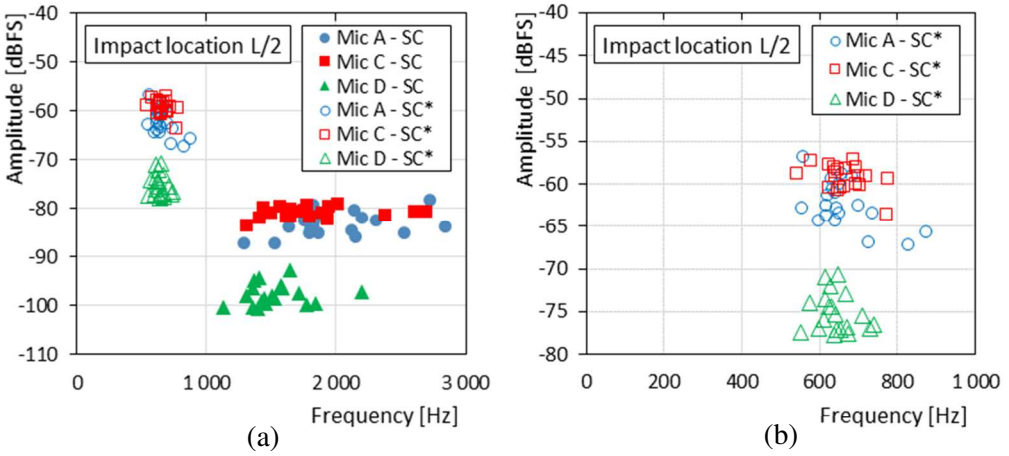

Figure 5-23 Spectral centroids (SC and SC) and mean amplitudes (A_{mean} and A_{mean}*) of acoustic impact tests performed on all specimens in simply supported conditions (midspan section): all values (a) and detail about only SC* and A_{mean}* couples*

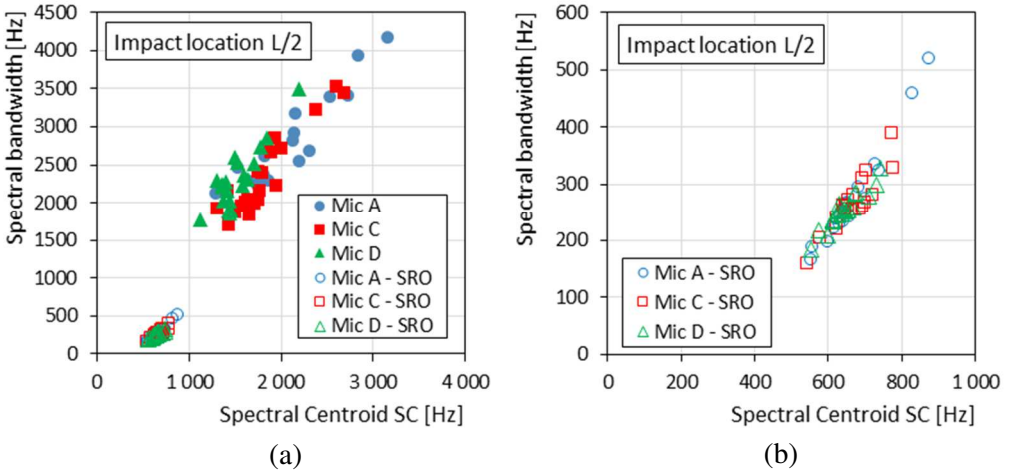

Figure 5-24 Spectral centroids (SC and SC) and spectral bandwidths (SB and SB*) of acoustic impact tests performed on all specimens in simply supported conditions (midspan section): all values (a) and detail about only SC* and SB* couples*

Figure 5-24 and Figure 5-25 present respectively the relation between the spectral centroid and spectral bandwidth (couples SC and SB) and the mean amplitude and

amplitude standard deviation values (couples A_{mean} and A_{std}). Not surprisingly there is a positive, almost linear, correlation between the centroid and average parameters (SC and A_{mean}) and the dispersion related parameters (SB and A_{std}).

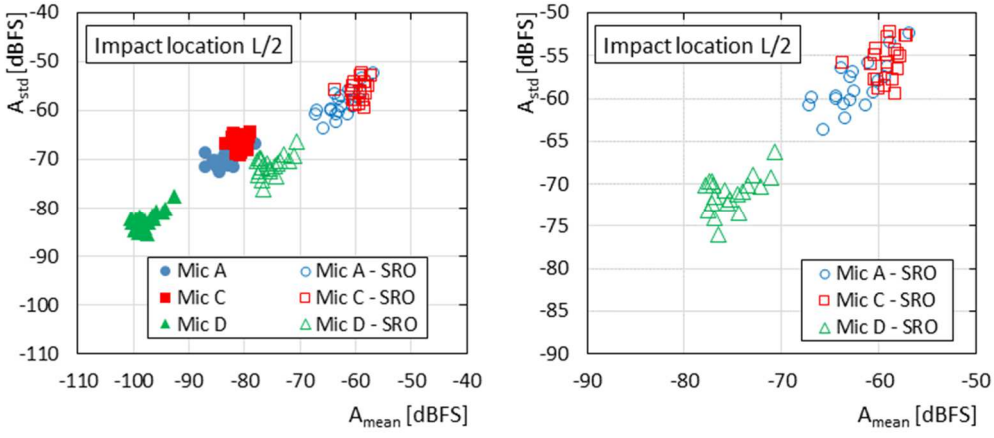

Figure 5-25 Mean amplitudes (A_{mean} and A_{mean}) and amplitude standard deviation (A_{std} and A_{std}*) of acoustic impact tests performed on all specimens in simply supported conditions (midspan section): all values (a) and detail about only A_{mean}* and A_{std}* couples*

INFLUENCE OF BOUNDARY CONDITIONS AND STATISTICAL ANALYSIS (T-TEST)

In this section will be reported the outcomes of the acoustic impact tests for the specimens tested varying the type of boundary conditions. Figure 5-26, Figure 5-27, and Figure 5-28 report the t-score values resulted from paired T-test performed to evaluate the influence of the type of boundary condition on the sound radiation temporal and spectral descriptors (before and after the imposition of the SRO limit). As regards the time-based parameters only few of the features exhibited significant t-score values, but also these outcomes were not consistent across the different microphones used for the recording. For this reason, it was decided to not use the temporal descriptors for further investigations. More interesting findings can be extrapolated from paired T-test carried out for the frequency-based parameters. Comparing the t-scores of specimens A and B (for both Figure 5-27 and Figure 5-28) one can see that the type of boundary condition has a larger effect on specimens A, especially when it comes to directly amplitude-based features (e.g. A_{mean} and A_{std}). The second important remark is related to the spectral centroid parameter SC^* calculated limiting the spectrum to the Spectral Roll-Off (SRO) value (Figure 5-28). The type of boundary condition appears to have limited if any influence on the spectral centroid SC^* parameters of both specimens A and B.

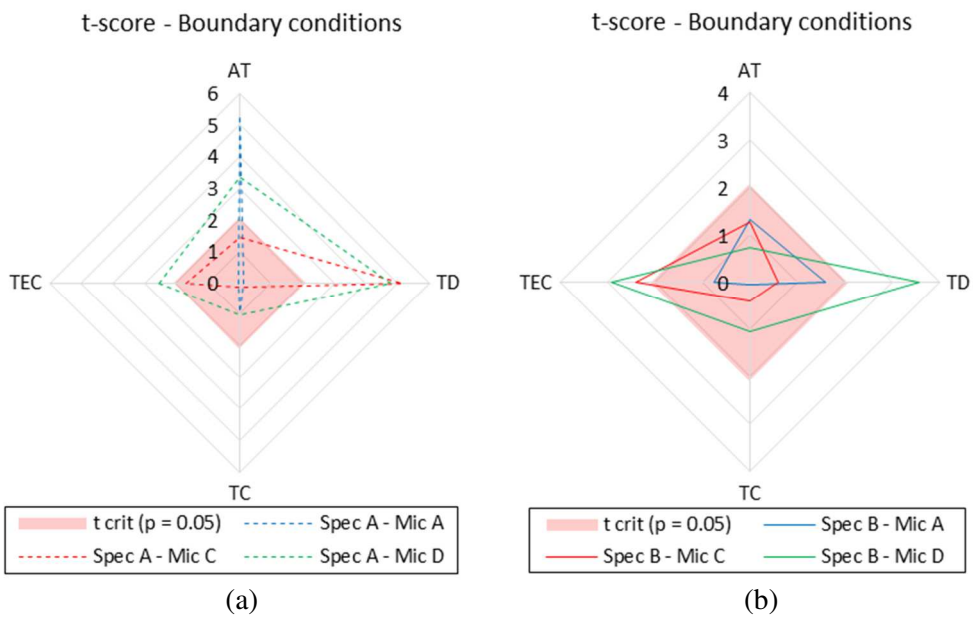

Figure 5-26 T-score values (influence of boundary conditions) of the temporal descriptors for the specimens A (a) and specimens B (b)

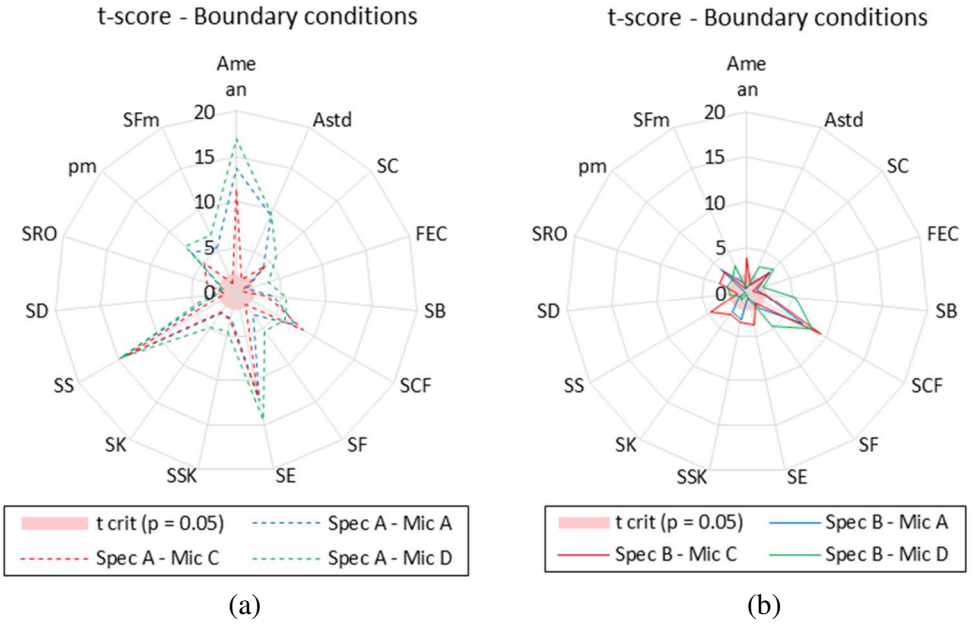

Figure 5-27 T-score values (influence of boundary conditions) of the spectral descriptors for the specimens A (a) and specimens B (b)

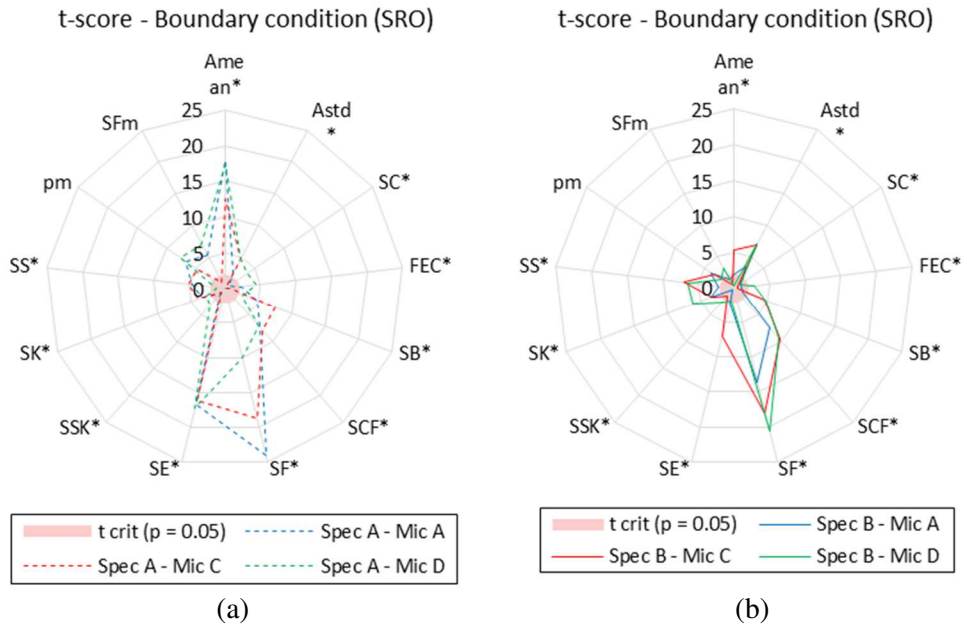

Figure 5-28 T-score values (influence of boundary conditions) of the spectral descriptors (limiting the spectrum to the SRO value) for the specimens A (a) and specimens B (b)

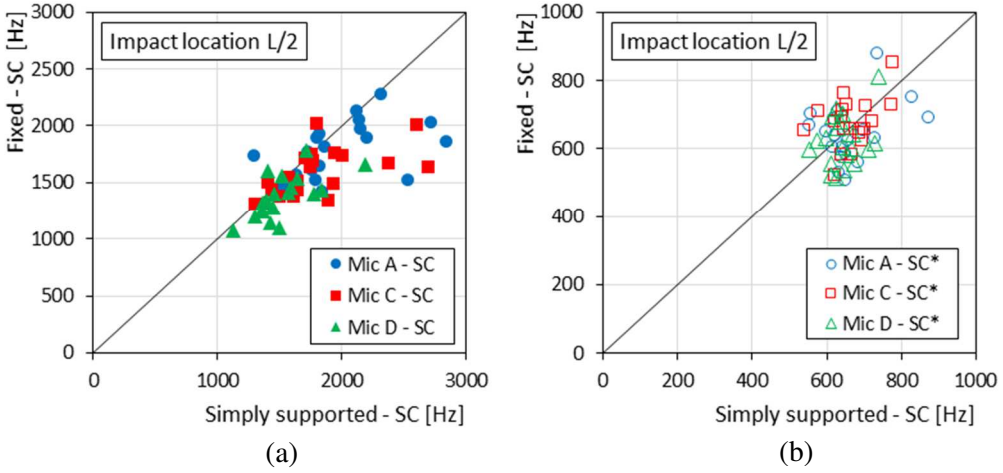

Figure 5-29 Correlation of spectral centroid values for specimen in simply supported and fixed-fixed boundary conditions for an impact at the midspan section. Spectral centroid obtained from the entire spectrum (a) and limiting the spectrum to the SRO value (b)

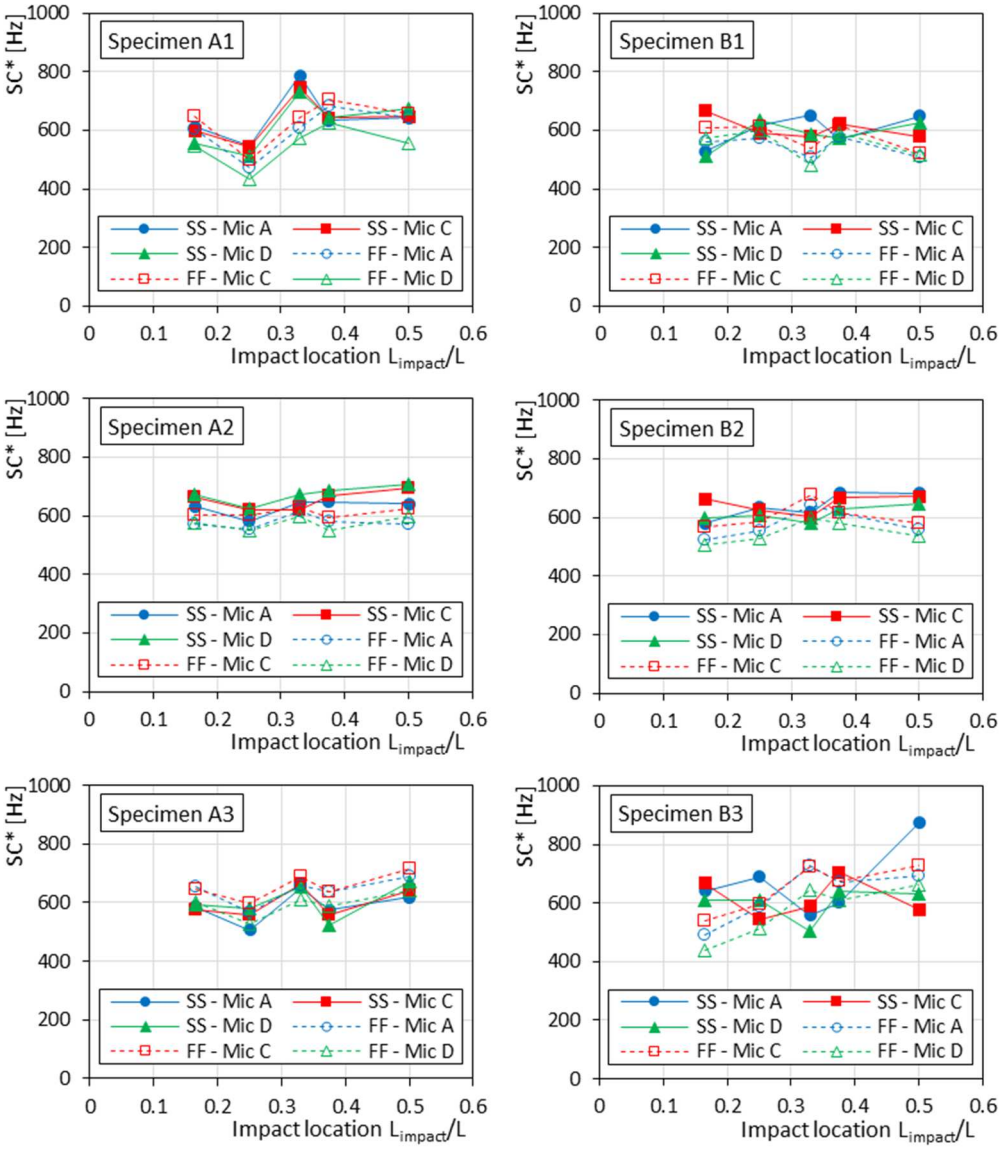

Figure 5-30 Spectral centroids SC in the different impact location for the six tested specimens under the two considered beam boundary conditions ("SS" stands for simply supported and "FF" for fixed-fixed)*

To further examine the relation between the spectral centroid parameters and the type of boundary conditions Figure 5-29 and Figure 5-30 report the correlation of SC and SC^* values in simply supported and fixed-fixed conditions for all specimens impacted in the midspan section, and the SC^* values, plotted in the different impact locations, for the six specimens selected for additional studies. The procedure of limiting the spectrum

to the SRO value is what allows to reveal the limited influence of the boundary conditions on the spectral centroid values (Figure 5-29). From Figure 5-30 it can be seen that even changing the position of the impact the consistency of the results remains unaltered, with the variation due to the type of boundary condition similar to the difference due to the use of different microphones. This finding can be explained by the fact that the spectral centroid is a weighted mean of all the signal frequency content and acknowledging that the hypothetical larger influence of the type of boundary condition on the sound and vibration behaviour of a structure is in the low frequency range. Considering a Euler-Bernoulli type of beam the ratio of the dynamic vibration fundamental frequency for a beam with fixed ends over pinned ends is equal to 2.25 and decreases for increasing mode number (and related increasing frequency), being equal to 1.27 and 1.17 respectively for the 4th and 6th bending mode.

INFLUENCE OF DAMAGE AND STATISTICAL ANALYSIS (T-TEST)

In this last section will be presented the outcomes of the acoustic impact tests performed on the six specimens (i.e. A1, A2, A3 and B1, B2, B3) selected for the test after the imposition of a chain-saw induced damage, simulating pass-through cracks perpendicular to the grain direction.

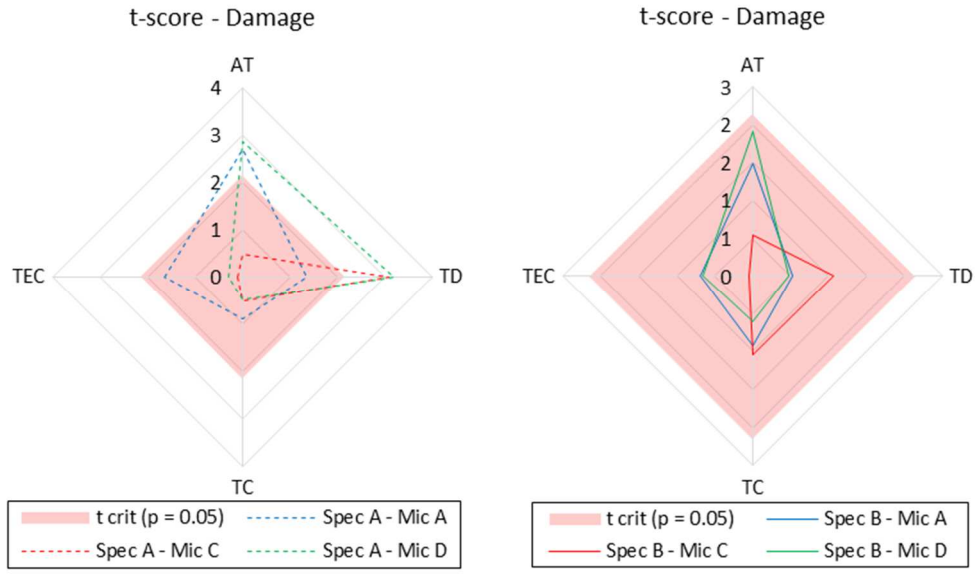

Figure 5-31 T-score values (influence of damage) of the temporal descriptors for the specimens A (a) and specimens B (b)

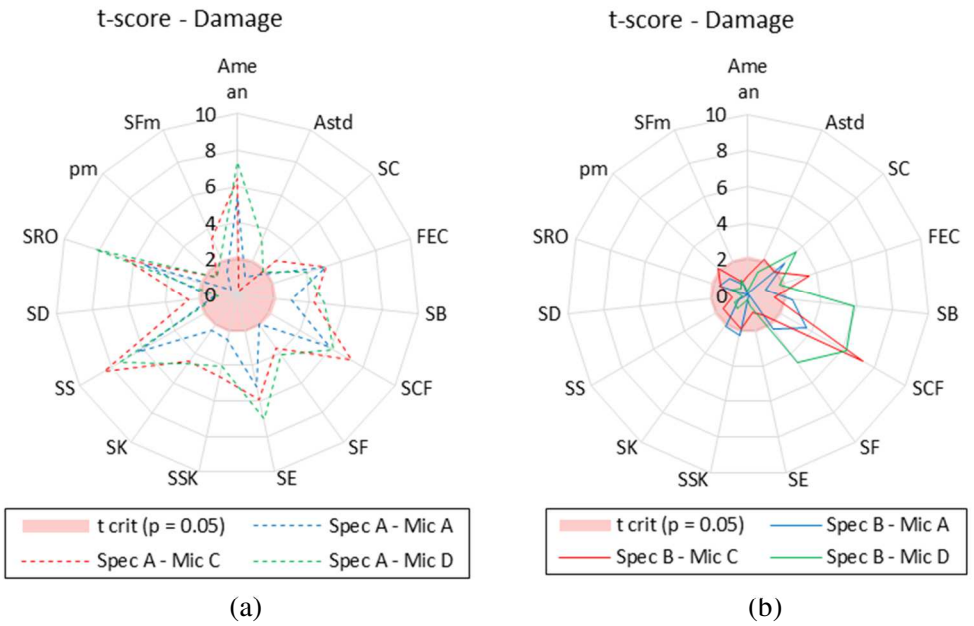

Figure 5-32 T-score values (influence of damage) of the spectral descriptors for the specimens A (a) and specimens B (b)

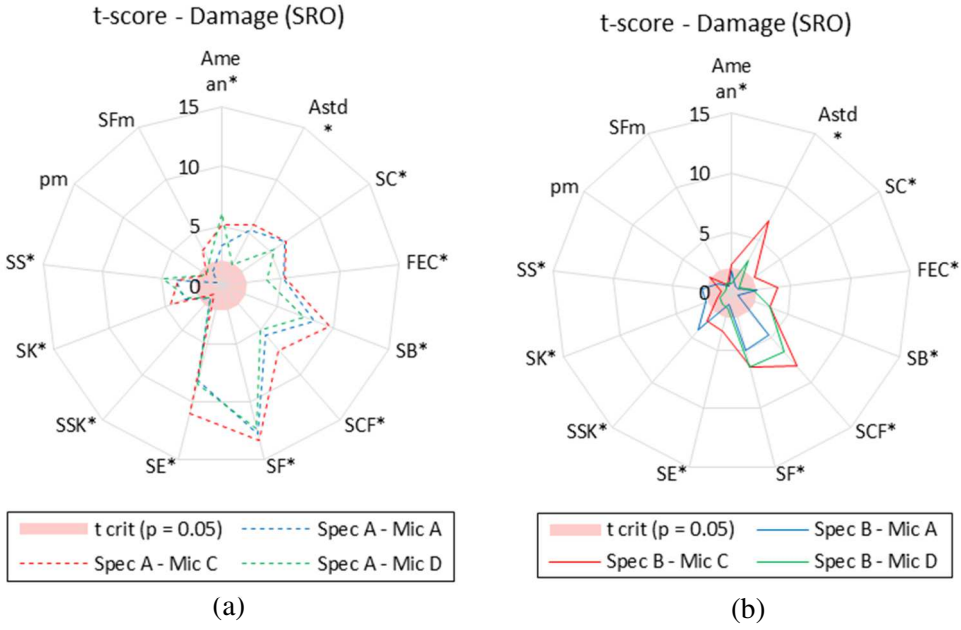

Figure 5-33 T-score values (influence of damage) of the spectral descriptors (limiting the spectrum to the SRO value) for the specimens A (a) and specimens B (b)

Figure 5-31, Figure 5-32, and Figure 5-33 report the t-score values resulted from paired T-test performed to evaluate the influence of damage on the sound radiation temporal and spectral descriptors (before and after the imposition of the SRO limit). Temporal descriptors exhibited limited influence from the applied damage compared to the intact specimens (i.e. low t-score values), therefore they are disregarded in the detailed commentary. Once again, more remarkable considerations can be drawn from the paired T-tests performed for the spectral descriptors. As already noted for the test under different boundary conditions, specimens A show a larger effect on the acoustic test due to the imposed damage compared to specimens B A plausible explanation for this behaviour may be the larger ratio r_{mass} between the mass of the hammer ($m_{hammer} \cong 0.5\ kg$) and the mass of the beam for specimens A ($r_{mass\,A} \cong 5\%$) with respect to specimens B ($r_{mass\,B} \cong 1\%$), which allows for a more effective energy transfer from the impact in the case of specimens A. It is interesting to note also that, differently for the tests on the type of boundary condition, the t-scores related to the SC^* parameter indicate a significant difference between the acoustic tests in undamaged and damaged conditions (especially for specimens A). This observation suggests that the SC^* parameter may be robust indicator for the presence of damage, insensitive to the type of boundary condition (often difficult to be properly defined during a preliminary on-site assessment).

Figure 5-34 shows the spectral centroids SC^* for the six examined specimens, tested in intact conditions (solid lines) and in damaged conditions (dashed lines) hitting the beam in five different positions. For a direct visual interpretation of the outcomes a schematic graphical representation of half of the beam (with the imposed damage depicted as a red rectangle) is layered on top of the SC^* charts. From the results of specimens A1 and A2 is evident how approaching the damage location the SC^* parameter undergoes an increase in frequency with the larger difference from the "undamaged" values in correspondence of the damage (specimen A2) or close to it (specimen A1). Specimen A3 displayed a singular response from the acoustic tests after the application of damage, with an almost constant increase of centroid frequencies ($\cong +300\ Hz$) in all the five impacted positions. Therefore, it was decided to impact the damaged specimen A3 directly at the location of damage (i.e. $0.07 \cdot L$ from the beam end) and this additional test exhibited an additional increase for the SC^* parameter ($\cong +200\ Hz$) with respect to the spectral centroids measured in the other five positions located outside the damaged portion. Specimens B on the other hand shown a more limited influence of the presence of damage on the SC^* parameter. For specimens B1 and B3 the acoustic tests carried out on the intact and on the damaged beam delivered almost equal results in term of spectral centroid values.

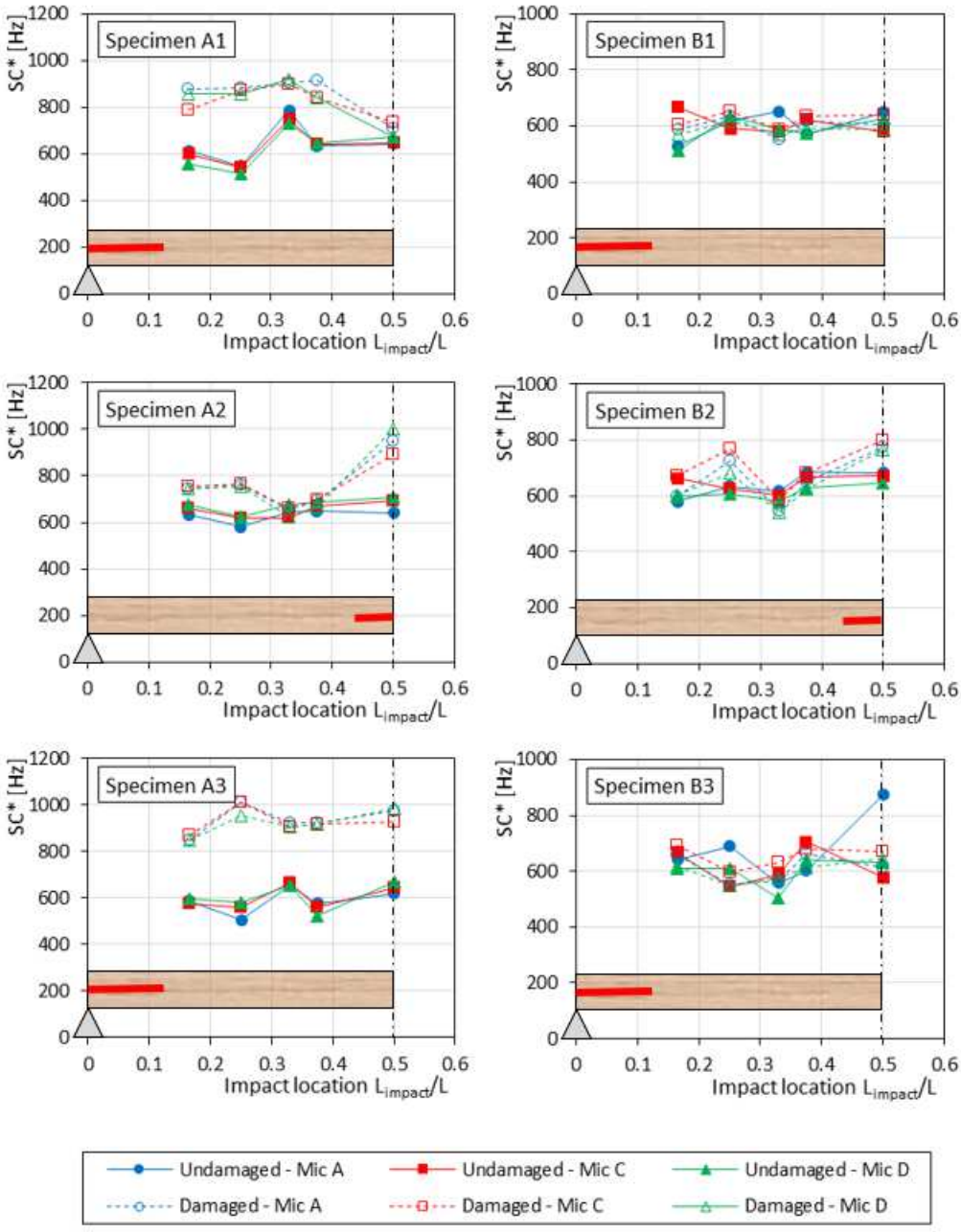

Figure 5-34 Spectral centroids SC in the different impact location for the six tested specimens in undamaged and damaged conditions (the graphic on the bottom of each chart shows the position of the applied damage)*

Specimen B2 instead exhibited a similar behaviour to specimen A2, with a slightly less pronounced, but still significant, increase in frequency value for the SC^* parameter measured at the location of damage. It is believed that this difference in behaviour between specimens A and specimens B can be attributed to the greater mass of specimens B, which limited the effect of damage on sound radiation from impact test outside the damaged beam section.

5.3 REFERENCES

[1] D. Riccadonna, G. Schiro, D. Casagrande, M. Piazza and I. Giongo, "On the use of sound spectral analysis for the in situ assessment of structural timber" Proceedings of the 11th International Conference on Structural Analysis of Historical Constructions SAHC, Cusco, Perú, 2018.

[2] European Committee for Standardization (2010). EN 408: Timber Structures – Structural timber and glued laminated timber – Determination of some physical and mechanical properties. CEN, Brussels, Belgium.

[3] European Committee for Standardisation (2002). EN 13813-2: Moisture content of a piece of sawn timber - Part 2: Estimation by electrical resistance method. CEN, Brussels, Belgium.

[4] European Committee for Standardization. 2016. EN 338: Structural timber – Strength classes. Brussels, Belgium: CEN.

[5] D. Riccadonna, I. Giongo, D. Casagrande and M. Piazza, "Acoustic testing for the preliminary assessment of timber beams – A pilot study" *International Journal of Architectural Heritage*, vol. 13, no. 7, 2019.

[6] MATLAB. (2020). 9.9.0.1467703 (R2020b). Natick, Massachusetts: The MathWorks Inc.

This page intentionally left blank.

6 CONCLUSIONS

This thesis presented a research work aimed at studying and developing a specific assessment method for existing timber structures based on the recording of the radiated sound from impact tests (using smartphone built-in microphones), and on the following analysis of the registered acoustic signal. It was highlighted that this technique could represent an improvement of the so-called tapping (sounding) method, known in literature (and in practice) as a qualitative approach for an approximate estimate of the timber element conditions. The use of a microphone allows to eliminate the subjectivity of human sound perception and permits to obtain reproducible outcomes within the limit of the microphone different technical specifications. The recording of the sound enables a more objective and scientific analysis of the acoustic signal properties. Finally, the suggested use of smartphone built-in microphones permits to retain the qualities of cost-effectiveness and speed of measurement of the "standard" tapping method, making this method an attractive solution for the preliminary stage of assessment. This means that the method could be used for the detection of supposed critical areas of the examined structure in the initial stage of the assessment procedure. These critical areas could then be examined more thoroughly with detailed NDT or SDT techniques, excluding the possible cases of false positive that "preliminary methods" may detect.

The currently available methods for the assessment of timber structures were described, with a particular emphasis on the stress-wave based techniques, to set up the literature background for the proposed method. A brief yet detailed compendium of the physics of waves propagation inside solid and fluid media was reported so as to provide a firm scientific base for the interpretation of sound radiation from vibrating structures. The theoretical study part continued with the exposition of the basic notions of acoustic, the presentation of the most relevant microphone technical specifications and the definition of the most relevant concepts of signal frequency analysis. At the end of this preparatory section, an original procedure (and the relative MATLAB code) to analyse and interpret the outcomes of the experimental part of the thesis is presented, with a selection of

proposed descriptive parameters to encapsulate the sound information in a set of data more manageable.

The experimental program was divided into two different campaigns, one focused on the study of the influence of decay on sound radiation and the other focused on the examination of the effect of damage on the acoustic impact test results. For both campaigns softwood timber beam specimens were analysed exclusively. Due to the exploratory nature of the study, several other parameters that may affect the results were considered and investigated: microphone-to-sound-source distance, impact tool type (i.e. "soft" and "hard" hammer tip), microphone type and element boundary conditions. As regard microphone-to-sound source distance an appropriate value was found to be 1 meter; shorter distances may increase the risk of signal clipping and the influence of proximity effect for MEMS microphone, while larger distances may reduce the available signal-to-noise ratio. Regarding the impact tool type to use, it was found that when the signal is expected to achieve high ranges of frequency content (e.g. impact in the longitudinal direction, relative smaller elements, etc.), a hammer tip realised with "hard" material (e.g. steel) is required for being able to excite the complete spectrum of the structure. For each campaign the main mechanical parameters (i.e. modulus of elasticity, global density and moisture content) of the tested specimens were measured and then used to obtain acoustic related features (e.g. sound radiation coefficient, acoustic critical frequency, etc.). With the purpose of comparing the results from acoustic impact testing of sound timber with the data from timber in decayed and damaged conditions, two-tailed paired T-tests were used, and t-score values were calculated for all the defined acoustic temporal and spectral descriptors. From the outcomes of the first investigation on timber decayed material, it was detected a strong correlation between the sound mean spectral amplitude values and the sound radiation coefficients. Decayed specimens, having smaller sound radiation coefficients, exhibited lower sound intensity as evidenced by the smaller values of mean spectral amplitudes. Regarding the second experimental campaign, one of the most interesting findings was related to the spectral centroid parameter. The spectral centroid demonstrated to be a promising robust parameter for the detection of damage, being relatively insensitive to the modification of the beam element boundary conditions but showing significant variations between acoustic tests in intact and damaged conditions.

Regarding the working hypotheses stated in the Chapter 1 Introduction, it was confirmed that wood decay, due to the reduction of Modulus of Elasticity (MOE) and surface hardness of the material, induces a decrease in the intensity of the acoustic response recorded from impact test. The reduction in frequency content was also observed comparing the spectra of timber specimens with equal geometric properties in sound and decayed conditions. When the comparison was extended to elements having

different span lengths the influence of decay on the frequency content of the signal (related to the reduction of MOE) was less discernible due to the acute effect of span length variation on the bending natural frequencies of the beam (correlated to the sound radiation). This result serves as an indication for the care which should be apply in an eventual practical application of the method in the definition of the geometrical constraints of the tested elements and the comparison of frequency content of element with similar geometries. With regard to the influence of mechanical damage, it was observed that the presence of pass-through cracks in the element cross-section causes a rise in frequency content of the acoustic signal, which is more noticeable if the impact location is closer to the site of damage and if the timber element overall dimensions are small. It is assumed that this increase in frequency content is likely due to the alteration of the flexural vibration behaviour, with the "summation" of the response of partial section of the element to the global vibration pattern of the structure.

However, given that the findings of this pilot research project are based on a limited number of specimens and under specific conditions, the results from such analyses should be treated with due caution. Future studies in this area should focus on increasing the number of available experimental data, including different timber species and timber products, and different element geometry (e.g. Cross-Laminated-Timber panels). An appreciable increase of the experimental database will not only make the findings more reliable but will also enable the adoption of advanced soft computing techniques for the analysis of the radiated sound. An important aspect of the research which should be investigated in future studies is the difference between laboratory (or otherwise controlled) conditions and on-site survey conditions. Specifically, two subjects to be assessed are the effect of surfaces close to the impact location, in other terms the effect of sound reflections on the acoustic signal, and the effect of background noise, in particular steady noise type. For the latter case, the adoption of noise cancelling algorithm should be examined as a possible counter-measure. Another promising area of research exploration for the proposed method could be the coupled use of accelerometers sensor and microphones. In fact, the close relation between the vibrations of the timber structure and the consequent sound radiation could be analysed more thoroughly (e.g. link between bending modes and sound frequency content, bending wave dispersion relation from Wavenumber Transform, etc.).

This page intentionally left blank.

ACKNOWLEDGMENTS

At the end of this important and stimulating period of my life there are a few people I would like to thank.

First of all, I am grateful to my supervisors prof Maurizio Piazza and Dr. Ivan Giongo for their invaluable assistance and expert guidance during the three years of the PhD program.

I would also like to thank several “colleagues” from the Timber and Masonry Research Group of the University of Trento (either former or present members) for their support and friendship during this journey: Dr. Stefano Bezzi, Mirko Capovilla, Marco Carlet, Davide Cassol, Dr. Daniele Casagrande, Andrea Gaspari, Dr. Ermes Rizzi, Dr. Gianni Schiro, Stefano Segatta, Francesco Smiroldo, and Giovanni Sommacal.

Finally, I want to acknowledge the help of the former undergraduate students Paolo Maria Vendramini, Federico Dallapè, Semir Nasufoski, and Edoardo Bertoni, and the direct and indirect support of all the staff of the Department of Civil, Environmental and Mechanical Engineering of the University of Trento (including the technicians of the LPMS laboratory, the administrative staff and all the professors and researchers).

The research work presented in the thesis was carried out within the framework of the ReLUIS-DPC network (Italian University Network of Seismic Engineering Laboratories and Italian Civil Protection Agency).

This page intentionally left blank.

ANNEX A – MATLAB CODE

IMPACT AUDIO ANALYSIS

```
clear all
close all
clc

set(0,'defaultfigurecolor',[1 1 1])

%% Import data and plot time history
% Reading of the audio file: y data are the amplitude of the
% signal in linear scale and fs is the sampling frequency
[y,fs] = audioread('example.wav');
% Trim the data to 0.1 seconds before impact and 1.4 seconds
% after impact
y_peak = max(y);
pos_t = find(y==y_peak);
low_y = pos_t -0.1*fs;
up_y = pos_t +1.4*fs;
y_trim = y(low_y:up_y);

% Temporal resolution
T = 1/fs;
% Length of the signal
L = length(y_trim);
% Temporal vector
t = (0:L-1)*T;
% Data in logarithmic scale (decibel full scale: dBFS)
y_dB = 20*log10(abs(y_trim));

% Graphic representation of the signal in the time domain
% (amplitude in linear scale and logarithmic scale (dBFS), time
% in seconds). Logarithmic scale useful to detect if all the
% signal is represented in the selected temporal section
```

```
figure(1)

subplot(2,1,1);
plot(t,y_trim,'b');
xlabel('Time [s]');
ylabel('Amplitude [lin]');

subplot(2,1,2);
plot(t,y_dB,'b');
xlabel('Time [s]');
ylabel('Amplitude [dBFS]');

%% Signal descriptors in the time domain
% Calculation of the signal features in the time domain: attack
% time (AT), time duration (TD), time centroid (TC) and time
% energy centroid (TEC)

t_peak = find(y_trim==y_peak);
tol = 0.01;

AT_init = find(abs(y_trim(1:t_peak)-0.1*y_peak)<tol,1);
AT_fin = find(abs(y_trim(1:t_peak)-0.9*y_peak)<tol,1,'last');
AT = t(AT_fin)-t(AT_init);

TD_fin = t_peak + find(abs(y_trim(t_peak:L)-
0.1*y_peak)<tol,1,'last');
TD = t(TD_fin)-t(AT_init);

TC =
sum(t(AT_init:TD_fin)*y_trim(AT_init:TD_fin))/sum(y_trim(AT_ini
t:TD_fin));

TEC =
sum(t(AT_init:TD_fin)*(y_trim(AT_init:TD_fin).^2))/sum(y_trim(A
T_init:TD_fin).^2);

disp(['Attack time AT [s] =' num2str(AT)]);
disp(['Time duration TD [s] =' num2str(TD)]);
disp(['Time centroid TC [s] =' num2str(TC)]);
disp(['Time energy centroid TEC [s] =' num2str(TEC)]);

% Graphic representation of the signal descriptors in the time
% domain
AT_y = [0.5*y_peak;0.5*y_peak];
AT_x = [t(AT_init);t(AT_fin)];

TD_y = [0;0];
TD_x = [t(AT_init);t(TD_fin)];

figure(2)
```

```
plot(t,y_trim,'b','linewidth',0.8);
xlabel('Time [s]');
ylabel('Amplitude [lin]');

hold on

scatter(t(t_peak),y_peak,'o','b','filled');
plot(AT_x,AT_y,'m','linewidth',1,'marker','v','MarkerFaceColor'
,'m');
plot(TD_x,TD_y,'g','linewidth',1,'marker','v','MarkerFaceColor'
,'g');
scatter(TC,0,72,'o','r','filled');
scatter(TEC,0,72,'s','c','filled');
yline(0.9*y_peak,'-.r','0.9*Peak','linewidth',0.8);
yline(0.1*y_peak,'-.r','0.1*Peak','linewidth',0.8);
xline(t(AT_init),'-.r','linewidth',0.8);
xline(t(AT_fin),'-.r','linewidth',0.8);
xline(t(TD_fin),'-.r','linewidth',0.8);

hold off

legend({'Signal','Peak','Attack time','Time duration','Time
centroid',...
    'Time energy
centroid'},'Location','southeast','color',[0.95 0.95 0.95],...
    'edgecolor','k','linewidth',0.7)

%% Windowing of the signal
% Definition of a rectangular window (aka "No window")
win = rectwin(L);
% Amplitude Correction Factor (ACF) to compensate for the
% reduction of signal amplitude after the window is applied
mean_win = mean(win);
ACF = 1/mean_win;
% Energy Correction Factor (ECF) to compensate for the
% reduction of signal energy after the window is applied
rms_w =rms(win);
ECF = 1/rms_w;
% Windowing of the signal
ywin = y_trim.*win;

% Graphic representation of the signal, the windowed signal and
% the applied window (note: if a rectangular window is applied
% the signal remains equal)
figure(3)
title('Window');
plot(t,y_trim,'b','linewidth',0.8)
xlabel('Time [s]');
ylabel('Amplitude [lin]');
hold on
```

```
plot(t,win,'g','linewidth',0.8)
hold on
plot(t,ywin,'r','linewidth',0.8)
hold on

hold off

legend({'Signal','Window','Windowed
signal'},'Location','southeast',...
    'color',[0.95 0.95 0.95],'edgecolor','k','linewidth',0.7)

%% Spectrum analysis using the Fast Fourier Transform (FFT)
% Zero-padding of the signal to apply the FFT (N is the closest
% power of two to the signal length)
N = 2^nextpow2(L);
Y = fft(ywin,N);
% Normalization of the two-sided spectrum (complex FFT)and use
% of the ACF
P2 = abs(Y)/N;
P2 = P2*ACF;
% One-sided spectrum neglecting the mirrored part of the two-
% sided spectrum (negative frequencies)
P1 = P2(1:N/2);
% Discarding the first value (DC frequency at 0 Hz) and the
% last value corresponding to the Nyquist frequency.
% Multiplying by a factor of 2 to account for the loss of
% symmetry and represent the right amplitude
P1 = (2*P1(2:end-1));

% Frequency spectrum resolution
F = fs/N;
% Frequency vector defined up to the Nyquist frequency (fs/2)
f = (2:(N/2-1))*F;
% Graphic representation of the spectrum: linear amplitude and
% logarithmic frequency axis
figure(4)
semilogx(f,P1,'b')
xlabel('Frequency [Hz]');
ylabel('Amplitude [lin]');
% Graphic representation of the spectrum: logarithmic amplitude
% (dBFS) and logarithmic frequency axis
P1db = 20*log10(P1);
figure(5)
semilogx(f,P1db,'b')
xlim([20 max(f)]);
xlabel('Frequency [Hz]');
ylabel('Amplitude [dBFS]');

%% Signal descriptors in the frequency domain
% Calculate spectrum peak value (f_peak, A_peak), mean
```

```
% amplitude (A_mean), spectral centroid (SC), spectral
% bandwidth (SB), frequency energy centroid (FEC), spectral
% crest factor (SCF), spectral flatness (SF), spectral entropy
% (SE), spectral skewness (SSK), spectral kurtosis (SK),
% spectral slope (SS), spectral decrease (SD) and spectral
% rolloff (SRO)

A_peak = max(P1db);
pos_fpeak = find(P1db==A_peak);
f_peak = f(pos_fpeak);

A_mean_lin = mean(P1);
A_mean = 20*log10(A_mean_lin);
A_std_lin = std(P1);
A_std = 20*log10(A_std_lin);

SC = sum(f*P1)/sum(P1);
FEC = sum(f*(P1.^2))/sum(P1.^2);
SB = (sum(((f-SC).^2)*P1)/sum(P1))^(1/2);
SCF = max(P1)/mean(P1);
SF = geomean(P1)/mean(P1);
SE = -sum(P1.*log(P1))/log(length(P1)-1);
SSK = sum(((f-SC).^3)*P1)/(SB^3*sum(P1));
SK = sum(((f-SC).^4)*P1)/(SB^4*sum(P1));

f_mean = mean(f);
SS = sum((f-f_mean)*(P1-A_mean_lin))/sum((f-f_mean).^2);

SD = 0;
for k = 2:length(P1)
    SD = SD + ((P1(k)-P1(1))/(k-1))/P1(k);
end

tot_en = sum(P1.^2);
energy = 0;
pos_f = 1;
while(energy <= 0.95* tot_en) && (pos_f < length(f))
    energy = energy + P1(pos_f).^2;
    pos_f = pos_f +1;
end
SRO = f(pos_f);

disp([' ']);
disp(['Peak amplitude A_peak [dBFS] =' num2str(A_peak)]);
disp(['Peak frequency f_peak [Hz] =' num2str(f_peak)]);
disp(['Mean amplitude A_mean [dBFS] =' num2str(A_mean)]);
disp(['Amplitude standard deviation A_std [dBFS] ='
num2str(A_std)]);
disp(['Spectral centroid SC [Hz] =' num2str(SC)]);
disp(['Frequency energy centroid FEC [Hz] =' num2str(FEC)]);
```

```
disp(['Spectral bandwidth SB [Hz] =' num2str(SB)]);
disp(['Spectral crest factor SCF [] =' num2str(SCF)]);
disp(['Spectral flatness SF [] =' num2str(SF)]);
disp(['Spectral entropy SE [] =' num2str(SE)]);
disp(['Spectral skewness SSK [] =' num2str(SSK)]);
disp(['Spectral kurtosis SK [] =' num2str(SK)]);
disp(['Spectral slope SS [1/Hz] =' num2str(SS)]);
disp(['Spectral decrease SD [] =' num2str(SD)]);
disp(['Spectral rolloff SRO [Hz] =' num2str(SRO)]);

% Graphic representation of the spectral slop in the frequency
% domain and using a linear scale for the amplitude axis

figure(6)
plot(f,P1,'b','linewidth',0.8)
xlim([20 max(f)]);
xlabel('Frequency [Hz]');
ylabel('Amplitude [lin]');

y_SS_lin = SS*(f-SC)+A_mean_lin;

hold on

plot(f,y_SS_lin,'c','linewidth',0.8);

hold off

legend({'Spectrum','Spectral
slope'},'Location','southeast','color',...
    [0.95 0.95 0.95],'edgecolor','k','linewidth',0.7)

% Graphic representation of the signal descriptors in the
% frequency domain

figure(7)
semilogx(f,P1db,'b','linewidth',0.8)
xlim([20 max(f)]);
xlabel('Frequency [Hz]');
ylabel('Amplitude [dBFS]');
grid on

hold on

scatter(f(pos_fpeak),A_peak,'o','b','filled');
plot([SC-
SB/2;SC+SB/2],[A_mean;A_mean],'m','linewidth',0.8,'marker','s',
...
    'MarkerFaceColor','m');
plot([SC;SC],[A_mean-
A_std/2;A_mean+A_std/2],'m','linewidth',0.8,'marker',...
```

```
    's','MarkerFaceColor','m');
scatter(SC,A_mean,72,'o','r','filled');
scatter(FEC,A_mean,72,'s','g','filled');

hold off

legend({'Spectrum','Peak','Spectral bandwidth','Amplitude
std',...
    'Spectral centroid','Frequency energy
centroid'},'Location',...
    'southwest','color',[0.95 0.95
0.95],'edgecolor','k','linewidth',0.7)

%% Signal descriptors in the frequency domain limited to the
SRO value
% Recalculate mean amplitude (A_mean*), spectral centroid
% (SC*), frequency energy centroid (FEC*) and spectral
% bandwidth (SB*) spectral crest factor (SCF*), spectral
% flatness (SF*), spectral entropy (SE*), spectral skewness
% (SSK*), spectral kurtosis (SK*), spectral slope (SS*),
% spectral decrease (SD*) limiting the spectrum data to the
% spectral rolloff frequency value

A_mean_lin_SRO = mean(P1(1:pos_f));
A_mean_SRO = 20*log10(A_mean_lin_SRO);
A_std_lin_SRO = std(P1(1:pos_f));
A_std_SRO = 20*log10(A_std_lin_SRO);

SC_SRO = sum(f(1:pos_f)*P1(1:pos_f))/sum(P1(1:pos_f));
FEC_SRO = sum(f(1:pos_f)*(P1(1:pos_f).^2))/sum(P1(1:pos_f).^2);
SB_SRO = (sum(((f(1:pos_f)-
SC_SRO).^2)*P1(1:pos_f))/sum(P1(1:pos_f)))^(1/2);
SCF_SRO = max(P1(1:pos_f))/mean(P1(1:pos_f));
SF_SRO = geomean(P1(1:pos_f))/mean(P1(1:pos_f));
SE_SRO = -
sum(P1(1:pos_f).*log(P1(1:pos_f)))/log(length(P1(1:pos_f))-1);
SSK_SRO = sum(((f(1:pos_f)-
SC_SRO).^3)*P1(1:pos_f))/(SB_SRO^3*sum(P1(1:pos_f)));
SK_SRO = sum(((f(1:pos_f)-
SC_SRO).^4)*P1(1:pos_f))/(SB_SRO^4*sum(P1(1:pos_f)));

f_mean_SRO = mean(f(1:pos_f));
SS_SRO = sum((f(1:pos_f)-f_mean_SRO)*(P1(1:pos_f)-
A_mean_lin_SRO))/...
    sum((f(1:pos_f)-f_mean_SRO).^2);

SD_SRO = 0;
for k = 2:length(P1(1:pos_f))
    SD_SRO = SD_SRO + ((P1(k)-P1(1))/(k-1))/P1(k);
end
```

```
disp([' ']);
disp(['Mean amplitude SRO A_mean* [dBFS] ='
num2str(A_mean_SRO)]);
disp(['Amplitude standard deviation SRO A_std* [dBFS] ='
num2str(A_std_SRO)]);
disp(['Spectral centroid SRO SC* [Hz] =' num2str(SC_SRO)]);
disp(['Frequency energy centroid SRO FEC* [Hz] ='
num2str(FEC_SRO)]);
disp(['Spectral bandwidth SRO SB* [Hz] =' num2str(SB_SRO)]);
disp(['Spectral crest factor SRO SCF* [] =' num2str(SCF_SRO)]);
disp(['Spectral flatness SRO SF* [] =' num2str(SF_SRO)]);
disp(['Spectral entropy SRO SE* [] =' num2str(SE_SRO)]);
disp(['Spectral skewness SRO SSK* [] =' num2str(SSK_SRO)]);
disp(['Spectral kurtosis SRO SK* [] =' num2str(SK_SRO)]);
disp(['Spectral slope SRO SS* [1/Hz] =' num2str(SS_SRO)]);
disp(['Spectral decrease SRO SD* [] =' num2str(SD_SRO)]);

% Graphic representation of the signal descriptors in the
% frequency domain calculated limiting the spectrum to the SRO
% value

figure(8)
semilogx(f(1:pos_f),P1db(1:pos_f),'b','linewidth',0.8)
xlim([20 max(f)]);
xlabel('Frequency [Hz]');
ylabel('Amplitude [dBFS]');
grid on

hold on

plot(f(pos_f:end),P1db(pos_f:end),'color',[0.8 0.8
0.8],'linewidth',0.8)
scatter(f(pos_fpeak),A_peak,'o','b','filled');
plot([SC_SRO-
SB_SRO/2;SC_SRO+SB_SRO/2],[A_mean_SRO;A_mean_SRO],'m',...
    'linewidth',0.8,'marker','s','MarkerFaceColor','m');
plot([SC_SRO;SC_SRO],[A_mean_SRO-
A_std_SRO/2;A_mean_SRO+A_std_SRO/2],...
    'm','linewidth',0.8,'marker','s','MarkerFaceColor','m');
scatter(SC_SRO,A_mean_SRO,72,'o','r','filled');
scatter(FEC_SRO,A_mean_SRO,72,'s','g','filled');
xline(f(pos_f),'-.r','linewidth',0.8);

hold off

legend({'Spectrum*','Discarded spectrum','Peak','Spectral
bandwidth*',...
    'Amplitude std*','Spectral centroid*','Frequency energy
centroid*'}...
```

```
    ,'Location','southwest','color',[0.95 0.95
0.95],'edgecolor','k',...
    'linewidth',0.7)

% Graphic representation of the spectral slop in the frequency
% domain and using a linear scale for the amplitude axis

figure(9)
plot(f(1:pos_f),P1(1:pos_f),'b','linewidth',0.8)
xlim([20 max(f)]);
xlabel('Frequency [Hz]');
ylabel('Amplitude [lin]');

y_SS_lin_SRO = SS_SRO*(f-SC_SRO)+A_mean_lin_SRO;

hold on

plot(f(pos_f:end),P1(pos_f:end),'color',[0.8 0.8
0.8],'linewidth',0.8)
plot(f,y_SS_lin_SRO,'c','linewidth',0.8);
xline(f(pos_f),'-.r','linewidth',0.8);

hold off

legend({'Spectrum','Discarded spectrum','Spectral
slope*'},'Location',...
    'southeast','color',[0.95 0.95
0.95],'edgecolor','k','linewidth',0.7)

% Matlab Audio features extractor algorithm (note: spectral
% spread = spectral bandwidth)

aFE =
audioFeatureExtractor("SampleRate",fs,'spectralCentroid',true,.
..
    'spectralSpread',true,'pitch',true,'spectralFlux',true);
features = extract(aFE,ywin);

idx = info(aFE);
SCm = mean(features(:,idx.spectralCentroid));
pm = mean(features(:,idx.pitch));
SFm = mean(features(:,idx.spectralFlux));

% Display spectral centroid and spectral flux over time using
% an Hamming window (1024 sample) with an overlap length of 512

figure(10)

tt = linspace(0,size(ywin,1)/fs,size(features,1));
```

```
subplot(3,1,1);
plot(tt,features(:,idx.spectralCentroid),'linewidth',0.7)
title('Spectral centroid & Spectral bandwidth')
xlabel('Time (s)')
ylabel('Frequency (Hz)')

hold on
plot(tt,features(:,idx.spectralSpread),'linewidth',0.7)
hold off

legend({'Spectral centroid','Spectral
bandwidth'},'Location','northeast',...
    'color',[0.95 0.95 0.95],'edgecolor','k','linewidth',0.7)

subplot(3,1,2);
plot(tt,features(:,idx.pitch))
title('Pitch')
xlabel('Time (s)')
ylabel('Frequency (Hz)')

subplot(3,1,3);
plot(tt,features(:,idx.spectralFlux))
title('Spectral flux')
xlabel('Time (s)')
ylabel('Amplitude (lin)')

% VECTOR RESUMING THE TIME DOMAIN AND FREQUENCY DOMAIN
% DESCRIPTORS

A_A_results =
[AT;TD;TC;TEC;A_peak;f_peak;A_mean;A_std;SC;FEC;SB;SCF;SF;...

SE;SSK;SK;SS;SD;SRO;pm;SFm;A_mean_SRO;A_std_SRO;SC_SRO;FEC_SRO;
SB_SRO;...
    SCF_SRO;SF_SRO;SE_SRO;SSK_SRO;SK_SRO;SS_SRO;SD_SRO];
```

IMPACT AUDIO TIME-FREQUENCY ANALYSIS

```
clear all
close all
clc

set(0,'defaultfigurecolor',[1 1 1])

%% Import data and plot time history
% Reading of the audio file: y data are the amplitude of the
% signal in linear scale and fs is the sampling frequency
[y,fs] = audioread('example.wav');
% Trim the data to 0.1 seconds before impact and 1.4 seconds
% after impact
y_peak = max(y);
pos_t = find(y==y_peak);
low_y = pos_t -0.1*fs;
up_y = pos_t +1.4*fs;
y_trim = y(low_y:up_y);

% Temporal resolution
T = 1/fs;
% Length of the signal
L = length(y_trim);
% Temporal vector
t = (0:L-1)*T;
% Data in logarithmic scale (decibel full scale: dBFS)
y_dB = 20*log10(abs(y_trim));

% Graphic representation of the signal in the time domain
% (amplitude in linear scale and logarithmic scale (dBFS), time
% in seconds). Logarithmic scale useful to detect if all the
% signal is represented in the selected temporal section
figure(1)

subplot(2,1,1);
plot(t,y_trim,'b');
xlabel('Time [s]');
ylabel('Amplitude [lin]');

subplot(2,1,2);
plot(t,y_dB,'b');
xlabel('Time [s]');
ylabel('Amplitude [dBFS]');

%% Windowing of the signal
% Definition of a rectangular window (aka "No window")
win = rectwin(L);
```

```
% Amplitude Correction Factor (ACF) to compensate for the
% reduction of signal amplitude after the window is applied
mean_win = mean(win);
ACF = 1/mean_win;
% Energy Correction Factor (ECF) to compensate for the
% reduction of signal energy after the window is applied
rms_w =rms(win);
ECF = 1/rms_w;
% Windowing of the signal
ywin = y_trim.*win;

% Graphic representation of the signal, the windowed signal and
% the applied window
figure(2)
title('Window');
plot(t,y_trim,'b','linewidth',0.8)
xlabel('Time [s]');
ylabel('Amplitude [lin]');
hold on
plot(t,win,'g','linewidth',0.8)
hold on
plot(t,ywin,'r','linewidth',0.8)
hold on

hold off

legend({'Signal','Window','Windowed
signal'},'Location','southeast',...
    'color',[0.95 0.95 0.95],'edgecolor','k','linewidth',0.7)

%% Matlab audio features extractor
% Matlab Audio feautures extractor algorithm - default Hamming
% window over 1024 samples with 512 overlap length (note:
% spectral spread = spectral bandwidth)

aFE =
audioFeatureExtractor("SampleRate",fs,'spectralCentroid',true,.
..

'spectralSpread',true,'spectralCrest',true,'spectralFlatness',t
rue,...

'spectralEntropy',true,'spectralSkewness',true,'spectralKurtosi
s'...

,true,'spectralSlope',true,'spectralDecrease',true,'spectralRol
loffPoint'...
    ,true,'spectralFlux',true,'pitch',true);
% setExtractorParams(aFE,"pitch","Method","CEP")
features = extract(aFE,ywin);
```

```
idx = info(aFE);
SCm = mean(features(:,idx.spectralCentroid));
SBm = mean(features(:,idx.spectralSpread));
SCFm = mean(features(:,idx.spectralCrest));
SFm = mean(features(:,idx.spectralFlatness));
SEm = mean(features(:,idx.spectralEntropy));
SSKm = mean(features(:,idx.spectralSkewness));
SKm = mean(features(:,idx.spectralKurtosis));
SSm = mean(features(:,idx.spectralSlope));
SDm = mean(features(:,idx.spectralDecrease));
SROm = mean(features(:,idx.spectralRolloffPoint));
SFluxm = mean(features(:,idx.spectralFlux));
pm = mean(features(:,idx.pitch));

% Display spectral centroid, spectral bandwidth and spectral
% rolloff varying over time

figure(3)

subplot(2,1,1)
tt = linspace(0,size(ywin,1)/fs,size(features,1));

plot(tt,features(:,idx.spectralCentroid),tt,features(:,idx.spec
tralSpread),...
    tt,features(:,idx.spectralRolloffPoint),'linewidth',0.7)
xlabel('Time [s]')
ylabel('Frequency [Hz]')

legend({'Spectral Centroid','Spectral Bandwidth','Spectral
Rolloff'},...
    'Location','northwest','color',[0.95 0.95
0.95],'edgecolor','k',...
    'linewidth',0.7)

subplot(2,1,2)
tt = linspace(0,size(ywin,1)/fs,size(features,1));

semilogy(tt,features(:,idx.spectralCentroid),tt,features(:,idx.
spectralSpread),...
    tt,features(:,idx.spectralRolloffPoint),'linewidth',0.7)
xlabel('Time [s]')
ylabel('Frequency [Hz]')

legend({'Spectral Centroid','Spectral Bandwidth','Spectral
Rolloff'},...
    'Location','northwest','color',[0.95 0.95
0.95],'edgecolor','k',...
    'linewidth',0.7)
```

```
% Normalize the other features by their mean and standard
% deviation and plot their variation over time

features_norm = (features -
mean(features,1))./std(features,[],1);

figure(4)

subplot(3,1,1)

plot(tt,features_norm(:,idx.spectralCrest),tt,features_norm(:,i
dx.spectralFlatness),...
    tt,features_norm(:,idx.spectralEntropy),'linewidth',0.7)
xlabel('Time [s]')
ylabel('Feature variation')
legend({'Spectral Crest','Spectral Flatness','Spectral
Entropy'},...
    'Location','northeast','color',[0.95 0.95
0.95],'edgecolor','k',...
    'linewidth',0.7)

subplot(3,1,2)

plot(tt,features_norm(:,idx.spectralSkewness),tt,features_norm(
:,idx.spectralKurtosis),...
    tt,features_norm(:,idx.spectralFlux),'linewidth',0.7)
xlabel('Time [s]')
ylabel('Feature variation')
legend({'Spectral Skewness','Spectral Kurtosis','Spectral
Flux'},...
    'Location','northeast','color',[0.95 0.95
0.95],'edgecolor','k',...
    'linewidth',0.7)

subplot(3,1,3)

plot(tt,features_norm(:,idx.spectralSlope),tt,features_norm(:,i
dx.spectralDecrease),...
    tt,features_norm(:,idx.pitch),'linewidth',0.7)
xlabel('Time [s]')
ylabel('Feature variation')
legend({'Spectral Slope','Spectral Decrease','Pitch'},...
    'Location','southeast','color',[0.95 0.95
0.95],'edgecolor','k',...
    'linewidth',0.7)

%% Spectrogram using the Short Time Fourier Transform (STFT)
% Spectrogram using the STFT (Hamming window, interval 1024
% samples, overlap length 512 samples)
```

```
figure(5)
spectrogram(ywin,1024,512,[],fs,'yaxis');
xlabel('Time [s]')
ylabel('Frequency [kHz]')

% Spectrogram with logarithmic frequency axis

[S,F,T] = spectrogram(ywin,1024,512,[],fs,'yaxis');

figure(6)
sh = surf(T,F,20*log10(abs(S)/1024));
% Linear scale magnitude
% sh = surf(T,F,abs(S)/1024);
view([0 90])
axis tight
xlabel('Time [s]')
ylabel('Frequency [Hz]')
c = colorbar;
c.Label.String = 'Power/frequency [dBFS/Hz]';
set(gca,'YScale','log')
set(sh,'LineStyle','none')
caxis([-150 inf])
ylim([-inf inf])

hold on
rectangle('Position',[T(1) F(2) T(end-1) F(end)])
hold off

% Spectrogram using the STFT (Hamming window, interval 4096
% samples, overlap length 2048 samples). A longer interval
% increases the frequency resolution but obviously decreases
% temporal resolution

figure(7)
spectrogram(ywin,4096,2048,[],fs,'yaxis');
xlabel('Time [s]')
ylabel('Frequency [kHz]')

% Spectrogram with logarithmic frequency axis

[SS,FF,TT] = spectrogram(ywin,4096,2048,[],fs,'yaxis');

figure(8)
shh = surf(TT,FF,20*log10(abs(SS)/4096));
% Linear magnitude
% shh = surf(TT,FF,abs(SS)/4096);
view([0 90])
axis tight
xlabel('Time [s]')
ylabel('Frequency [Hz]')
```

```
c = colorbar;
c.Label.String = 'Power/frequency [dBFS/Hz]';
set(gca,'YScale','log')
set(shh,'LineStyle','none')
caxis([-150 inf])
ylim([F(2) inf])

hold on
rectangle('Position',[TT(1) F(2) TT(end-1) FF(end)])
hold off

%% Scalogram using Continuos Wavelet Transform (CWT)
% Scalogram using the CWT (default value: Morse wavelet -
% symmetry parameter (gamma) equal to 3 and the time-bandwidth
% product equal to 60). Time-bandwidth set to 120 (max
% admissible value) leads to larger spreads in time and
% narrower spreads in frequency

[wt,f] = cwt(ywin,fs,'TimeBandwidth',120);
% [wt,f] = cwt(ywin,'bump',fs);

% Scalogram representation of the signal limited to the first
% 0.5 seconds. The white line marks what is known as the cone
% of influence and shows areas in the scalogram potentially
% affected by edge-effect artifacts.

figure(9)
cwt(ywin,fs,'TimeBandwidth',120);
% cwt(ywin,'bump',fs);
xlim([0 0.5])

% Scalogram representation of the signal limited to the first
% 0.5 seconds using a contour plot. 10 magnitude levels used to
% plot the isolines

figure(10)
contour(t,f,abs(wt),30);
set(gca,'YScale','log');
xlim([0 0.5])
ylim([100 22050])
grid on
grid minor
xlabel('Time [s]')
ylabel('Frequency [Hz]')
c = colorbar;
c.Label.String = 'Magnitude';

% Extract 3 ridges with the highest energy content of the
% signal along the frequency domain. The penalty value for
% changing frequency is set to 200
```

```
[fridge,iridge,lridge] = tfridge(wt,f,200,'NumRidges',3);
rvals = wt(lridge);

% Find the most frequent values of the 3 identified ridges
% limiting the time to half the signal duration

m = mode(fridge(1:round(length(t)/2),:));
fridge_new = repmat(m,length(fridge),1);

hold on;
plot(t,fridge_new,'r--','linewidth',0.8);
hold off;

% 3D representation of the CWT and ridges using a contour plot

figure(11)
contour3(t,f,abs(wt),50);
set(gca,'YScale','log');
xlim([0 0.5]);
ylim([100 22050])
grid on
grid minor
view([50 50])
xlabel('Time [s]')
ylabel('Frequency [Hz]')
zlabel('Magnitude')

hold on
plot3(t,fridge_new,abs(rvals),'r','linewidth',1);
hold off
```

MICROPHONE OCTAVE EQUALIZER

```
clear all
close all
clc

set(0,'defaultfigurecolor',[1 1 1])

%% Import data and plot time history
% Reading of the audio file: y data are the amplitude of the
% signal in linear scale and fs is the sampling frequency
[y,fs] = audioread('example.wav');
% Trim the data to 0.1 seconds before impact and 1.4 seconds
% after impact
y_peak = max(y);
pos_t = find(y==y_peak);
low_y = pos_t -0.1*fs;
up_y = pos_t +1.4*fs;
y_trim = y(low_y:up_y);

% Temporal resolution
T = 1/fs;
% Length of the signal
L = length(y_trim);
% Temporal vector
t = (0:L-1)*T;
% Data in logarithmic scale (decibel full scale: dBFS)
y_dB = 20*log10(abs(y_trim));

%% Sound equalization
% Equalize the sound using the UMIK-1 calibration file (FRF -
% 1/3 octave) Define the equalizer filter
equalizer = graphicEQ('Bandwidth','1/3
octave','Structure','Cascade',...
    'SampleRate',fs);
equalizer.Gains = [-24.61,-25.38,-22.46,-17.25,-15.36,-9.93,-
6.41,-0.78,...
    -0.58,6.73,8.55,4.80,3.93,1.75,0.45,0.84,-2.41,-7.14,-
8.68,-1.05,...
    -6.40,-3.91,-4.47,-4.82,-1.40,-5.65,-12.25,-5.25,-3.21,-
10.72];
visualize(equalizer)

y_equal = equalizer(y_trim);
y_equal_tot = equalizer(y);
% Data in logarithmic scale (decibel full scale: dBFS)
y_equal_dB = 20*log10(abs(y_equal));
```

```
%% Graphic representation in the time domain
% Graphic representation of the signal in the time domain
% (amplitude in linear scale and logarithmic scale (dBFS), time
% in seconds). Logarithmic scale useful to detect if all the
% signal is represented in the selected temporal section
figure(1)

subplot(2,1,1);
plot(t,y_trim,'b','linewidth',0.8);
xlabel('Time [s]');
ylabel('Amplitude [lin]');

hold on
plot(t,y_equal,'g','linewidth',0.8);
hold off

legend({'Signal','Equalized signal'},'Location','southeast',...
    'color',[0.95 0.95 0.95],'edgecolor','k','linewidth',0.7)

subplot(2,1,2);
plot(t,y_dB,'b','linewidth',0.8);
xlabel('Time [s]');
ylabel('Amplitude [dBFS]');

hold on
plot(t,y_equal_dB,'g','linewidth',0.8);
hold off

legend({'Signal','Equalized signal'},'Location','southeast',...
    'color',[0.95 0.95 0.95],'edgecolor','k','linewidth',0.7)

%% Spectrum analysis using the Fast Fourier Transform (FFT)
% Zero-padding of the signal to apply the FFT (N is the closest
% power of two to the signal length)
N = 2^nextpow2(L);
Y = fft(y_trim,N);
Y_eq = fft(y_equal,N);
% Normalization of the two-sided spectrum (complex FFT)
P2 = abs(Y)/N;
P2_eq = abs(Y_eq)/N;
% One-sided spectrum neglecting the mirrored part of the two-
% sided spectrum (negative frequencies)
P1 = P2(1:N/2);
P1_eq = P2_eq(1:N/2);
% Discarding the first value (DC frequency at 0 Hz) and the
% last value corresponding to the Nyquist frequency.
% Multiplying by a factor of 2 to account for the loss of
% symmetry and represent the right amplitude
P1(2:end-1) = (2*P1(2:end-1));
P1_eq(2:end-1) = (2*P1_eq(2:end-1));
```

```
% Frequency spectrum resolution
F = fs/N;
% Frequency vector defined up to the Nyquist frequency (fs/2)
f = (1:N/2)*F;

% Graphic representation of the spectrum: logarithmic amplitude
% (dBFS) and logarithmic frequency axis
P1db = 20*log10(P1);
P1_eq_db = 20*log10(P1_eq);

figure(2)
semilogx(f,P1db,'b','linewidth',0.8)
xlim([20 max(f)]);
xlabel('Frequency [Hz]');
ylabel('Amplitude [dBFS]');

hold on
semilogx(f,P1_eq_db,'g','linewidth',0.8)
hold off

legend({'Spectrum','Spectrum
(equalized)'},'Location','southeast',...
    'color',[0.95 0.95 0.95],'edgecolor','k','linewidth',0.7)

%% Export the equalized audio in a '.wave' file format

filename = 'example_equalized.wav';
audiowrite(filename,y_equal_tot,fs,'BitsPerSample',16);
```